TECHNISCHE UNIVERSITÄT MÜNCHEN

Department Chemie

Institute for Advanced Study

Design and Synthesis of Novel αIIbβ3 Integrin Antagonists

Markus Bollinger

Vollständiger Abdruck der von der Fakultät für Chemie der Technischen Universität München zur Erlangung des akademischen Grades eines

Doktors der Naturwissenschaften

genehmigten Dissertation.

Vorsitzender: Univ.-Prof. Dr. Stephan A. Sieber

Prüfer der Dissertation:

1. Univ.-Prof. Dr. Dr. h.c. Horst Kessler
2. Univ.-Prof. Dr. Hans-Jürgen Wester

Die Dissertation wurde am 9. Oktober 2012 bei der Technischen Universität München eingereicht und durch die Fakultät für Chemie am 30. November 2012 angenommen.
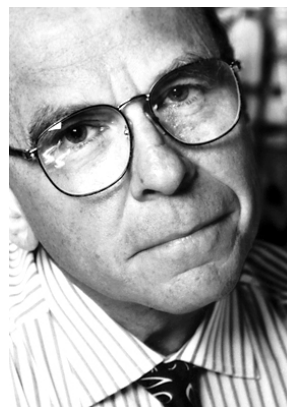
meinen Eltern

„SEARCHING FOR NEW REACTIVITY"

by

K. Barry Sharpless
The Scripps Research Institute
La Jolla, USA

> In 1938, three years before I was born, a live coelancath was taken from the waters [...] remained big news for years, fueling an enthusiasm for "creatures" that persisted for decades.
> [...] As a kid, I passionately wanted to be one who caught the next coelacanth, the first to see something that was beyond reasoning, even beyond imagining.

K. Barry Sharpless won the Nobel Prize in Chemistry 2001 for his work on chirally catalyzed oxidation reactions.

Die vorliegende Arbeit wurde im Zeitraum von September 2008 bis Oktober 2012 am Institute for Advanced Study - Department Chemie - der Technischen Universität München unter der Leitung von Herrn Prof. Dr. Dr. h. c. Horst Kessler angefertigt.

Danksagung

Mein ganz besonderer Dank gilt meiner Mama und meinem Papa, der leider viel zu früh verstorben ist. Ihr wart mir stets ein starker familiärer Rückhalt und habt mich zu dem Menschen gemacht, der ich heute bin.

Danke!

The following publications resulted from the work of this Ph. D. thesis:

Jagasia, R.; Holub, J. M.; **Bollinger, M.**; Kirshenbaum, K.; Finn, M.G.
Peptide Cyclization and Cyclodimerization by Cu^I-Mediated Azide-Alkyne Cyclo-
addition. *J. Org. Chem.* **2009**, *74*, 2964-2974.

Bollinger, M.; Manzenrieder, F.; Kolb, R.; Bochen, A.; Neubauer, S.; Marinelli, L.;
Limongelli, V.; Novellino, E.; Moessmer, G.; Pell, R.; Lindner, W.; Fanous, J.; Hoff-
man, A.; Kessler, H.
Tailoring of Integrin Ligands: Probing the Charge Capability of the Metal Ion-De-
pendent Adhesion Site. *J. Med. Chem.* **2012**, *55*, 871-882.

Bollinger, M.; Yousefi, B. H.; Bochen, A.; Laitinen, I.; Petzold, T.; Schwaiger, M.;
Kessler, H.; Wester, H-J.
Direct One-Step ^{18}F-Labeling of a New Highly Active αIIbβ3 Integrin Antagonist via
Nucleophilic Aromatic Substitution. October, **2012**, *Manuscript in preparation.*

**The following conference oral presentations resulted from the work of this Ph.
D. thesis:**

Jagasia, R.; Holub, J. M.; **Bollinger, M.**; Kirshenbaum, K.; Finn, M.G.
Peptide cyclodimerization by the Cu(I)-mediated azide-alkyne cycloaddition reaction.
Abstracts of Papers, 234th ACS National Meeting, Boston, MA, United States, August
19-23, **2007**.

Bollinger, M. Integrins as Therapeutic Targets. Tagung des Doktorandenforums "Na-
tur " Wannseeforum, der Studienstiftung des deutschen Volkes, June 2–5, **2011**, Ber-
lin, Deutschland.

The following poster presentations resulted from the work of this Ph. D. thesis:

Bollinger, M.; Manzenrieder, F.; Kolb, R.; Marinelli, L.; Limongelli, V.; Kessler, H.
Probing the Charge Capability of the MIDAS: Phosphinic- and Phosphonic Acid Containing Compounds as New Potent αIIbβ3 Integrin Antagonists.
31st European Peptide Symposium 2010, September 5–9, **2010**, Copenhagen, Denmark.

Bollinger, M.; Manzenrieder, F.; Kolb, R.; Bochen, A.; Marinelli, L.; Limongelli, V.; Pell, R.; Lindner, W.; Kessler, H.
Probing the Charge Capability of the MIDAS: Phosphinic- and Phosphonic Acid Containing Compounds as New Potent αIIbβ3 Integrin Antagonists.
5th International Peptide Symposium 2010, December 4-9, **2010**, Kyoto, Japan.

Bollinger, M.; Manzenrieder, F.; Bochen, A.; Moessmer, G.; Kessler, H.
Platelet Aggregation Inhibition by a New Class of Glycoprotein IIb/IIIa Inhibitors.
22nd American Peptide Symposium 2011, June 25-30, **2011**, San Diego, USA.

The following patent resulted from the work of this Ph. D. thesis:

Bollinger, M.; Yousefi, B. H.; Schwaiger, M.; Kessler, H.; Wester, H-J.
^{18}F-Labeling of Unprotected Small Molecules. October, **2012**, *Patent in preparation.*

INDEX

1 INTRODUCTION

The science of medicinal chemistry deals with the design and discovery of new compounds that are suitable for use as therapeutic agents or clinical diagnostics. They should interfere with biological receptors in the appropriate biochemical pathological pathways in order to cure or diagnose diseases. The process of drug development requires scientists from a wide range of disciplines such as chemistry, biology, biochemistry, medicine and computational sciences, amongst others. One of the most famous and essential drugs in modern medicine is acetylsalicylic acid, traded as Aspirin[®]. More than 50,000 tons of acetylsalicylic acid are produced per year.[1] On August 10, 1897, *Felix Hoffmann*, a German chemist at the Bayer Company, succeeded first to synthesize acetylsalicylic acid in a chemically pure and stable form.[1-4] This was the beginning of an outstanding success story, which is still ongoing. By the middle of the 20th century Aspirin[®] was solely used as an anti-inflammatory, antipyretic, and analgesic drug. Since the last decades, it is known that acetylsalicylic acid also possesses an antithrombotic effect due to inhibition of platelet function by acetylation of cyclooxygenase 1 (COX-1).[2] COX-1 oxidizes arachidonic acid to prostaglandin H_2 (PGH$_2$), a precursor of the prothrombotic thromboxane A_2 (TXA$_2$). In addition to the prostaglandin-dependent antithrombotic action of Aspirin[®], other antiplatelet drugs are known (Figure 12, top) including ADP antagonists (clopidogrel, prasugrel, ticagrelor) and the well-established glycoprotein (GP) IIb/IIIa (integrin αIIbβ3) antagonists such as abciximab, a Fab fragment of a humanized murine monoclonal antibody against αIIbβ3, eptifibatide, a cyclic heptapeptide containing the recognition sequence lysine-glycine-aspartic acid (KGD) and tirofiban (Aggrastat[®]), a non-peptidic tyrosine derivative, respectively.[5, 6]

The αIIbβ3 integrin is the most abundant platelet surface membrane glycoprotein. It mediates the final common pathway of platelet aggregation.[5-7] Due to the primary expression on activated platelets and the biological relevance in platelet aggregation, thrombus formation and coronary artery diseases, the integrin αIIbβ3 represents an attractive target for medicinal chemistry and pharmaceutical research. Therefore, the main focus of this thesis is related to the αIIbβ3 integrin and the synthesis of novel

αIIbβ3 integrin antagonists. The research carried out within this work can be categorized into three topics, which are briefly summarized below:

The aim of the first project is the bioisosteric replacement of the conserved carboxylic acid functionality in integrin ligands. Up to now, the carboxylic acid group in all integrin ligands (with exception of the recently found hydroxamic acid moiety[8]) including αIIbβ3 inhibitors is essential for the coordination of the bivalent metal cation at the metal ion-dependent adhesion site (MIDAS) of the receptor and is therefore responsible for activities in the low nanomolar range. For this reason, the main objectives of this project are to investigate, whether the MIDAS region can tolerate other bioisosteric groups, and furthermore, can compensate for negative excess charge. It was planned to substitute the carboxylic acid group by phosphorus-containing residues such as phosphinic-, phosphonic-, or thiophosphonic acids (Figure 1). The alterations of the pK_a values could provide insights in the binding mode of the metal-ligand-interaction and improve the pharmacokinetic properties of this new class of integrin antagonists. So far, a substitution of this group by phosphorus moieties in biologically active ligands failed. The investigated glycoprotein IIb/IIIa inhibitors may be promising candidates for novel and potent antithrombotic drugs.
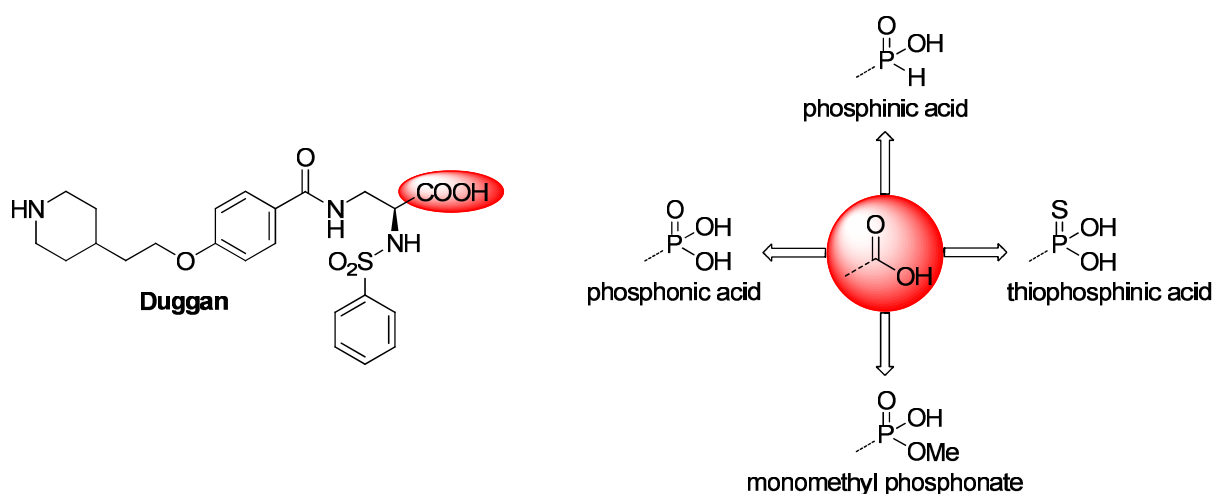
Figure 1 │ Bioisosteric replacement of the carboxylic MIDAS binding motif by phosphinic-, phosphonic-, thiophosphonic acid, and monomethyl phosphonate for the development of new αIIbβ3 integrin antagonists.

The association of the αIIbβ3 integrin within the pathological process of thrombus formation has been described (Figure 7).[5] Consequently, noninvasive imaging of the αIIbβ3 receptor using positron emission tomography (PET) could yield information

concerning the platelet aggregation status and an improved spatial resolution of the thrombus position within the body. Thus, αIIbβ3 PET tracers have been the subject of increasing interest over recent years for preclinical and clinical imaging studies. In the second project of this thesis, the synthesis and evaluation of a novel radiotracer for Molecular Imaging of activated platelets, involved in thrombus formation, is described. A highly active and selective αIIbβ3 integrin antagonist is radiolabeled by a direct one-step nucleophilic aromatic substitution. The [¹⁸F]fluoride was incorporated into the unprotected precursor in the last reaction step. The radiosynthesis and the subsequent biological evaluation of the labeled compound are subjects of the present efforts.
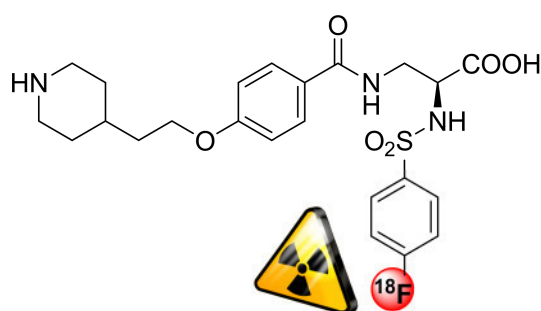
Figure 2 │ Development of a novel ¹⁸F radiotracer for targeting activated αIIbβ3 integrins.

Additionally, part three, which is not connected to the integrin field, discusses the head-to-tail peptide cyclodimerization using click chemistry. Recently, *Punna et al.*[9] found that on-resin cyclization of a peptide via copper(I)-catalyzed azide-alkyne cycloaddition (CuAAC) did not yield the desired cyclic monomer but rather only the head-to-tail cyclic dimer. These observations motivated us to evaluate the scope and mechanism of this Cu(I)-mediated azide-alkyne cycloaddition reaction. Accordingly, several peptide libraries have been constructed to understand the mechanism of this on-resin head-to-tail cyclodimerization phenomenon.
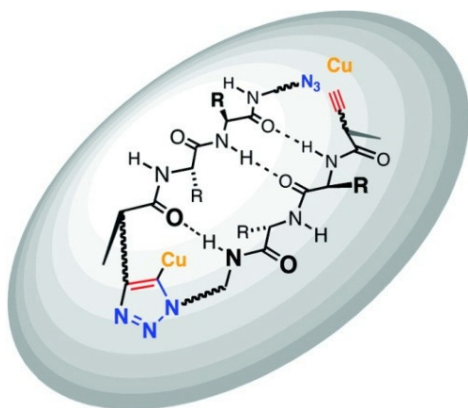
Figure 3 │ Schematic view of head-to-tail peptide cyclodimerization by copper(I)-catalyzed azide-alkyne cycloaddition. The intermolecular hydrogen bonds are shown as dashed lines.[10] Reprinted with permission from *The Journal of Organic Chemistry*, 2009, 74 (8), 2964–2974. Copyright © 2009 American Chemical Society.

2 *BIOLOGICAL BACKROUND*

2.1 *Integrin Family*

Integrins constitute an important class of transmembrane cell adhesion receptors, which are nearly universally found on all metazoa.[11-13] Twenty four integrin hetero-dimers are known and represent the main cellular anchor molecule that mediate cell-matrix and cell-cell interaction.[14] The contact of cells with its neighboring cells and extracellular matrix components mediated via integrins is for most cells a crucial property for survival.[15] Integrins facilitate transmembrane connections to the cytoskeleton. However, integrins are usually found in an inactive, non-ligand binding conformation and require signaling from inside of the cell to become activated.[16] Once activated, integrins mediate many different outside-inside signaling pathways.[17] Integrins are involved in many biological and pathological processes such as angiogenesis, apoptosis, cell migration, proliferation, cardiovascular disorders, and thrombosis.[18-20] Therefore inhibition of integrin function has been a major challenge in chemical biology and especially in medicinal chemistry, since the discovery in the late 1980s.[19]

In 1986, the term "integrin" was introduced by *Tamkum et al.*[21] to emphasize the role of the adhesion receptor proteins of the extracellular matrix (ECM) as an integral membrane complex involved in the transmembrane association between the extracellular matrix and the cytoskeleton. The finding of fibronectin being an ECM protein which is strongly involved in cell adhesion led to the identification of the arginine-glycine-aspartic acid (RGD) sequence as pivotal recognition motif of integrin binding.[22] By now, many different recognition motifs are known from several natural integrin ligands.[23]

The development of new subtypes of selective and highly active integrin ligands is of utmost importance. One of the goals would be to explore the importance of the individual integrin subtypes in the biology of integrin function and further better understanding the biochemical regulation of cell adhesion and bidirectional signal transduction on a molecular basis. Therefore, the inhibition of integrin function is an ongo-

ing major challenge in medicinal chemistry. In the last decades, great efforts have been applied by pharmaceutical companies as well as academic institutions to discover new compounds for the inhibition of integrin function.[24] An example is Cilengitide,[25] a cyclic RGD pentapeptide, cyclo(RGDf-*N*(Me)V-), that is currently in clinical phase III for the treatment of brain tumors (glioblastomas) and in phase II for other cancer types. It constituted the first anti-angiogenic small molecule targeting the integrins αvβ3, αvβ5, and α5β1.[26]

All integrins are non-covalently associated heterodimers of an α subunit and a β subunit. Both subunits are type I transmembrane glycoproteins, containing large extracellular domains (700-1100 residues) and mostly short cytoplasmic domains (30-50 residues) linked by a single transmembrane helix.[27] The extracellular domain of the β subunit contains a metal ion-dependent adhesion site (MIDAS) in the ligand binding domain.[14] Up to now, 18 different α and 8 different β subunits are known in mammals, which can assemble to form 24 individual dimers.[28, 29] An overview of the possible combinations of α and β subunits is given in Figure 4.
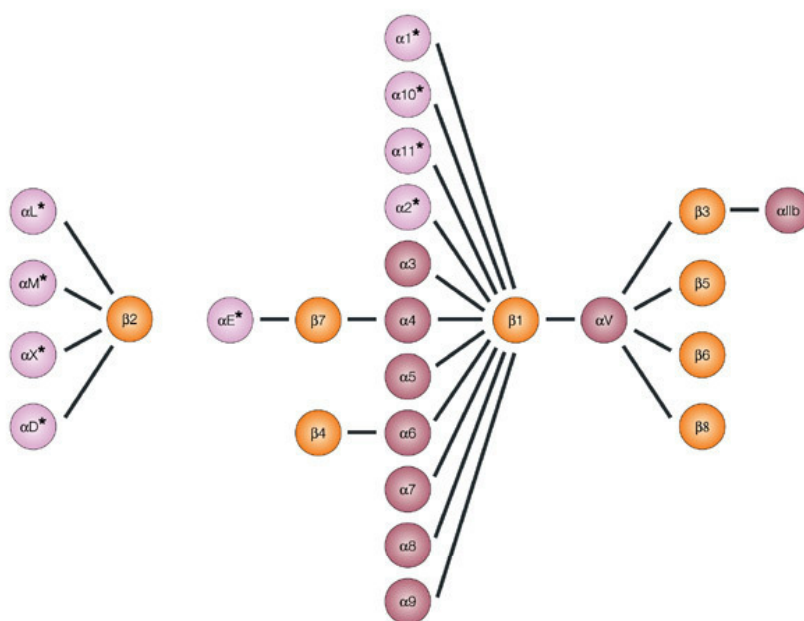
Nature Reviews | Drug Discovery

Figure 4 | Integrin heterodimer composition.[29] Reprinted by permission from Macmillan Publishers Ltd: *Nature Reviews Drug Discovery* 2003, 2, 703-716, Copyright © 2003, license number 2957620741653. Integrin α- and β-subunits form 24 heterodimers that recognize distinct but overlapping ligands. Half of the α-subunits contain I domains (asterisked).

2.2 The αIIbβ3 Integrin

One major subtype of integrins, the β3-integrins, includes the platelet receptor αIIbβ3 (see Figure 4). It recognizes the common RGD binding motif in its natural ligand, the plasma protein fibrinogen. The αIIbβ3 integrin is the most abundant integrin on the surface of platelets and plays a key role in thrombosis. It is solely expressed on platelets and megakaryocytes (platelet-producing cells in the bone marrow).[5, 7] Integrin αIIbβ3 [also referred to glycoprotein (GP) IIb/IIIa] is the main receptor involved in platelet aggregation in primary hemostasis. Formation of inter-platelet bridges via GPIIb/IIIa is mainly mediated by the plasma protein fibrinogen and to a lesser extent by the *von Willebrand* factor (see Figure 7). Therefore, the inhibition of the final common pathway of platelet aggregation by αIIbβ3 receptor antagonists such as tirofiban[30] is a clinically proven concept for acute antithrombotic therapy.[5, 31-33]

To carry out its adhesive tasks, the αIIbβ3 integrin has to be activated. During activation, integrins undergo conformational shape changes through their subunits, which will be discussed in the following.

A major breakthrough was the first crystal structure of the αIIbβ3 extracellular head group, co-crystallized with the fibrinogen-mimetic drug tirofiban,[30] elucidated by *Springer et al.*[34] in 2004 (pdb code 2vdm). This study provided knowledge about the active site (ligand binding site) of the αIIbβ3 receptor and significant new insights, on a molecular level, into the allosteric regulation mechanism of the conformation and the ligand affinity of the platelet integrin αIIbβ3.[34] For the mechanism of integrin activation, *Springer et al.*[34] postulated, based on electron microscopy and X-ray data, a model with three different overall conformations of the extracellular domain:[34, 35]

- low-affinity, bent conformation (inactive, Figure 5a)
- high-affinity, extended conformation (primed with closed headpiece, Figure 5b)
- ligand-bound (activated with open headpiece, Figure 5c)

In the bent conformation, the head group of the integrin points inwards towards the cell surface and exhibits low affinity for ligands. However, there is an equilibrium between bent and extended conformation regulated by proteins (e.g. talin), which bind to the short intracellular domains of the integrins. In this extended conformation, the head group points away from the surface and is accessible for other molecules, which thus can bind with higher affinity.[34-36]
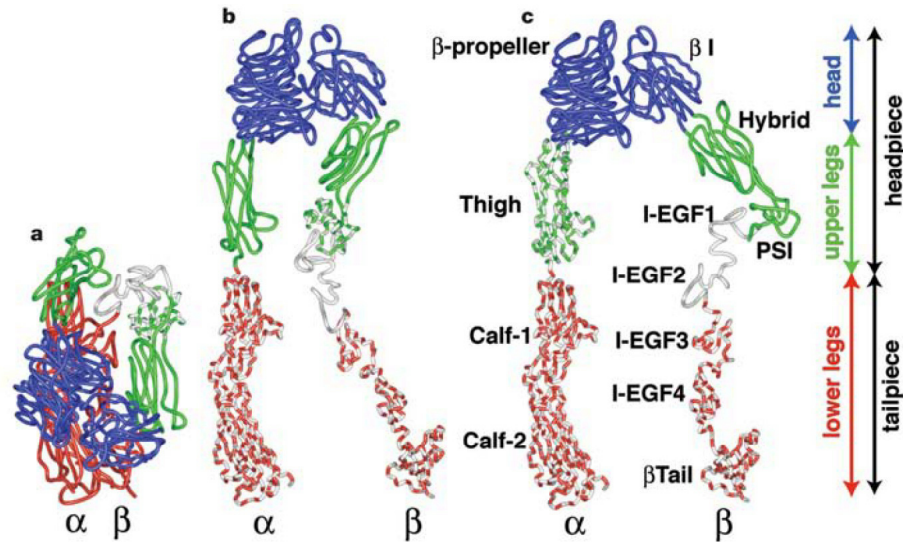
Figure 5 | Integrin activation states.[34] Adapted by permission from Macmillan Publishers Ltd: *Nature* 2004, 432, 59-67, Copyright © 2004, license number 2957630213342. Different overall conformations of the extracellular domain are depicted. **(a)** bent, **(b)** extended, and **(c)** ligand-bound form.

The major ligand binding site of the platelet integrin $\alpha IIb\beta 3$ (the αI-domain is not present in $\alpha IIb\beta 3$) is located at a groove between the β-propeller of the α subunit and the βI-domain of the β subunit (Figure 5c). Both integrin subunits are involved in ligand binding. In case of tirofiban, the carboxylic acid function of the tyrosine scaffold is involved in the crucial coordination of the bivalent metal cation at the metal-ion-dependent adhesion site (MIDAS), which is present in all integrins (Figure 6 and Figure 13). Five of six possible coordination sites of the bivalent cation are coordinated by the integrin in an octahedral shape.[14, 34] The protonated piperidine moiety of tirofiban points toward the αIIb subunit, forming a salt bridge interaction with (αIIb)-Asp224 and an H-bond with the (αIIb)-Ser225 backbone CO group. In the $\alpha IIb\beta 3$ integrin, the basic moiety of the corresponding ligand (here piperidine) is bound in the αIIb subunit via an end-on interaction, whereas in $\alpha v\beta 3$ a ligand is bound side-on. These distinctions in the binding mode can be used to selectively address the $\alpha IIb\beta 3$ integrin.[37] Figure 6 shows the binding mode of tirofiban in $\alpha IIb\beta 3$.[38]
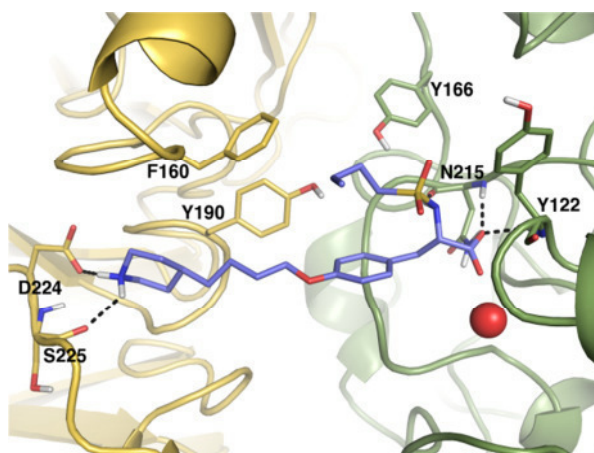
Figure 6 | Binding mode of tirofiban in αIIbβ3.[38] The αIIb domain is displayed as a yellow cartoon, while the β3 domain is colored in green. The interacting residues and the ligand are shown as licorice, while the magnesium ion is represented as a red sphere. For the sake of clarity, only the polar hydrogens are displayed. Adapted with permission from *Journal of Medicinal Chemistry*, 2012, 55, 871–882. Copyright © 2012 American Chemical Society.

2.3 Arterial Thrombus Formation

Thrombus formation is a quite complex process, which requires several temporarily and spatially tightly regulated events. In a resting state, platelets patrol the vasculature in close proximity to the vessel wall. An atherosclerotic plaque rupture accompanies the exposure of subendothelial matrix proteins such as collagen, fibronectin, laminin and *von Willebrand* factor (vWF). Collagens resemble the most thrombogenic matrixes and are recognized by different platelet receptors. Initially GPIb mediates interaction to collagen via blood derived and deposited vWF. This transient interaction leads to platelet deceleration and allows other platelet receptors to bind. Subsequent binding of glycoprotein GP VI[39], which is so far understood to be the most important collagen receptor, can induce platelet activation which goes along with a conformational change of the αIIbβ3 integrin (extended conformation with high-affinity for fibrinogen; Figure 5b). On unstimulated platelets there are ~60.000 αIIbβ3 dimers expressed on the surface. However, an additional, smaller pool of intracellular vesicular stored αIIbβ3 dimers can be transferred to the platelet surface.[40] Activated glycoprotein IIb/IIIa reveals its binding site for fibrinogen (the predominant aggregation mediating protein) and thus, fibrinogen, which contains two RGD-binding sequences, can bridge two plates and lead to aggregation.[5, 6, 31] A detailed description of the process of thrombus formation is given in Figure 7.
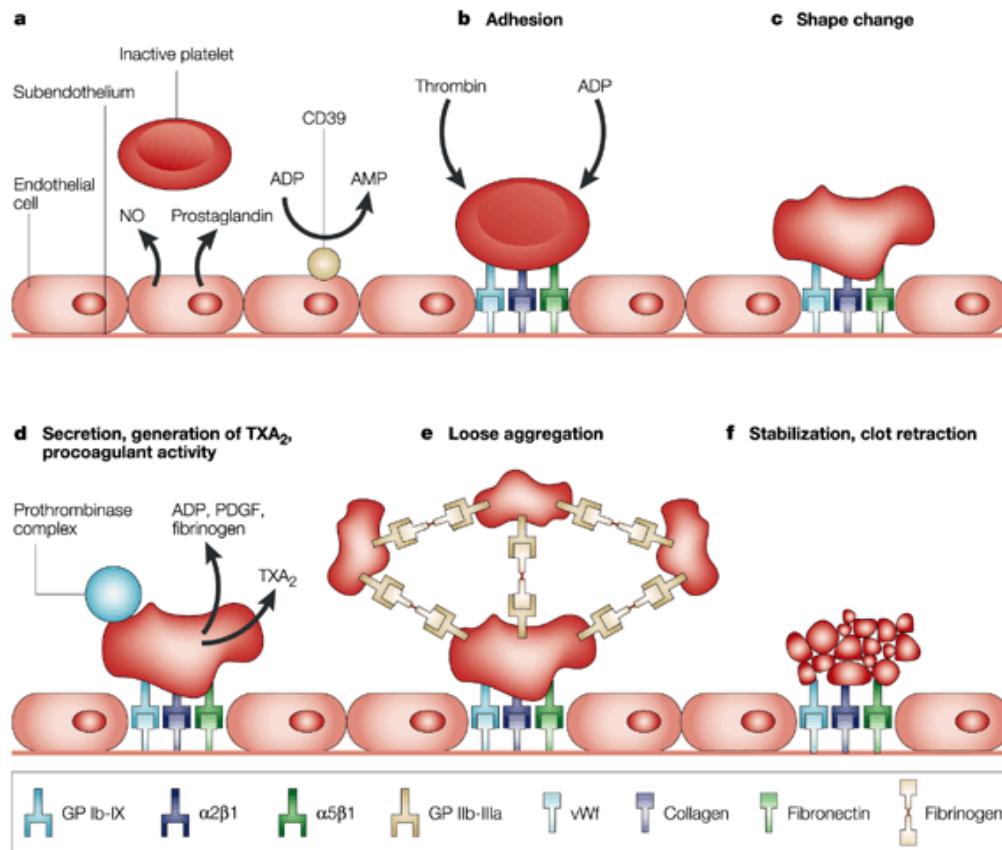
Figure 7 | The role of platelets in thrombus formation.[5] Reprinted by permission from Macmillan Publishers Ltd: *Nature Reviews Drug Discovery* 2003, 2, 15-28, Copyright © 2003, license number 2957631110707. **(a)** Circulating platelets are usually kept in an inactive state by prostacyclin and nitric oxide (NO) released by the endothelial cells that line the walls of blood vessels. Endothelial cells also express CD39 on their surface, which inhibits platelet activation by converting adenosine diphosphate (ADP), a potent inducer of platelet activation, into adenosine monophosphate (AMP). **(b, c)** At sites where the blood vessel wall has been injured, the platelets adhere to the exposed subendothelium through interactions between collagen, *von Willebrand* factor and fibronectin and their receptors on the platelets, integrin α2β1, glycoprotein Ib-IX (GP Ib-IX) and integrin α5β1, respectively. Both thrombin and ADP cause platelets to change into an active conformation. **(d)** Activated platelets secrete ADP, platelet-derived growth factor, and fibrinogen from storage granules in the platelet, and thromboxane A_2 (TXA_2), produced by immediate biosynthesis. ADP and TXA_2 cause circulating platelets to change shape and become activated. **(e)** Glycoprotein IIb/IIIa receptors on the surface of activated platelets bind fibrinogen, leading to the formation of fibrinogen bridges between the platelets, resulting in platelet aggregation. This, and the simultaneous formation of a fibrin mesh (not shown), lead to the formation of a platelet thrombus. **(f)** Clot retraction then leads to formation of a stable thrombus.[5]

3 GENERAL SECTION

This chapter is intended to give a short overview of some adopted techniques and topics of peripheral interest that are not discussed in detail in the publication and manuscript respectively. However, they are important for the understanding of the context.

3.1 Enantioselective Liquid Chromatography

Due to its broad applicability ranging from trace analysis of enantiomeric impurities to multi-kilogram-scale preparative enantioseparations,[41] enantioselective high performance liquid chromatography (HPLC), often referred chiral HPLC, has become a powerful and versatile tool for analysis and separation of enantiomers in the last decades.[42] Since enantiomerically pure compounds are of immense importance in pharmaceutical industry chiral HPLC plays an important role in the development of new drugs.

The enantiomer separation of the racemic phosphorus-containing $\alpha IIb\beta 3$ integrin antagonists[38] was performed, in a direct approach, on quinine-based chiral zwitterionic ion-exchange-type stationary phases [ZWIX-CSPs, Quinine-type (8S, 9R), Figure 8] developed by the *Lindner Group*.[43] They comprise strong cation and weak anion exchanger motifs within the chiral selector moiety. Covalent attachment of such a chiral selector onto modified silica gel yields a zwitterionic chiral stationary phase (CSP) suitable for enantiomer separation via chromatography. Figure 8 shows the used quinine-based ZWIX-selectors and CSPs for the enantiomer separation in *Bollinger et al.*.[38]

Due to the zwitterionic nature, the ZWIX-CSPs are able to resolve chiral zwitterionic (amphoteric) compounds (e.g. free amino acids or small peptides), which are generally poorly or even not retained and thus not separated on uni-ionic CSPs. Main interaction forces between the zwitterionic chiral selector and the analytes (selectands) are characterized by a simultaneous double ion pairing process. Thus, the protonat-

ed tertiary amine of the quinuclidine ring and the dissociated sulfonic acid of the chiral selector can undergo double-ionic attraction with zwitterionic analytes. These undirected electrostatic forces are supported by additional directed interactions like π-π stacking, hydrogen bonding, van der Waals and steric interactions which are in a concerted action responsible for enantiodiscrimination and thus resolution of the enantiomers.[44, 45] Detailed studies on the molecular recognition mechanism identified the crucial role of the carbamate group of the quinidine based chiral selector as it supports the formation of directed hydrogen bonds with the amide group of *N*-acyl protected α-amino acid derivatives.[46, 47] This results in a stereochemically fixed molecular recognition model with the consequence of a chromatographically corresponding elution order. The selectand enantiomer of the lower complex stability with the quinine based chiral selector will elute in front of the stronger complexing analyte enantiomer. It relates to the relative stability constants of the diastereomeric intermediate associates and is directly proportional to the observed chromatographic selectivity value α. Based on this concept we can state that the elution order keeps constant for ionizable enantiomers bearing an amide group located in the vicinity to the acid group and the chiral C-atom. For these constellations the stereochemically controlled isosteric molecular chiral recognition model stays fixed for any type of α-amino acid whether it is related to carboxylic-, phosphinic- or phosphonic acids.[48, 49] In the case of phosphonic acids, the additional electrostatic interaction of a second ion pair, supports only retention but in a non-stereodiscriminating way. Consequently, we can assume that the elution order keeps constant within the herein presented peptidomimetics[38] having a chiral α amino acid motif in its structure. With standard analytes of known absolute configuration and the given configuration of the chiral centers of the quinine moiety of the chiral selector [quinine-type (8*S*, 9*R*)], the chromatographic elution order was verified and from these data it was concluded that the first eluted enantiomers of the resolved phosphinic - and phosphonic acid derivative had to have the (*R*)-configuration, being isosteric with the (*S*)-configuration of a corresponding α amino carboxylic acid derivative following the Cahn-Ingold-Prelog convention. Moreover, enantiomer elution order could be inverted by switching from the quinine- to the pseudoenantiomeric quinidine-based CSP [quinidine-type (8*R*, 9*S*)], which underlined that the cinchona alkaloid moiety plays a pivotal role in the chiral recognition process.[43]
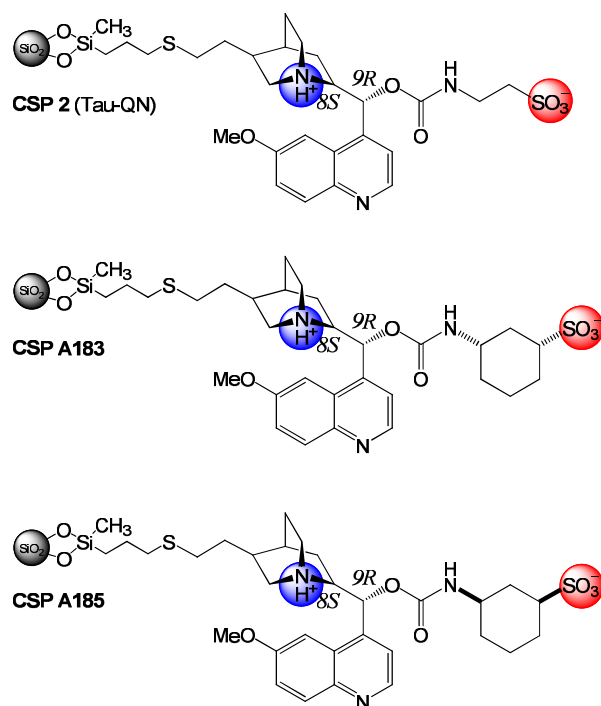
Figure 8 | Chemical structures of the quinine-based chiral zwitterionic ion exchange-type stationary phases [ZWIX-CSP, Quinine-type (8*S*, 9*R*)]: **CSP 2** (Tau-QN), **CSP A183** and **CSP A185**. Stereoconfiguration at the cyclohexan moiety of **CSP A183** and **CSP A185** has not yet determined.

Figure 9 shows some examples of the remarkable enantiodiscrimanation properties of one of the ZWIX-CSPs mentioned above.
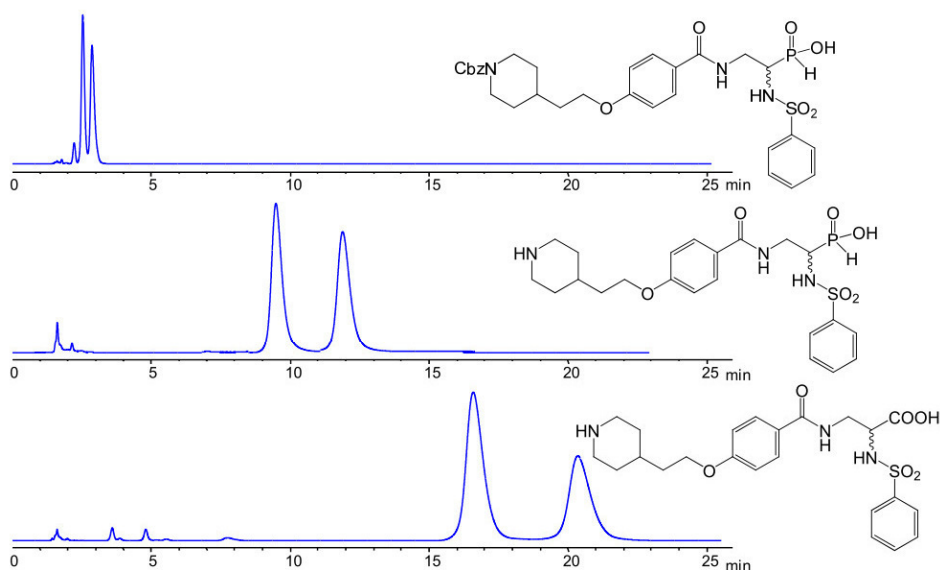
Figure 9 | HPLC enantiomer separations of peptidomimetics on quinine-based chiral zwitterionic ion exchange-type stationary phase. Experimental conditions: **CSP A185**, MeOH, 50 mM HOAc, 25 mM NH$_3$, 25 °C, flow rate 1.0 mL/min, UV detection, t$_0$ = 1.51 min.

3.2 ^{31}P Phosphorus NMR Spectroscopy

The enantiopurity of the thiophosphonic acid[38] (exemplary, Figure 10) obtained from enantioseparation conducted on one of the ZWIX-CSPs[43] (see Figure 8) was confirmed independently by NMR spectroscopy. ^{31}P NMR spectroscopy in combination with α-cyclodextrin as suitable chiral solvating agent represents a powerful technique for the direct determination of the enantiomeric purity of the synthesized compounds.[50] One of the biggest advantages of NMR spectroscopy in relation to other methods is that it directly detects even weak interactions between the chiral agent and the target molecules. However, the pH of the solution influences the enantiodiscrimination process and has to be adjusted.

^{31}P with spin ½ is the only naturally occurring phosphorus isotope. Its sensitivity is among the highest spin ½ nuclei, however, compared to that of the proton it is only 6.6%. The sensitivity of the ^{31}P NMR signal is proportional to $(\gamma_P/\gamma_H)^3$ where γ_P and γ_H is the gyromagnetic ratio of phosphorus and hydrogen, respectively.[51] ^{31}P NMR signals typically appear as singlet resonances in the presence of proton decoupling and are therefore intense. Furthermore, most molecules suitable for ^{31}P NMR-screening possess only one phosphorus atom and are therefore mostly represented by only one ^{31}P-signal in the spectrum.[52] The ubiquitous disadvantage of ^{1}H NMR, namely signal overlapping, is thereby reduced. The integrin antagonists described by *Bollinger et al.*[38] contain also one ^{31}P nucleus and are therefore suitable reporters in ^{31}P NMR based drug screening.

Here, proton-decoupled ^{31}P-1D-NMR spectra for racemic, (*R*)-thiophosphonic acid, and (*S*)-thiophosphonic acid (each 5.0 mM) respectively, with α-cyclodextrin (50 mM) were recorded. For enantiodiscrimination of the racemic thiophosphonic acid, α-cyclodextrin was used as chiral discriminating agent.[50] The signal for the (*R*)-enantiomer was then found at 51.3 ppm, whereas the corresponding (*S*)-enantiomer was detected at 51.1 ppm (Figure 10, middle and bottom). For the racemic mixture, both signals were obtained (Figure 10, top). This is due to the presence of the two enantiomers which are in fast exchange in the NMR time scale between free and bound conformations.[50]

These spectra unequivocally confirm the remarkable enantiodiscrimination properties of the used ZWIX-CSPs[43] for resolving chiral zwitterionic analytes.
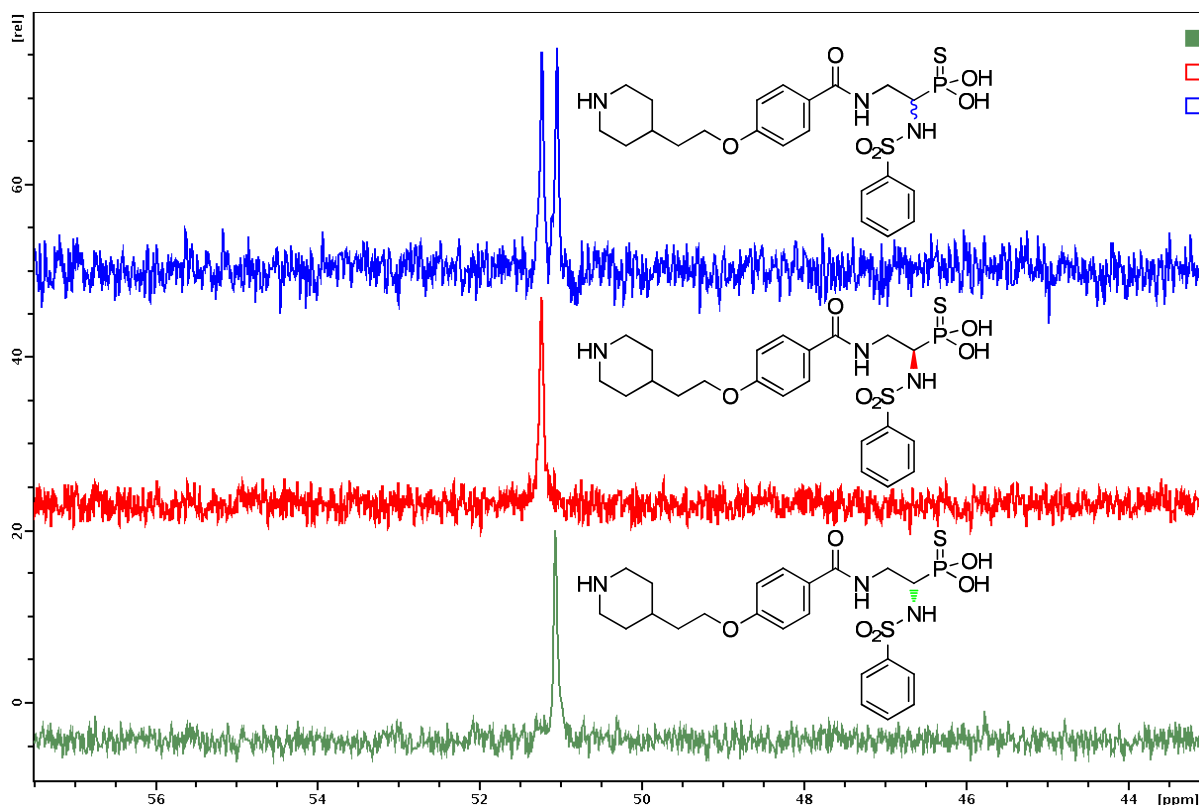
Figure 10 | Enantiomeric purity determination by means of ^{31}P NMR. ^{31}P NMR spectra recorded at 295 K on a 250 MHz *Bruker* AV spectrometer of a mixture of (top) racemic, (middle) (*R*)-thiophosphonic acid and (bottom) (*S*)-thiophosphonic acid with α-cyclodextrin 50 mM (1:10 ratio) in DMSO-d$_6$, (pH 2.5).

3.3 In vitro Inhibition of Integrin αIIbβ3

The biological *in vitro* evaluation was performed in-house at the Technische Universität München. To validate the inhibition properties of the integrin inhibitors against αIIbβ3, a competitive ELISA assay (αIIbβ3-fibrinogen assay) was performed using soluble integrin αIIbβ3 and the immobilized natural ligand fibrinogen. The amount of bound integrin was determined by specific antibodies in an enzyme-linked immunosorbent assay (enzyme: HRP horseradish peroxidase). The activity of the HRP was measured with an appropriate HRP substrate, which is converted into a colored product. The readout was the absorbance at 450 nm, from which the amount of integrin and thus the IC$_{50}$ value could be calculated. Figure 11 schematically shows the performed αIIbβ3-fibrinogen assay.[38]
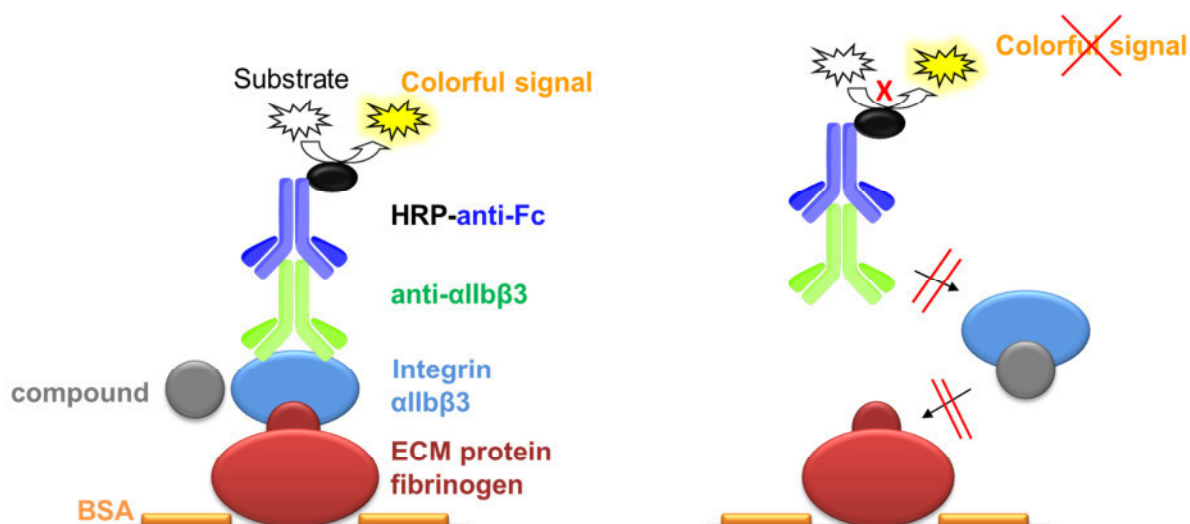
Figure 11 | Schematic representation of the αIIbβ3-fibirinogen assay. Compounds were tested for their ability to inhibit the binding of soluble integrin αIIbβ3 to the immobilized natural ligand fibrinogen (ECM protein): **(1.)** Coating the plate with fibrinogen; **(2.)** Uncoated positions are blocked with BSA; **(3.)** Incubation with the corresponding compound and soluble integrin αIIbβ3; **(4.)** Detecting antibody (anti-αIIbβ3) is added, which binds to the antigen of the αIIbβ3 integrin; **(5.)** HRP-anti-FC conjugate is added, which binds to the detecting antibody; **(6.)** Appropriate HRP substrate is added and is oxidized by HRP → colorimetric signal readout (450 nm). After each step there is a washing step.

3.4 Platelet Aggregation in Whole Blood

In Europe, the Multiplate® system is one of the most common platelet aggregometers using whole blood. It is applied for the analysis of platelet function using various agonists and is sensitive for the detection of Aspirin®, clopidogrel, prasugrel, or αIIbβ3 antagonists, e.g. tirofiban (Figure 12, top). The detection principle of the Multiplate® analyzer is based on electrical impedance. In contrast to non-thrombogenic (inactive) platelets, activated platelets can adhere to the sensor wires (silver-coated), resulting in an increase of the electrical resistance between the wires (Figure 12, at the bottom left).The change in resistance is recorded continuously and the so-called area under the curve (AUC) is used for data analysis.[53] Platelets can be stimulated by thrombin receptor-activated peptide 6 (TRAP-6) via the thrombin receptor, and various other antagonists.[53, 54]
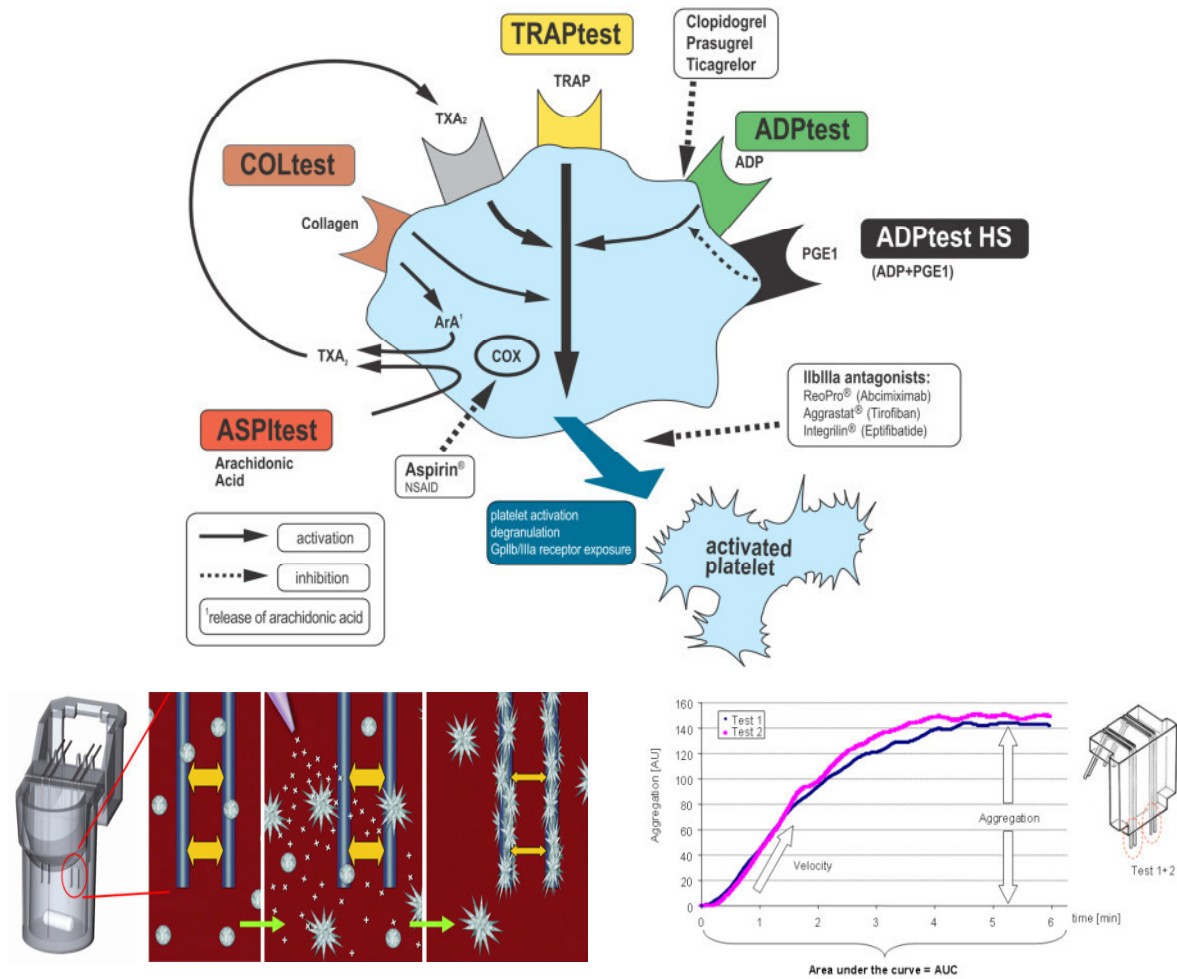
Figure 12 │ Impedance-based platelet aggregometry using the Multiplate® system. Reprinted by permission from Verum Diagnostica GmbH, München, Germany, Copyright © 2008. (top) Multiplate® tests and main platelet activation/inhibition pathways, (at the bottom left) Detection principle: impedance aggregometry, (at the bottom right) Multiplate® data analysis.

In collaboration with Dr. Mößmer, Institut für Klinische Chemie und Pathobiochemie, Klinikum rechts der Isar, München, a selection of four ligands was tested[38] using impedance-based platelet aggregometry[55, 56] in hirudin-anticoagulated TRAP-6-activated whole blood. These studies were aimed to compare the potencies of binding to isolated platelet integrin $\alpha IIb\beta 3$ (*in vitro*, IC_{50} values) with the predicted inhibitory potencies for the complex biological process of platelet aggregation in whole blood (*ex vivo*, EC_{50} values).

The assays showed that the ability of the phosphinic acid analog to inhibit *ex vivo* platelet aggregation is similar to the potency of tirofiban (Aggrastat®) whereas the inhibiting activity of the corresponding phosphonic acid compound is lower by about one order of magnitude. The phosphonic monomethylester showed intermediate efficacy. These findings correlate with the IC_{50} values measured *in vitro* (Chapter 3.3).[38]

4 RESULTS AND DISCUSSION

This chapter primarily outlines those results that have already been published in peer-reviewed journals or have been included in a manuscript draft. In order to allow straightforward reading and to avoid redundant information, the contents are only briefly summarized. For obtaining detailed information the reader is referred to the corresponding publication or manuscript draft given in the appendix.

4.1 Phosphorus-containing αIIbβ3 Integrin Antagonists

Inhibition of integrin function is a major challenge in medicinal chemistry. Tirofiban is an intravenously administered synthetic αIIbβ3 receptor antagonist drug that specifically inhibits fibrinogen-dependent platelet aggregation.[30] The carboxylic acid group in integrin ligands is essential for the coordination of the bivalent metal cation at the metal ion-dependent adhesion site (MIDAS) of all integrins.[14] It is the most conserved functionality in all integrin ligands. Recently, the first successful bioisosteric replacement of the carboxyl group with the pharmacologically favorable hydroxamic acid group has been described.[8] Based on these results, we were interested in the question if the MIDAS tolerates any other bioisosteric group and negative excess charge. Being aware that phosphinic- and phosphonic acids possess very good coordination properties for bivalent metal cations, we assumed that tirofiban analog structures with the above-mentioned motive are highly valuable compounds.

The following publication by *Bollinger et al.*[38] describes the rational design and multistep synthesis of phosphinic- and phosphonic acid analog tirofiban derivatives to gain insights into the binding modes of ligands to the MIDAS region under physiological conditions. For the biological *in vitro* and *ex vivo* evaluation of the new compounds, resolution of racemic amino phosphoric acids was required.

The phosphinic acid derivative, bearing a single negative charge, has similar activity for αIIbβ3 as compared to the known carboxylic acid derivative (1.2 nM vs. 0.81 nM). However, the phosphonic acid compound (22.7 nM), being double negatively

charged, gave a 20-fold lower activity than the phosphinic acid. Interestingly, when the phosphonic acid was converted into the monomethyl phosphonate, the compound regained activity (3.3 nM). Obviously, the additional negative charge in the phosphonic acid destabilizes ligand binding in the MIDAS region. We used modeling, docking and *ab-initio* calculations of the ligand-receptor-interactions as well as ^{31}P NMR studies on the protonation state of the phosphorus containing derivatives to support the hypothesis that the unoccupied binding site at the octahedral coordinated bivalent metal cation does not tolerate the bulky and double negatively charged phosphonic acid moiety as compared to the phosphinic acid analog. In conclusion, the results outline the requirement of low negative charge in addition to spatial demands for this replacement.

In detail, the results are presented and discussed in the following publication. (For the complete article and Supporting Information see Appendix I. Reprinted with permission from *Journal of Medicinal Chemistry*, 2012, 55, 871–882. Copyright © 2012 American Chemical Society.)

Tailoring of Integrin Ligands: Probing the Charge Capability of the Metal Ion-Dependent Adhesion Site

Markus Bollinger, Florian Manzenrieder, Roman Kolb, Alexander Bochen, Stefanie Neubauer, Luciana Marinelli, Vittorio Limongelli, Ettore Novellino, Georg Moessmer, Reinhard Pell, Wolfgang Lindner, Joseph Fanous, Amnon Hoffman, and Horst Kessler. *Journal of Medicinal Chemistry* **2012**, *55*, 871-882.
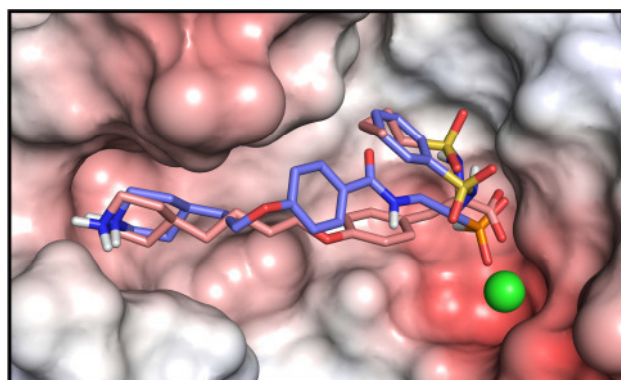
Figure 13 | Bioisosteric replacement of the carboxylic MIDAS binding motif. An overlay of the binding conformations of a phosphinic acid ligand (blue) and the drug tirofiban (pink) into the binding site of the integrin αIIbβ3. The magnesium ion is represented as a green sphere in this picture. Reprinted with permission from *Journal of Medicinal Chemistry*, 2012, 55, 871–882. Copyright © 2012 American Chemical Society.

4.2 Development of a Novel ^{18}F-labeled αIIbβ3 Integrin Antagonist

This project was a collaboration with Prof. Dr. Wester and Dr. Yousefi from the Department of Pharmaceutical Radiochemistry, Technische Universität München. A manuscript entitled "Direct One-Step ^{18}F-Labeling of a New Highly Active αIIbβ3 Integrin Antagonist via Nucleophilic Aromatic Substitution" by **Markus Bollinger**, Behrooz H. Yousefi, Alexander Bochen, Iina Laitinen, Tobias Petzold, Markus Schwaiger, Horst Kessler, and Hans-Jürgen Wester is drafted (for the complete manuscript and Supporting Information see Appendix II).

The αIIbβ3 receptor is the most abundant integrin on the surface of platelets, and therefore plays a key role in the process of thrombus formation. Thus, αIIbβ3 PET tracers have been the subject of increasing interest over recent years for preclinical and clinical imaging studies. In this work a highly active ^{18}F-labeled αIIbβ3 integrin antagonist was synthesized and evaluated as molecular imaging agent of activated platelets. To gain a potential radiotracer, a novel no-carrier-added (n.c.a.) direct nucleophilic radiofluorination method was developed to label the unprotected *para*-nitro-precursor **4** in presence of protic functions (Figure 14, green labels).

Briefly, three synthesis approaches were conducted. First, a fully protected precursor was applied to obtain the desired ^{18}F-labeled radiotracer. However, we could not detect the product. Consequently, we have not pursued this strategy. Instead, we tried the radiosynthesis with the *N*-Boc protected precursor (free carboxylic acid). However, although the synthesis of the labeled intermediate worked straightforward, the Boc-deprotection in the last step was inconvenient and therefore this approach was not applicable. Finally, we ended up with the above-mentioned synthetic pathway via direct fluorination of the unprotected *para*-nitro-precursor **4** with a radiochemical yield of 19% (Figure 14).

The novel radiotracer (^{19}F reference compound **5**) was biologically evaluated. Antagonist **5** exhibits *in vitro* and *ex vivo* affinity in the low nanomolar range (IC$_{50}$ 0.99 nM; EC$_{50}$ 16.8 nM) combined with suitable lipophilicity and plasma protein binding, high *in vivo* stability and fast washout from blood circulation. In addition, biodistribution results showed the tracer excretes fast via the gastrointestinal system. These initial results encouraged us to carry out further investigations. Ongoing animal studies are

planned and the applicability of [^{18}F]**5** as PET tracer for the detection of deep vein thrombosis in mouse models is in progress.
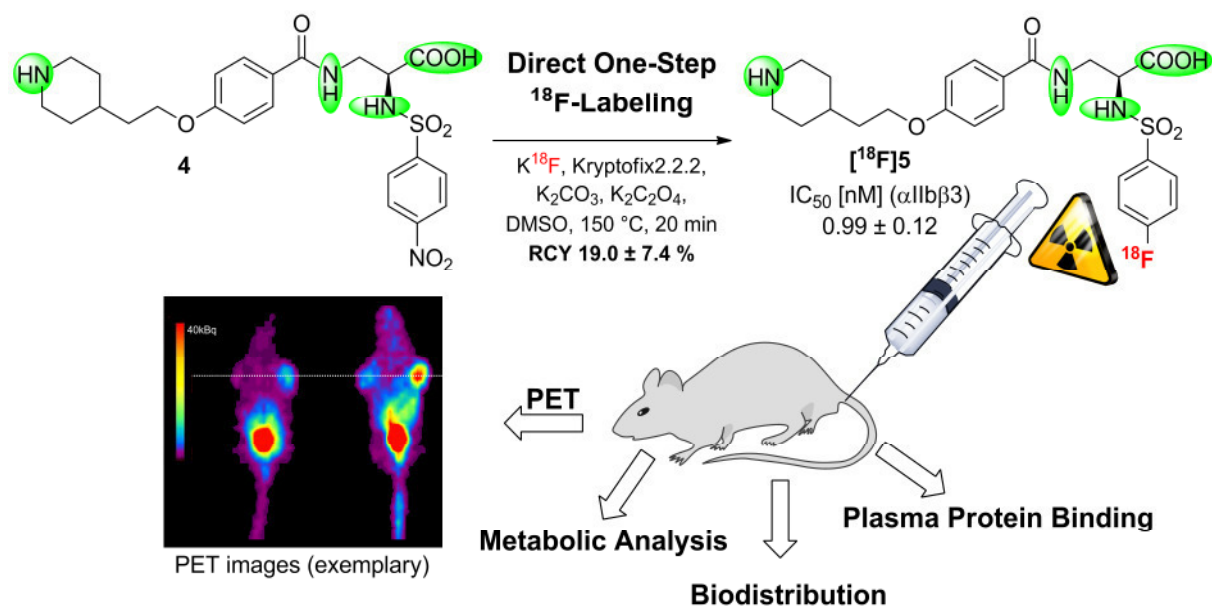
Figure 14 │ Development of a novel ^{18}F-labeled αIIbβ3 radiotracer. RCY = radiochemical yield.

4.3 Cyclodimerization by the Cu^I-mediated Azide-Alkyne Reaction

The following project was performed in cooperation with Dr. Jagasia from the group of Prof. M. G. Finn at the Scripps Research Institute (La Jolla, CA, USA). The results from this cooperation have been published as cited below.[10] For detailed characterization of the synthesized peptide libraries, please refer to the experimental section and the Supporting Information of the publication (Appendix III).

Peptide Cyclization and Cyclodimerization by Cu^I-Mediated Azide-Alkyne Cycloaddition.
Reshma Jagasia, Justin M. Holub, **Markus Bollinger**, Kent Kirshenbaum, and M. G. Finn. *The Journal of Organic Chemistry* **2009**, *74*, 2964-2974.

The cyclization of peptides is commonly applied when determining bioactive conformations and generating lead structures in drug discovery.[57, 58] Cyclic peptides and related structures are of sustained interest as biologically active compounds, in gen-

eral because of their ability to display protein-like epitopes with restricted conformational flexibility. Cyclic peptides play an important role in drug development research and material sciences. The conformational flexibility relative to their linear (or not fixed) analogs is drastically decreased, which can lead to increased binding affinity (Figure 15, matched case). However, receptor affinity can be lost if the peptide is not constrained in its proper, biologically active conformation (Figure 15, mismatched case). On the other hand, cyclized peptides may offer enhanced bioavailability, increased metabolic stability against proteolytic degradation, and better receptor selectivity (Figure 15).[57, 59] However, the synthesis of large cyclic peptides is still a great challenge. Common strategies for peptide cyclization are the intra-molecular linkage via amide bonds, esters, disulfide bridges using the cysteine side chain moieties, or olefin metathesis.[60] So far, a major disadvantage of almost all cyclization strategies, either performed in solution or on solid phase, is that they require particular attention to side chain protecting groups. The reactive motifs for cyclization must be synthetically incorporated into the peptide and deprotected selectively at the time of cyclization. An alternative approach is described by *Finn* and *Sharpless,*[9, 61, 62] in which the peptide is cyclized by the 1,3-dipolar [2+3] copper(I)-catalyzed regioselective (1,4-regioisomer) alkyne-azide cycloaddition reaction. This high yielding reaction provides fast access to an enormous variety of cyclic peptides and is amenable to many reaction conditions. The azide and alkyne units can be incorporated into the peptide sequences during solid phase peptide synthesis (SPPS) without special protecting groups. Both functionalities remain inert until exposed to Cu(I) catalyst.
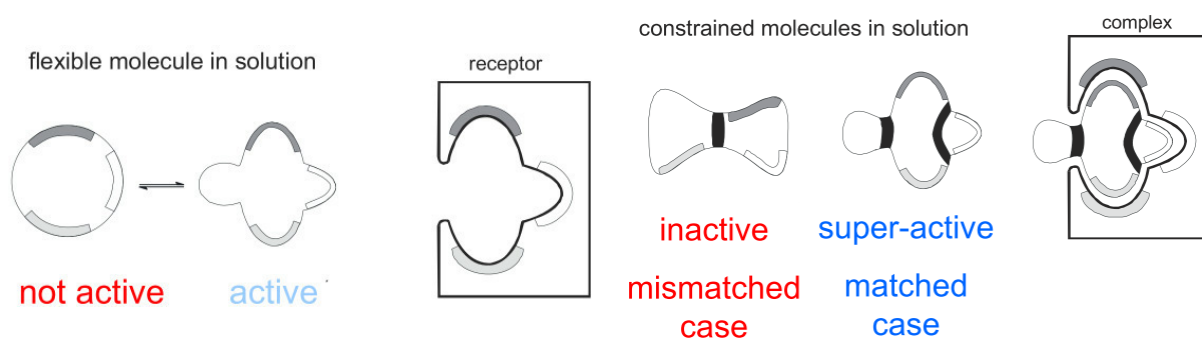
Figure 15 | Comparison of a flexible and a fixed molecule in solution.[63]

Recently, *Punna et al.*[9] reported that on-resin cyclization of a peptide via the copper(I)-catalyzed azide-alkyne cycloaddition (CuAAC) reaction did not yield the desired cyclic monomer but rather only the head-to-tail cyclic dimer. To elucidate the scope and robustness of this peptide cyclodimerization phenomenon, an extensive study was conducted to understand the effects of varying peptide sequence, peptide length, resin type, solvent-dependent effects, reagent concentrations, proximity of the alkyne to the resin, as well as the need for peptide side chains and secondary amide bonds.

For this study, solid phase peptide synthesis (SPPS), developed by *Merrifield*,[64] was applied for the synthesis of the linear peptides, using rink amide MBHA (4-methylbenzhydrylamine) resin with orthogonal Fmoc/*tert*butyl protecting groups (Fmoc-SPPS).[65-68] This technique facilitates the stepwise assembling of the peptide by coupling temporarily *N*-Fmoc-protected amino acids to each other. The deprotection of the base-labile Fmoc group under mild conditions (20% piperidine in NMP) is orthogonal to the acid-labile permanent protection groups of the side chains and to the resin-anchorage. The use of a great excess of coupling reagents leads to an almost quantitative coupling reaction (for more details see Supporting Information[10]).

To enable the cyclization via click chemistry,[62] the alkyne was introduced as a propargylglycine unit, located near the resin-bound *C*-terminus, while the azide group was incorporated as 5-azidopentanoic acid at the *N*-terminus. The optimized on-resin copper(I)-catalyzed [2+3] azide-alkyne cycloaddition reaction was carried out in a mixture of 20% DMSO in MeCN. Finally, deprotection of the acid-labile side-chain protecting groups (Pbf and Trt), as well as cleavage from the resin, was performed with 95% trifluoroacetic acid (TFA), 2.5% triiospropylsilane (TIPS) and 2.5% water yielding the cyclic dimeric **p2/NC peptide** as a final product (Scheme 1, further examples are described in the publication[10]).

The careful analysis of the comprehensive peptide libraries concluded that the cyclodimerization process is independent of peptide sequence, sensitive to the proximity of the alkyne to the resin, sensitive to solvent composition, facile for α- and β-peptides but not for γ-peptides, and inhibited by the inclusion of tertiary amide linkages. For peptides with less than six residues, the corresponding cyclic monomers were predominantly obtained. These results suggest that cyclodimerization depends on the ability of the peptides to form inter-chain hydrogen bonds (Figure 3 and Fig-

ure 18). Therefore, cyclodimerization is solvent dependent, as solvent has a strong influence on the formation of such hydrogen bonds. This novel class of constrained cyclic dimeric peptides offers potential as promising peptide drug candidates due to the asset of two identical binding sites.
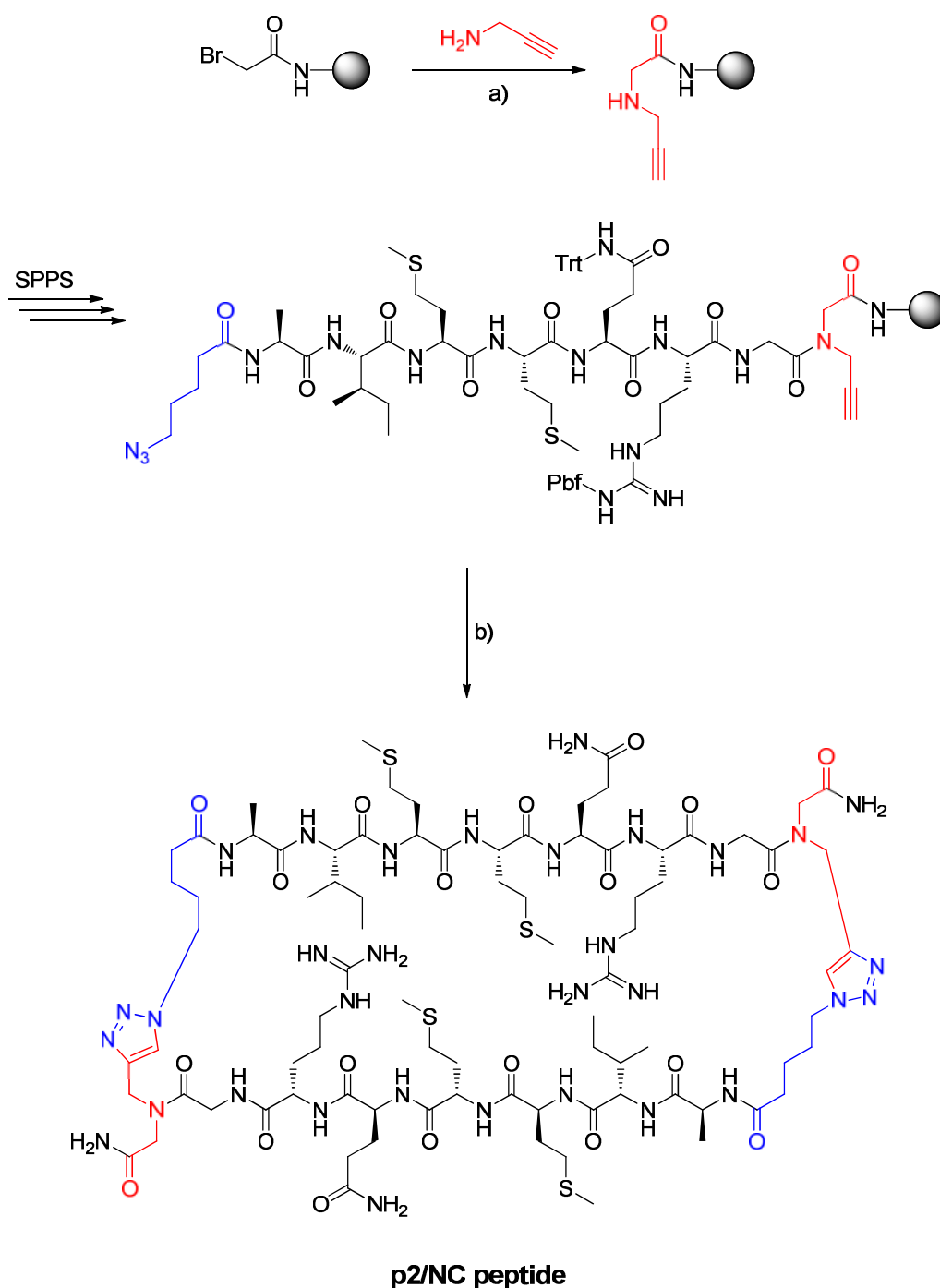
Scheme 1 | Peptide cyclodimerization by azide-alkyne cycloaddition. a) DIEA, DMF, RT, 16 h b) 1. 5 mM CuI, 2,6-lutidine, MeCN/DMSO (4:1), N_2, atm, RT, 16 h; 2. 95% TFA, 2.5% TIPS, 2.5% H_2O, atm, RT, 3 h.

5 SUMMARY

The scope of this work was the design and synthesis of highly active antagonists for the αIIbβ3 integrin receptor, based on a non-peptidic selective αIIbβ3 integrin ligand, developed by *Duggan et al.*(Figure 16).[69]
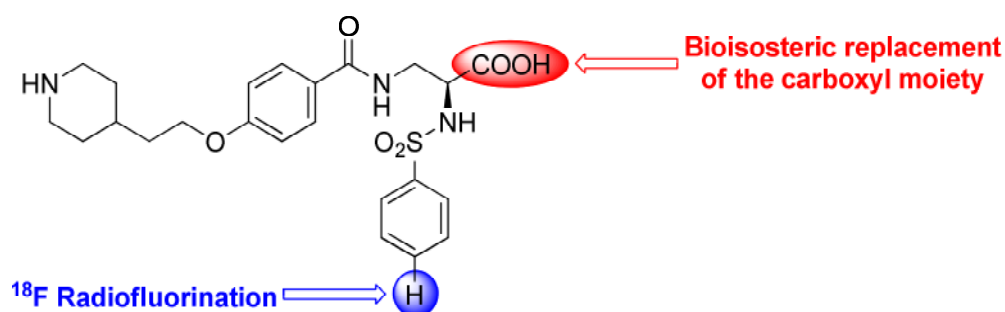
Figure 16 | Tirofiban analog and αIIbβ3 integrin antagonist, developed by *Duggan et al.*.[69] The red and blue spheres indicate the different moieties, which were modified in this thesis.

Integrins constitute an important class of heterodimeric cell-adhesion receptors that are involved in many severe pathological processes. The research on integrins and their functions in various biological and pathological processes therefore is one of the most interesting topics in the field of medicinal chemistry. Progress in this sector can lead to enormous improvements in cancer diagnosis and therapy, implant materials, antithrombotic therapies and many other areas of medicine.

Following a bioisosteric replacement approach, the ubiquitous carboxylic acid pharmacophore in integrin ligands has been successfully substituted by phosphorus-containing moieties for the first time. The introduction of a phosphinic acid residue and phosphonate monomethylesters, respectively, gave αIIbβ3 integrin inhibitors with *in vitro* and *ex vivo* activities in the low nanomolar range. In contrast, the replacement by phosphonic acid or thiophosphonic acid resulted in a strong decrease of binding affinity. These relevant observations will stimulate and guide the design of new generations of novel integrin targeting compounds with improved pharmacophoric properties.
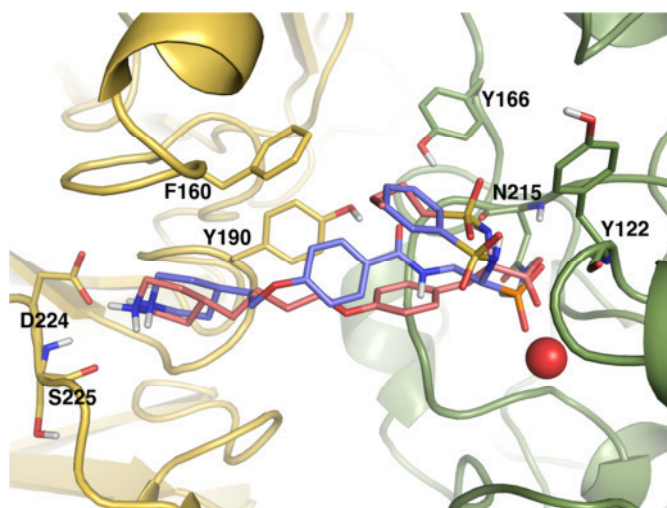
Figure 17 │ Superimposition of the X-ray binding conformation of tirofiban (pink) and phosphinic acid (blue) derived from docking calculations. The αIIb domain is displayed as yellow cartoon, while the β3 subunit is in green. The magnesium ion is represented as red sphere. For the sake of clarity only the polar hydrogens are displayed. Four selected ligands with different activities towards αIIbβ3 are shown on the right.[38]
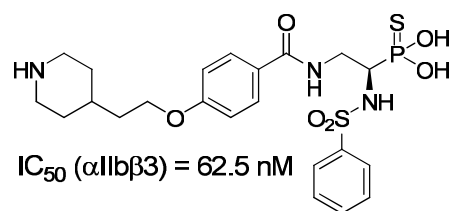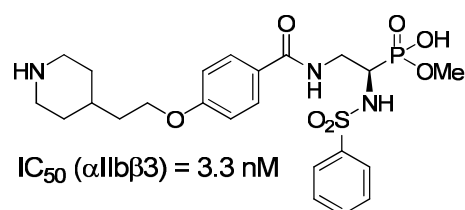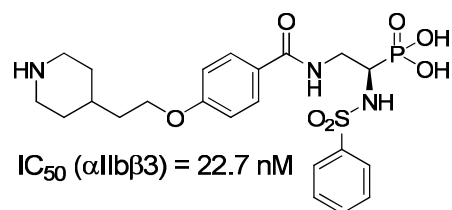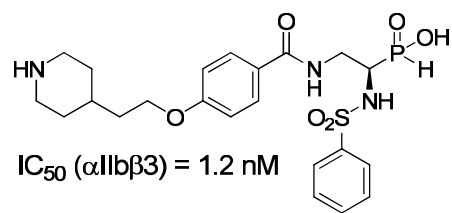
The association of the αIIbβ3 integrin with platelets and thrombus formation has been shown in chapter 2.[5] Therefore, by imaging the αIIbβ3 receptor with a positron emission tomography (PET) tracer, valuable information to diagnose thrombosis and embolism should be obtained. In order to enable Duggan's ligand[69] (Figure 16, blue sphere) for the application in PET-screening, a direct nucleophilic substitution synthesis approach was developed. The introduction of a nitro group in the *para*-position of the aromatic moiety allowed ^{18}F radiofluorination. In conclusion, the first successful direct ^{18}F-labeling procedure in the presence of protic functional groups is reported in this thesis. So far, temporary protecting groups were required for these functionalities, which had to be finally cleaved. The preliminary biological evaluation results indicate that the novel radiotracer is a potent candidate for PET imaging of activated αIIbβ3 integrin. Additional *in vitro* and *in vivo* studies are currently ongoing to further investigate the applicability for the detection of deep vein thrombosis.

The last project (not related to the integrin field) was to evaluate the mechanism of a on resin peptide cyclodimerization phenomenon originally described by *Punna et al.*.[9] For this purpose, different libraries of head-to-tail cyclized peptides were created. Via systematic modifications in the linear peptide sequence and careful evaluation of the different parameters, significant new insights into the mechanism of this cyclodimerization process were obtained (Figure 18). The key element for the dimerization of two linear peptide sequences is the ability of the peptides to form inter-chain hydrogen bonds. This novel cycloaddition reaction opens new routes for the synthesis of cyclic macromolecules.
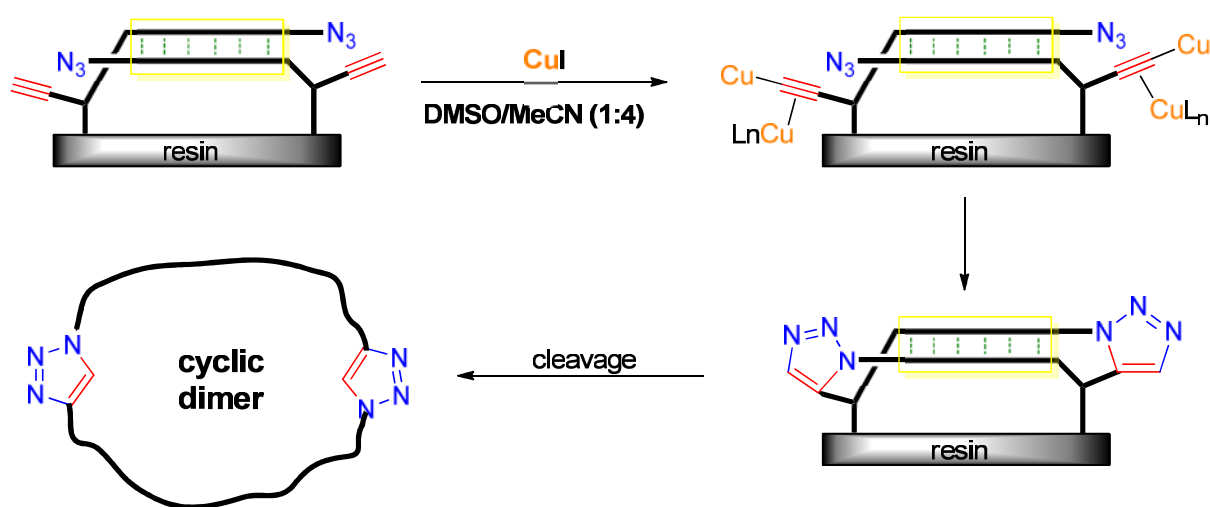
Figure 18 | Schematic illustration of the proposed mechanism for on-resin cyclodimerization via the copper(I)-catalyzed azide-alkyne cycloaddition (CuAAC) reaction. Due to the head-to-tail hydrogen bonding patterns (dashed green lines) the reacting interstrand alkyne and azide moieties are in close proximity to each other and can react.

6 REFERENCES

(1) Aspirin®. *http://www.aspirin.de/de/index.php*.

(2) Schrör, K. Aspirin and Platelets: The Antiplatelet Action of Aspirin and Its Role in Thrombosis Treatment and Prophylaxis. *Semin. Thromb. Hemost.* **1997,** *23*, 349-356.

(3) Schrör, K. 100 Jahre erfolgreiche Arzneimittelforschung: Geschichte von Acetyl-salicylsäure. *Pharm. Unserer Zeit* **2009,** *38*, 306-313.

(4) Miner, J.; Hoffhines, A. The Discovery of Aspirin's Antithrombotic Effects. *Tex. Heart Inst. J.* **2007,** *34*, 179-186.

(5) Bhatt, D. L.; Topol, E. J. Scientific and Therapeutic Advances in Antiplatelet Therapy. *Nat. Rev. Drug Discovery* **2003,** *2*, 15-28.

(6) Madan, M.; Berkowitz, S. D.; Tcheng, J. E. Glycoprotein IIb/IIIa Integrin Blockade. *Circulation* **1998,** *98*, 2629-2635.

(7) Hato, T.; Ginsberg, M. H.; Shattil, S. J. Integrin $\alpha_{IIb}\beta_3$. In *Platelets*, Michelson, A., Ed. Academic/Elsevier Science, New York: **2002**; pp 105-116.

(8) Heckmann, D.; Laufer, B.; Marinelli, L.; Limongelli, V.; Novellino, E.; Zahn, G.; Stragies, R.; Kessler, H. Breaking the Dogma of the Metal-Coordinating Carboxylate Group in Integrin Ligands: Introducing Hydroxamic Acids to the MIDAS To Tune Potency and Selectivity. *Angew. Chem., Int. Ed.* **2009,** *48*, 4436-4440.

(9) Punna, S.; Kuzelka, J.; Wang, Q.; Finn, M. G. Head-to-Tail Peptide Cyclodimerization by Copper-Catalyzed Azide-Alkyne Cycloaddition. *Angew. Chem., Int. Ed.* **2005,** *44*, 2215-2220.

(10) Jagasia, R.; Holub, J. M.; Bollinger, M.; Kirshenbaum, K.; Finn, M. G. Peptide Cyclization and Cyclodimerization by Cu^I-Mediated Azide-Alkyne Cycloaddition. *J. Org. Chem.* **2009,** *74*, 2964-2974.

(11) Arnaout, M. A.; Mahalingam, B.; Xiong, J. P. Integrin Structure, Allostery, and Bidirectional Signaling. *Annu. Rev. Cell Dev. Biol.* **2005,** *21*, 381-410.

(12) Hynes, R. O. Integrins: Bidirectional, Allosteric Signaling Machines. *Cell* **2002,** *110*, 673-687.

(13) Whittaker, C. A.; Hynes, R. O. Distribution and Evolution of von Willebrand/Integrin A Domains: Widely Dispersed Domains with Roles in Cell Adhesion and Elsewhere. *Mol. Biol. Cell* **2002,** *13*, 3369-3387.

(14) Humphries, M. J. Integrin Structure. *Biochem. Soc. Trans.* **2000,** *28*, 311-339.

(15) Meredith, J. E., Jr.; Fazeli, B.; Schwartz, M. A. The Extracellular Matrix as a Cell Survival Factor. *Mol. Biol. Cell* **1993,** *4*, 953-961.

(16) Moser, M.; Legate, K. R.; Zent, R.; Fässler, R. The Tail of Integrins, Talin, and Kindlins. *Science* **2009,** *324*, 895-899.

(17) Giancotti, F. G.; Ruoslahti, E. Integrin Signaling. *Science* **1999,** *285*, 1028-1032.

(18) Mousa, S. A. Anti-integrin as novel drug-discovery targets: potential therapeutic and diagnostic implications. *Curr. Opin. Chem. Biol.* **2002,** *6*, 534-541.

(19) Cox, D.; Brennan, M.; Moran, N. Integrins as therapeutic targets: lessons and opportunities. *Nat. Rev. Drug Discovery* **2010,** *9*, 804-820.

(20) Goodman, S. L.; Picard, M. Integrins as therapeutic targets. *Trends Pharmacol. Sci.* **2012,** *33*, 405-412.

(21) Tamkun, J. W.; DeSimone, D. W.; Fonda, D.; Patel, R. S.; Buck, C.; Horwitz, A. F.; Hynes, R. O. Structure of Integrin, a Glycoprotein Involved in the Transmembrane Linkage between Fibronectin and Actin. *Cell* **1986,** *46*, 271-282.

(22) Pierschbacher, M. D.; Ruoslahti, E. Cell attachment activity of fibronectin can be duplicated by small synthetic fragments of the molecule. *Nature* **1984,** *309*, 30-33.

(23) Barczyk, M.; Carracedo, S.; Gullberg, D. Integrins. *Cell Tissue Res.* **2010,** *339*, 269-280.

(24) Meyer, A.; Auernheimer, J.; Modlinger, A.; Kessler, H. Targeting RGD Recognizing Integrins: Drug Development, Biomaterial Research, Tumor Imaging and Targeting. *Curr. Pharm. Des.* **2006,** *12*, 2723-2747.

(25) Dechantsreiter, M. A.; Planker, E.; Mathä, B.; Lohof, E.; Hölzemann, G.; Jonczyk, A.; Goodman, S. L.; Kessler, H. *N*-Methylated Cyclic RGD Peptides as Highly Active and Selective $\alpha_V\beta_3$ Integrin Antagonists. *J. Med. Chem.* **1999,** *42*, 3033-3040.

(26) Mas-Moruno, C.; Rechenmacher, F.; Kessler, H. Cilengitide: The First Anti-Angiogenic Small Molecule Drug Candidate. Design, Synthesis and Clinical Evaluation. *Anti-Cancer Agents Med. Chem.* **2011,** *10*, 753-768.

(27) Hoefling, M.; Kessler, H.; Gottschalk, K. E. The Transmembrane Structure of Integrin $\alpha IIb\beta 3$: Significance for Signal Transduction. *Angew. Chem., Int. Ed.* **2009,** *48*, 6590-6593.

(28) Humphries, J. D.; Byron, A.; Humphries, M. J. Integrin ligands at a glance. *J. Cell Sci.* **2006,** *119*, 3901-3903.

(29) Shimaoka, M.; Springer, T. A. Therapeutic Antagonists and Conformational Regulation of Integrin Function. *Nat. Rev. Drug Discovery* **2003,** *2*, 703-716.

(30) Hartman, G. D.; Egbertson, M. S.; Halczenko, W.; Laswell, W. L.; Duggan, M. E.; Smith, R. L.; Naylor, A. M.; Manno, P. D.; Lynch, R. J.; Zhang, G.; Chang, C. T.-C.; Gould, R. J. Non-Peptide Fibrinogen Receptor Antagonists. 1. Discovery and Design of Exosite Inhibitors. *J. Med. Chem.* **1992,** *35,* 4640-4642.

(31) Tello-Montoliu, A.; Jover, E.; Rivera, J.; Valdés, M.; Angiolillo, D. J.; Marín, F. New Perspectives in Antiplatelet Therapy. *Curr. Med. Chem.* **2012,** *19,* 406-427.

(32) Topol, E. J.; Moliterno, D. J.; Herrmann, H. C.; Powers, E. R.; Grines, C. L.; Cohen, D. J.; Cohen, E. A.; Bertrand, M.; Neumann, F. J.; Stone, G. W.; DiBattiste, P. M.; Demopoulos, L. Comparison of two platelet glycoprotein IIb/IIIa inhibitors, tirofiban and abciximab, for the prevention of ischemic events with percutaneous coronary revascularization. *N. Engl. J. Med.* **2001,** *344,* 1888-1894.

(33) Cannon, C. P.; Weintraub, W. S.; Demopoulos, L. A.; Vicari, R.; Frey, M. J.; Lakkis, N.; Neumann, F. J.; Robertson, D. H.; DeLucca, P. T.; DiBattiste, P. M.; Gibson, C. M.; Braunwald, E. Comparison of early invasive and conservative strategies in patients with unstable coronary syndromes treated with the glycoprotein IIb/IIIa inhibitor tirofiban. *N. Engl. J. Med.* **2001,** *344,* 1879-1887.

(34) Xiao, T.; Takagi, J.; Coller, B. S.; Wang, J. H.; Springer, T. A. Structural basis for allostery in integrins and binding to fibrinogen-mimetic therapeutics. *Nature* **2004,** *432,* 59-67.

(35) Mould, A. P.; Humphries, M. J. Cell biology: Adhesion articulated. *Nature* **2004,** *432,* 27-28.

(36) Shattil, S. J.; Kim, C.; Ginsberg, M. H. The final steps of integrin activation: the end game. *Nat. Rev. Mol. Cell Biol.* **2010,** *11,* 288-300.

(37) Gottschalk, K. E.; Kessler, H. The Structures of Integrins and Integrin-Ligand Complexes: Implications for Drug Design and Signal Transduction. *Angew. Chem., Int. Ed.* **2002,** *41,* 3767-3774.

(38) Bollinger, M.; Manzenrieder, F.; Kolb, R.; Bochen, A.; Neubauer, S.; Marinelli, L.; Limongelli, V.; Novellino, E.; Moessmer, G.; Pell, R.; Lindner, W.; Fanous, J.; Hoffman, A.; Kessler, H. Tailoring of Integrin Ligands: Probing the Charge Capability of the Metal Ion-Dependent Adhesion Site. *J. Med. Chem.* **2012,** *55,* 871-882.

(39) Jung, S. M.; Moroi, M.; Soejima, K.; Nakagaki, T.; Miura, Y.; Berndt, M. C.; Gardiner, E. E.; Howes, J.-M.; Pugh, N.; Bihan, D.; Watson, S. P.; Farndale, R. W. Constitutive Dimerization of Glycoprotein VI (GPVI) in Resting Platelets Is Essential for Binding to Collagen and Activation in Flowing Blood. *J. Biol. Chem.* **2012,** *287,* 30000-30013.

(40) Wagner, C. L.; Mascelli, M. A.; Neblock, D. S.; Weisman, H. F.; Coller, B. S.; Jordan, R. E. Analysis of GPIIb/IIIa Receptor Number by Quantification of 7E3 Binding to Human Platelets. *Blood* **1996,** *88,* 907-914.

(41) Andersson, S.; Allenmark, S. G. Preparative chiral chromatographic resolution of enantiomers in drug discovery. *J. Biochem. Biophys. Methods* **2002,** *54,* 11-23.

(42) Lämmerhofer, M. Chiral recognition by enantioselective liquid chromatography: Mechanisms and modern chiral stationary phases. *J. Chromatogr., A* **2010,** *1217,* 814-856.

(43) Hoffmann, C. V.; Pell, R.; Lämmerhofer, M.; Lindner, W. Synergistic Effects on Enantioselectivity of Zwitterionic Chiral Stationary Phases for Separations of Chiral Acids, Bases, and Amino Acids by HPLC. *Anal. Chem. (Washington, DC, U. S.)* **2008,** *80,* 8780-8789.

(44) Hoffmann, C. V.; Reischl, R.; Maier, N. M.; Lämmerhofer, M.; Lindner, W. Stationary phase-related investigations of quinine-based zwitterionic chiral stationary phases operated in anion-, cation-, and zwitterion-exchange modes. *J. Chromatogr., A* **2009,** *1216,* 1147-1156.

(45) Lämmerhofer, M.; Lindner, W. Quinine and quinidine derivatives as chiral selectors I. Brush type chiral stationary phases for high-performance liquid chromatography based on cinchonan carbamates and their application as chiral anion exchangers. *J. Chromatogr., A* **1996,** *741,* 33-48.

(46) Maier, N. M.; Schefzick, S.; Lombardo, G. M.; Feliz, M.; Rissanen, K.; Lindner, W.; Lipkowitz, K. B. Elucidation of the Chiral Recognition Mechanism of Cinchona Alkaloid Carbamate-type Receptors for 3,5-Dinitrobenzoyl Amino Acids. *J. Am. Chem. Soc.* **2002,** *124,* 8611-8629.

(47) Mandl, A.; Nicoletti, L.; Lämmerhofer, M.; Lindner, W. Quinine versus carbamoylated quinine-based chiral anion exchangers. A comparison regarding enantioselectivity for N-protected amino acids and other chiral acids. *J. Chromatogr., A* **1999,** *858,* 1-11.

(48) Zarbl, E.; Lämmerhofer, M.; Hammerschmidt, F.; Wuggenig, F.; Hanbauer, M.; Maier, N. M.; Sajovic, L.; Lindner, W. Direct liquid chromatographic enantioseparation of chiral α- and β-aminophosphonic acids employing quinine-derived chiral anion exchangers: determination of enantiomeric excess and verification of absolute configuration. *Anal. Chim. Acta* **2000,** *404,* 169-177.

(49) Lämmerhofer, M.; Hebenstreit, D.; Gavioli, E.; Lindner, W.; Mucha, A.; Kafarski, P.; Wieczorek, P. High-performance liquid chromatographic enantiomer separation and determination of absolute configurations of phosphinic acid analogues of dipeptides and their α-aminophosphinic acid precursors. *Tetrahedron: Asymmetry* **2003,** *14,* 2557-2565.

(50) Rudzinska, E.; Dziedziola, G.; Berlicki, L.; Kafarski, P. Enantiodifferentiation of α-Hydroxyalkanephosphonic Acids in ^{31}P NMR with Application of α-Cyclodextrin as Chiral Discriminating Agent. *Chirality* **2010,** *22,* 63-68.

(51) Manzenrieder, F.; Frank, A. O.; Kessler, H. Phosphorus NMR Spectroscopy as a Versatile Tool for Compound Library Screening. *Angew. Chem., Int. Ed.* **2008,** *47,* 2608-2611.

(52) Manzenrieder, F.; Frank, A. O.; Huber, T.; Dorner-Ciossek, C.; Kessler, H. Synthesis and biological evaluation of phosphino dipeptide isostere inhibitor of human β-secretase (BACE1). *Bioorg. Med. Chem.* **2007,** *15*, 4136-4143.

(53) Multiplate®. *http://www.multiplate.net/en/index.php*.

(54) Weber, M.; Gerdsen, F.; Gutensohn, K.; Schoder, V.; Eifrig, B.; Hossfeld, D. K. Enhanced platelet aggregation with TRAP-6 and collagen in platelet aggregometry in patients with venous thromboembolism. *Thromb. Res.* **2002,** *107*, 325-328.

(55) Tóth, O.; Calatzis, A.; Penz, S.; Losonczy, H.; Siess, W. Multiple electrode aggregometry: A new device to measure platelet aggregation in whole blood. *Thromb. Haemostasis* **2006,** *96*, 781-788.

(56) Halimeh, S.; de Angelis, G.; Sander, A.; Edelbusch, C.; Rott, H.; Thedieck, S.; Mesters, R.; Schlegel, N.; Nowak-Göttl, U. Multiplate® Whole Blood Impedance Point of Care Aggregometry: Preliminary Reference Values in Healthy Infants, Children and Adolescents. *Klin. Padiatr.* **2010,** *222*, 158-163.

(57) Kessler, H. Conformation and Biological Activity of Cyclic Peptides. *Angew. Chem., Int. Ed.* **1982,** *21*, 512-523.

(58) Haubner, R.; Finsinger, D.; Kessler, H. Stereoisomeric Peptide Libraries and Peptidomimetics for Designing Selective Inhibitors of the $\alpha_v\beta_3$ Integrin for a New Cancer Therapy. *Angew. Chem., Int. Ed.* **1997,** *36*, 1374-1389.

(59) Biron, E.; Chatterjee, J.; Ovadia, O.; Langenegger, D.; Brueggen, J.; Hoyer, D.; Schmid, H. A.; Jelinek, R.; Gilon, C.; Hoffman, A.; Kessler, H. Improving Oral Bioavailability of Peptides by Multiple N-Methylation: Somatostatin Analogues. *Angew. Chem., Int. Ed.* **2008,** *47*, 2595-2599.

(60) Berezowska, I.; Chung, N. N.; Lemieux, C.; Wilkes, B. C.; Schiller, P. W. Dicarba Analogues of the Cyclic Enkephalin Peptides H-Tyr-*c*[D-Cys-Gly-Phe-D(or L)-Cys]NH$_2$ Retain High Opioid Activity. *J. Med. Chem.* **2007,** *50*, 1414-1417.

(61) Kolb, H. C.; Finn, M. G.; Sharpless, K. B. Click Chemistry: Diverse Chemical Function from a Few Good Reactions. *Angew. Chem., Int. Ed.* **2001,** *40*, 2004-2021.

(62) Rostovtsev, V. V.; Green, L. G.; Fokin, V. V.; Sharpless, K. B. A Stepwise Huisgen Cycloaddition Process: Copper(I)-Catalyzed Regioselective "Ligation" of Azides and Terminal Alkynes. *Angew. Chem., Int. Ed.* **2002,** *41*, 2596-2599.

(63) Laufer, B. Synthesis of highly active and selective peptides and peptidomimetics. Ph. D. Thesis, Technische Universität München, München, **2009**.

(64) Merrifield, R. B. Solid Phase Peptide Synthesis. I. The Synthesis of a Tetrapeptide. *J. Am. Chem. Soc.* **1963,** *85*, 2149-2154.

(65) Carpino, L. A.; Han, G. Y. The 9-Fluorenylmethoxycarbonyl Amino-Protecting Group. *J. Org. Chem.* **1972,** *37*, 3404-3409.

(66) Carpino, L. A.; Sadat-Aalaee, D.; Chao, H. G.; DeSelms, R. H. ((9-Fluorenylmethyl)oxy)carbonyl (FMOC) Amino Acid Fluorides. Convenient New Peptide Coupling Reagents Applicable to the FMOC/*tert*-Butyl Strategy for Solution and Solid-Phase Syntheses. *J. Am. Chem. Soc.* **1990,** *112*, 9651-9652.

(67) Fields, G. B.; Noble, R. L. Solid phase peptide synthesis utilizing 9-fluorenylmethoxycarbonyl amino acids. *Int. J. Pept. Prot. Res.* **1990,** *35*, 161-214.

(68) Carpino, L. A. 1-Hydroxy-7-azabenzotriazole. An Efficient Peptide Coupling Additive. *J. Am. Chem. Soc.* **1993,** *115*, 4397-4398.

(69) Duggan, M. E.; Duong, L. T.; Fisher, J. E.; Hamill, T. G.; Hoffman, W. F.; Huff, J. R.; Ihle, N. C.; Leu, C. T.; Nagy, R. M.; Perkins, J. J.; Rodan, S. B.; Wesolowski, G.; Whitman, D. B.; Zartman, A. E.; Rodan, G. A.; Hartman, G. D. Nonpeptide $\alpha_v\beta_3$ Antagonists. 1. Transformation of a Potent, Integrin-Selective $\alpha_{IIb}\beta_3$ Antagonist into a Potent $\alpha_v\beta_3$ Antagonist. *J. Med. Chem.* **2000,** *43*, 3736-3745.

7 APPENDIX

7.1 Appendix I: Tailoring of Integrin Ligands

Tailoring of Integrin Ligands: Probing the Charge Capability of the Metal Ion-Dependent Adhesion Site.
Journal of Medicinal Chemistry **2012**, *55*, 871-882. Reprinted with permission from *Journal of Medicinal Chemistry*, 2012, *55*, 871–882. Copyright © 2012 American Chemical Society.

7.2 Appendix II: Development of a Novel αIIbβ3 Radiotracer

Direct One-Step ^{18}F-Labeling of a New Highly Active αIIbβ3 Integrin Antagonist via Nucleophilic Aromatic Substitution.
Manuscript, October, **2012.**

7.3 Appendix III: Peptide Cyclization and Cyclodimerization

Peptide Cyclization and Cyclodimerization by Cu^{I}-Mediated Azide-Alkyne Cycloaddition.
The Journal of Organic Chemistry **2009**, *74*, 2964-2974. Reprinted with permission from *The Journal of Organic Chemistry*, 2009, 74 (8), 2964–2974. Copyright © 2009 American Chemical Society.

APPENDIX I

Tailoring of Integrin Ligands: Probing the Charge Capability of the Metal Ion-Dependent Adhesion Site

Markus Bollinger,[†] Florian Manzenrieder,[†] Roman Kolb,[†] Alexander Bochen,[†] Stefanie Neubauer,[†] Luciana Marinelli,[‡] Vittorio Limongelli,[‡] Ettore Novellino,[‡] Georg Moessmer,[§] Reinhard Pell,[||] Wolfgang Lindner,[||] Joseph Fanous,[⊥] Amnon Hoffman,[⊥] and Horst Kessler*,[†,@]

[†]Institute for Advanced Study and Center of Integrated Protein Science, Department Chemie, Technische Universität München, Lichtenbergstrasse 4, 85747 Garching, Germany

[‡]Dipartimento di Chimica Farmaceutica e Tossicologica, Università di Napoli "Federico II", Via D. Montesano, 49-80131 Napoli, Italy

[§]Institut für Klinische Chemie und Pathobiochemie, Klinikum rechts der Isar, Technische Universität München, Ismaninger Strasse 22, 81675 München, Germany

[||]Institute of Analytical Chemistry, University of Vienna, Währinger Strasse 38, A-1090 Vienna, Austria

[⊥]School of Pharmacy, Faculty of Medicine, The Hebrew University of Jerusalem, P.O. Box 12065, Jerusalem 91120, Israel

[@]Chemistry Department, Faculty of Science, King Abdulaziz University, P.O. Box 80203, Jeddah 21589, Saudi Arabia

Ⓢ Supporting Information

ABSTRACT: Intervention in integrin-mediated cell adhesion and integrin signaling pathways is an ongoing area of research in medicinal chemistry and drug development. One key element in integrin−ligand interaction is the coordination of the bivalent cation at the metal ion-dependent adhesion site (MIDAS) by a carboxylic acid function, a consistent feature of all integrin ligands. With the exception of the recently discovered hydroxamic acids, all bioisosteric attempts to replace the carboxylic acid of integrin ligands failed. We report that phosphinates as well as monomethyl phosphonates represent excellent isosters, when introduced into integrin antagonists for the platelet integrin αIIbβ3. The novel inhibitors exhibit in vitro and ex vivo activities in the low nanomolar range. Steric and charge requirements of the MIDAS region were unraveled, thus paving the way for an in silico prediction of ligand activity and in turn the rational design of the next generation of integrin antagonists.
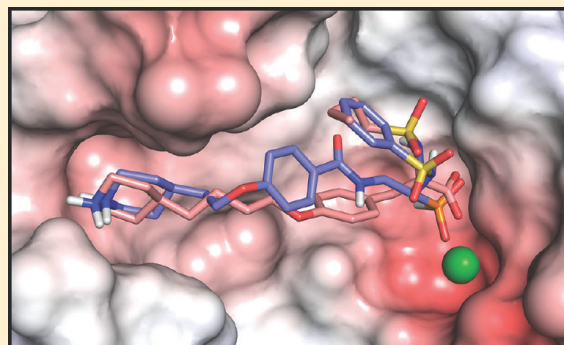
■ INTRODUCTION

Integrin signaling is profoundly implicated in numerous physiological processes, such as tissue remodeling or angiogenesis, as well as in important pathological disorders such as thrombosis, cancer, osteoporosis, and autoimmune diseases. Because of their biological relevance in many diseases, integrins represent highly important targets for medicinal chemistry.[1,2] From a structural point of view, integrins are heterodimers of a noncovalently linked α-subunit and a β-subunit. Each domain is composed of an extracellular domain, a single membrane-spanning helical domain, and a short cytoplasmic tail. The β-subunit contains a metal ion-dependent adhesion site (MIDAS) in the ligand binding domain.[3−5] Among the 24 known integrins, a number of them, known as the RGD-dependent integrins, recognize the tripeptide sequence arginine-glycine-aspartic acid (RGD) of extracellular matrix (ECM) proteins (e.g., fibronectin for α5β1, fibrinogen for platelet integrin αIIbβ3, and vitronectin for αvβ3 and other αv integrins) or other ligands, such as ADAMs, snake venoms, or viruses

(FMD).[1,6,7] Constraining and mimicking RGD has successfully been used to develop thousands of integrin ligands, all containing an essential carboxylate moiety as a metal-coordinating group in the MIDAS. Recently, we found hydroxamic acids as a first potent isosteric replacement of the carboxylic group in integrins αvβ3 and α5β1.[8] The known tendency of phosphate groups to coordinate bivalent metal ions (calcium, manganese, or magnesium) prompted us to develop new phosphorus-containing integrin ligands with the aim of unraveling the steric and electrostatic requirements of the MIDAS region and obtaining significant new insights into the binding mode of integrins for further optimizing integrin ligands.

To date, extensive efforts have been made to discover and develop integrin antagonists for clinical applications. However, only for three integrins[9] (αIIbβ3, α4β1, and αLβ2), of the 24
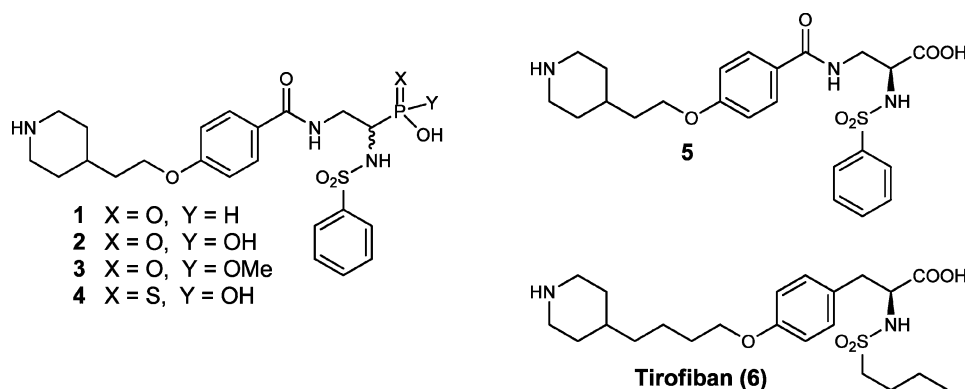
Figure 1. Bioisosteric replacement of the carboxylic MIDAS binding motif for the development of new αIIbβ3 integrin antagonists: phosphinic acid **1**, phosphonic acid **2**, monomethyl phosphonic acid **3**, thiophosphonic acid **4**, tirofiban analogue **5**, and tirofiban **6**.

Scheme 1. Synthesis of Integrin Ligands 1–4[a]
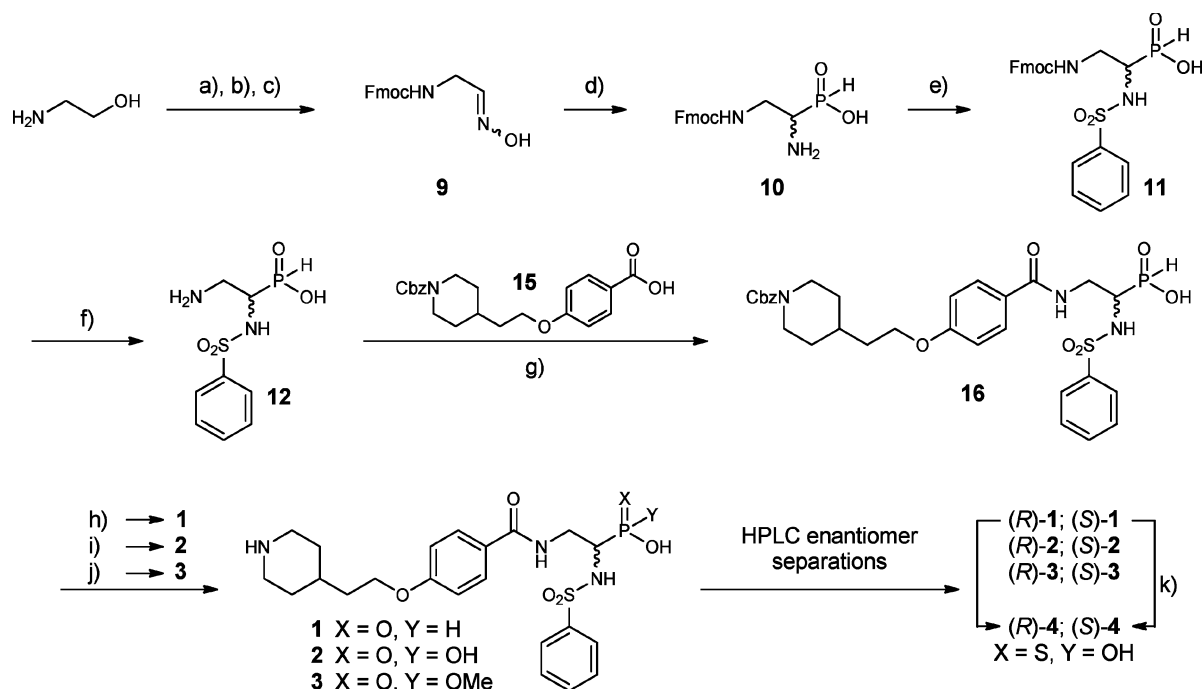
[a](a) Fmoc-Cl, 10% Na$_2$CO$_3$, room temperature (RT), 2 h; (b) IBX, DMSO, RT, 16 h; (c) NH$_2$OH·HCl, DIEA, DCM, RT, 16 h; (d) anhydrous crystalline H$_3$PO$_2$, MeOH, reflux, 4 h; (e) PhSO$_2$Cl, 10% Na$_2$CO$_3$, dioxane, RT, 3 h; (f) 20% piperidine/DMF, RT, 2 h; (g) HATU, DIEA, DMF, RT, 16 h; (h) TFA/H$_2$O/TIPS, RT, 16 h; (i) (1) BSA, air, DCM, RT, 1 h; (2) TFA/H$_2$O/TIPS, 16 h; (j) (1) BSA, air, DCM, RT, 1 h; (2) EDC·HCl, DMAP, MeOH, RT, 1 h; (3) TFA/H$_2$O/TIPS, 16 h; (k) BSA, sulfur, DCM, RT, 1 h. All compounds were purified by RP-HPLC (for more details, see the Supporting Information).

known, have small molecular ligands been approved as drugs. Candidates for other integrins, such as αvβ3, are in clinical phase III trials.[10] In contrast, significant advances have been made in targeting platelet integrin αIIbβ3.[9,11] In fact, the αIIbβ3 integrin inhibitor tirofiban[12] is being successfully used in acute antithrombotic therapy;[12–14] thus, inhibition of this receptor is now a validated way of inhibiting fibrinogen-dependent platelet aggregation.

In this work, integrin antagonists **1–4** (Figure 1) were developed on the basis of tirofiban analogue **5** (Figure 1) previously described by Duggan et al.[15] Compounds **1–4** allow us to explore the sensitivity of the MIDAS region for coordination of differently charged groups. Synthetic methods

for obtaining the desired compounds **1–4** have been developed (Scheme 1). Enantiomers due to the chiral center in α-position of the phosphorus-containing group were resolved via chromatography on chiral columns and tested independently. The ability of the novel ligands to inhibit the binding of integrin αIIbβ3 to its corresponding ECM protein fibrinogen was tested in a competitive ELISA, and the efficacy of the most active compounds was proven in ex vivo experiments. To understand the dependency of the charge of the metal-coordinating group and the corresponding biological activities, we studied the protonation states of compounds **1–4** by means of extensive theoretical calculations and ^{31}P NMR titration experiments. The combination of ab initio calculations and molecular

Table 1. Biological Evaluation of Activities of Ligands 1−6 on Integrin $\alpha IIb\beta 3$
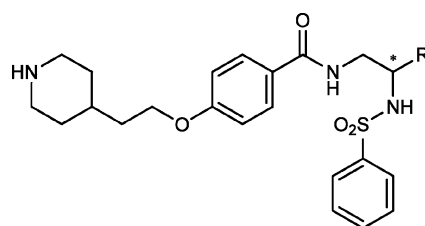
compd	R	IC_{50}^{a} (nM) ($\alpha IIb\beta 3$)	EC_{50}^{b} (nM) ($\alpha IIb\beta 3$)
(R)-1	PHOOH	1.2 ± 0.06	7.8 ± 0.9
(S)-1		6.3 ± 0.73	
(R)-2	$PO(OH)_2$	22.7 ± 2.7	276 ± 15.6
(S)-2		136 ± 10.7	
(R)-3	PO(OH)(OMe)	3.3 ± 0.4	40.8 ± 1.9
(S)-3		1154 ± 272	
(R)-4	$PS(OH)_2$	62.5 ± 6.0	
(S)-4		1322 ± 498	
(S)-5	COOH	0.81 ± 0.05	
(R)-5		4.4 ± 0.3	
6	tirofiban	0.95 ± 0.09	13.6 ± 3.3

[a]IC_{50} values were derived from a competitive ELISA using immobilized fibrinogen and soluble integrin $\alpha IIb\beta 3$. [b]Effective concentrations (EC_{50}) of some key compounds for inhibition of platelet aggregation were derived from aggregation measurements using multiple-electrode aggregometry in hirudin-anticoagulated TRAP-6-activated blood.

docking simulations has defined the binding modes of the new ligands **1** and **2** identifying the molecular requisites for achieving a high inhibitory activity, and on the basis of these, a prediction of the activity of **3** and **4** was successfully executed.

■ CHEMISTRY

To prepare compounds **1−4**, two major fragments (**12** and **15**) were connected via an amide bond (Scheme 1). For the synthesis of **12**, commercially available 2-aminoethanol was Fmoc-protected followed by oxidation with IBX.[16,17] The corresponding aldehyde **8** was converted with hydroxylamine hydrochloride in DCM to oxime **9** in high yield.[18] Refluxing oxime **9** with anhydrous crystalline phosphinic acid in dry methanol resulted in racemic phosphinate intermediate **10**,[18,19] which was sulfonylated upon treatment with phenylsulfonyl chloride in aqueous Na_2CO_3 to provide Fmoc-protected derivative **11**. Fmoc deprotection and purification by reverse-phase high-performance liquid chromatography (RP-HPLC) afforded fragment **12** as a racemic mixture.

The second fragment containing the arginine mimic as a piperidine moiety had already been described by Duggan et al.[15] Herein, Cbz protection was used instead of the more acid labile Boc group, to avoid any deprotection of the secondary amine during synthesis. Furthermore, during purification of **13**, the Cbz group allows UV detection. 2-[N-(Benzyloxycarbonyl)-piperidin-4-yl]ethanol (**13**) was coupled to methyl-4-hydroxybenzoate via Mitsunobu reaction with tributylphosphine and 1,1'-(azodicarbonyl)dipiperidine.[20,21] Saponification of methyl ester **14** gave benzoic acid derivative **15**. Activation of **15** by use of O-(7-azabenzotriazol-1-yl)-N,N,N',N'-tetramethyluronium hexafluorophosphate (HATU) and subsequent condensation with **12** gave Cbz-protected precursor **16**.

Deprotection of **16** with trifluoroacetic acid yielded molecular probe **1**, while the conversion of phosphinic acid **16** to the bis(trimethylsilyl)phosphonite intermediate, which was oxidized by atmospheric oxygen, afforded after Cbz deprotection phosphonic acid ligand **2** in high yield. When

this process was applied to **1** and an excess of sulfur was added, thiophosphonic acid **4** was obtained. Furthermore, Cbz-protected phosphonic acid **2** undergoes rapid monoesterification at room temperature in the presence of N-[3-(dimethylamino)propyl]-N'-ethylcarbodiimide (EDC) and 2 equiv of 4-dimethylaminopyridine (DMAP) in dry methanol. Without DMAP, the reaction results in exclusive formation of the dimethyl ester and no desired product **3** is observed.

We decided to synthesize all molecular probes as racemic mixtures, as "libraries of enantiomers". However, for a more detailed biological evaluation, it was necessary to determine the activity of the optically pure compounds.

Enantiomer separation was successfully performed on quinine-based chiral zwitterionic ion-exchange-type stationary phases developed by Hoffmann et al.[22] Here, a sulfonic acid derivative of quinine served as a zwitterionic chiral selector.[23] The concept of the resolution of the racemic ampholytes, as compounds **1−3** can be classified, is based on a simultaneous ion pair formation of the zwitterionic chiral selector motif of the chiral stationary phase with the individual enantiomers of the analytes. These two diastereomerically behaving selector−(R)-enantiomer and selector−(S)-enantiomer associates are the basis for the enantiomer separations.[22] The preference and magnitude of molecular recognition and chiral discrimination are based on the stereochemical properties of the chiral selector and the ampholytes that include additional intermolecular interaction sites like hydrogen bonding and $\pi - \pi$ interactions that determine the overall chromatographic enantioselectivity and elution order.

For N-acyl-protected amino acid-type analytes with known absolute configurations, we formulated a general model of intermolecular interactions and chromatographic elution order that correlates with the absolute configuration of the α-carbon of an α-amino acid.[24,25] Accordingly, we assigned the stereocenter of compounds **1−3**, taking into account the isosteric behavior of the analytes and the Cahn−Ingold−Prelog
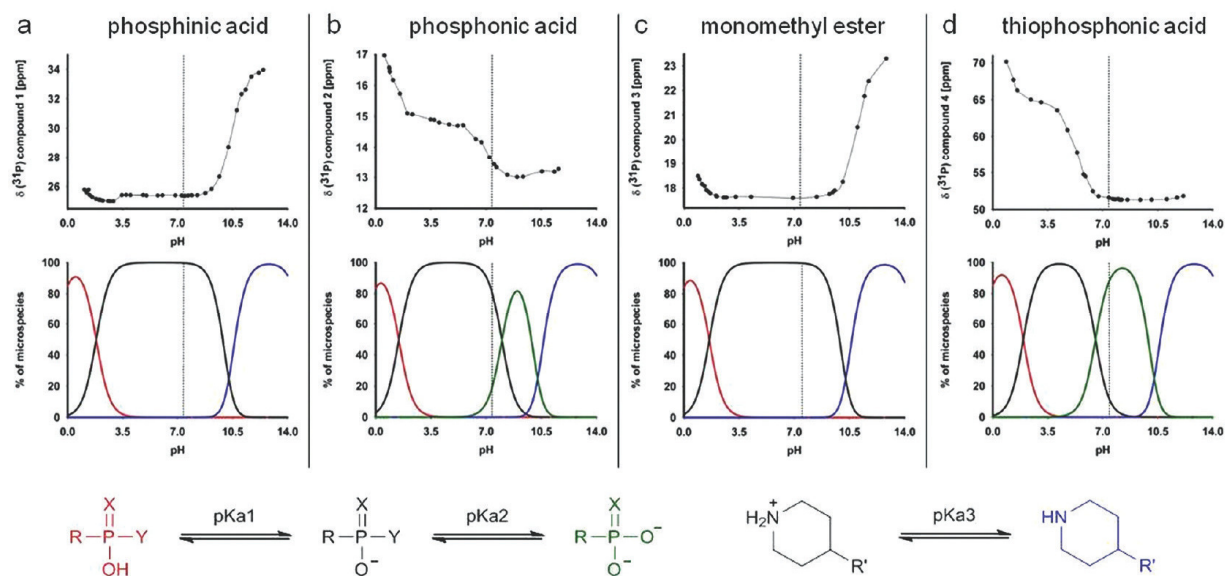
Figure 2. Assessing the protonation state of the molecular probes. Comparison of ^{31}P NMR titration curves (top) and computed microspecies distributions (middle) for molecular probes **1–4** (a–d, respectively). The physiological pH of 7.2 is shown as a dotted line to highlight the presence of either a single protonation state [horizontal line for **1** (a), **3** (c), and **4** (d)] or two protonation states [descending line for **2** (b)]. In the calculated microspecies distribution (bottom), structures of the most dominant protonation states are shown. The dotted line and the intersection with the presentation of microspecies represent the protonation states at the physiological pH of 7.2.

(CIP) convention (for more details, see the Supporting Information).

RESULTS

In Vitro Inhibition of Integrin αIIbβ3. To validate the inhibition properties of the compounds against αIIbβ3, a competitive ELISA (αIIbβ3 fibrinogen assay) was performed using soluble integrin αIIbβ3 and the immobilized natural ligand fibrinogen.[26,27] The clinically used αIIbβ3 inhibitor tirofiban was used as an internal control (Table 1, IC$_{50}$).

Carboxylic acid (S)-**5** is similar in potency to tirofiban (**6**), whereas the (R)-configuration is 6 times less active (0.8 nM vs 4.4 nM). Isosteric replacement of the carboxylic acid with a phosphinic acid results in retained activity depending on its relative configuration [1.2 nM for (R)-**1** and 6.3 nM for (S)-**1**]. However, the phosphonic acid derivatives **2** are 20 times less active [22.7 nM for (R)-**2** and 136 nM for (S)-**2**] than phosphinic acid **1**, clearly indicating that additional negative charge is not well tolerated in the MIDAS. Being aware that phosphonic acid **2** might exist in several different protonation states at the given pH, we used thiophosphonic acid **4** as a molecular probe existing only in the double-negative protonation state (Figure 2). The higher IC$_{50}$ of **4** [62.5 nM for (R)-**4** and 1322 nM for the less favored (S)-**4** enantiomer] indicates that the additional charge in phosphonates and thiophosphonates reduces the binding affinity for the MIDAS. To further prove and underline this concept, we evaluated monomethyl ester **3** of phosphonic acid **2**, resulting in the elimination of the additional negative charge. The (R)-**3** phosphonic methyl ester regains nearly all of the activity (3.3 nM) compared to the phosphinic acid (R)-**1**, whereas the (S)-**3** methyl ester is far less potent (1154 nM). This could indicate a steric hindrance by the methyl group pointing toward the binding pocket. Similar indications were obtained from the docking calculations (for more details, see the Supporting Information).

Platelet Aggregation in Whole Blood. In an attempt to compare the potencies of binding of various compounds to isolated platelet integrin αIIbβ3 (IC$_{50}$) with their predicted inhibitory potency for the complex biological process of platelet aggregation, the effects of synthetic ligands (R)-**1**, (R)-**2**, (R)-**3**, and tirofiban on ex vivo platelet aggregation were assessed using impedance-based platelet aggregometry[28,29] in hirudin-anticoagulated TRAP-6-activated whole blood (Table 1, EC$_{50}$).

Phosphinic acid (R)-**1** was found to behave like tirofiban in terms of platelet aggregation inhibition, whereas phosphonic acid derivative (R)-**2** was ~20 times less potent. Phosphonic methyl ester (R)-**3** showed intermediate efficacy. There is a very good correlation between the inhibitory potencies of compounds in the ELISA (IC$_{50}$) and their inhibitory potencies in the platelet aggregation assay (EC$_{50}$).

In Vitro Permeability Study. We have tested pharmacokinetic properties (including disposition and membrane permeability) of ligands **1–3** and tirofiban (**6**) by evaluating their permeability properties with an enterocyte monolayer derived from human colonic carcinoma cells (Caco-2 model).[30] This model is commonly used to predict the degree of intestinal permeability of therapeutic compounds as well as to gain a certain indication regarding their likelihood of penetrating the brain. The results could not differentiate between the permeability properties of the four compounds in cases where all of them exhibit poor permeability properties ($P_{app} < 1 \times 10^{-8}$ cm/s). It should be noted that the permeability of mannitol (positive control) used in this study was 2.4×10^{-6} cm/s. The permeability mechanism of mannitol is paracellular, using the pores between the cells (tight junctions), with no transcellular component. The fact that all of the tested tirofiban analogues had significantly lower permeability values indicates that the charged moiety of these analogues (at physiological pH, 7.2) restricted the paracellular transport properties in an effective manner. However, to validate this argument, we prepared the corresponding dimethyl ester of **2** [inactive in the
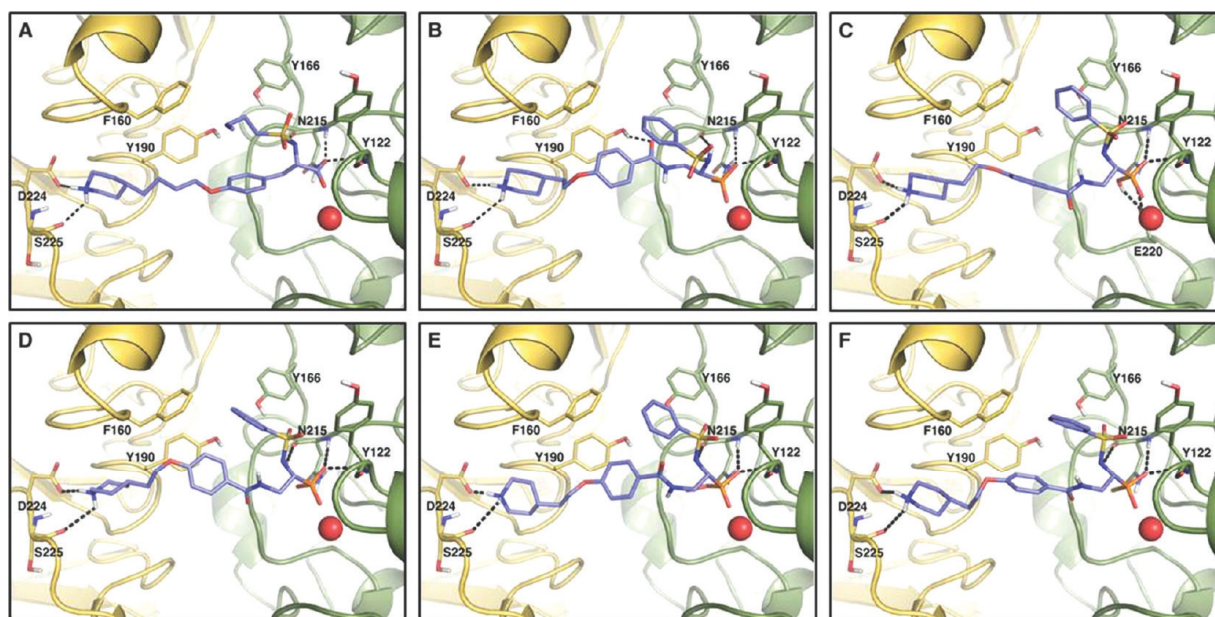
Figure 3. Modes of binding of tirofiban (A), (*R*)-**1** (B), (*R*)-**2** in the overall neutral form (C) and in the overall anionic form (D), (*R*)-**3** (E), and (*R*)-**4** (F). The αIIb domain is displayed as a yellow cartoon, while the β3 domain is colored green. The interacting residues and the ligands are shown as licorice, while the magnesium ion is represented as a red sphere. For the sake of clarity, only the polar hydrogens are displayed. The stereoview version of each complex is provided in Figure S3 of the Supporting Information.

αIIbβ3 fibrinogen assay (data not shown] and tested its permeability. Unfortunately, this compound also exhibited poor permeability.

Assessment of the Protonation State of 1−4. To elucidate the molecular properties responsible for the different activity profiles of the investigated compounds (Table 1) and the mechanism of recognition between the inhibitors and the αIIbβ3 integrin receptor (see the docking section), we conducted an extensive computational study. First, the protonation states of compounds **1−4** were computed for each compound, and the distribution of microspecies between pH 0 and 14 was calculated with the Marvin Sketch package. The results were validated via titration experiments monitored by ^{31}P NMR chemical shifts that are very sensitive to ionization state[31−35] (Figure 2; for more details, see the Supporting Information).

While **1** and **3** are characterized by two pK_a values, corresponding to the acidities of the phosphorus acid moiety (pK_{a1}) and the piperidinium group (pK_{a3}), for **2** and **4** a total of three pK_a values are found [phosphonic and thiophosphonic acid (pK_{a1} and pK_{a2}, respectively) and piperidinium group (pK_{a3})]. The experimental as well as the calculated (in parentheses) pK_a values show that at the physiological pH of 7.2 all piperidine moieties are protonated with pK_{a3} values of 10.44 (10.48) for **1**, 10.06 (10.48) for **2**, 11.02 (10.57) for **3**, and 12.03 (10.58) for **4**. Furthermore, the first acid functionality of the phosphorus unit (pK_{a1}) of all compounds **1−4** is present in the completely deprotonated form at pH 7.2 with pK_{a1} values of greater than 1.56 (1.90) for **1**, 1.01 (1.63) for **2**, 1.13 (1.63) for **3**, and 1.27 (1.94) for **4**. All in all, we found that the experimental NMR results fully corroborate the trends in the computational calculations.

At the physiological pH of 7.2, the piperidine moiety (pK_{a3}) of **1** is protonated and the phosphinate group (pK_{a1}) is fully deprotonated (Figure 2a). For **2**, two microspecies can be

found at physiological pH, both having a protonated piperidine unit; however, in one case, the phosphonic acid is monoanionic (~86% in silico and 63% in vitro), and in the other case, it is in the dianionic form (~14% in silico and 37% in vitro) (Figure 2b). To further investigate the effect of the charge of the different substituents on the phosphorus atom, two more molecular probes, **3** and **4**, were studied. In particular, the thiophosphonate group of compound **4**, like the phosphonate group of **2**, coexists at neutral pH as mono- and dianionic species, but a shift toward the dianionic form (~82% in silico and 99% in vitro) was observed (Figure 2d). The in vitro measurements showed that the second acid functionality (pK_{a2}) of compounds **2** and **4** is more acidic than calculated. For **2** a pK_{a2} of 6.97 (7.99) and for **4** a pK_{a2} of 5.27 (6.53) can be extracted from the obtained data points. Compound **3**, like **1**, possesses only one single microspecies (Figure 2c).

Molecular Docking and Electrostatic Potential Calculations of 1−4. Compounds **1−4** were docked into the αIIbβ3 RGD binding site with the aid of AutoDock version 4.0.[36,37] Both enantiomers were studied. Results of the (*S*)-enantiomers are reported in the Supporting Information along with an explanation of the lower inhibitory potency observed for (*S*)-**1**, (*S*)-**2**, and (*S*)-**3** with respect to those of the corresponding (*R*)-enantiomers.

As for (*R*)-**1**, in accordance with the protonation state assessment (Figure 2a), only the neutral ligand form (piperidine moiety protonated, phosphinate deprotonated) was used for docking simulations. As a result, a binding mode highly similar to that of tirofiban was observed (Figure 3A,B and Figure S2 of the Supporting Information). In fact, the phosphinate group coordinates the magnesium ion occupying in the MIDAS the same region that hosts the carboxylate group of tirofiban. In particular, one of the oxygen atoms coordinates the metal, while the other one engages two H-bonds with the backbone NH groups of (β3)-Asn215 and (β3)-Tyr122, like
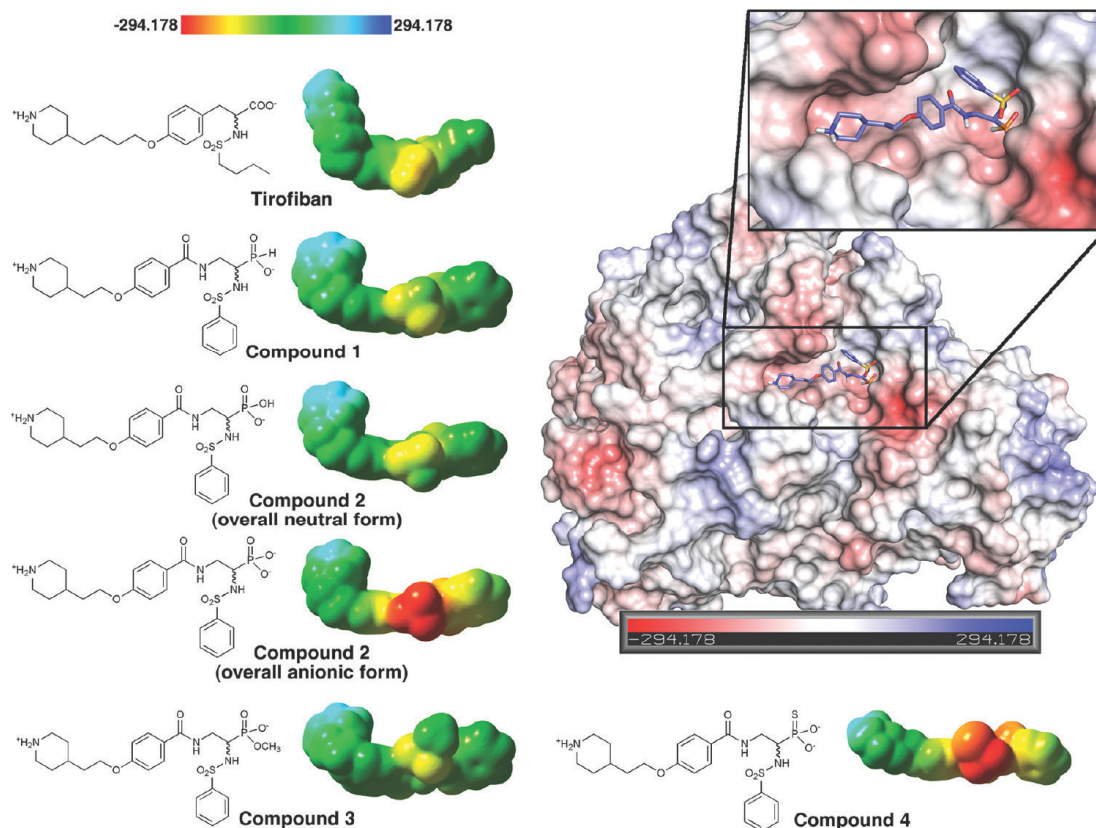
Figure 4. Electrostatic potential mapped onto the molecular surface of tirofiban, **1**, **2** in the overall neutral form and in the anionic form, **3**, and **4**. At the top right, the electrostatic surface of the integrin $\alpha IIb\beta 3$ binding site complexed with compound (R)-**1** is shown. Both for ligands and for the protein, the scale of the electrostatic potential ranges from -294.178 (red) to 294.178 (blue) $k_b T/e_c$.

tirofiban in $\alpha IIb\beta 3$ and Cilengetide in $\alpha v\beta 3$ [Protein Data Bank (PDB) entries 2vdm and 1L5G]. The benzenesulfonamide moiety forms H-bonds with the $(\beta 3)$-Asn215 backbone CO group, while the phenyl ring occupies the aromatic pocket formed by (αIIb)-Phe160, (αIIb)-Tyr190, and $(\beta 3)$-Tyr166. The aromatic ring of the *p*-hydroxybenzoate scaffold is close enough to form a $\pi-\pi$ interaction with (αIIb)-Tyr190, the hydroxyl group of which is involved in an H-bond interaction with the inhibitor amide CO group. This allows the piperidine moiety to point toward the αIIb subunit, where the protonated nitrogen group makes a salt bridge interaction with the (αIIb)-Asp224 side chain and an H-bond with the (αIIb)-Ser225 backbone CO group. All these favorable interactions are certainly responsible for the low nanomolar activity of (R)-**1** toward the $\alpha IIb\beta 3$ receptor.

Because phosphonic acid **2** is present at the physiological pH of 7.2 both in the monoanionic form and in the dianionic form (Figure 2b), docking calculations for (R)-**2** were performed for both protonation states, and the results showed a binding conformation similar to that of tirofiban and (R)-**1** (Figure 3C,D). This suggests that although the phosphonic group is bulkier than the phosphinate moiety, it can fit in the MIDAS region. Nevertheless, because (R)-**2** shows reduced activity compared to that of (R)-**1** (Table 1), reasons different from the steric hindrance should be responsible for the experimentally observed lower activity. In this regard, it has to be clarified that all docking algorithms, either based on classical force fields[38] or based on empirical free energy scoring functions[39] or knowledge-based scoring functions,[40] cannot accurately predict

properties like the exact metal coordination geometry or particular charge effects. Thus, to overcome this limitation and to shed light on the different activity profiles of (R)-**1** and (R)-**2**, more accurate computational techniques must be used. Recent progress made in the force field parametrization of bivalent ions[41] and some theoretical studies on a Mg^{2+} protein[42,43] would suggest the use of molecular dynamics-based approaches to sample more accurately the specific ligand–protein interaction of each complex. Another possibility might be to perform QM/MM calculations to accurately describe the ligand–protein interaction at the binding site. Unfortunately, both these approaches are computationally time intensive and are useful for the study of only a few compounds. To perform calculations on most of the ligands of the series in a reasonable computational time, we decided to conduct quantum mechanical calculations only on the ligands, thus elucidating their different electrostatic potential profiles.

Quantum mechanical calculations revealed that (R)-**1** has an electrostatic potential profile highly similar to that of tirofiban, particularly with regard to the metal-coordinating group, while (R)-**2** is similar to tirofiban only in its neutral form (Figure 4). In fact, with regard to (R)-**2**, the electrostatic potential of the phosphonate group in the dianionic form, existing at physiological pH, is highly negative. Indeed, if on one hand this improves the coordination of the metal ion, on the other hand, it causes electrostatic repulsion effects with the surrounding atoms in the MIDAS such as the backbone CO groups of $(\beta 3)$-Asn215 and $(\beta 3)$-Asp217 or the $(\beta 3)$-Glu220 side chain (Figures 3D and 4). Thus, our computational study

of (R)-**1** and (R)-**2** suggests that electrostatic properties, more than steric features, are the crucial factors for the different activities of the two compounds.

Also in the case of (R)-**3** and (R)-**4**, it was not possible to predict the αIIbβ3 activities solely on the basis of the docking calculations (see Figure 3E,F for the predicted binding modes and the Supporting Information for further details about docking). As shown in Figure 4, the electrostatic potential profile calculated for (R)-**3** is highly similar to those of tirofiban and (R)-**1**, while compound (R)-**4**, like (R)-**2**, has a highly negative potential localized on the thiophosphonate group (dianionic form). Those results are in perfect line with the ELISA data reported in Table 1. In fact, (R)-**4** possesses a reduced activity because of the preponderance (~82% in silico and 99% in vitro) of its dianionic form, which has the less favorable electrostatic profile for its interaction with αIIbβ3. Accordingly, (R)-**3** has an electrostatic potential profile and an activity comparable to those of (R)-**1**.

■ DISCUSSION

The strong binding affinity of phosphorus ligands for bivalent metal ions stimulated us to investigate those groups as pharmacophores for binding to the MIDAS region of integrins. As a proof of principle, we investigated analogues of αIIbβ3 integrin inhibitor **5**, previously described by Duggan et al.,[15] which is structurally related to the drug tirofiban (**6**) and exhibits a similar binding affinity. The essential carboxyl group of **5** was modified by different phosphorus-containing groups. We found that phosphinate groups as well as a phosphonate monomethyl ester are suitable isosteres for the carboxyl group in integrin ligands while phosphonate and thiophosphonate groups could not be used for this purpose. Docking of ligands **1**–**4** in the αIIbβ3 receptor did not reveal substantial differences with respect to the tirofiban binding mode (Figure 3 and Figure S2 of the Supporting Information), thus excluding steric effects as a reason for different binding potencies. On the basis of ab initio studies, the high affinity of phosphinate **1** and phosphonate monomethyl ester **3** can be attributed to the lower negative charge of the ligand metal binding groups, if compared to those of **2** and **4** (Figure 4). The differences in charges among compounds **1** and **4** have been investigated both by theoretical calculations and by ^{31}P NMR measurements. In phosphonate **2** and thiophosphonate **4** at neutral pH, there are considerable amounts of dianionic species in the equilibrium (Figure 2). Obviously, the high negative charge is not tolerated by the MIDAS region, which is already negatively charged (Figure 4).

The dominating charge effect is accompanied by second-order steric effects induced by substituents in α-position to the phosphorus atom expressed in the different acceptance of stereoisomers. Synthesis and the biological assays of the pure (R)- and (S)-stereoisomers of **5** reveal that the (R)-enantiomer is ~5 times less active than the (S)-enantiomer. The same general trend was found for compounds **1**–**4**, bearing in mind the fact that according to the CIP rules the notation in the phosphorus compounds is reversed (Table 1). Molecular docking revealed that in the case of compounds **1**–**4**, although the (S)-enantiomers are also able to bind the receptor, they lose a number of favorable interactions within the binding pocket, particularly in the case of phosphonic compounds (S)-**2** and (S)-**3** (see the Supporting Information for details).

In the biological evaluation of the new αIIbβ3 antagonists, we have shown that the in vitro binding affinity fully correlates with the ex vivo prevention of platelet aggregation measured by multiple-electrode aggregometry in hirudin-anticoagulated TRAP-6-activated blood. Both assays yield the same order of activities for all tested compounds. Approximately 10-fold higher EC_{50} values are required compared to inhibition of binding of integrin to fibrinogen (Table 1, IC_{50}).

The pharmacotherapeutic activity of tirofiban is provided following intravenous administration and is confined to the systemic blood circulation. The results of the permeability studies can be regarded as an indication that the new ligands will also be restricted to the central compartment. Thus, once administered by a parenteral route, the molecules will be distributed within the central compartment where they produce their antiplatelet aggregation activity. In case the novel analogues will be further developed for clinical use (e.g., for molecular imaging), the restricted distribution predicted for these analogues ensures minimal side effects that could be derived by interaction with peripheral tissues, including the central nervous system. Thus, the poor membrane permeability contributes to the safety profile of these analogues. Pharmacokinetically wise, the polar moieties of these analogues at the physiological pH of 7.2 did not allow passive diffusion across the biological membrane, like enterocytes. It also inhibited the transport via the tight junctions pores as evidenced by the significantly lower permeability compared to that of mannitol.

In summary, we here report a successful case of drug design on the αIIbβ3 integrin that allowed us to identify the molecular and electrostatic requisites for achieving strong αIIbβ3 inhibition. In particular, we have found that even a space-demanding group such as methyl phosphonate (R)-**3** can bind to the αIIbβ3 MIDAS without strongly affecting the activity. We have found that highly negatively charged metal-coordinating groups are not well tolerated in the αIIbβ3 MIDAS. All these findings, on one hand, are extremely useful for an easy and quick tuning of both the steric and electrostatic features of αIIbβ3 inhibitors; on the other hand, they demonstrate that docking calculations together with more rigorous computational procedures, such as ab initio studies, can be successfully used in rational design of new inhibitors active on integrin receptors different from αIIbβ3.

The modification of the carboxylate group into a phosphinate or a phosphonate monomethyl ester yields an attractive new way of optimizing integrin ligands. The successful design of non-carboxylate-containing ligands as integrin antagonists surely opens a new era in the design and finding of novel integrin ligands.

■ EXPERIMENTAL SECTION

All technical solvents were distilled prior to use. Dry solvents were purchased from Aldrich, Fluka, or Merck. Reactions sensitive to oxygen or water were performed in flame-dried reaction vessels under an argon atmosphere (99.996%). Fmoc-protected amino acids and coupling reagents were purchased from Novabiochem (Schwalbach, Germany), Iris Biotech GmbH (Marktredwitz, Germany), and Medalchemy (Alicante, Spain). All other chemicals and organic solvents were purchased from commercial suppliers at the highest purity available and used without further purification.

TLC monitoring was performed on Merck DC silica gel plates (60 F-254 on aluminum foil). Spots were detected by UV absorption at 254 nm and/or by staining with a 5% solution of ninhydrin in ethanol or mostain [6.25 g of phosphomolybdic acid, 2.5 g of cerium(IV) sulfate, and 15 mL of sulfuric acid in 235 mL of water] or potassium permanganate (5% in 1 N aqueous NaOH).

Flash column chromatography was performed using silica gel 60 (40−63 μm) from Merck at a pressure of 1−1.5 atm.

Analytical HPLC was performed using Amersham Pharmacia Biotech Äkta Basic 10F equipment, with a P-900 pump system, a reversed-phase YMC-ODS-A C$_{18}$ column (12 nm pore size, 5 μm particle size, 250 mm × 4.6 mm), and UV detection (UV-900; 220 and 254 nm). The system was run at a flow rate of 1.0 mL/min over 30 min using H$_2$O (0.1% TFA) and MeCN (0.1% TFA) as solvents.

Semipreparative HPLC was performed using Waters equipment: System Breeze; pump system 1525, UV detector 2487 dual (220 and 254 nm); Driver Software Breeze version 3.20; column material, YMC-ODS-A C$_{18}$ (12 nm pore size, 5 μm particle size, 250 mm × 20 mm), YMC-ODS-AQ C$_{18}$ (12 nm pore size, 5 μm particle size, 250 mm × 20 mm), or YMCbasic (proprietary, 5 μm particle size, 250 mm × 20 mm).

HPLC−ESI-MS analyses were performed on a Hewlett-Packard Series HP 1100 system with a Finnigan LCQ mass spectrometer using a YMC-Hydrosphere C$_{18}$ column (12 nm pore size, 3 μm particle size, 125 mm × 2.1 mm) or a YMC-Octyl C$_8$ column (20 nm pore size, 5 μm particle size, 250 mm × 2.1 mm). The system uses H$_2$O (0.1% formic acid) and MeCN (0.1% formic acid) as eluents.

High-resolution mass spectrometry was conducted on a Thermo Finnigan LTQ-FT (ESI-ICR) spectrometer.

^{1}H NMR, ^{13}C NMR, and ^{31}P NMR spectra were recorded at 295 K on 500 MHz Bruker DMX, 360 MHz Bruker AV, and a 250 MHz Bruker AV spectrometers, respectively (Bruker, Karlsruhe, Germany). Chemical shifts (δ) are given in parts per million. The following solvent peaks were used as internal standards: DMSO-d_5, 2.50 ppm (^{1}H NMR) and 39.52 ppm (^{13}C NMR); CHCl$_3$, 7.26 ppm (^{1}H NMR) and 77.16 ppm (^{13}C NMR); MeOH-d_3, 3.31 ppm (^{1}H NMR) and 49.00 ppm (^{13}C NMR).[44] With MeOH-d_3 as the solvent, standard pulse sequences provided by Bruker were used to eliminate the solvent peak (watergate, P3919GP; presaturation, ZGPR). For ^{31}P NMR spectra, 85% phosphoric acid was used as an external standard.

Duggan ligand (S)-5 was synthesized according to literature procedures,[15] starting from $N^α$-Fmoc-L-2,3-diaminopropionic acid. Synthesis of the corresponding (R)-enantiomer was conducted as described here, starting from $N^α$-Boc-$N^β$-Fmoc-D-2,3-diaminopropionic acid. Standard peptide coupling techniques were employed.

All yields are not optimized. The analytical data of compounds 7−18 are listed in the Supporting Information. All tested compounds were ≥95% pure as determined by RP-HPLC-(MS).

1-(Phenylsulfonamido)-2-{4-[2-(piperidin-4-yl)ethoxy]-benzamido}ethylphosphinic Acid (1). A mixture of TFA, TIPS, and water [5 mL, 95:2.5:2.5 (v/v/v) TFA/TIPS/H$_2$O] was added to 16 (36.0 mg, 0.057 mmol) and the mixture stirred at room temperature (RT) for 16 h. Purification by semi-preparative RP-HPLC and lyophilization gave 1 (23.5 mg, 0.047 mmol, 83%) as a white solid: ^{1}H NMR (500 MHz, MeOH-d_3, RT) δ 8.53 (br s, 1 H), 8.24 (br s, 1 H), 8.10 (t, ^3J = 5.0 Hz, 1 H), 7.83 (d, ^3J = 7.6 Hz, 2 H), 7.66 (d, ^3J = 9.0 Hz, 2 H), 7.42 (t, ^3J = 7.3 Hz, 1 H), 7.37 (t, ^3J = 7.5 Hz, 2 H), 6.93 (d, ^3J = 9.0 Hz, 2 H), 6.83 (d, ^1J = 531.3 Hz, 1 H), 4.11 (t, ^3J = 6.2 Hz, 2 H), 3.66−3.48 (m, 3 H), 3.43−3.34 (m, 2 H), 3.07−2.87 (m, 2 H), 2.11−1.94 (m, 2 H), 1.96−1.84 (m, 1 H), 1.80 (dt, ^3J = 6.3 Hz, ^3J = 6.3 Hz, 2 H), 1.46 (dt, ^3J = 14.9 Hz, ^3J = 3.9 Hz, 2 H); ^{13}C NMR (126 MHz, MeOH-d_3, RT) δ 169.9, 163.2, 142.6, 133.6, 130.4, 130.2, 128.0, 127.7, 115.2, 66.6, 54.9 (d, $^1J_{PC}$ = 99 Hz), 45.5, 39.4 (d, $^2J_{PC}$ = 5 Hz), 36.2, 32.4, 30.1; ^{31}P NMR (101 MHz, D$_2$O/H$_2$O, RT) δ 25.4 (pH 7.3); MS (ESI) m/z 430.2 [M − PHOOH]$^+$, 496.2 [M + H]$^+$, 518.2 [M + Na]$^+$, 991.1 [2M + H]$^+$, 1013 [2M + Na]$^+$, 1029.2 [2M + K]$^+$; RP-HPLC t_R = 10.5 min (10−90% in 30 min); HRMS (ESI) m/z calcd for C$_{22}$H$_{31}$N$_3$O$_6$P^{32}S 496.1671 [M + H]$^+$, found 496.1665.

1-(Phenylsulfonamido)-2-{4-[2-(piperidin-4-yl)ethoxy]-benzamido}ethylphosphonic Acid (2). A mixture of TFA, TIPS, and water [5 mL, 95:2.5:2.5 (v/v/v) TFA/TIPS/H$_2$O] was added to 17 (24.1 mg, 0.037 mmol) and the mixture stirred at RT for 16 h. Purification by semipreparative RP-HPLC and lyophilization gave 2 (15.0 mg, 0.029 mmol, 79%) as a white solid: ^{1}H NMR (500 MHz, MeOH-d_3, RT) δ 8.47 (br s, 1 H), 8.18 (br s, 1 H), 8.12−8.05 (m, 1

H), 7.84 (d, ^3J = 7.4 Hz, 2 H), 7.70 (d, ^3J = 8.9 Hz, 2 H), 7.49−7.32 (m, 3 H), 6.95 (d, ^3J = 8.9 Hz, 2 H), 4.13 (t, ^3J = 6.0 Hz, 2 H), 3.96−3.85 (m, 1 H), 3.73−3.62 (m, 1 H), 3.55−3.44 (m, 1 H), 3.43−3.35 (m, 2 H), 3.07−2.93 (m, 2 H), 2.08−1.99 (m, 2 H), 1.98−1.87 (m, 1 H), 1.82 (dd, ^3J = 12.4 Hz, ^3J = 6.1 Hz, 2 H), 1.51 (m, 2 H); ^{13}C NMR (126 MHz, D$_2$O/CD$_3$CN/NaOH, RT) δ 167.7, 160.9, 141.4, 131.5, 128.6, 128.5, 125.6, 125.2, 113.7, 65.5, 52.1 (d, ^1J = 134 Hz), 44.8, 41.5 (d, ^2J = 5 Hz), 35.1, 32.1, 31.8; ^{31}P NMR (101 MHz, D$_2$O/H$_2$O, RT) δ 13.7 (pH 7.2); MS (EI) m/z 430.1 [M − PO(OH)$_2$]$^+$, 494.3 [M − OH]$^+$, 512.2 [M + H]$^+$, 1023.1 [2M + H]$^+$, 1045.1 [2M + Na]$^+$; RP-HPLC t_R = 10.2 min (10−90% in 30 min); HRMS (ESI) m/z calcd for C$_{22}$H$_{31}$N$_3$O$_7$P^{32}S 512.1615 [M + H]$^+$, found 512.1616.

Methyl-1-(phenylsulfonamido)-2-{4-[2-(piperidin-4-yl)-ethoxy]benzamido}ethylphosphonate (3). A mixture of TFA, TIPS, and water [5 mL, 95:2.5:2.5 (v/v/v) TFA/TIPS/H$_2$O] was added to 18 (16.7 mg, 0.025 mmol) and the mixture stirred at RT for 16 h. Purification by semipreparative RP-HPLC and lyophilization gave 3 (10.4 mg, 0.020 mmol, 78%) as a white solid: ^{1}H NMR (500 MHz, MeOH-d_3, RT) δ 8.60−8.40 (m, 1 H), 8.18 (t, ^3J = 5.2 Hz, 1 H), 7.88 (d, ^3J = 8.0 Hz, 2 H), 7.74 (d, ^3J = 9.0 Hz, 2 H), 7.49 (t, ^3J = 7.2 Hz, 1 H), 7.44 (t, ^3J = 7.5 Hz, 2 H), 7.18−7.11 (m, 1 H), 6.95 (d, ^3J = 9.0 Hz, 2 H), 4.11 (t, ^3J = 6.2 Hz, 2 H), 3.73 (ddd, ^3J = 16.8 Hz, ^3J = 13.3 Hz, ^3J = 8.1 Hz, 1 H), 3.65 (ddd, ^2J = 19.2 Hz, ^3J = 9.8 Hz, ^3J = 4.9 Hz, 1 H), 3.53−3.49 (m, 1 H), 3.42−3.35 (m, 2 H), 3.35 (d, ^3J = 10.5 Hz, 3 H), 3.06−2.32 (m, 2 H), 2.06−1.97 (m, 2 H), 1.97−1.86 (m, 1 H), 1.80 (dt, ^3J = 6.5 Hz, ^3J = 6.3 Hz, 2 H), 1.52−1.39 (m, 2 H); ^{13}C NMR (126 MHz, MeOH-d_3, RT) δ 169.7, 163.1, 142.9, 133.5, 130.3, 130.1, 128.1, 127.7, 115.2, 66.5, 52.7 (d, ^2J = 6.3 Hz), 50.9 (d, ^1J = 147.1 Hz), 45.5, 42.4 (d, ^2J = 6.1 Hz), 36.2, 32.4, 30.1; ^{31}P NMR (101 MHz, D$_2$O/H$_2$O, RT) δ 17.6 (pH 6.91); MS (ESI) m/z 494.2 [M − OMe]$^+$, 526.2 [M + H]$^+$, 548.2 [M + Na]$^+$, 1051.1 [2M + H]$^+$, 1073.1 [2M + Na]$^+$, 1576.0 [3M + H]$^+$; RP-HPLC t_R = 10.8 min (10−90% in 30 min); HRMS (ESI) m/z calcd for C$_{23}$H$_{33}$N$_3$O$_7$P^{32}S 526.1777 [M + H]$^+$, found 526.1769.

1-(Phenylsulfonamido)-2-{4-[2-(piperidin-4-yl)ethoxy]-benzamido}ethylthiophosphonic Acid (4). N,O-Bis-(trimethylsilyl)acetamide (BSA, 18.6 μL, 0.076 mmol) was added to a mixture of 1 (9.60 mg, 0.019 mmol) and sulfur powder (1.86 mg, 0.058 mmol) in DCM (dry, 5 mL) at 0 °C under an argon atmosphere.[34] The mixture was allowed to warm to RT and stirred for 1 h. Concentration in vacuo and purification by semipreparative RP-HPLC gave 4 (7.34 mg, 0.014 mmol, 72%) as a white solid: ^{1}H NMR (500 MHz, MeOD-d_4, RT) δ 7.87 (d, ^3J = 7.8 Hz, 2 H), 7.75 (d, ^3J = 8.6 Hz, 2 H), 7.46 (dd, ^3J = 8.9 Hz, ^3J = 15.9 Hz, 1 H), 7.42 (t, ^3J = 7.4 Hz, 2 H), 6.96 (d, ^3J = 8.6 Hz, 2 H), 4.13 (t, ^3J = 6.0 Hz, 2 H), 3.80 (dt, ^3J = 11.4 Hz, ^3J = 4.5 Hz, 2 H), 3.65−3.56 (m, 1 H), 3.42−3.36 (m, 2 H), 3.04−2.95 (m, 2 H), 2.07−1.99 (m, 2 H), 1.98−1.87 (m, 1 H), 1.85−1.79 (m, 1 H), 1.53−1.42 (m, 2 H); ^{13}C NMR (126 MHz, MeOD-d_4, RT) δ 169.7, 163.1, 142.6, 133.4, 130.3, 129.9, 128.2, 127.7, 115.1, 66.5, 56.8 (d, ^1J = 114.7 Hz), 45.3, 42.3 (d, ^2J = 11.3 Hz), 36.2, 32.3, 30.0; ^{31}P NMR (101 MHz, D$_2$O/H$_2$O, RT) δ 51.8 (pH 6.73); MS (ESI) m/z 494.2 [M − 2OH]$^+$, 510.2 [M − OH]$^+$, 528.1 [M + H]$^+$, 550.2 [M + Na]$^+$, 1055.0 [2M + H]$^+$; RP-HPLC t_R = 19.1 min (10−50% in 30 min); HRMS (ESI) m/z calcd for C$_{22}$H$_{31}$N$_3$O$_6$P^{32}S$_2$ 528.1392 [M + H]$^+$, found 528.1374.

(9H-Fluoren-9-yl)methyl (2-Hydroxyethyl)carbamate (7). 9-Fluorenylmethoxycarbonyl chloride (Fmoc-Cl, 1.55 g, 6.00 mmol) was added to a solution of 2-aminoethanol (0.330 g, 5.40 mmol) in 10% aqueous Na$_2$CO$_3$ (50 mL) and the mixture stirred for 2 h at RT. The reaction mixture was extracted with ethyl acetate (3 × 50 mL). The organic phases were combined, washed with aqueous HCl (1 M, 2 × 50 mL) and brine (1 × 50 mL), and dried over MgSO$_4$. Concentration in vacuo and purification by column chromatography (silica gel, 5:1 ethyl acetate/hexane) gave 7 as a white solid (1.48 g, 5.22 mmol, 97%): TLC R_f = 0.5 (5:1 ethyl acetate/hexane) (UV). ^{1}H NMR and ^{13}C NMR spectra were identical to those previously reported.[45]

(9H-Fluoren-9-yl)methyl (2-Oxoethyl)carbamate (8). IBX (7.78 g, 27.8 mmol) was added to a solution of 7 (6.06 g, 21.4 mmol) in DMSO (20 mL) and the mixture stirred at RT for 16 h.[17] DCM (1 L) was added to the reaction mixture, and the resulting white

suspension was stirred for 0.5 h, prior to filtration through Celite. The organic layer was washed with aqueous saturated Na_2CO_3 (3 × 300 mL) and brine (2 × 300 mL). Each extraction was followed by filtration through Celite, if necessary. Drying over $MgSO_4$ and concentration in vacuo resulted in a yellow crude product, which was purified by column chromatography (silica gel, 5:1 ethyl acetate/hexane) to give 8 (4.81 g, 17.1 mmol, 80%) as a white solid: TLC R_f = 0.8 (5:1 ethyl acetate/hexane) (UV). ^{1}H NMR and ^{13}C NMR spectra were identical to those previously reported.[45]

(9H-Fluoren-9-yl)methyl [2-(Hydroxyimino)ethyl]carbamate (9). DIEA (15.3 mL, 89.7 mmol) was added to a mixture of 8 (4.21 g, 15.0 mmol) and hydroxylammonium chloride (3.12 g, 44.9 mmol) in DCM (dry, 40 mL) and the mixture stirred at RT for 16 h.[18] Concentration in vacuo and purification by column chromatography (silica gel, 3:1 ethyl acetate/hexane) gave 9 (2.45 g, 8.27 mmol, 55%) as a slightly yellow colored solid.

2-{N-[(9H-Fluoren-9-yl)methoxy]carbonylamino}-1-aminoethylphosphinic Acid (10). Commercial 60 wt % aqueous phosphinic acid (40.0 g, 364 mmol) was lyophilized to obtain anhydrous crystalline H_3PO_2, which was subsequently added to a solution of 9 (2.10 g, 7.09 mmol) in methanol (dry, 100 mL). The reaction mixture was heated to reflux for 4 h and then concentrated in vacuo.[18,19] The residue was dissolved in aqueous HCl (3 M, 200 mL) and washed with diethyl ether (3 × 100 mL). The pH was adjusted to 1.5 by addition of solid Na_2CO_3. The resulting precipitate was isolated and purified by RP-HPLC to give 10 (1.25 g, 3.61 mmol, 51%) as a colorless solid.

2-{N-[(9H-Fluoren-9-yl)methoxy]carbonylamino}-1-(phenylsulfonamido)ethylphosphinic Acid (11). Benzenesulfonyl chloride (0.507 mL, 3.97 mmol) was added to a solution of 10 (0.310 g, 0.895 mmol) in dioxane and aqueous Na_2CO_3 [50 mL, 1:1 dioxane/aqueous Na_2CO_3 (10 wt %)] and stirred at RT for 3 h. The solvent was removed in vacuo and the residue dissolved in water (100 mL). The aqueous phase was acidified (pH 1) by addition of aqueous HCl (3 M) and extracted with ethyl acetate (3 × 50 mL). The combined organic phases were washed with brine (3 × 50 mL) and dried over Na_2SO_4. Concentration in vacuo and lyophilization from dioxane gave 11 (0.382 g, 0.785 mmol, 88%) as a white solid.

2-Amino-1-(phenylsulfonamido)ethylphosphinic Acid (12). A solution of piperidine (20%) in DMF (v/v, 50 mL) was added to 11 (0.672 g, 1.38 mmol) and the mixture stirred at RT for 2 h. Concentration in vacuo and purification by RP-HPLC and lyophilization gave 12 (0.253 g, 0.96 mmol, 69%) as a white solid.

2-[N-(Benzyloxycarbonyl)piperidin-4-yl]ethanol (13). Benzyl chloroformate (Cbz-Cl, 6.05 mL, 42.38 mmol) was added to a solution of 2-(piperidin-4-yl)ethanol (5.00 g, 38.7 mmol) in a dioxane/aqueous 10% Na_2CO_3 mixture (1:1, 250 mL) and the mixture stirred at RT for 1 h. The reaction mixture was concentrated in vacuo and the residue dissolved with ethyl acetate (100 mL). The organic phase was washed with aqueous saturated $NaHCO_3$ (2 × 50 mL), aqueous HCl (1 M, 2 × 50 mL), and brine (1 × 50 mL). Drying over $MgSO_4$ was followed by column chromatography (silica gel, 5:1 ethyl acetate/hexane) to give 13 (7.46 g, 28.2 mmol, 73%) as a colorless liquid.

Methyl 4-[2-N-(Benzyloxycarbonyl)piperidin-4-ylethyloxy]benzoate (14). 13 (1.17 g, 4.43 mmol) was added to a solution of methyl 4-hydroxybenzoate (0.62 g, 4.08 mmol) and tributylphosphine (1.31 mL, 5.25 mmol) in THF (dry, 40 mL) at 0 °C under an argon atmosphere. A solution of 1,1'-(azodicarbonyl)dipiperidine (ADDP, 1.32 g, 5.23 mmol) in THF (dry, 15 mL) was added within 5 h by the help of a syringe pump, and the reaction mixture was stirred at RT for 16 h.[20,21] The white precipitate was removed by filtration and destroyed. The filtrate was concentrated in vacuo and the residue dissolved in ethyl acetate (100 mL). The organic phase was washed with saturated aqueous Na_2CO_3 (3 × 50 mL), dried over $MgSO_4$, and concentrated in vacuo. Purification by column chromatography (silica gel, 1:2 ethyl acetate/hexane) and crystallization from methanol gave 14 (1.39 g, 3.50 mmol, 86%) as a white solid.[15]

4-[2-N-(Benzyloxycarbonyl)piperidin-4-ylethyloxy]benzoic Acid (15). Aqueous NaOH (1 M, 100 mL) was added to a solution of 14 (0.50 g, 1.26 mmol) in ethanol (100 mL) and stirred at RT for 16 h. The reaction mixture was concentrated in vacuo, and the residue

was dissolved in water (100 mL) and acidified (pH 1) with HCl (12 M, 10 mL). A white precipitate formed, which was extracted with ethyl acetate (3 × 100 mL). The combined organic phases were washed with brine (1 × 100 mL) and dried over $MgSO_4$. Concentration in vacuo and lyophilization from dioxane gave 15 (0.47 g, 1.23 mmol, 97%) as a white solid.[15]

2-({4-[2-N-(Benzyloxycarbonyl)piperidin-4-yl]ethoxy}benzamido)-1-(phenylsulfonamido)ethylphosphinic Acid (16). HATU (168 mg, 0.442 mmol), 15 (170 mg, 0.443 mmol), and DIEA (452 μL, 2.66 mmol) were dissolved in DMF (dry, 10 mL), and the mixture was stirred at RT for 15 min. A solution of 12 (117 mg, 0.443 mmol) in DMF (dry, 3 mL) was added and the mixture stirred at RT for 16 h. Concentration in vacuo and purification by RP-HPLC gave 16 (234 mg, 0.372 mmol, 84%) as a white solid.

2-({4-[2-N-(Benzyloxycarbonyl)piperidin-4-yl]ethoxy}benzamido)-1-(phenylsulfonamido)ethylphosphonic Acid (17). N,O-Bis(trimethylsilyl)acetamide (BSA, 98 μL, 0.400 mmol) was added to a solution of 16 (10.1 mg, 0.016 mmol) in DCM (5 mL) and the mixture stirred at RT for 1 h under an ambient atmosphere. Concentration in vacuo, purification by semipreparative HPLC, and lyophilization gave 17 (9.68 mg, 0.015 mmol, 93%) as a white solid.

Methyl 2-(4-{2-[1-(Benzyloxycarbonyl)piperidin-4-yl]ethoxy}benzamido)-1-(phenylsulfonamido)ethylphosphonate (18). EDC·HCl (25.8 mg, 0.134 mmol) and DMAP (8.3 mg, 0.068 mmol) were added to a solution of 17 (21.7 mg, 0.034 mmol) in methanol (dry, 5 mL), and the mixture was stirred at RT for 2 h. Concentration in vacuo and purification via semipreparative RP-HPLC gave 18 (17.4 mg, 0.026 mmol, 78%) as a white solid.

Integrin Binding Assay (Fibrinogen–αIIbβ3 Assay). The inhibiting activity of the integrin antagonists was determined in a solid-phase binding assay using coated extracellular matrix protein fibrinogen and soluble αIIbβ3 integrin.[26] The assay was based on a previously reported method with some modifications.[27] Flat-bottom 96-well ELISA plates (BRAND, Wertheim, Germany) were coated overnight at 4 °C with 100 μL of 10 μg/mL fibrinogen per well (Calbiochem, Darmstadt, Germany) in carbonate buffer [15 mM Na_2CO_3 and 35 mM $NaHCO_3$ (pH 9.6)]. Wells were then washed three times with PBST buffer [137 mM NaCl, 2.7 mM KCl, 10 mM Na_2HPO_4, 2 mM KH_2PO_4, and 0.01% Tween 20 (pH 7.4)] and blocked for 1 h at room temperature with 150 μL of TSB buffer [20 mM Tris-HCl, 150 mM NaCl, 1 mM $CaCl_2$, 1 mM $MgCl_2$, 1 mM $MnCl_2$ (pH 7.5), and 1% BSA] per well. After being washed three times with PBST, equal amounts of controls (tirofiban, Sigma-Aldrich) or test compounds were mixed with 5.0 μg/mL human integrin αIIbβ3 (Enzyme Research Laboratory, Swansea, U.K.), resulting in a final TSB buffer dilution of 0.00013 to 10 μM for the inhibitors and 2.5 μg/mL for integrin αIIbβ3; 100 μL of these solutions was incubated per well for 1 h at room temperature. The plate was washed three times with PBST buffer, and 100 μL of 2.0 μg/mL primary antibody (mouse anti-human CD41b, BD Biosciences, Heidelberg, Germany) per well was added to the plate. After incubation for 1 h at room temperature, the plate was washed three times with PBST, and 100 μL of 1.0 μg/mL secondary peroxidase-labeled antibody (anti-mouse IgG-POD, Sigma-Aldrich) per well was added to the plate and the plate incubated for 1 h at room temperature. After the plate had been washed three times with PBST, the plate was developed by addition of 50 μL of SeramunBlau fast (Seramun Diagnostic GmbH, Heidesee, Germany) per well and incubated for 5 min at room temperature. The reaction was stopped with 50 μL of 3 M H_2SO_4 per well, and the absorbance was measured at 450 nm with a plate reader (POLARstar Galaxy, BMG Labtechnologies). Each compound concentration was tested in duplicate, and the resulting inhibition curves were analyzed using OriginPro version 7.5G; the inflection point describes the IC_{50} value. Each plate contained tirofiban as an internal control.

In Vitro Permeability Study (Caco-2 test). *Growth and Maintenance of Cells.* Caco-2 cells were obtained from ATCC (Manassas, VA) and then grown in 75 cm[2] flasks with approximately 0.5 × 10^{6} cells/flask at 37 °C in a 5% CO_2 atmosphere at a relative humidity of 95%. The culture growth medium consisted of Dulbecco's modified Eagle's medium (DMEM) supplemented with 10% heat-

inactivated fetal bovine serum (FBS), 1% nonessential amino acids, 2 mM L-glutamine, 2 mM sodium pyruvate, and a 2 mM penicillin/streptomycin solution.

Preparation of Cells. For transport studies, cells in a passage range of 52–60 were seeded at a density of 25×10^5 cells/cm^2 on untreated culture inserts of a polycarbonate membrane with 0.4 μm pores and a surface area of 1.1 cm^2. The culture inserts containing the Caco-2 monolayer were placed in 24 transwell plates (12 mm, Costar). The culture medium was changed every other day. Transport studies were performed 21–23 days after seeding, when the cells were fully differentiated and the TEER values were stable (300–500 Ω cm^2).

Caco-2 Assay. The transport study (apical to basolateral, A to B) was initiated by removal of medium from both sides of the monolayer and replacement with apical buffer (600 μL) and basolateral buffer (1500 μL), both warmed to 37 °C. The cells were incubated for 30 min at 37 °C with shaking (100 cycles/min). After the incubation period, the buffers were removed and replaced with 1500 μL of basolateral buffer at the basolateral side. Test solutions were preheated to 37 °C and added (600 μL) to the apical side of the monolayer; 50 μL samples were taken from the apical side immediately at the beginning of the experiment, resulting in an apical volume of 550 μL during the experiment. For the period of the experiment, cells were kept at 37 °C with shaking. At predetermined times (30, 60, 90, 120, and 150 min), 200 μL samples were taken from the basolateral side and replaced with the same volume of fresh basolateral buffer to maintain a constant volume. A mass balance was performed for each tested compound to detect instability and/or nonspecific binding of the peptides. For the basolateral to apical study (B to A), compounds were placed in the basolateral chamber, followed by sampling of the apical side, in the same manner used for the A to B protocol.

Blood Samples. Venous blood was collected from a healthy volunteer who had refrained from taking any medication affecting platelet function for the two preceding weeks. Blood was drawn by peripheral venipuncture into 4.5 mL plastic tubes containing recombinant hirudin as an anticoagulant (specified final concentration of 25 μg/mL of blood). Measurements were performed 0.5–4 h after venipuncture.

Platelet Aggregation Assay. Platelet aggregation in hirudin-anticoagulated whole blood with thrombin receptor-activating peptide (TRAP-6, final concentration of 33 μM) as an activator was measured using an impedance-based multiple-electrode platelet aggregometer (Multiplate, Dynabyte Informationssysteme GmbH, Munich, Germany)[28,29] according to the manufacturer's instructions, i.e., at 37 °C, minicuvettes with 175 μL of blood, 175 μL of isotonic saline, and 12 μL of TRAP-6 reagent (1 mM). The only modification was the use of a serial saline dilution of integrin inhibitors instead of pure saline. The increase in electrical impedance was recorded for 6 min and transformed into arbitrary aggregation units, and the area under the curve (AUC) was calculated. Reported AUC values represent the average from two electrode pairs per cuvette. Inhibition curves were analyzed using OriginPro version 7.5G; the inflection point indicates the half-maximal effective concentration (EC$_{50}$).

Protonation State Calculations. The estimation of pK_a values of compounds 1–4 was conducted using the calculator plugin Marvin 5.3, 2010, from ChemAxon (http://www.chemaxon.com). The estimation is computed through an algorithm that uses the empirically calculated atomic charges for each protonation state of a subset of molecules.[46] Each atom of the query molecule is identified in one of the atom's subsets, and via the algorithm, the pK_a is finally calculated. The concentration of the different microspecies formed by a molecule at a given pH is predicted using the distribution coefficient (D), calculated using the previously computed pK_a values.[47]

Molecular Electrostatic Potential Calculations. For tirofiban (6) and compounds 1–4, the electrostatic potential was calculated by means of Gaussian03 and mapped onto the electron density surface for each compound. The isovalue of 0.0004 electron/Bhor^3 was chosen for the definition of the density surface, while the electrostatic potential was computed at the Hartree–Fock level of theory using the 6-31G* basis set with a scale of −294.178 (red) to 294.178 (blue) $K_b T/e_c$. The electrostatic potential of the αIIbβ3 receptor was calculated using the parm99 Amber force field[48,49] through apbs, which is an adaptive Poisson–Boltzmann solver.[50]

Docking Simulations. *Redocking Experiment.* The reliability of AutoDock for this system was assessed through the redocking of the αIIbβ3 cocrystallized ligand, tirofiban (PDB entry 2vdm). The X-ray binding conformation of tirofiban has been clearly predicted by AutoDock among the poses with the best scoring function values (Figure 3A). One may notice that for tirofiban the (S)-enantiomer is the bioactive one, while for the phosphorus-containing compounds, because of the change in priority according to the Cahn–Ingold–Prelog rules, the (R)-enantiomers are the bioactive ones. Molecular docking calculations for tirofiban and compounds 1–4 were conducted using the three-dimensional X-ray structure of αIIbβ3 in the apo form (PDB entry 2vdm) through AutoDock (version 4.0).[36,37] The apo form of αIIbβ3 was obtained via removal of tirofiban from the X-ray complex.

Ligand Setup. The structures of the inhibitors were first generated using the PRODRG server.[51] Then the ligands and the protein were charged using the Gasteiger partial charge[52] and converted to AutoDock format files using AutoDockTools (ADT 1.5.4).

Docking Setup. The docking area was defined by a box, centered approximately on the center of mass of tirofiban cocrystallized with the protein. Grid points (60 × 60 × 60) with 0.375 Å spacing were calculated around the docking area for all the ligand atom types using AutoGrid4. For each ligand, 100 separate docking calculations were performed. Each docking calculation consisted of 2.5×10^6 energy evaluations using the Lamarckian genetic algorithm local search (GALS) method. Otherwise, default docking parameters were applied. The docking conformations were clustered on the basis of the root-mean-square deviation (rmsd of 2 Å) calculated for the Cartesian coordinates of the ligand atoms and then were ranked on the basis of AutoDock scoring function. The binding mode figures were generated using PyMOL (http://www.pymol.org), while the molecular electrostatic potential surfaces were rendered using GaussView.

■ ASSOCIATED CONTENT

ⓢ Supporting Information

Analytical data of compounds 7–18, HPLC enantiomer separation, ^{31}P NMR titration of compounds 1–4, docking of molecular probes (R)-3 and (R)-4, docking of (S)-enantiomers, and supporting figures. This material is available free of charge via the Internet at http://pubs.acs.org.

■ AUTHOR INFORMATION

Corresponding Author

*Institute for Advanced Study and Center of Integrated Protein Science, Department Chemie, Technische Universität München, Lichtenbergstrasse 4, 85747 Garching, Germany. Phone: +49 (0) 89 289 13300. Fax: +49 (0) 89 289 13210. E-mail: kessler@tum.de.

■ ACKNOWLEDGMENTS

■ ABBREVIATIONS

ADAMs, disintegrin and metalloprotease; AUC, area under the curve; CIP, Cahn–Ingold–Prelog; DMAP, 4-(dimethylamino)-pyridine; ECM, extracellular matrix; EDC, N-[3-(dimethylamino)propyl]-N′-ethylcarbodiimide; ELISA, enzyme-linked immunosorbent assay; FMD, foot-and-mouth disease; HATU, O-(7-azabenzotriazol-1-yl)-N,N,N′,N′-tetrame-

thyluronium hexafluorophosphate; IBX, *o*-iodoxybenzoic acid; MIDAS, metal ion-dependent adhesion site; RGD, arginine-glycine-aspartic acid

■ REFERENCES

(1) Meyer, A.; Auernheimer, J.; Modlinger, A.; Kessler, H. Targeting RGD recognizing integrins: Drug development, biomaterial research, tumor imaging and targeting. *Curr. Pharm. Des.* **2006**, *12*, 2723−2747.

(2) Mousa, S. A. Anti-integrin as novel drug-discovery targets: Potential therapeutic and diagnostic implications. *Curr. Opin. Chem. Biol.* **2002**, *6*, 534−541.

(3) Humphries, M. J. Integrin structure. *Biochem. Soc. Trans.* **2000**, *28*, 311−339.

(4) Arnaout, M. A.; Mahalingam, B.; Xiong, J. P. Integrin structure, allostery, and bidirectional signaling. *Annu. Rev. Cell Dev. Biol.* **2005**, *21*, 381−410.

(5) Hynes, R. O. Integrins: Bidirectional, allosteric signaling machines. *Cell* **2002**, *110*, 673−687.

(6) Humphries, J. D.; Byron, A.; Humphries, M. J. Integrin ligands at a glance. *J. Cell Sci.* **2006**, *119*, 3901−3903.

(7) Ruoslahti, E. RGD and other recognition sequences for integrins. *Annu. Rev. Cell Dev. Biol.* **1996**, *12*, 697−715.

(8) Heckmann, D.; Laufer, B.; Marinelli, L.; Limongelli, V.; Novellino, E.; Zahn, G.; Stragies, R.; Kessler, H. Breaking the dogma of the metal-coordinating carboxylate group in integrin ligands: Introducing hydroxamic acids to the MIDAS to tune potency and selectivity. *Angew. Chem., Int. Ed.* **2009**, *48*, 4436−4440.

(9) Cox, D.; Brennan, M.; Moran, N. Integrins as therapeutic targets: Lessons and opportunities. *Nat. Rev. Drug Discovery* **2010**, *9*, 804−820.

(10) Mas-Moruno, C.; Rechenmacher, F.; Kessler, H. Cilengitide: The first anti-angiogenic small molecule drug candidate. Design, synthesis and clinical evaluation. *Anti-Cancer Agents Med. Chem.* **2011**, *10*, 753−768.

(11) Shimaoka, M.; Springer, T. A. Therapeutic antagonists and conformational regulation of integrin function. *Nat. Rev. Drug Discovery* **2003**, *2*, 703−716.

(12) Hartman, G. D.; Egbertson, M. S.; Halczenko, W.; Laswell, W. L.; Duggan, M. E.; Smith, R. L.; Naylor, A. M.; Manno, P. D.; Lynch, R. J.; Zhang, G.; Chang, C. T.-C.; Gould, R. J. Non-peptide fibrinogen receptor antagonists. 1. Discovery and design of exosite inhibitors. *J. Med. Chem.* **1992**, *35*, 4640−4642.

(13) Topol, E. J.; Moliterno, D. J.; Herrmann, H. C.; Powers, E. R.; Grines, C. L.; Cohen, D. J.; Cohen, E. A.; Bertrand, M.; Neumann, F. J.; Stone, G. W.; DiBattiste, P. M.; Demopoulos, L. Comparison of two platelet glycoprotein IIb/IIIa inhibitors, tirofiban and abciximab, for the prevention of ischemic events with percutaneous coronary revascularization. *N. Engl. J. Med.* **2001**, *344*, 1888−1894.

(14) Cannon, C. P.; Weintraub, W. S.; Demopoulos, L. A.; Vicari, R.; Frey, M. J.; Lakkis, N.; Neumann, F. J.; Robertson, D. H.; DeLucca, P. T.; DiBattiste, P. M.; Gibson, C. M.; Braunwald, E. Comparison of early invasive and conservative strategies in patients with unstable coronary syndromes treated with the glycoprotein IIb/IIIa inhibitor tirofiban. *N. Engl. J. Med.* **2001**, *344*, 1879−1887.

(15) Duggan, M. E.; Duong, L. T.; Fisher, J. E.; Hamill, T. G.; Hoffman, W. F.; Huff, J. R.; Ihle, N. C.; Leu, C. T.; Nagy, R. M.; Perkins, J. J.; Rodan, S. B.; Wesolowski, G.; Whitman, D. B.; Zartman, A. E.; Rodan, G. A.; Hartman, G. D. Nonpeptide $\alpha_v\beta_3$ antagonists. 1. Transformation of a potent, integrin-selective $\alpha_{IIb}\beta_3$ antagonist into a potent $\alpha_v\beta_3$ antagonist. *J. Med. Chem.* **2000**, *43*, 3736−3745.

(16) Frigerio, M.; Santagostino, M.; Sputore, S. A user-friendly entry to 2-iodoxybenzoic acid (IBX). *J. Org. Chem.* **1999**, *64*, 4537−4538.

(17) Frigerio, M.; Santagostino, M. A mild oxidizing reagent for alcohols and 1,2-diols: o-Iodoxybenzoic acid (IBX) in DMSO. *Tetrahedron Lett.* **1994**, *35*, 8019−8022.

(18) Liboska, R.; Pícha, J.; Hanclová, I.; Budešínský, M.; Sanda, M.; Jiráček, J. Synthesis of methionine- and norleucine-derived phosphinopeptides. *Tetrahedron Lett.* **2008**, *49*, 5629−5631.

(19) Zhukov, Y. N.; Khomutov, A. R.; Osipova, T. I.; Khomutov, R. M. Synthesis of phosphinic analogs of sulfur-containing amino acids. *Russ. Chem. Bull.* **1999**, *48*, 1348−1351.

(20) Heckmann, D.; Meyer, A.; Laufer, B.; Zahn, G.; Stragies, R.; Kessler, H. Rational design of highly active and selective ligands for the $\alpha 5\beta 1$ integrin receptor. *ChemBioChem* **2008**, *9*, 1397−1407.

(21) Marugán, J. J.; Manthey, C.; Anaclerio, B.; Lafrance, L.; Lu, T.; Markotan, T.; Leonard, K. A.; Crysler, C.; Eisennagel, S.; Dasgupta, M.; Tomczuk, B. Design, synthesis, and biological evaluation of novel potent and selective $\alpha_v\beta_3/\alpha_v\beta_5$ integrin dual inhibitors with improved bioavailability. Selection of the molecular core. *J. Med. Chem.* **2005**, *48*, 926−934.

(22) Hoffmann, C. V.; Pell, R.; Lämmerhofer, M.; Lindner, W. Synergistic effects on enantioselectivity of zwitterionic chiral stationary phases for separations of chiral acids, bases, and amino acids by HPLC. *Anal. Chem.* **2008**, *80*, 8780−8789.

(23) Hoffmann, C. V.; Reischl, R.; Maier, N. M.; Lämmerhofer, M.; Lindner, W. Stationary phase-related investigations of quinine-based zwitterionic chiral stationary phases operated in anion-, cation-, and zwitterion-exchange modes. *J. Chromatogr., A* **2009**, *1216*, 1147−1156.

(24) Maier, N. M.; Schefzick, S.; Lombardo, G. M.; Feliz, M.; Rissanen, K.; Lindner, W.; Lipkowitz, K. B. Elucidation of the chiral recognition mechanism of cinchona alkaloid carbamate-type receptors for 3,5-dinitrobenzoyl amino acids. *J. Am. Chem. Soc.* **2002**, *124*, 8611−8629.

(25) Lämmerhofer, M.; Hebenstreit, D.; Gavioli, E.; Lindner, W.; Mucha, A.; Kafarski, P.; Wieczorek, P. High-performance liquid chromatographic enantiomer separation and determination of absolute configurations of phosphinic acid analogues of dipeptides and their α-aminophosphinic acid precursors. *Tetrahedron: Asymmetry* **2003**, *14*, 2557−2565.

(26) Mas-Moruno, C.; Beck, J. G.; Doedens, L.; Frank, A. O.; Marinelli, L.; Cosconati, S.; Novellino, E.; Kessler, H. Increasing $\alpha v\beta 3$ selectivity of the anti-angiogenic drug cilengitide by N-methylation. *Angew. Chem., Int. Ed.* **2011**, *50*, 9496−9500.

(27) Chatterjee, J.; Ovadia, O.; Zahn, G.; Marinelli, L.; Hoffman, A.; Gilon, C.; Kessler, H. Multiple N-methylation by a designed approach enhances receptor selectivity. *J. Med. Chem.* **2007**, *50*, 5878−5881.

(28) Tóth, O.; Calatzis, A.; Penz, S.; Losonczy, H.; Siess, W. Multiple electrode aggregometry: A new device to measure platelet aggregation in whole blood. *Thromb. Haemostasis* **2006**, *96*, 781−788.

(29) Halimeh, S.; Angelis, G.; Sander, A.; Edelbusch, C.; Rott, H.; Thedieck, S.; Mesters, R.; Schlegel, N.; Nowak-Gottl, U. Multiplate whole blood impedance point of care aggregometry: Preliminary reference values in healthy infants, children and adolescents. *Klin. Paediatr.* **2010**, *222*, 158−163.

(30) Artursson, P.; Karlsson, J. Correlation between oral drug absorption in humans and apparent drug permeability coefficients in human intestinal epithelial (Caco-2) cells. *Biochem. Biophys. Res. Commun.* **1991**, *175*, 880−885.

(31) Kelley, J. L.; McLean, E. W.; Crouch, R. C.; Averett, D. R.; Tuttle, J. V. [[(Guaninylalkyl)phosphinico]methyl]phosphonic acids. Multisubstrate analogue inhibitors of human erythrocyte purine nucleoside phosphorylase. *J. Med. Chem.* **1995**, *38*, 1005−1014.

(32) Manzenrieder, F.; Frank, A. O.; Kessler, H. Phosphorus NMR spectroscopy as a versatile tool for compound library screening. *Angew. Chem., Int. Ed.* **2008**, *47*, 2608−2611.

(33) Stirtan, W. G.; Withers, S. G. Phosphonate and α-fluorophosphonate analogue probes of the ionization state of pyridoxal 5′-phosphate (PLP) in glycogen phosphorylase. *Biochemistry (Moscow, Russ. Fed.)* **1996**, *35*, 15057−15064.

(34) Selvam, C.; Goudet, C.; Oueslati, N.; Pin, J. P.; Acher, F. C. L-(+)-2-Amino-4-thiophosphonobutyric acid (L-thioAP4), a new potent agonist of group III metabotropic glutamate receptors: Increased distal acidity affords enhanced potency. *J. Med. Chem.* **2007**, *50*, 4656−4664.

(35) Castellino, S.; Leo, G. C.; Sammons, R. D.; Sikorski, J. A. ^{31}P, ^{15}N, and ^{13}C NMR of glyphosate: Comparison of pH titrations to the herbicidal dead-end complex with 5-enolpyruvoylshikimate-3-phos-

phate synthase. *Biochemistry (Moscow, Russ. Fed.)* **1989**, *28*, 3856–3868.

(36) Morris, G. M.; Goodsell, D. S.; Halliday, R. S.; Huey, R.; Hart, W. E.; Belew, R. K.; Olson, A. J. Automated docking using a Lamarckian genetic algorithm and an empirical binding free energy function. *J. Comput. Chem.* **1998**, *19*, 1639–1662.

(37) Huey, R.; Morris, G. M.; Olson, A. J.; Goodsell, D. S. A semiempirical free energy force field with charge-based desolvation. *J. Comput. Chem.* **2007**, *28*, 1145–1152.

(38) Jones, G.; Willett, P.; Glen, R. C.; Leach, A. R.; Taylor, R. Development and validation of a genetic algorithm for flexible docking. *J. Mol. Biol.* **1997**, *267*, 727–748.

(39) Rarey, M.; Kramer, B.; Lengauer, T.; Klebe, G. A fast flexible docking method using an incremental construction algorithm. *J. Mol. Biol.* **1996**, *261*, 470–489.

(40) Gohlke, H.; Hendlich, M.; Klebe, G. Knowledge-based scoring function to predict protein-ligand interactions. *J. Mol. Biol.* **2000**, *295*, 337–356.

(41) Oelschlaeger, P.; Klahn, M.; Beard, W. A.; Wilson, S. H.; Warshel, A. Magnesium-cationic dummy atom molecules enhance representation of DNA polymerase β in molecular dynamics simulations: Improved accuracy in studies of structural features and mutational effects. *J. Mol. Biol.* **2007**, *366*, 687–701.

(42) Rucker, R.; Oelschlaeger, P.; Warshel, A. A binding free energy decomposition approach for accurate calculations of the fidelity of DNA polymerases. *Proteins* **2010**, *78*, 671–680.

(43) Xiang, Y.; Oelschlaeger, P.; Florian, J.; Goodman, M. F.; Warshel, A. Simulating the effect of DNA polymerase mutations on transition-state energetics and fidelity: Evaluating amino acid group contribution and allosteric coupling for ionized residues in human Pol β. *Biochemistry (Moscow, Russ. Fed.)* **2006**, *45*, 7036–7048.

(44) Gottlieb, H. E.; Kotlyar, V.; Nudelman, A. NMR chemical shifts of common laboratory solvents as trace impurities. *J. Org. Chem.* **1997**, *62*, 7512–7515.

(45) Porcheddu, A.; Giacomelli, G.; Piredda, I.; Carta, M.; Nieddu, G. A practical and efficient approach to PNA monomers compatible with Fmoc-mediated solid-phase synthesis protocols. *Eur. J. Org. Chem.* **2008**, *2008*, 5786–5797.

(46) Dixon, S. L.; Jurs, P. C. Estimation of pKa for organic oxyacids using calculated atomic charges. *J. Comput. Chem.* **1993**, *14*, 1460–1467.

(47) Csizmadia, F.; Tsantili-Kakoulidou, A.; Panderi, I.; Darvas, F. Prediction of distribution coefficient from structure. 1. Estimation method. *J. Pharm. Sci.* **1997**, *86*, 865–871.

(48) Cornell, W. D.; Cieplak, P.; Bayly, C. I.; Gould, I. R.; Merz, K. M.; Ferguson, D. M.; Spellmeyer, D. C.; Fox, T.; Caldwell, J. W.; Kollman, P. A. A second generation force field for the simulation of proteins, nucleic acids, and organic molecules. *J. Am. Chem. Soc.* **1995**, *117*, 5179–5197.

(49) Wang, J.; Cieplak, P.; Kollman, P. A. How well does a restrained electrostatic potential (RESP) model perform in calculating conformational energies of organic and biological molecules? *J. Comput. Chem.* **2000**, *21*, 1049–1074.

(50) Baker, N. A.; Sept, D.; Joseph, S.; Holst, M. J.; McCammon, J. A. Electrostatics of nanosystems: Application to microtubules and the ribosome. *Proc. Natl. Acad. Sci. U.S.A.* **2001**, *98*, 10037–10041.

(51) Schüttelkopf, A. W.; van Aalten, D. M. F. PRODRG: A tool for high-throughput crystallography of protein-ligand complexes. *Acta Crystallogr.* **2004**, *D60*, 1355–1363.

(52) Gasteiger, J.; Marsili, M. Iterative partial equalization of orbital electronegativity: A rapid access to atomic charges. *Tetrahedron* **1980**, *36*, 3219–3228.

Supporting Information

Tailoring of Integrin Ligands: Probing the Charge Capability of the Metal-Ion-Dependent Adhesion Site

Markus Bollinger,[1] Florian Manzenrieder,[1] Roman Kolb,[1] Alexander Bochen,[1] Stefanie Neubauer,[1] Luciana Marinelli,[2] Vittorio Limongelli,[2] Ettore Novellino,[2] Georg Moessmer,[3] Reinhard Pell,[4] Wolfgang Lindner,[4] Joseph Fanous,[5] Amnon Hoffman[5] and Horst Kessler[1,6*]

[1] *Institute for Advanced Study and Center of Integrated Protein Science, Department Chemie, Technische Universität München, Lichtenbergstrasse 4, 85747 Garching, Germany.*

[2] *Dipartimento di Chimica Farmaceutica e Tossicologica, Università di Napoli "Federico II", Via D. Montesano, 49-80131 Napoli, Italy.*

[3] *Institut für Klinische Chemie und Pathobiochemie, Klinikum rechts der Isar, Technische Universität München, Ismaninger Strasse 22, 81675 München, Germany.*

[4] *Institute of Analytical Chemistry, University of Vienna, Währinger Strasse 38, A-1090 Vienna, Austria.*

[5] *School of Pharmacy, Faculty of Medicine, The Hebrew University of Jerusalem, POB 12065, Jerusalem 91120, Israel.*

[6] *Chemistry Department, Faculty of Science, King Abdulaziz University, P.O. Box 80203, Jeddah 21589, Saudi Arabia.*

Table of Contents

Analytical data of compounds 7-18

(9*H*-Fluoren-9-yl)methyl (2-hydroxyethyl)carbamate (7).

MS (ESI): $^m/_z$ = 179.2 [Fmoc-CO$_2$]$^+$, 284.1 [M+H]$^+$, 306.2 [M+Na]$^+$; RP-HPLC: t_R = 20.0 min (10-90% in 30 min); HRMS (ESI): $^m/_z$ calcd for C$_{17}$H$_{17}$NO$_3$Na: 306.1106 [M+Na]$^+$, found: 306.1101.

(9*H*-Fluoren-9-yl)methyl (2-oxoethyl)carbamate (8).

MS (ESI): $^m/_z$ = 179.2 [Fmoc-CO$_2$]$^+$, 282.0 [M+H]$^+$; RP-HPLC: t_R = 19.57 min (10-90% in 30 min); HRMS (ESI): $^m/_z$ calcd for C$_{17}$H$_{16}$NO$_3$: 282.1230 [M+H]$^+$, found: 282.1125.

(9*H*-Fluoren-9-yl)methyl [2-(hydroxyimino)ethyl]carbamate (9).

TLC: R_f = 0.7 (ethyl acetate/hexane = 3:1) [UV]; ^{1}H NMR (500 MHz, DMSO-d$_6$, RT): δ (ppm) = 11.06 (s, 1 H, C$H^{\alpha E/Z}$), 10.73 (s, 1 H, C$H^{\alpha E/Z}$), 7.89 (d, ^3J = 7.6 Hz, 2 H), 7.69 (d, ^3J = 7.6 Hz, 2 H), 7.42 (t, ^3J = 7.6 Hz, 2 H), 7.33 (t, ^3J = 6.9 Hz, 2 H), 6.58 (t, ^3J = 3.9 Hz, 1 H), 4.35 (d, ^3J = 6.8 Hz, 1 H), 4.31 (d, ^3J = 6.9 Hz, 1 H), 4.23 (m, 1 H), 3.82 (dd, ^3J = 5.6 Hz, ^3J = 4.0 Hz, 2 H), 3.71 (t, ^3J = 5.6 Hz, 2 H), 3.33 (br. s, 1 H); ^{13}C NMR (126 MHz, DMSO-d$_6$, RT): δ (ppm) = 156.2, 149.2, 146.5, 143.8, 140.7, 127.6, 127.0, 125.1, 120.1, 65.5, 46.7, 36.4; MS (ESI): $^m/_z$ = 179.2 [Fmoc-CO$_2$]$^+$, 297.0 [M+H]$^+$; RP-HPLC: t_R = 21.6 (**9**), 19.9 (**8**, decomposition of **9** with TFA) (10-90% in 30 min).

2-[*N*-((9*H*-Fluoren-9-yl)methoxy)carbonylamino)]-1-aminoethyl phosphinic acid (10).

^{1}H NMR (500 MHz, DMSO-d$_6$, RT): δ (ppm) = 8.09 (br. s, 2 H), 7.89 (d, ^3J = 7.4 Hz, 2 H), 7.69 (d, ^3J = 7.4 Hz, 2 H), 7.42 (t, ^3J = 7.4 Hz, 2 H), 7.33 (t, ^3J = 7.4 Hz, 2 H), 7.01 (d, ^3J = 520 Hz, 1 H), 4.32 (d, ^3J = 6.8 Hz, 2 H), 4.23 (d, ^3J = 6.8 Hz, 1 H), 3.43 (m, 1 H), 3.32 (m, 1 H), 3.00 (m, 1 H); ^{13}C NMR (126 MHz, DMSO-d$_6$, RT): δ (ppm) = 156.2, 143.8, 140.7, 127.6, 127.1, 125.1, 120.1, 65.7, 49.7 (d, $^1J_{PC}$ = 83.2 Hz), 46.6, 38.5; ^{31}P NMR (101 MHz, DMSO-d$_6$, RT): δ (ppm) = 12.2; MS (ESI): $^m/_z$ = 179.2 [Fmoc-CO$_2$]$^+$, 347.0 [M+H]$^+$, 369.3 [M+Na]$^+$, 693.0 [2M+H]$^+$, 715.0 [2M+Na]$^+$, 731.1 [2M+K]$^+$, 1039.0 [3M+H]$^+$, 1061.0 [3M+Na]$^+$, 1077.0 [3M+K]$^+$; RP-HPLC: t_R = 15.4 min (10-90% in 30 min); HRMS (ESI): $^m/_z$ calcd for C$_{17}$H$_{20}$N$_2$O$_4$P: 347.1161 [M+H]$^+$, found: 347.1155.

2-[*N*-((9*H*-Fluoren-9-yl)methoxy)carbonylamino)]-1-(phenylsulfonamido)ethyl phosphinic acid (11).

^{1}H NMR (500 MHz, DMSO-d_6, RT): δ (ppm) = 8.03 (br. d, ^3J = 7.5 Hz, 1 H), 7.89 (d, ^3J = 7.5 Hz, 2 H), 7.81 (d, ^3J = 7.5 Hz, 2 H), 7.66 (d, ^3J = 7.4 Hz, 2 H), 7.56 (t, ^3J = 7.4 Hz, 1 H), 7.50 (t, ^3J = 7.4 Hz, 2 H), 7.42 (t, ^3J = 7.5 Hz, 2 H), 7.33 (t, ^3J = 7.5 Hz, 2 H), 7.01 (t, ^3J = 5.3 Hz, 1 H), 6.78 (d, ^1J = 535 Hz, 1 H), 4.17-4.13 (m, 2 H), 4.12-4.05 (m, 1 H), 3.53-3.42 (m, 1 H), 3.29-3.16 (m, 1 H), 3.07-2.96 (m, 1 H); ^{13}C NMR (126 MHz, DMSO-d_6, RT): δ (ppm) = 155.6, 143.7, 141.2, 140.6, 132.2, 128.9, 127.5, 127.0, 126.3, 125.1, 119.9, 65.5, 46.5, 38.6 (C$^\alpha$ n.o.); ^{31}P NMR (101 MHz, DMSO-d_6, RT): δ (ppm) = 23.9; MS (ESI): $^m/_z$ = 179.3 [Fmoc-CO$_2$]$^+$, 487.3 [M+H]$^+$, 509.4 [M+Na]$^+$, 973.1 [2M+H]$^+$, 995.0 [2M+Na]$^+$, 1011.1 [2M+K]$^+$, 1458.7 [3M+H]$^+$, 1480.7 [3M+Na]$^+$, 1497.8 [3M+K]$^+$, 1945.2 [4M+H]$^+$, 1967.5 [4M+Na]$^+$, 1983.5 [4M+K]$^+$; RP-HPLC: t_R = 20.5 min (10-90% in 30 min); HRMS (ESI): $^m/_z$ calcd for C$_{23}$H$_{22}$N$_2$O$_6$P^{32}S: 485.0936 [M-H]$^-$, found: 485.0932.

2-Amino-1-(phenylsulfonamido)ethyl)phosphinic acid (12).

^{1}H NMR (500 MHz, MeOD-d_4, RT): δ (ppm) = 7.95 (d, ^3J = 7.4 Hz, 2 H), 7.66 (t, ^3J = 7.4 Hz, 1 H), 7.59 (t, ^3J = 7.4 Hz, 2 H), 6.46 (d, $^1J_{PH}$ = 530 Hz, 1 H), 3.75-3.70 (m, 1 H), 3.29-3.23 (m, 1 H), 3.09-3.00 (m, 1 H); ^{13}C NMR (90 MHz, MeOD-d_4, RT): δ (ppm) = 141.8, 134.2, 130.5, 128.3, 52.5 (d, ^1J = 90.0 Hz), 40.1 (d, ^2J = 4.4 Hz); ^{31}P NMR (101 MHz, DMSO-d_6, RT): δ (ppm) = 15.9; MS (ESI): $^m/_z$ = 265.2 [M+H]$^+$, 529.1 [2M+H]$^+$, 551.1 [2M+Na]$^+$, 792.9 [3M+H]$^+$, 814.9 [3M+Na]$^+$, 1056.8 [4M+H]$^+$; RP-HPLC: t_R = 6.1 min (10-90% in 30 min); HRMS (ESI): $^m/_z$ calcd for C$_8$H$_{14}$N$_2$O$_4$P^{32}S: 265.0412 [M+H]$^+$, found: 265.0407.

2-[*N*-(benzyloxycarbonyl)piperidine-4-yl]ethanol (13).

TLC: R_f = 0.5 (ethyl acetate/hexane = 5:1) [UV]; ^{1}H NMR (360 MHz, CDCl$_3$, RT): δ (ppm) = 7.34-7.30 (m, 4 H), 7.30-7.25 (m, 1 H), 5.08 (s, 2 H), 4.22-4.02 (m, 2 H), 3.63 (t, ^3J = 6.6 Hz, 2 H), 2.83-2.63 (m, 2 H), 2.54 (br. s, 1 H), 1.72-1.61 (m, 2 H), 1.61-1.53 (m, 1 H), 1.46 (dt, ^3J = 6.6 Hz, ^3J = 6.6 Hz, 2 H), 1.17-1.02 (m, 2 H); ^{13}C NMR (91 MHz, CDCl$_3$, RT): δ (ppm) = 155.4, 136.9, 128.5, 128.0, 127.9, 67.1, 60.0, 44.3, 39.2, 32.5, 32.1; MS (ESI): $^m/_z$ = 264.1 [M+H]$^+$; RP-HPLC: t_R = 18.8 min (10-

90% in 30 min); HRMS (ESI): $^m/_z$ calcd for $C_{15}H_{22}NO_3$: 264.1600 [M+H]$^+$, found: 264.1595.

Methyl 4-[2-*N*-(benzyloxycarbonyl)piperidine-4-ylethyl-oxy]benzoate (14).

TLC: R_f = 0.4 (ethyl acetate/hexane = 1:2) [UV]; ^{1}H NMR (360 MHz, CDCl$_3$, RT): δ (ppm) = 7.96 (d, ^3J = 8.9 Hz, 2 H), 7.36-7.31 (m, 4 H), 7.31-7.26 (m, 1 H), 6.87 (d, ^3J = 8.9 Hz, 2 H), 5.11 (s, 2 H), 4.27-4.08 (m, 2 H), 4.02 (t, ^3J = 6.0 Hz, 2 H), 3.85 (s, 3 H), 2.87-2.69 (m, 2 H), 1.78-1.65 (m, 5 H), 1.26-1.09 (m, 2 H); ^{13}C NMR (91 MHz, CDCl$_3$, RT): δ (ppm) = 166.9, 162.8, 155.4, 137.0, 131.7, 128.6, 128.1, 128.0, 122.7, 114.1, 67.1, 65.6, 52.0, 44.2, 35.7, 32.9, 32.1; MS (ESI): $^m/_z$ = 398.2 [M+H]$^+$, 420.4 [M+Na]$^+$, 615.9 [(3M+K+H)/2]$^{2+}$, 1214.0 [3M+Na]$^+$; RP-HPLC: t_R = 29.2 min (10-90% in 30 min); HRMS (ESI): $^m/_z$ calcd for $C_{23}H_{27}NO_5Na^{23}$: 420.1787 [M+Na]$^+$, found: 420.1781.

4-[2-*N*-(benzyloxycarbonyl)piperidine-4-ylethyloxy]-benzoic acid (15).

TLC: R_f = 0.5 (ethyl acetate/hexane = 1:1 + 1 % AcOH) [UV]; ^{1}H NMR (500 MHz, DMSO-d$_6$, RT): δ (ppm) = 12.62 (s, 1 H), 7.87 (d, ^3J = 8.8 Hz, 2 H), 7.40-7.28 (m, 5 H), 7.00 (d, ^3J = 8.8 Hz, 2 H), 5.06 (s, 2 H), 4.07 (t, ^3J = 5.9 Hz, 2 H), 4.03-3.95 (m, 2 H), 2.92-2.67 (m, 2 H), 1.76-1.60 (m, 5 H), 1.16-1.01 (m, 2 H); ^{13}C NMR (91 MHz, DMSO-d$_6$, RT): δ (ppm) = 167.0, 162.2, 154.3, 137.1, 131.3, 128.4, 127.8, 127.5, 122.8, 114.2, 66.0, 65.5, 43.6, 34.9, 32.2, 31.4; MS (ESI): $^m/_z$ = 384.0 [M+H]$^+$, 767.0 [2M+H]$^+$, 789.3 [2M+Na]$^+$, 805.2 [2M+K]$^+$, 1171.8 [3M+Na]$^+$; RP-HPLC: t_R = 24.7 min (10-90% in 30 min); HRMS (ESI): $^m/_z$ calcd for $C_{22}H_{24}NO_5$: 382.1660 [M-H]$^-$, found: 382.1654.

2-{4-[2-*N*-(benzyloxycarbonyl)piperidine-4-yl)ethoxy]-benzamido}-1-(phenylsulfonamido)ethylphosphinic acid (16).

^{1}H NMR (500 MHz, MeOD-d$_4$, RT): δ (ppm) = 7.80 (d, ^3J = 6.9 Hz, 2 H), 7.58 (d, ^3J = 8.9 Hz, 2 H), 7.39-7.26 (m, 8 H), 6.98 (d, ^3J = 567 Hz, 1 H), 6.92 (d, ^3J = 8.9 Hz, 2 H), 5.11 (s, 2 H), 4.19-4.12 (m, 2 H), 4.11 (t, ^3J = 6.0 Hz, 2 H), 3.89-3.82 (m, 1 H), 3.62 (ddd, ^2J = 14.1 Hz, ^3J = 5.2 Hz, ^3J = 5.2 Hz, 1 H), 3.51 (ddd, ^2J = 14.1 Hz, ^3J = 9.6 Hz, ^3J = 8.5 Hz, 1 H), 3.02-2.70 (m, 2 H), 1.88-1.68 (m, 5 H), 1.27-1.09 (m, 2 H); ^{13}C NMR (126 MHz, MeOD-d$_4$, RT): δ (ppm) = 170.3, 163.6, 157.1, 142.3, 138.4, 133.8, 130.5, 130.3, 129.7, 129.2, 129.0, 128.0, 126.9, 115.3, 68.4, 67.0, 54.0 (d,

^1J = 106.5 Hz), 45.5, 38.6 (^2J = 7.0 Hz), 36.8, 34.3, 33.3; ^{31}P NMR (101 MHz, MeOD-d_4, RT): δ (ppm) = 29.1; MS (ESI): $^m/_z$ = 630.1 [M+H]$^+$, 652.2 [2M+H]$^+$, 668.2 [M+K]$^+$, 1259.1 [2M+H]$^+$, 1281.1 [2M+Na]$^+$, 1297.2 [2M+K]$^+$; RP-HPLC: t_R = 22.3 min (10-90% in 30 min); HRMS (ESI): $^m/_z$ calcd for $C_{30}H_{37}N_3O_8P^{32}S$: 630.2039 [M+H]$^+$, found: 630.2034.

2-{4-[2-*N*-(benzyloxycarbonyl)piperidine-4-yl)ethoxy]-benzamido}-1-(phenyl-sulfonamido)ethylphosphonic acid (17).

^{1}H NMR (500 MHz, MeOH-d_3, RT): δ (ppm) = 8.11 (t, ^3J = 5.3 Hz, 2 H), 7.85 (dd, ^3J = 8.2 Hz, ^3J = 1.2 Hz, 2 H), 7.68 (d, ^3J = 9.0 Hz, 2 H), 7.45-7.23 (m, 8 H), 6.93 (d, ^3J = 9.0 Hz, 2 H), 5.10 (s, 2 H), 4.18-4.11 (m, 2 H), 4.10 (t, ^3J = 6.1 Hz, 2 H), 3.88-3.74 (m, 1 H), 3.65 (ddd, ^2J = 9.1 Hz, ^3J = 4.8 Hz, ^3J = 4.8 Hz, 1 H), 3.59-3.48 (m, 1 H), 2.95-2.73 (m, 2 H), 1.87-1.66 (m, 5 H), 1.26-1.09 (m, 2 H); ^{13}C NMR (126 MHz, MeOH-d_3, RT): δ (ppm) = 169.9, 163.3, 157.0, 142.9, 138.3, 133.4, 130.3, 130.0, 129.6, 129.1, 128.9, 128.0, 127.4, 115.2, 68.3, 66.8, 52.5 (d, ^1J = 151.5 Hz), 45.3, 42.0 (d, ^2J = 6.7 Hz), 36.7, 34.2, 33.2; ^{31}P NMR (101 MHz, MeOH-d_3, RT): δ (ppm) = 17.2; MS (EI): $^m/_z$ = 646.1 [M+H]$^+$, 668.2 [M+Na]$^+$, 684.2 [M+K]$^+$, 1291.0 [2M+H]$^+$, 1313.1 [2M+Na]$^+$, 1329.1 [2M+K]$^+$; RP-HPLC: t_R = 21.4 min (10-90% in 30 min); HRMS (ESI): $^m/_z$ calcd for $C_{30}H_{37}N_3O_9P^{32}S$: 646.1988 [M+H]$^+$, found: 646.1986.

Methyl 2-{4-[2-(1-(benzyloxycarbonyl)piperidine-4-yl)-ethoxy]benzamido}-1-(phenylsulfonamido)ethyl-phospho-nate (18).

^{1}H NMR (500 MHz, MeOD-d_4, RT): δ (ppm) = 7.83 (d, ^3J = 6.8 Hz, 2 H), 7.66 (d, ^3J = 8.7 Hz, 2 H), 7.44-7.25 (m, 8 H), 6.93 (d, ^3J = 8.7 Hz, 2 H), 5.10 (s, 2 H), 4.19-4.12 (m, 2 H), 4.12-4.08 (m, 2 H), 4.08-4.01 (m, 1 H), 3.63 (d, ^3J = 10.7 Hz, 4 H), 3.51-3.43 (m, 1 H), 2.97-2.73 (m, 2 H), 1.85-1.69 (m, 5 H), 1.26-1.11 (m, 2 H); ^{13}C NMR (126 MHz, MeOD-d_4, RT): δ (ppm) = 170.1, 163.4, 157.0, 142.9, 138.2, 133.4, 130.4, 130.0, 129.5, 129.1, 128.8, 127.9, 127.1, 115.1, 68.2, 66.8, 53.5 (d, ^2J = 6.5 Hz), 51.2 (d, ^1J = 156.1 Hz), 45.3, 41.3 (d, ^2J = 9.1 Hz), 36.7, 34.2, 33.1; ^{31}P NMR (101 MHz, MeOD-d_4, RT): δ (ppm) = 21.2; MS (EI): $^m/_z$ = 616.2 [M-CO$_2$]$^+$, 660.1 [M+H]$^+$, 682.2 [M+Na]$^+$; RP-HPLC: t_R = 22.5 min (10-90% in 30 min); HRMS (ESI): $^m/_z$ calcd for $C_{30}H_{37}N_3O_9P^{32}S$: 660.2145 [M+H]$^+$, found: 660.2141.

HPLC enantiomer separation

Isocratic semi-preparative chromatographic resolution of phosphinic acid **1**, phosphonic acid **2** and phosphonic acid monomethylester **3** was performed on a 1100 Series HPLC system from *Agilent Technologies* (Waldbronn, Germany) equipped with an autosampler, binary pump, degasser for the mobile phase, multiple wavelength detector (MWD) and a 6-column switching valve. Due to partial racemization during synthesis of compounds **5** it was also necessary to purify them. For automated fraction collection a 2/10-switching valve from *Agilent Technologies* was connected to the flow path just behind the UV-detector. UV-detection was accomplished at 254 nm.

The employed stationary phases were taurine-based **CSP2**, **CSP A183** and **CSP A185** (120 Å pore size, particle size 5 μm each, see Figure S1), which were packed in-house into stainless steel columns (150 x 4 mm). For separation of the carboxylic acids **5** CSP A185 was used, whereas for the separation of phosphinic- **1** and phosphonic acid **2** CSP A183 was used. Phosphonic acid monomethylester **3** was separated on taurine based CSP 2.

As mobile phase 5 mM HOAc and 5 mM NH_4Ac in MeOH was used (for separation of phosphonic acid **2** 95 mM HOAc and 5 mM NH_4Ac in MeOH was used). MeOH was of HPLC-grade from *Merck* (Darmstadt, Germany), mobile phase additives acetic acid and ammonium acetate were of analytical grade (*Sigma-Aldrich*, Taufkirchen, Germany). The flow rate was set to 1.0 mL/min, column temperature was not thermostat-controlled and therefore varied between 25°C and 34°C.

Phosphinic acid **1** was dissolved in a acetonitrile/water/2,5% TFA mixture at a concentration of 16 mg/mL. Phosphonic acid **2** was dissolved in a acetonitrile/water/methanol/2,5% TFA mixture at a concentration of 9 mg/mL and phosphonic acid monomethylester **3** was dissolved in a acetonitrile/water/0,5% TFA mixture at a concentration of 18 mg/mL.

In a series of injections, the enantiomers were separated and collected in two fractions, which were concentrated in vacuum. The purity of the collected enantiomers was assessed analytically using the same conditions as for the semi-preparative separation. The following enantiomeric excess was determined:

(*R*)-**1**: ≥96% ee	(*R*)-**2**: ≥90% ee	(*R*)-**3**: ≥97% ee	(*S*)-**5**: ≥97% ee
(*S*)-**1**: ≥92% ee	(*S*)-**2**: ≥85% ee	(*S*)-**3**: ≥96% ee	(*R*)-**5**: ≥97% ee

^{31}P NMR titration of compounds 1-4

For each data point an individual ^{31}P NMR spectra was recorded at 295 K on a 250 MHz *Bruker* AV spectrometer. Compounds **1-4** (each about 2 mg) were dissolved in H_2O (0.5 mL) including 10% D_2O. Adjustment of the pH of the solution was achieved with small volumes aqueous NaOH (1.0 M) and HCl (1.0 M) solutions. The ^{31}P NMR chemical shifts of each compound were plotted against the measured pH. To extract and evaluate the individual pKa values the obtained data points were plotted in *Origin* 7.5 SR6 (*OriginLab* Corp., Northampton, MA). The appropriate intervals for each pKa transition were selected and plotted in individual graphs. A sigmoidal fit was applied and the inflection point calculated giving the corresponding pKa value. In case of pKa1 of compound **1** an additional data point had to be set (pH = -2.0/ $\delta(^{31}P)$ = 25.5932; $\delta(^{31}P)$ = 25.5932 represents the highest measured value for pH = 1.2), due to unsatisfactory data points in the pH range of 0 to 1.2. The resulted pKa1 for compound **1** represents the lower limit for the real pKa1 and is therefore written as pKa1 > 1.56.

Thereby, the set of molecular probes used in this study gradually shifts from mono anionic (**1**, **2**) to almost dianionic form (**4**) as regards the metal-coordinating group. Conversely, **3** is a probe for the steric influence on the MIDAS binding, due to the single negative charge and a methoxy substituent.

Docking of molecular probes (*R*)-3 and (*R*)-4

In one of the best scored binding conformations calculated by the docking program, compound (*R*)-**4** binds to the MIDAS similar to Tirofiban with the sulfur atom pointing inner in the binding site and the two oxygens involved one in the metal coordination and the other in the H-bond interactions with (β3)-Asn215 and (β3)-Tyr122. All the other main interactions between the ligand and the receptor are conserved like those involving the phenylsulphonamide moiety in the β3 region and those of the piperidine ring in the αIIb subunit (see Figure 3).

A binding conformation similar to that of (*R*)-**4** was found among the best solutions also in the case of (*R*)-**3**. In this binding pose the methylphosphonic group coordinates the magnesium with one oxygen while the other H-bonds with (β3)-Asn215 and (β3)-Tyr122. The ester group points in the inner part of the binding pocket similar to what was found for the sulfur atom of (*R*)-**4**. The benzensulfonamide moiety fills properly the β3 region with the sulfonamide group H-bonding with the backbone CO of (β3)-Asn215 (see Figure 3). On the other side, the *para*-hydroxy-benzoate scaffold of (*R*)-**3** engages π-π interactions with (αIIb)-Tyr190 and the piperidine moiety is able to form in the αIIb domain the strong interactions with (αIIb)-Asp224 and (αIIb)-Ser225.

Similarly to (*R*)-**1** and (*R*)-**2**, also for (*R*)-**3** and (*R*)-**4** the docking calculations did not provide significant differences in the binding mode to the αIIbβ3 receptor.

Docking of the (*S*)-enantiomers

In order to understand how the different chirality of the carbon bearing phosphinic/phosphonic group influences the inhibitory activity, docking calculations on the corresponding (*S*)-enantiomers of the most potent compounds of the series, (*R*)-**1**, (*R*)-**2** and (*R*)-**3**, were performed. The results showed that in the (*S*)-configuration all the three compounds are able to coordinate the metal, however some differences in the binding mode are found if compared with the corresponding (*R*)-enantiomers (see Supporting Figure S4).

In particular, while in the αIIb region the piperidine moiety conserves the interactions with (αIIb)-Asp224 and (αIIb)-Ser225, in the β3 region a loss of the H-bond between the sulfonamide group and (β3)-Asn215 is observed and the benzenesulfonamide moiety is not located in the αIIb/β3 aromatic pocket. Moreover, while in (*S*)-**1**, one oxygen of the phosphinate group coordinates the metal and the other H-bonds with

(β3)-Asn215 and (β3)-Tyr122 as usual, in (*S*)-**2** the (*S*) configuration induces a change in the metal coordination geometry with a consequent loss and weakening of the H-bonds formed with (β3)-Asn215 and (β3)-Tyr122, respectively. Differently, in case of (*S*)-**3**, due to the (*S*) configuration and the bulkiness of the methylester group, all the favorable interactions established with the β3 region by (*R*)-**3** are lost except for the metal-coordination (see Supporting Figure S4D). Thus, the loss of one [(*S*)-**1**] or more interactions [(*S*)-**3**] is the reason behind the lower inhibitory potency of (*S*)-compounds if compared with the (*R*)-enantiomers (see Table 1).
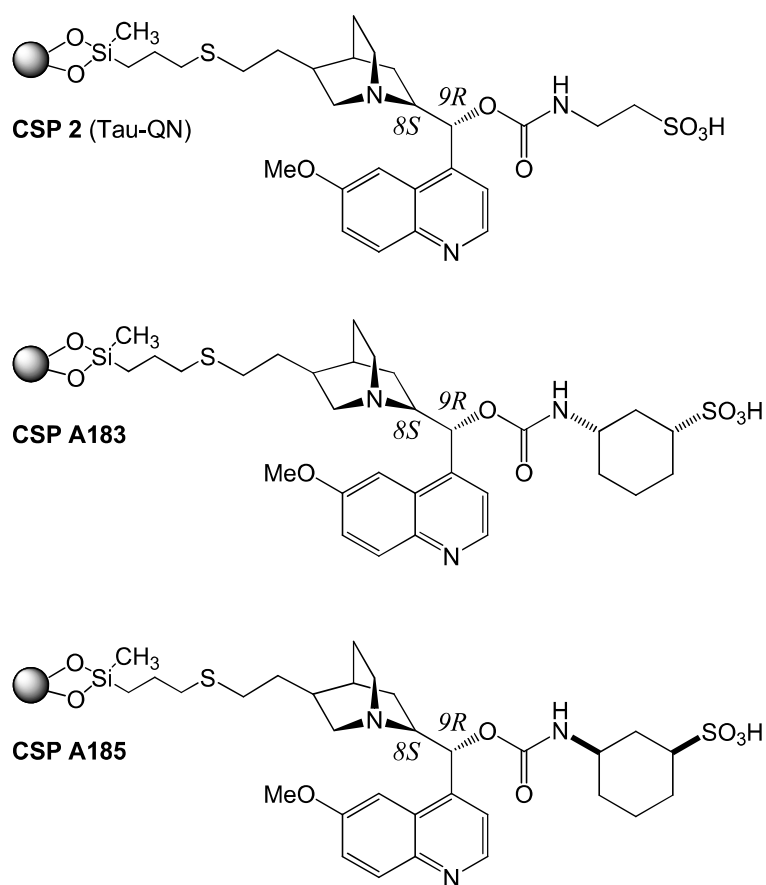
Figure S1. Chemical structures of the quinine based chiral zwitterionic ion-exchange-type stationary phases **CSP 2** (Tau-QN), **CSP A183** and **CSP A185**. Stereoconfiguration at the cyclohexan moiety of **CSP A183** and **CSP A185** has not yet determined.
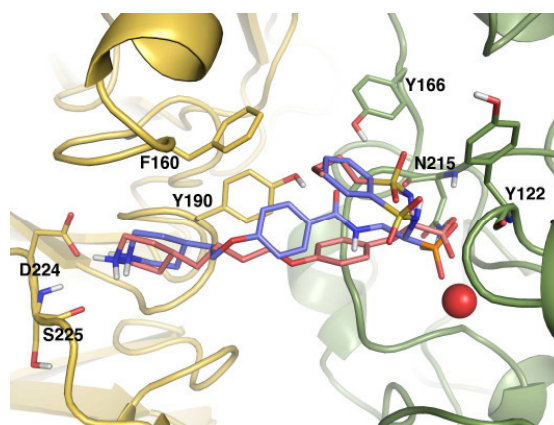
Figure S2. Superimposition of the X-ray binding conformation of Tirofiban (pink) and the binding mode of (*R*)-**1** (blue) derived from the docking calculations. The αIIb domain is displayed as yellow cartoon while the β3 subunit in green. The interacting residues and the ligands are in licorice while the magnesium ion is represented as red sphere. For the sake of clarity only the polar hydrogens are displayed.
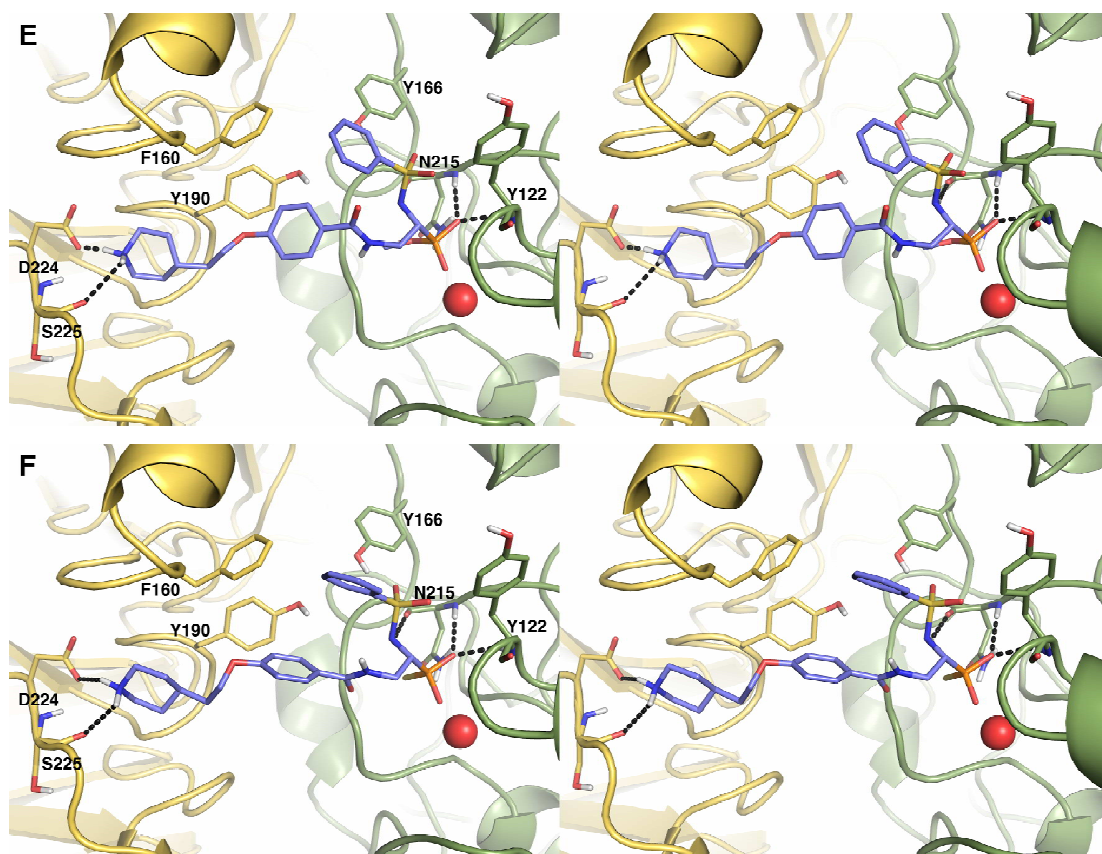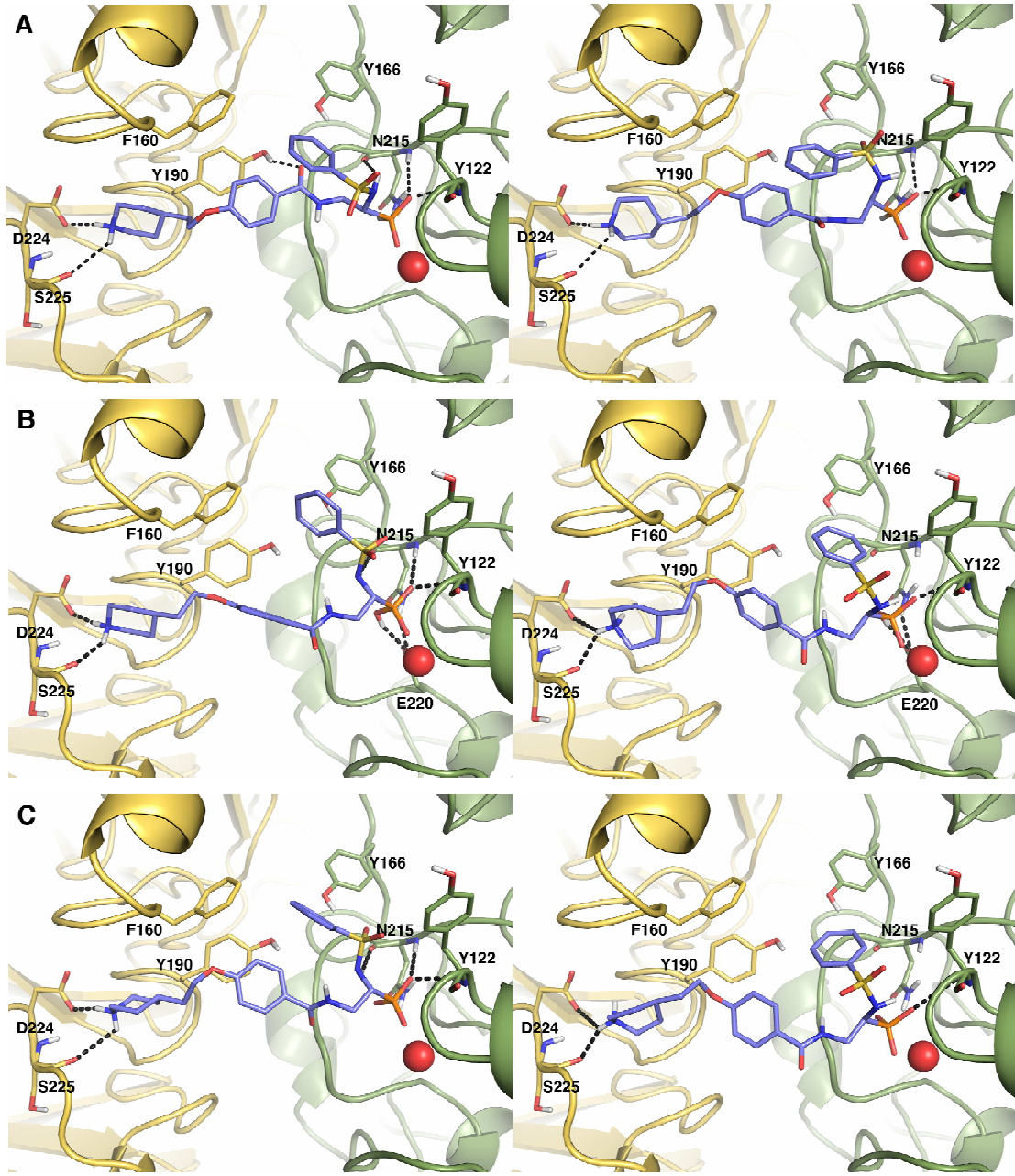
S12
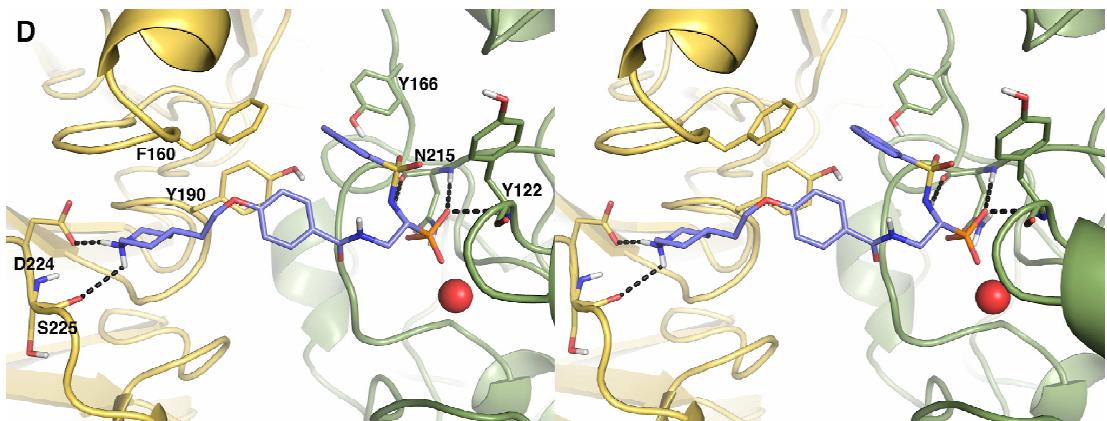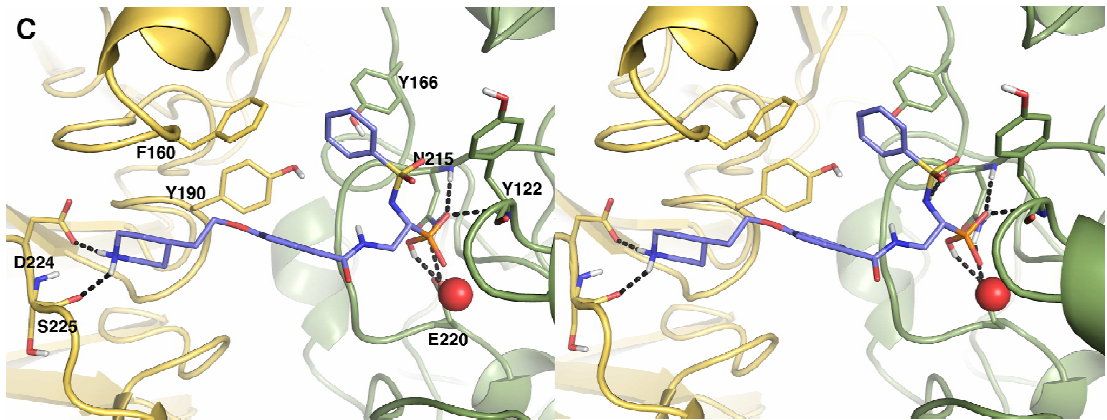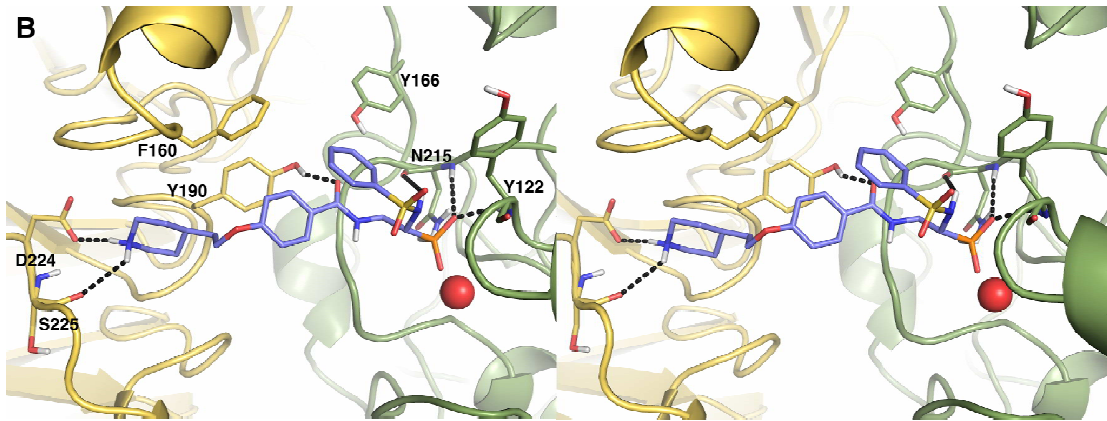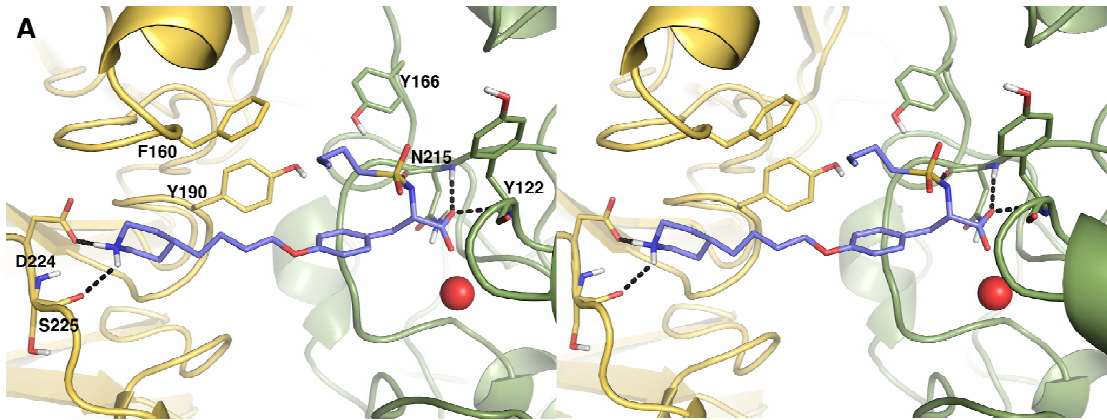
Figure S3. Stereoview of the binding mode of Tirofiban (A), (*R*)-**1** (B), (*R*)-**2** in the overall neutral form (C) and in the overall anionic form (D), (*R*)-**3** (E), and (*R*)-**4** (F). The αIIb domain is displayed as yellow cartoon while the β3 one in green. The magnesium ion is represented as red sphere. For the sake of clarity only the polar hydrogens are displayed.
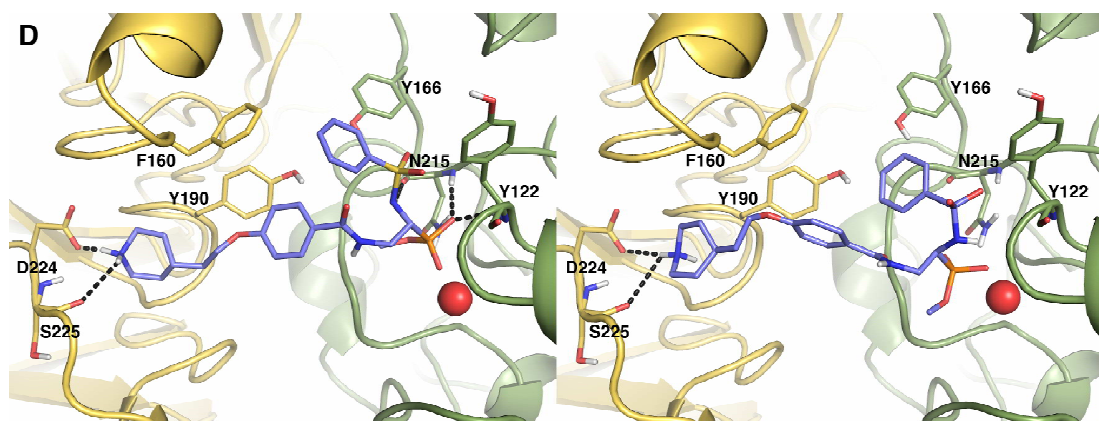
Figure S4. Comparison between the binding mode of the (*R*)-enantiomers (left) and (*S*)-enantiomers (right) of **1** (A), **2** in the overall neutral form (B) and in the overall anionic form (C), and **3** (D). The αIIb domain is displayed as yellow cartoon while the β3 one in green. The interacting residues and the ligands are in licorice while the magnesium ion is represented as red sphere. For the sake of clarity only the polar hydrogens are displayed.

APPENDIX II

Direct One-Step ^{18}F-Labeling of a New Highly Active αIIbβ3 Integrin Antagonist via Nucleophilic Aromatic Substitution**

Markus Bollinger[1#], Behrooz H. Yousefi[2,3#], Alexander Bochen[1], Iina Laitinen[3], Tobias Petzold[4], Markus Schwaiger[3], Horst Kessler[1,5*], and Hans-Jürgen Wester[2,3]

[1] *Institute for Advanced Study and Center of Integrated Protein Science, Department Chemie, Technische Universität München, Lichtenbergstrasse 4, 85747 Garching, Germany.*

[2] *Department of Pharmaceutical Radiochemistry, Technische Universität München, Walther-Meissner-Strasse 3, 85748 Garching, Germany.*

[3] *Department of Nuclear Medicine, Klinikum rechts der Isar, Technische Universität München, Ismaninger Strasse 22, 81675 Munich, Germany.*

[4] *Department of Cardiology, German Heart Centre Munich, Lazarettstrasse 36, 80363 Munich, Germany.*

[5] *Chemistry Department, Faculty of Science, King Abdulaziz University, P.O. Box 80203, Jeddah 21589, Saudi Arabia.*

Keywords: αIIbβ3 Integrin Inhibitor, Thrombosis, ^{18}F-Labeling, Nucleophilic Aromatic Substitution, Radiopharmaceuticals, Radiochemistry, Integrin Ligands, Fluorination

[*] Correspondence to:

Horst Kessler

Email: kessler@tum.de

Tel.:   +49 (0) 89 289 13300

Fax: +49 (0) 89 289 13210

[#] These authors contributed equally.

Thromboembolic diseases are the most common causes of morbidity and mortality in industrialized countries. The aggregation of platelets via the integrin αIIbβ3 is profoundly implicated in the biological process of thrombus formation.[1] Therefore, diagnosis of the activated αIIbβ3 integrin is of utmost importance and Molecular Imaging of thrombus formation in the arteries remains a clinical challenge. So far, only one imaging agent has been FDA approved for clinical use. ^{99m}Tc-apcitide (AcuTect), a cyclic RGD (Arg-Gly-Asp) peptide mimetic is indicated for noninvasive single photon emission computer tomography (SPECT) of acute deep vein thrombosis (DVT).[2-5] However, the resolution of SPECT is limited and the development of a highly active ligand for positron emission tomography (PET) imaging is essential to achieve higher resolution. ^{18}F represents an ideal radionuclide for PET due to its optimal half-life of 109.7 min and a low β^+-energy (0.64 MeV).[6] But the most common no-carrier-added (n.c.a.) nucleophilic aromatic ^{18}F-labeling is still a daily challenge for pharmaceutical radiochemists. Ideally the radioactive fluorine should be directly incorporated in the molecule in the last reaction step without further chemical transformations. Here we report a direct fluorination method for a one-step ^{18}F-labeling of a fully unprotected nitro-precursor via n.c.a. nucleophilic aromatic substitution. To our knowledge, this is the first ^{18}F-labeled αIIbβ3 integrin antagonist with subnanomolar activity, selectivity for the platelet receptor αIIbβ3 and probably the first facile n.c.a nucleophilic aromatic substitution in presence of protic functions.

Cardiac infarctions, strokes, peripheral vascular disease and pulmonary embolism are mostly triggered off thrombus formation. Integrin αIIbβ3, often called as glycoprotein (GP) IIb/IIIa, is the most abundant platelet surface receptor, which is solely expressed on platelets and megakaryocytes. In primary hemostasis the αIIbβ3 integrin is essential for platelet aggregation.[1, 7] Therefore, the inhibition of the common pathway of platelet aggregation by αIIbβ3 receptor antagonists such as tirofiban[8] is a clinically proven concept for acute antithrombotic therapy. A novel radiolabeled antagonist, (S)-2-(4-[^{18}F]fluorophenylsulfonamido)-3-(4-(2-(piperidin-4-yl)ethoxy)benzamido)propanoic acid ([^{18}F]-**5**), was synthesized, characterized and evaluated by *in vivo* and *in vitro* experiments.

Thus, radiolabeled αIIbβ3 inhibitors which are capable to selectively bind to activated platelets are promising candidates for the imaging of thrombosis. Recently several imaging agents, targeting the platelet integrin αIIbβ3, have been reported.[2] Among

the different imaging techniques such as magnetic resonance imaging (MRI), ultrasound (US) or SPECT, PET is one of the most sensitive noninvasive molecular imaging techniques for *in vivo* studies. Widely used radioisotopes in PET imaging are for example ^{11}C, ^{18}F or ^{68}Ga, whereas fluorine-18 turned out to have several advantages over the others.[6] However, the introduction of ^{18}F into the appropriate biological target molecule often turned out to be challenging because of unwanted functional groups, such as phenol, amide, amine or carboxylic acids with their protic functions are present. Therefore, nucleophilic aromatic radiofluorination in such complex molecules is commonly only performed on protected precursors. Often time-consuming and laborious multi-step reactions are necessary. It is essential to develop facile and straightforward labeling methods in order to facilitate the development of new radiopharmaceutical.

In our study as a model compound, *p*-nitrobenzenesulfonamide, was labeled consistent with the literature[9] with insufficient analytical yield (3-5%). The same labeling procedure was not successful for nitro compounds **3**, **4** and **7**, although activated and protected benzenesulfonamides with nitro and trimethylammonium triflate leaving groups show very good conversion of 15-80% to ^{18}F-labeled compounds.[10, 11]

In our hypothesis the presence of weak basic, less nucleophilic salts like potassium oxalate or triflate unprotected precursors might be used for direct radiofluorination for compounds containing protic functions such as carboxylic acid and amino groups, which is usually considered as impossible. We combined our radiofluorination approach with the development of a highly active radiotracer for the platelet integrin αIIbβ3.
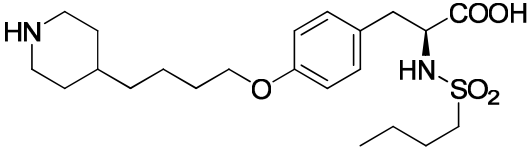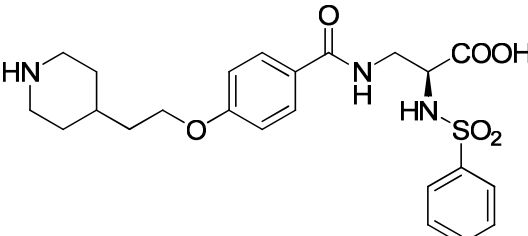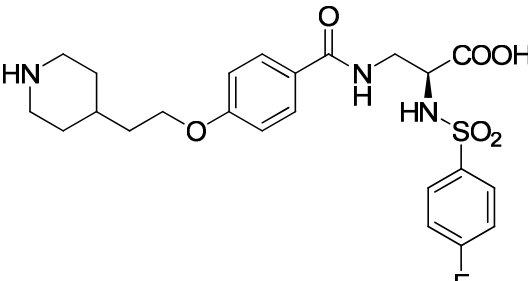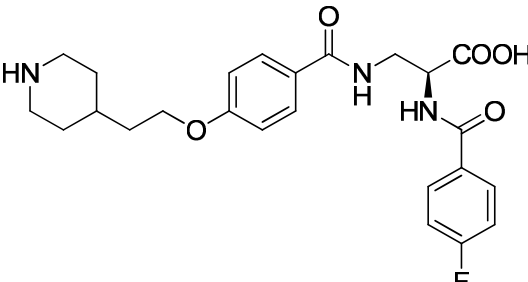
Based on our previous docking studies on αIIbβ3 antagonists,[12] we assumed that compound **11**[13] could tolerate a fluorination in *para*-position of the phenyl ring. The inhibiting activities of the synthesized compounds against αIIbβ3 were evaluated in a competitive enzyme-linked immunosorbent assay (ELISA) using immobilized fibrinogen and soluble αIIbβ3 integrin (Table 1, Supporting Information). The carboxylic acid **5** exhibited binding affinity to the αIIbβ3 integrin similar to tirofiban or **11**, proving that the introduction of the fluorine in *para*-position of **11** did not influence the activity, whereas the amide bond in **6** has a massive impact on the αIIbβ3 binding affinity (0.99 vs. 37.6 nM). This can be explained by the different geometry between the 90° twisted sulfonamide and the planar carboxamide.[14] Therefore, **6** which is

easy to prepare using activated 4-[^{18}F]fluorobenzoic acid[15] as labeling reagent is not suitable as potential radiotracer.

To validate the *ex vivo* inhibitory potency of **5** towards platelet aggregation, impedance-based platelet aggregometry was performed, using ADP and collagen activated mouse blood (blood was pooled from six animals), respectively. Collagen and ADP were used, as both addresses different stimuli in the process of platelet activation, contributing to arterial thrombosis *in vivo*. The assay was based on a previously reported method with some modifications.[12] As shown in Table 1, fluorinated compound **5** [16.8 nM (ADP); 19.4 nM (collagen)] is almost as potent as tirofiban (13.6 nM) in terms of *ex vivo* platelet aggregation (EC$_{50}$ value of tirofiban was measured in human whole blood, whereas for **5** pooled mouse blood was used). The small differences between ADP and collagen activated blood might be explained by the higher potency of collagen to fully activate platelets (additional adhesive properties of collagen) in contrast to ADP (for more details see Supporting Information).

The impressive *in vitro* and *ex vivo* activities of **5** in the low nanomolar range promoted us to focus our research on this compound. For the radiosynthesis of the desired product, we used different protected and unprotected *para*-nitrobenzenesulfonamid-precursors (Scheme 2). The *para* substitution pattern was chosen because of the better spatial accessibility in the nucleophilic substitution.
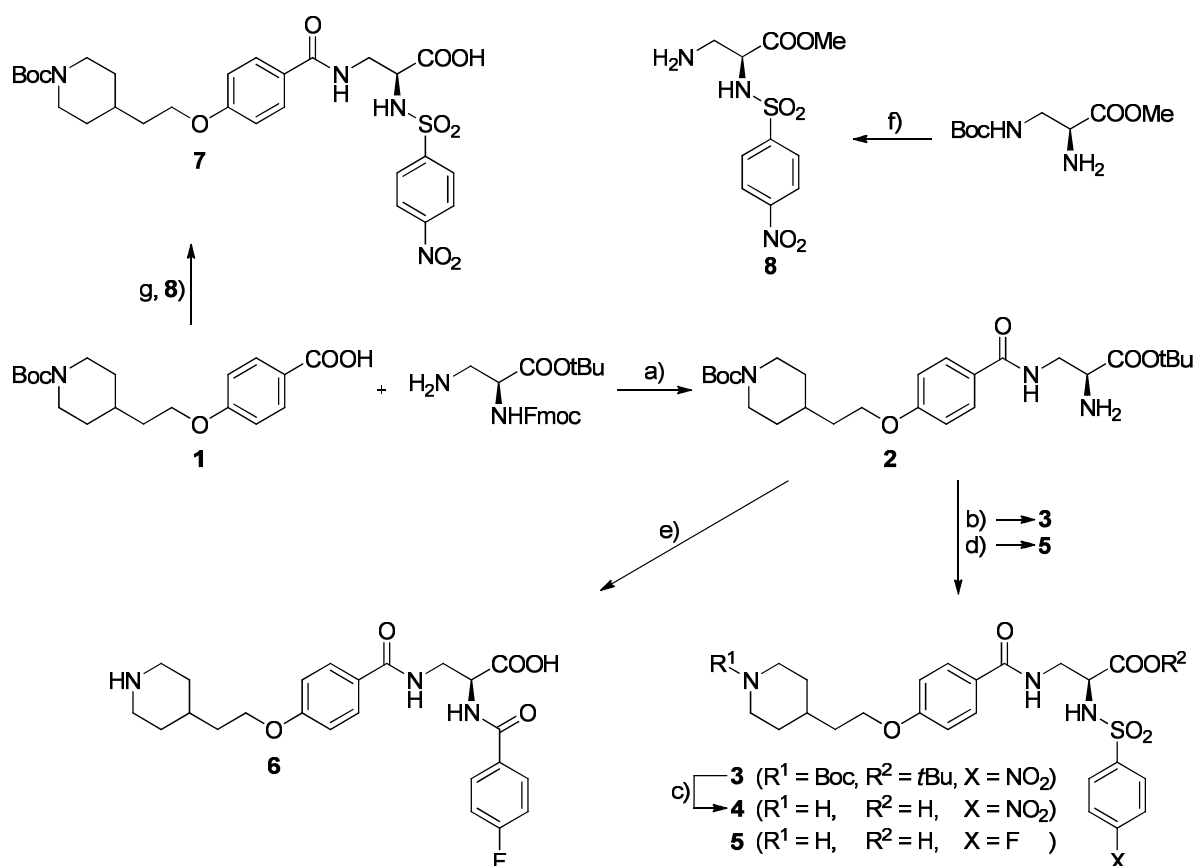
Table 1 | IC_{50}/EC_{50} values of integrin ligands for the platelet integrin αIIbβ3.

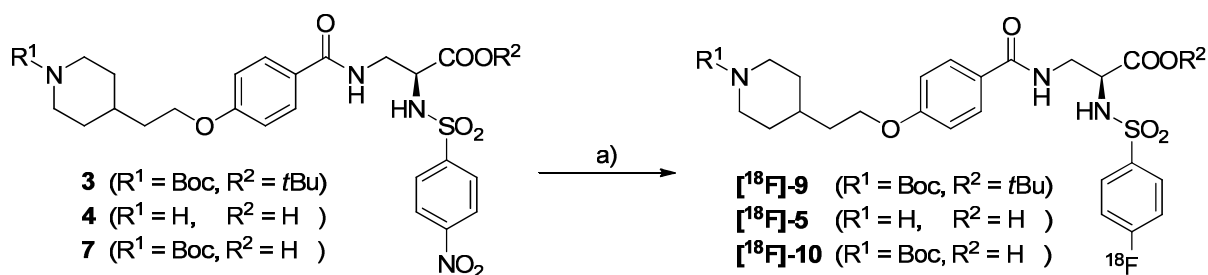| Compound	Structure	IC_{50} [nM] (αIIbβ3)[a]	EC_{50} [nM] (αIIbβ3)[b]
tirofiban		0.95 ± 0.09[12]	13.6 ± 3.3[12]
11		0.81 ± 0.05[12]	
5		0.99 ± 0.12	16.8 ± 1.8[c] 19.4 ± 2.1[d]
6		37.6 ± 5.9	

[a] IC_{50} values [nM] were derived from a competitive ELISA using immobilized fibrinogen and soluble integrin αIIbβ3. [b] Effective concentrations (EC_{50}) of some key compounds for inhibition of platelet aggregation were derived from aggregation measurements using multiple electrode aggregometry in hirudin-anticoagulated TRAP-6,[12] ADP[c], and collagen[d], respectively, activated blood. (for details see the Supporting Information).

The synthetic pathway, which summarizes the synthesis of all precursors (**3**, **4** and **7**) and ^{19}F reference compounds (**5** and **6**), is shown in Scheme 1. The Boc-protected N-terminal moiety **1** was synthesized according to literature procedures [12, 13] For this Mitsunobu-type reaction we used methyl-4-hydroxybenzoate, Boc-protected alcohol, tributylphosphine and 1,1'-(azodicarbonyl)dipiperidide (ADDP). After saponification of the corresponding methyester, **1** was activated by the use of O-(7-azabenzotriazol-1-yl)-N,N,N',N',-tetramethyluronium hexafluorophosphate (HATU) and eventually condensed with N^α-Fmoc-L-diaminopropionic acid tert-butyl ester. Fmoc-deprotection and purification by RP-HPLC afforded building block **2**. The corresponding free amin **2** was sulfonylated upon treatment with the particular para-substituted benzenesulfonyl chlorides in DCM and acylated with activated 4-fluorobenzoic acid (HATU, DIEA in DMF), respectively. To yield ligands **4-6** the last step of the synthesis was the cleavage of the protecting groups under acidic conditions. For the N-Boc protected precursor **7**, **1** was coupled to **8** in the presence of HATU followed by saponification of the methyl ester using lithium hydroxide in methanol/water to yield the desired product (for details see Supporting Information).

The suitable radiolabeling (Scheme 2, optimized conditions) of the protected and unprotected precursor compounds **3**, **4** and **7** were studied by nucleophilic substitution of the nitro group by n.c.a. $[K^+ \subset 2.2.2]^{18}F^-$ in presence of $[K^+ \subset 2.2.2]CO_3$ or $[K^+ \subset 2.2.2]CO_3$ and $[K^+ \subset 2.2.2]C_2O_4$ in CH_3CN, tBuOH/CH_3CN and DMSO at temperature 100-150 °C for 10-60 min. Experiments using the fully protected precursor **3** unfortunately failed but radiofluorination of **4** by n.c.a. $[K^+ \subset 2.2.2]^{18}F^-$ in presence of $[K^+ \subset 2.2.2]CO_3$ and $[K^+ \subset 2.2.2]C_2O_4$ in DMSO at 150 °C for 20 min yielded the desired ^{18}F-labeled product [^{18}F]**5** with radiochemical yields of 19.0 ± 7.4%. Similarly, the ^{18}F-labeling of N-Boc protected precursor **7** to yield [^{18}F]**10** was successfully performed with 10.0 ± 1.6% radiochemical yields (not optimized condition). However, this synthetic route is abandoned because of unpractical final Boc-deprotection with TFA. The direct one-step ^{18}F-labeling of the totally unprotected precursor **4** afforded [^{18}F]**5** was used for further evaluation of the integrin tracer in vivo and in vitro.

Scheme 1 | Synthesis of *para*-nitro substituted precursors **3,4** and **7** and ^{19}F-reference compounds **5** and **6**. a) 1. HATU, DIEA, DMF, RT, 16 h; 2. 20% piperidine/DMF, RT, 2 h; b) 4-Nitrobenzenesulfonyl chloride, DIEA, DCM, RT, 5 h; c) HCl$_{(aq)}$, dioxane, RT, 1 h; d) 1. 4-Fluorobenzenesulfonyl chloride, DIEA, DCM, RT, 5 h; 2. HCl$_{(aq)}$, dioxane, RT, 1 h; e) 1. HATU, 4-Fluorobenzoic acid, DIEA, DMF, RT, 16 h; 2. HCl$_{(aq)}$, dioxane, RT, 1 h; f) 1. 4-Nitrobenzenesulfonyl chloride, DIEA, DCM, RT, 5 h; 2. TFA, DCM, RT, 1 h; g) 1. HATU, 7, DIEA, DMF, RT, 16 h; 2. LiOH, methanol, H$_2$O, RT, 16 h. All compounds were purified by RP-HPLC (for more details see Supporting Information).

Scheme 2 | Radiosynthesis of ^{18}F-labeled compounds. a) K[18]F, Kryptofix 2.2.2, K$_2$CO$_3$, K$_2$C$_2$O$_4$, DMSO, 150 °C, 20min (optimized conditions).

The radiofluorination of **4** was studied using different amount of precursor at a reaction temperature of 150 °C. After 30 min reaction time the mixture was analyzed by HPLC (Figure 1). 5 mg of precursor gave the highest radiochemical yield. Furthermore, the radiofluorination of 5 mg of **4** was analyzed after 10-60 min by radio TLC. Figure 2 shows, that an optimal reaction time is 20 min for this radiolabeling. The labelings at 100 °C and 120 °C using similar conditions were not successful. Fluorinations at higher temperatures than 150 °C could not be performed due to possible decomposition of the precursor and the solvent.

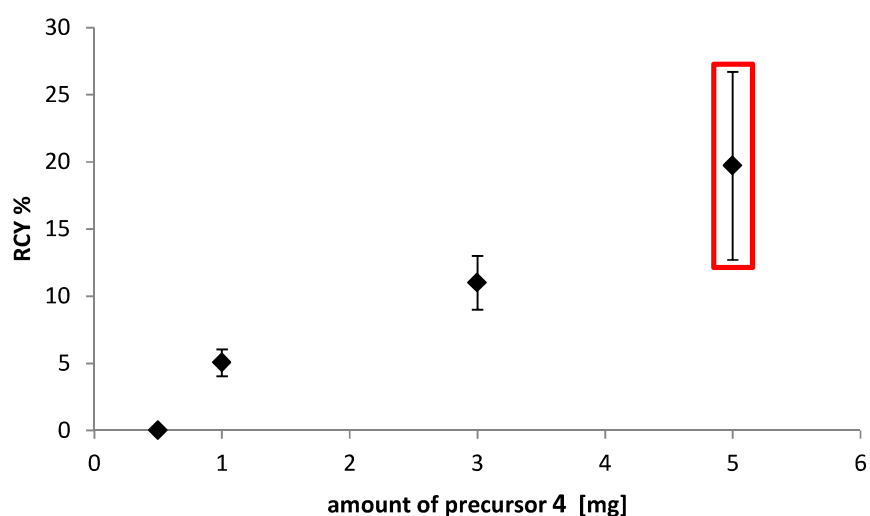**Figure 1** │ Precursor concentration dependence of the radiochemical yield: $K^{18}F$, Kryptofix 2.2.2, K_2CO_3, $K_2C_2O_4$, DMSO, 150 °C, 30min.
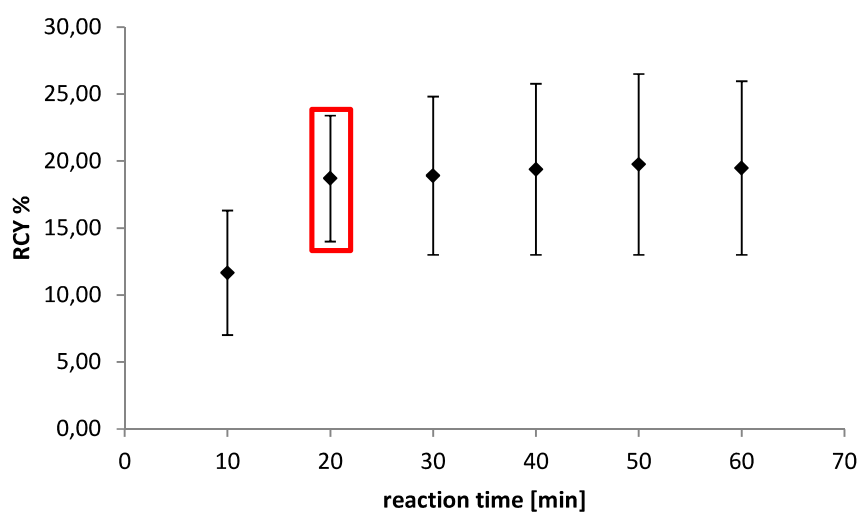

Figure 2 │ Reaction time dependence of the radiochemical yield: 5 mg of precursor **4**, $K^{18}F$, Kryptofix 2.2.2, K_2CO_3, $K_2C_2O_4$, DMSO, 150 °C.

The log $P_{oct/PBS}$ value of [^{18}F]**5** was determined (log $P_{oct/PBS}$ = -2.18 ± 0.02, n=6). The plasma protein binding of [^{18}F]**5** in human serum was measured and showed that only a small portion of [^{18}F]**5** was found to bind to plasma protein (8.61% ± 0.75, n= 6).

[^{18}F]**5** was formulated for the *in vivo* injections accordingly: the HPLC purified radiotracer was loaded on a RP-SPE cartridge, eluted with EtOH and formulated with isotonic saline. Healthy C57Bl/6 male mice (weight: 27.8 ± 0.3 g) were injected with [^{18}F]**5** (dose: 10.3 ± 0.8 MBq) for biodistribution and metabolism studies.

The biodistribution (Table 2) results suggest that there is no significant defluorination and the tracer excreted rapidly via gastrointestinal system. There is very little accumulation of the tracer in the muscle and heart, showing potential for *in vivo* PET imaging of thrombosis.

Table 2 | Biodistribution results of [^{18}F]**5** using healthy C57Bl/6 male mice (n=3).

Organ	30 min p.i. (%ID/g) Mean ± sd	60 min p.i. (%ID/g) Mean ± sd
Blood	4.0 ±0.5	1.0 ± 0.4
Heart	0.9 ± 0.1	0.3 ± 0.1
Lung	2.2 ± 0.4	3.3 ± 1.9
Liver	20.0 ± 2.6	13.7 ± 2.5
Gallbladder*	1.0 ± 0.2	2.9 ± 1.4
Pancreas	0.3 ± 0.1	2.5 ± 1.4
Spleen	14.3 ± 2.1	7.8 ± 0.2
Kidney	1.4 ± 1.0	0.7 ± 0.2
Adrenal gland	1.2 ± 0.9	0.7 ± 0.7
Small intestine	20.5 ± 2.1	18.3 ± 5.0
Large intestine	0.3 ± 0.4	0.2 ± 0.1
Stomach	16.5 ± 1.2	1.4 ± 1.2
Bladder (emptied)*	1.2 ± 0.8	1.6 ± 1.0
Muscle	0.1 ± 0.0	0.1 ± 0.0
Skull bone	0.8 ± 0.1	0.3 ± 0.0

*%ID (ID = injected dose)

Radio TLC analyses[16] of mouse urine, spleen and liver homogenates 30 and 60 min after injection of [^{18}F]**5** in wild type mice (n = 3) in Table 3 show major part of the tracers were excreted intact in urine (≥ 99% intact tracer). The results suggest that [^{18}F]**5** is partially excreted intact via urine, and partly metabolised in liver and spleen.

Table 3 | Amount of non-metabolised intact tracer in urine, spleen and liver of mice injected with [^{18}F]**5** (% Intact tracer ± sd, n= 3).

Time p.i.	Urine	Spleen	liver
30 min	99.4 ± 0.2	13.6 ± 1.6	86.4 ± 1.7
60 min	98.9 ± 0.2	0	78.0 ± 1.9

In vivo distribution of [^{18}F]**5** can be seen to have rapid blood clearance within first minutes after injection with some retention in the circulation (Figure 3). The uptake in the bone is minimal and does not change over one hour, suggesting that [^{18}F]**5** is not defluorinated (Figure 3). Time activity curves (TAC) showed fast excretion of the tracer partly via urine, and partly via gastrointestinal (GIT) system (Figure 4). TAC analyses of blood, muscle and heart confirmed that [^{18}F]**5** is suitable for thrombus imaging in mouse model due to very low background binding to these organs (Figure 3 and 5). However, activity seen in GIT may hinder the imaging in this region (Figure 5d).
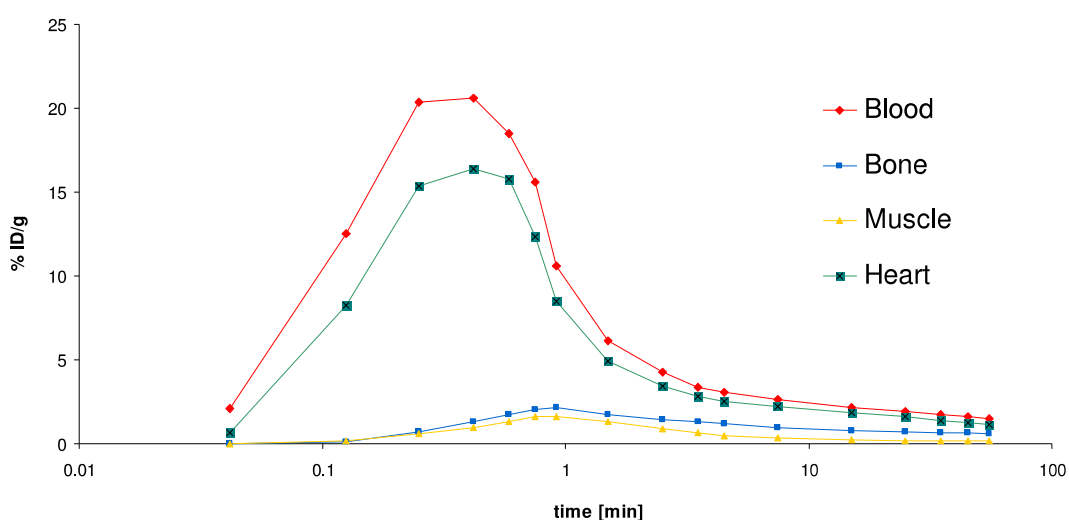

Figure 3 | Blood clearance and *in vivo* biodistribution of radiotracer [^{18}F]**5** to bone, muscle and heart (n=4).
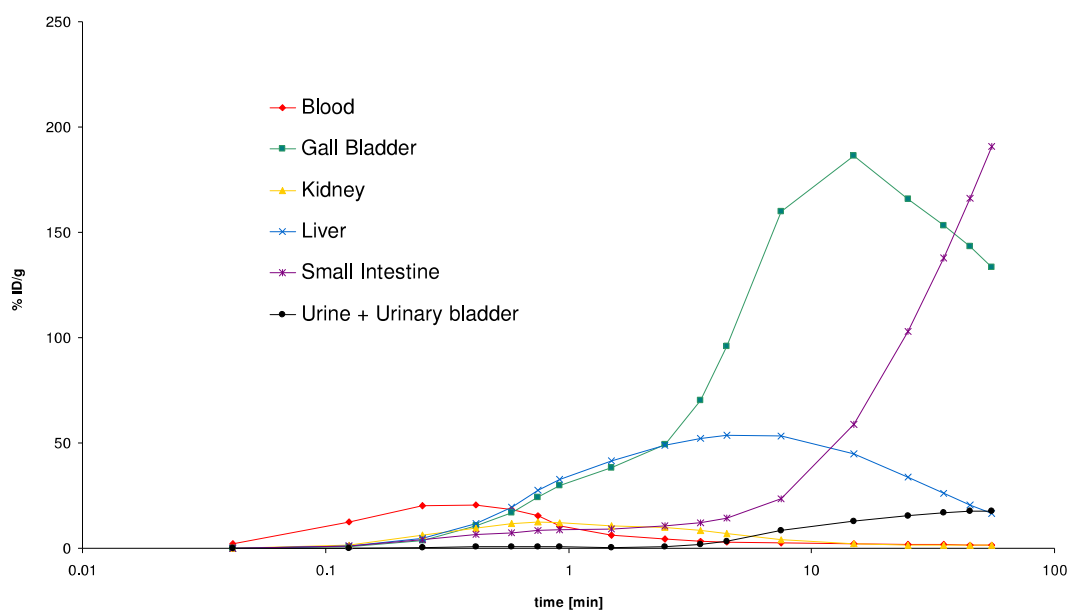
Figure 4 | Excretion profile of [^{18}F]**5**: Time activity curves of blood, gall bladder, kidney liver, small intestine, and urine (n=4).
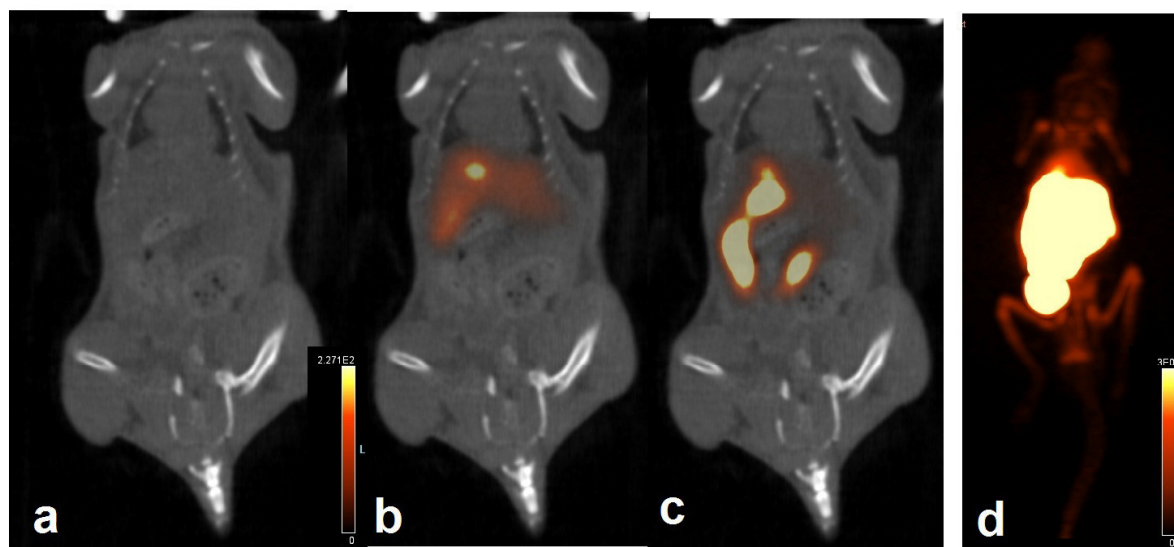

Figure 5 | Example of *in vivo* biodistribution of [^{18}F]**5**. **a)** CT image, coronal slide; **b)** Overlay of PET image 10 min post injection; **c)** Overlay 60 min post injection; **d)** PET maximum intensity projection at 60 min (scaled to show background).

In conclusion, we report here the first successful direct ^{18}F-labeling procedure in the presence of unprotected protic functional groups. So far, temporary protecting groups were required for these functionalities, which had to be finally cleaved with trifluoroacetic acid (TFA). However, it is known that TFA makes a ^{19}F-exchange with

the ^{18}F-labeled compound and therefore decreases the specific activity. Further advantages of the presented no-carrier-added direct radiofluorination are the short reaction times, a simple work-up, and the highly reproducibility, respectively. The presented n.c.a direct radiofluorination procedure is highly reproducible and provides a facile one-step approach of nucleophilic fluorination of peptidomimic and small molecules. We showed this novel approach on the example of a highly active αIIbβ3 integrin antagonist.

In summary, we successfully synthesized and evaluated the novel ^{18}F-labeled αIIbβ3 binding radiotracer [^{18}F]**5**. The preliminary biological results indicate that [^{18}F]**5** might be a potent candidate for the visualization of activated platelets involved in thromboembolic disorders.

References

(1) Bhatt, D. L.; Topol, E. J. Scientific and Therapeutic Advances in Antiplatelet Therapy. *Nat. Rev. Drug Discovery* **2003,** *2*, 15-28.

(2) Wiethoff, A. J.; Makowski, M. R.; Katoh, M.; Spuentrup, E.; Botnar, R. M. Molecular Imaging of Thrombosis. *Curr. Cardiovasc. Imaging Rep.* **2010,** *3*, 34-41.

(3) Bates, S. M.; Lister-James, J.; Julian, J. A.; Taillefer, R.; Moyer, B. R.; Ginsberg, J. S. Imaging Characteristics of a Novel Technetium Tc 99m-Labeled Platelet Glycoprotein IIb/IIIa Receptor Antagonist in Patients With Acute Deep Vein Thrombosis or a History of Deep Vein Thrombosis. *Arch. Intern. Med.* **2003,** *163*, 452-456.

(4) Mousa, S. A.; Bozarth, J. M.; Edwards, S.; Carroll, T.; Barrett, J. Novel technetium-99m-labeled platelet GPIIb/IIIa receptor antagonists as potential imaging agents for venous and arterial thrombosis. *Coronary Artery Disease* **1998,** *9*, 131-141.

(5) Zhou, Y.; Chakraborty, S.; Liu, S. Radiolabeled Cyclic RGD Peptides as Radiotracers for Imaging Tumors and Thrombosis by SPECT. *Theranostics* **2011,** *1*, 58-82.

(6) Ametamey, S. M.; Honer, M.; Schubiger, P. A. Molecular Imaging with PET. *Chem. Rev.* **2008,** *108*, 1501-1516.

(7) Hato, T.; Ginsberg, M. H.; Shattil, S. J. Integrin $a_{IIb}b_3$. In *Platelets*, Michelson, A., Ed. Academic/Elsevier Science, New York: 2002; pp 105-116.

(8) Hartman, G. D.; Egbertson, M. S.; Halczenko, W.; Laswell, W. L.; Duggan, M. E.; Smith, R. L.; Naylor, A. M.; Manno, P. D.; Lynch, R. J.; Zhang, G.; Chang, C. T.-C.; Gould, R. J. Non-Peptide Fibrinogen Receptor Antagonists. 1. Discovery and Design of Exosite Inhibitors. *J. Med. Chem.* **1992,** *35*, 4640-4642.

(9) Shiue, G. G.; Schirrmacher, R.; Shiue, C.-Y.; Alavi, A. A. Synthesis of fluorine-18 labeled sulfonureas as β-cell imaging agents. *J. Labelled Compd. Radiopharm.* **2001,** *44*, 127-139.

(10) Becaud, J.; Mu, L.; Karramkam, M.; Schubiger, P. A.; Ametamey, S. M.; Graham, K.; Stellfeld, T.; Lehmann, L.; Borkowski, S.; Berndorff, D.; Dinkelborg, L.; Srinivasan, A.; Smits, R.; Koksch, B. Direct One-Step ^{18}F-Labeling of Peptides via Nucleophilic Aromatic Substitution. *Bioconjugate Chem.* **2009,** *20*, 2254-2261.

(11) Andries, J.; Lemoine, L.; Le Bars, D.; Zimmer, L.; Billard, T. Synthesis and biological evaluation of potential 5-HT$_7$ receptor PET radiotracers. *Eur. J. Med. Chem.* **2011,** *46*, 3455-3461.

(12) Bollinger, M.; Manzenrieder, F.; Kolb, R.; Bochen, A.; Neubauer, S.; Marinelli, L.; Limongelli, V.; Novellino, E.; Moessmer, G.; Pell, R.; Lindner, W.; Fanous, J.; Hoffman, A.; Kessler, H. Tailoring of Integrin Ligands: Probing the Charge Capability of the Metal Ion-Dependent Adhesion Site. *J. Med. Chem.* **2012,** *55*, 871-882.

(13) Duggan, M. E.; Duong, L. T.; Fisher, J. E.; Hamill, T. G.; Hoffman, W. F.; Huff, J. R.; Ihle, N. C.; Leu, C. T.; Nagy, R. M.; Perkins, J. J.; Rodan, S. B.; Wesolowski, G.; Whitman, D. B.; Zartman, A. E.; Rodan, G. A.; Hartman, G. D. Nonpeptide $\alpha_v\beta_3$ Antagonists. 1. Transformation of a Potent, Integrin-Selective $\alpha_{IIb}\beta_3$ Antagonist into a Potent $\alpha_v\beta_3$ Antagonist. *J. Med. Chem.* **2000,** *43,* 3736-3745.

(14) Vijayadas, K. N.; Davis, H. C.; Kotmale, A. S.; Gawade, R. L.; Puranik, V. G.; Rajamohanan, P. R.; Sanjayan, G. J. An unusual conformational similarity of two peptide folds featuring sulfonamide and carboxamide on the backbone. *Chem. Commun.* **2012,** *48,* 9747-9749.

(15) Marik, J.; Sutcliffe, J. L. Fully automated preparation of n.c.a. 4-[18F]fluorobenzoic acid and *N*-succinimidyl 4-[18F]fluorobenzoate using a Siemens/CTI chemistry process control unit (CPCU). *Appl. Radiat. Isot.* **2007,** *65,* 199-203.

(16) Yousefi, B. H.; Manook, A.; von Reutern, B.; Schwaiger, M.; Drzezga, A.; Wester, H.-J.; Henriksen, G. Development of an improved radioiodinated 2-phenylimidazo[1,2-α]pyridine for non-invasive imaging of amyloid plaques. *MedChemComm* **2012,** *3,* 775-779.

Abstract / TOC

αIIbβ3 is the most abundant integrin on the surface of platelets, and therefore plays a key role in the process of thrombus formation. Thus, αIIbβ3 PET tracer has been the subject of increasing interest over recent years for preclinical and clinical imaging studies. In this work we developed a highly active ^{18}F-labeled αIIbβ3 integrin antagonist and evaluated as molecular imaging agent of activated platelets. A novel n.c.a. direct radiofluorination method was developed using unprotected nitro-precursor in presence of protic functions. [^{18}F]5 exhibits high *in vitro* affinity in the low nanomolar range combined with suitable lipophilicity and low plasma protein binding, high *in vivo* stability and fast washout from blood circulation. In addition biodistribution results showed the tracer excretes fast via gastrointestinal system and has minimum binding to tissues surrounding the potential imaging targets.

Further animal studies are planned and the applicability of [^{18}F]5 as PET tracer for the detection of deep vein thrombosis in mouse models are in progress.

Supporting Information

Direct One-Step ^{18}F-Labeling of a New Highly Active αIIbβ3 Integrin Antagonist via Nucleophilic Aromatic Substitution

Markus Bollinger[1#], Behrooz H. Yousefi[2,3#], Alexander Bochen[1], Iina Laitinen[3], Tobias Petzold[4], Markus Schwaiger[3], Horst Kessler[1,5*], and Hans-Jürgen Wester[2,3]

[1] *Institute for Advanced Study and Center of Integrated Protein Science, Department Chemie, Technische Universität München, Lichtenbergstrasse 4, 85747 Garching, Germany.*

[2] *Department of Pharmaceutical Radiochemistry, Technische Universität München, Walther-Meissner-Strasse 3, 85748 Garching, Germany.*

[3] *Department of Nuclear Medicine, Klinikum rechts der Isar, Technische Universität München, Ismaninger Strasse 22, 81675 Munich, Germany.*

[4] *Department of Cardiology, German Heart Centre Munich, Lazarettstrasse 36, 80363 Munich, Germany.*

[5] *Chemistry Department, Faculty of Science, King Abdulaziz University, P.O. Box 80203, Jeddah 21589, Saudi Arabia.*

[#]These authors contributed equally.

Contents

1. Synthesis of Precursors and [19]F Reference Compounds

Materials and Methods

All technical solvents were distilled prior to use. Dry solvents were purchased from *Aldrich*, *Fluka* or *Merck*. Protected amino acids and coupling reagents were purchased from *Novabiochem* (Schwalbach, Germany), *Iris Biotech GmbH* (Marktredwitz, Germany) and *Medalchemy* (Alicante, Spain). All other chemicals and organic solvents were purchased from commercial suppliers at the highest purity available and used without further purification.

Analytical HPLC was performed using *Amersham Pharmacia Biotech* Äkta Basic 10F equipment, with a P-900 pump system, a reversed-phase *YMC*-ODS-A C_{18} column (12 nm pore size, 5 μm particle size, 250 mm x 4.6 mm), and UV detection (UV-900, 220 and 254 nm). The system was run at a flow rate of 1.0 mL/min over 30 min using H_2O (0.1% TFA) and MeCN (0.1% TFA) as solvents.

Semipreparative HPLC was performed using *Waters* equipment: System Breeze; Pump System 1525, UV-Detector 2487 Dual (220 and 254 nm); Driver Software Breeze vers. 3.20; Column material: *YMC*-ODS-A C_{18} (12 nm pore size, 5 μm particle size, 250 mm x 20 mm), *YMC*-ODS-AQ C_{18} (12 nm pore size, 5 μm particle size, 250 mm x 20 mm) or *YMC*basic (proprietary, 5 μm particle size, 250 mm x 20 mm).

HPLC-ESI-MS analyses were performed on a *Hewlett Packard* Series HP 1100 with a *Finnigan LCQ* mass spectrometer using a *YMC*-Hydrosphere C_{18} column (12 nm pore size, 3 μm particle size, 125 mm x 2.1 mm, 9 min gradient elution, flow rate 0.55 mL/min) or *YMC*-Octyl C_8 column (20 nm pore size, 5 μm particle size, 250 mm x 2.1 mm, 30 min gradient elution, flow rate 0.2 mL/min). The system uses H_2O (0.1% formic acid) and MeCN (0.1% formic acid) as eluents.

High resolution mass spectrometry was recorded on a *Thermo Finnigan* LTQ-FT (ESI-ICR) spectrometer.

^{1}H NMR and ^{13}C NMR spectra were recorded at 295 K on a 500 MHz *Bruker* DMX (*Bruker*, Karlsruhe, Germany). Chemical shifts (δ) are given in parts per million

(ppm). Following solvent peaks were used as internal standards: DMSO-d_5: 2.50 ppm (^{1}H NMR) and 39.52 ppm (^{13}C NMR).[1]

All yields are not optimized. Standard peptide coupling techniques were employed. All tested compounds exhibited radiochemical and chemical purities ≥95% as determined by RP-HPLC-(MS).

All compounds were characterized by ^{1}H, ^{13}C NMR, HPLC, HPLC-MS and high resolution MS.

## Compound Preparation and Analytical Data
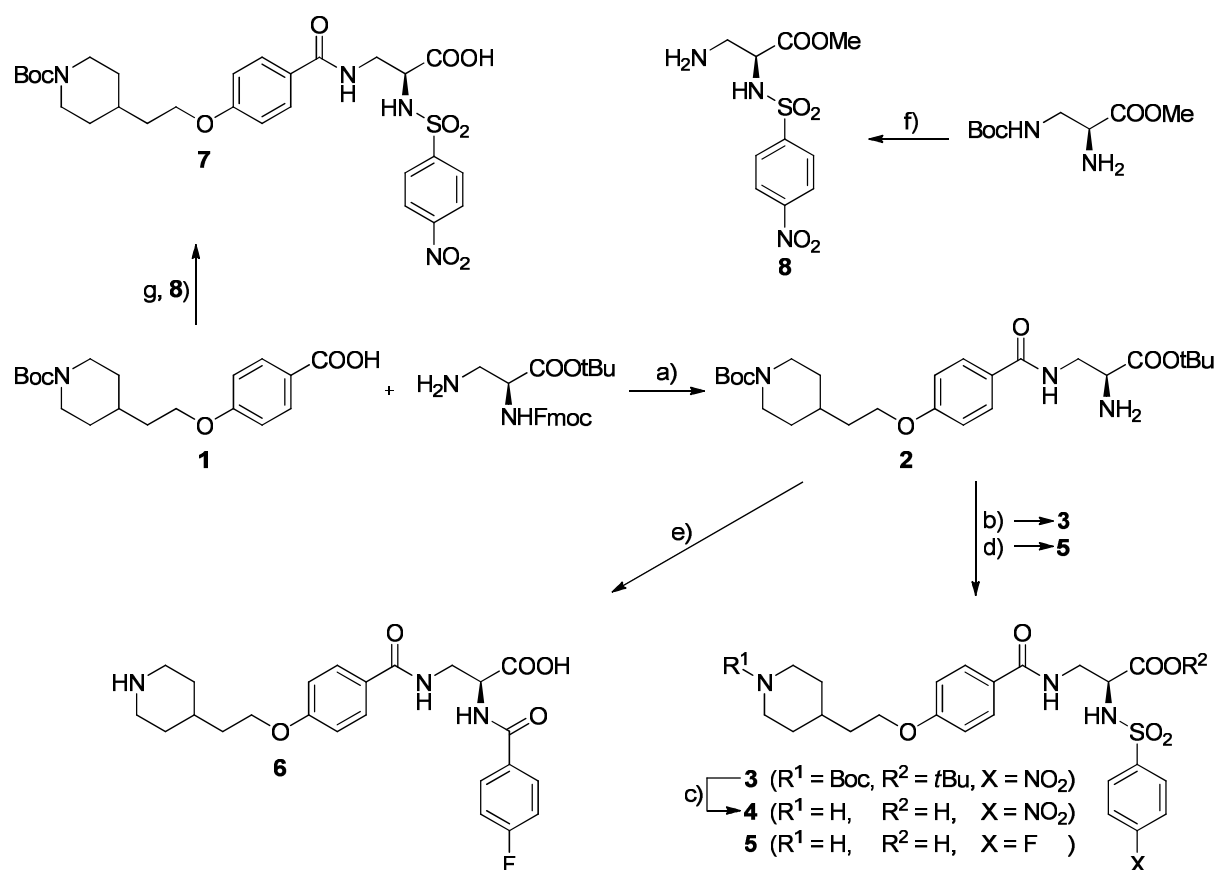
Supplementary Scheme 1. Synthesis of *para*-nitro substituted precursors **3,4** and **7** and ^{19}F-reference compounds **5** and **6**. a) 1. HATU, DIEA, DMF, RT, 16 h; 2. 20% piperidine/DMF, RT, 2 h; b) 4-Nitrobenzenesulfonyl chloride, DIEA, DCM, RT, 5 h; c) HCl$_{(aq)}$, dioxane, RT, 1 h; d) 1. 4-Fluorobenzenesulfonyl chloride, DIEA, DCM, RT, 5 h; 2. HCl$_{(aq)}$, dioxane, RT, 1 h; e) 1. HATU, 4-Fluorobenzoic acid, DIEA, DMF, RT, 16 h; 2. HCl$_{(aq)}$, dioxane, RT, 1 h; f) 1. 4-Nitrobenzenesulfonyl chloride, DIEA, DCM, RT, 5 h; 2. TFA, DCM, RT, 1 h; g) 1. HATU, 7, DIEA, DMF, RT, 16 h; 2. LiOH, methanol, H$_2$O, RT, 16 h. All compounds were purified by RP-HPLC.

4-[2-*N*-(*tert*-Butyloxycarbonyl)piperidin-4-ylethoxy]benzoic acid (1)
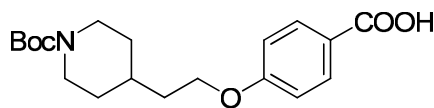
Chemical Formula: $C_{19}H_{27}NO_5$
Exact Mass: 349,18892
Molecular Weight: 349,42138

1 was synthesized according to literature procedures.[2, 3]

3-{4-[2-*N*-(*tert*-Butyloxycarbonyl)piperidin-4-ylethoxy]benzoylamino}-2-(*S*)-aminopropionic acid *tert*-butyl ester (2)
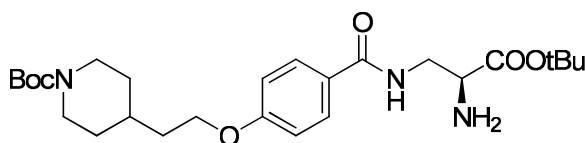

Chemical Formula: $C_{26}H_{41}N_3O_6$
Exact Mass: 491,29954
Molecular Weight: 491,62024

HATU (182 mg, 0.479 mmol), **1** (167 mg, 0.479 mmol) and DIEA (814 µL, 4.79 mmol) were dissolved in DMF (dry, 5 mL) and stirred at RT for 15 min. A solution of N^{α}-Fmoc-*L*-Diaminopropionic acid *tert*-butyl ester hydrochloride (201 mg, 0.479 mmol) in DMF (dry, 3 mL) was added and stirred at RT for 16 h. The solvent was removed in vacuo and the residue was dissolved in a solution of piperidine (20%) in DMF (v/v, 10 mL) and stirred at RT for 2 h. Concentration in vacuo and purification by RP-HPLC and lyophilization gave **2** (223 mg, 0.454 mmol, 95%) as a white solid.

^{1}H NMR (500 MHz, DMSO-d_6, RT): δ (ppm) = 8.55 (t, ^3J = 5.8 Hz, 1 H), 8.35 (br s, 2 H), 7.81 (d, ^3J = 8.8 Hz, 2 H), 7.03 (d, ^3J = 8.9 Hz, 2 H), 4.14-4.03 (m, 3 H), 3.98-3.86 (m, 2 H), 3.73-3.63 (m, 2 H), 2.83-2.57 (m, 2 H), 1.71-1.58 (m, 5 H), 1.38 (s, 18 H), 1.09-1.01 (m, 2 H). **^{13}C NMR** (126 MHz, DMSO-d_6, RT): δ (ppm) = 167.1, 166.6, 161.3, 153.8, 129.2, 125.7, 114.0, 83.1, 78.5, 65.5, 52.6, 35.0, 32.3, 28.1, 27.4. **MS** (ESI): $^m/_z$ = 336.3 [M-Boc-^{t}Bu+3H]$^+$, 380.1 [M-2^{t}Bu+3H]$^+$, 436.1 [M-^{t}Bu+2H]$^+$, 492.1 [M+H]$^+$, 514.2 [M+Na]$^+$, 982.9 [2M+H]$^+$. **RP-HPLC** (10-90% in 30 min): t_R = 21.5 min. **HR-MS** (ESI): calcd. for $C_{26}H_{42}N_3O_6^+$ 492.30681; found: 492.30707.

3-{4-[2-*N*-(*tert*-Butyloxycarbonyl)piperidin-4-ylethoxy]benzoylamino}-2-(*S*)-4-nitrophenylsulfonyl-aminopropionic acid *tert*-butyl ester (3)

Chemical Formula: $C_{32}H_{44}N_4O_{10}S$
Exact Mass: 676,27781
Molecular Weight: 676,77756
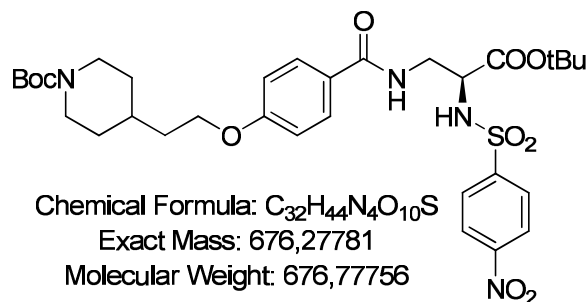
4-Nitrobenzenesulfonyl chloride (47.3 mg, 0.214 mmol) was added to a solution of **2** (105 mg, 0.214 mmol) and DIEA (363 µL, 2.14 mmol) in DCM (dry, 10 mL). The resulting yellow solution was stirred at RT for 5 h. Concentration in vacuo and purification by RP-HPLC and lyophilization gave the fully-protected precursor **3** (132 mg, 0.195 mmol, 91%) as a white solid.

¹H NMR (500 MHz, DMSO-d$_6$, RT): δ (ppm) = 8.74 (d, ^3J = 9.2 Hz, 1 H), 8.27 (t, ^3J = 5.7 Hz, 1 H), 8.24 (d, ^3J = 9.0 Hz, 2 H), 7.95 (d, ^3J = 9.0 Hz, 2 H), 7.64 (d, ^3J = 8.8 Hz, 2 H), 6.92 (d, ^3J = 8.8 Hz, 2 H), 4.15-4.10 (m, 1 H), 4.04 (t, ^3J = 6.0 Hz, 2 H), 3.98-3.88 (m, 2 H), 3.53-3.29 (m, 2 H), 2.81-2.61 (m, 2 H), 1.74-1.61 (m, 5 H), 1.39 (s, 9 H), 1.20 (s, 9 H), 1.09-1.01 (m, 2 H). **¹³C NMR** (126 MHz, DMSO-d$_6$, RT): δ (ppm) = 168.8, 165.6, 161.1, 153.8, 149.2, 146.6, 128.9, 128.0, 125.6, 124.4, 113.8, 81.4, 78.4, 65.4, 55.6, 35.1, 32.3, 28.1, 27.3. **MS** (ESI): $^m/_z$ = 521.2 [M-Boc-^{t}Bu+3H]$^+$, 565.0 [M-2^{t}Bu+3H]$^+$, 577.2 [M-^{t}Bu-CO$_2$+2H]$^+$, 621.0 [M-^{t}Bu+2H]$^+$, 676.8 [M+H]$^+$, 699.1 [M+Na]$^+$, 1253.0 [2M-Boc+2H]$^+$, 1353.0 [2M+H]$^+$, 1375.0 [2M+Na]$^+$. **RP-HPLC** (10-90% in 30 min): t_R = 30.1 min. **HR-MS** (ESI): calcd. for $C_{32}H_{45}N_4O_{10}S^+$ 677.28509; found: 677.28479.

3-[4-(2-Piperidin-4-ylethoxy)benzoylamino]-2-(*S*)-4-nitrophenylsulfonyl-aminopropionic acid (4)

Chemical Formula: $C_{23}H_{28}N_4O_8S$
Exact Mass: 520,16278
Molecular Weight: 520,55542
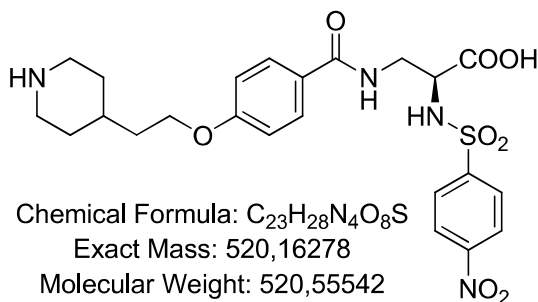
3 (50.0 mg, 73.9 μmol) was dissolved in a 3 : 1 mixture of dioxane and concentrated aqueous HCl (~0.1 M). After stirring for 1 h the solvents were removed under reduced pressure. The resulting fully-deprotected precursor was purified using preparative reverse phase HPLC. Purification by RP-HPLC and lyophilization gave **4** (37.3 mg, 71.7 μmol, 97%) as a white solid.

¹H NMR (500 MHz, DMSO-d_6, RT): δ (ppm) = 12.96 (br s, 1 H), 8.64 (d, ^3J = 8.9 Hz, 1 H), 8.48 (d, ^2J = 9.0 Hz, 1 H), 8.21 (t, ^3J = 5.8 Hz, 1 H), 8.19 (d, ^2J = 9.0 Hz, 1 H), 8.12 (d, ^3J = 8.8 Hz, 2 H), 7.91 (d, ^3J = 8.8 Hz, 2 H), 7.59 (d, ^3J = 8.8 Hz, 2 H), 6.87 (d, ^3J = 8.8 Hz, 2 H), 4.18-4.12 (m, 1 H), 4.05 (t, ^3J = 6.2 Hz, 2 H), 3.58-3.51 (m, 1 H), 3.31-3.23 (m, 3 H), 2.93-2.83 (m, 2 H), 1.93-1.86 (m, 2 H), 1.85-1.75 (m, 1 H), 1.74-1.66 (m, 2 H), 1.37-1.31 (m, 2 H). **¹³C NMR** (126 MHz, DMSO-d_6, RT): δ (ppm) = 171.2, 165.6, 160.9, 148.9, 146.7, 128.9, 127.8, 125.6, 124.2, 113.6, 65.1, 55.3, 43.2, 41.1, 34.6, 30.3, 28.4. **MS** (ESI): $^m/_z$ = 521.2 [M+H]⁺, 1040.9 [2M+H]⁺, 1063.0 [2M+Na]⁺. **RP-HPLC** (10-90% in 30 min): t_R = 13.1 min. **HR-MS** (ESI): calcd. for $C_{23}H_{29}N_4O_8S^+$ 521.17006; found: 521.17001.

3-[4-(2-Piperidin-4-ylethoxy)benzoylamino]-2-(*S*)-4-fluorophenylsulfonyl-aminopropionic acid (5)

Chemical Formula: $C_{23}H_{28}FN_3O_6S$
Exact Mass: 493,16828
Molecular Weight: 493,54832
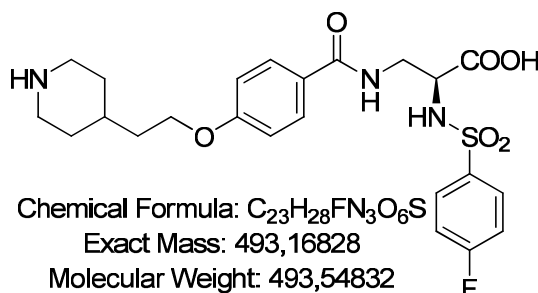
4-Fluorobenzenesulfonyl chloride (41.6 mg, 0.214 mmol) was added to a solution of **2** (105 mg, 0.214 mmol) and DIEA (363 µL, 2.14 mmol) in DCM (dry, 10 mL). After stirring for 5 h at RT the solvent was removed under reduced pressure and the residue was re-dissolved in a 3 : 1 mixture of dioxane and concentrated aqueous HCl (~0.1 M). After stirring for 1 h the solvents were removed in vacuo. Purification by RP-HPLC and lyophilization gave **5** (98.2 mg, 0.199 mmol, 93%) as a white solid.

^{1}H NMR (500 MHz, DMSO-d_6, RT): δ (ppm) = 12.80 (br s, 1 H), 8.53 (br s, 1 H), 8.34-8.26 (m, 2 H), 8.22 (br s, 1 H), 7.78 (dd, ^3J = 8.6 Hz, $^4J_{CF}$ = 5.3 Hz, 2 H), 7.70 (d, ^3J = 8.8 Hz, 2 H), 7.26 (t, ^3J = 8.8 Hz, 2 H), 6.96 (d, ^3J = 8.8 Hz, 2 H), 4.08 (t, ^3J = 6.2 Hz, 2 H), 4.06-4.0 (m, 1 H), 3.54-3.46 (m, 1 H), 3.35-3.29 (m, 1 H), 3.29-3.22 (m, 2 H), 2.92-2.81 (m, 2 H), 1.90-1.83 (m, 2 H), 1.82-1.73 (m, 1 H), 1.73-1.66 (m, 2 H), 1.39-1.27 (m, 2 H). **^{13}C NMR** (126 MHz, DMSO-d_6, RT): δ (ppm) = 171.2, 165.9, 164.0 (d, $^1J_{CF}$ = 249.6 Hz), 160.9, 137.4 (d, $^4J_{CF}$ = 2.9 Hz), 129.4 (d, $^3J_{CF}$ = 9.5 Hz), 129.0, 126.1, 116.0 (d, $^2J_{CF}$ = 22.6 Hz), 113.9, 65.2, 55.2, 43.2, 41.3, 34.6, 30.3, 28.4. **MS** (ESI): $^m/_z$ = 494.2 [M+H]$^+$, 987.1 [2M+H]$^+$. **RP-HPLC** (10-90% in 30 min): t_R = 13.5 min. **HR-MS** (ESI): calcd. for $C_{23}H_{29}FN_3O_6S^+$ 494.17556; found: 494.17579.

3-[4-(2-Piperidin-4-ylethoxy)benzoylamino]-2-(*S*)-4-fluorobenzamidopropionic acid (6)

Chemical Formula: $C_{24}H_{28}FN_3O_5$
Exact Mass: 457,20130
Molecular Weight: 457,49462
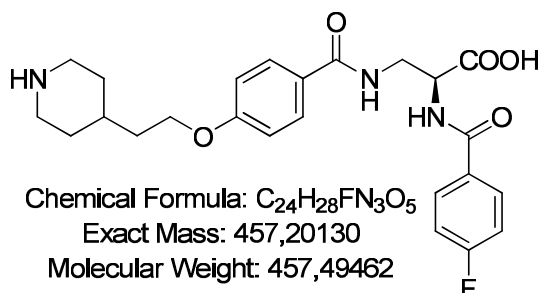
The title compound was prepared from **2**. Deprotected amin **2** (10.0 mg, 20.3 μmol) was dissolved in DMF (dry, 5 mL). A solution of HATU (7.73 mg, 20.3 μmol), 4-fluorobenzoic acid (2.85 mg, 20.3 μmol) and DIEA (34.6 μL, 203 μmol) in DMF (dry, 5 mL) was added and stirred at RT for 16 h. After evaporation of the DMF, the residue was re-dissolved in a 3 : 1 mixture of dioxane and concentrated aqueous HCl (~0.1 M). After stirring for 1 h the solvents were removed under reduced pressure. Purification by RP-HPLC and lyophilization gave **6** (8.10 mg, 17.7 μmol, 87%) as a white solid.

^{1}H NMR (500 MHz, DMSO-d_6, RT): δ (ppm) = 12.77 (br s, 1 H), 8.80 (d, ^3J = 7.4 Hz, 1 H), 8.56 (t, ^3J = 5.9 Hz, 1 H), 8.53-8.40 (m, 1 H), 8.25-8.08 (m, 1 H), 7.92 (dd, ^3J = 8.7 Hz, $^4J_{CF}$ = 5.7 Hz, 2 H), 7.79 (d, ^3J = 8.8 Hz, 2 H), 7.33 (t, ^3J = 8.8 Hz, 2 H), 6.98 (d, ^3J = 8.8 Hz, 2 H), 4.62-4.55 (m, 1 H), 4.06 (t, ^3J = 6.2 Hz, 2 H), 3.82-3.75 (m, 1 H), 3.70-3.60 (m, 1 H), 3.29-3.20 (m, 2 H), 2.91-2.80 (m, 2 H), 1.89-1.81 (m, 2 H), 1.81-1.71 (m, 1 H), 1.71-1.65 (m, 2 H), 1.38-1.27 (m, 2 H). **^{13}C NMR** (126 MHz, DMSO-d_6, RT): δ (ppm) = 171.8, 166.6, 165.3 162.0 (d, $^1J_{CF}$ = 262 Hz), 157.6, 130.4 (d, $^4J_{CF}$ = 3 Hz), 130.0 (d, $^3J_{CF}$ = 9.3 Hz), 129.1, 126.3, 115.4 (d, $^2J_{CF}$ = 21.9 Hz), 114.0, 65.2, 53.2, 43.2, 43.1, 34.6, 30.2, 28.4. **MS** (ESI): $^m/_z$ = 458.2 [M+H]$^+$, 480.2 [M+Na]$^+$, 915.2 [2M+H]$^+$, 937.2 [2M+Na]$^+$, 1372.1 [3M+H]$^+$. **RP-HPLC** (10-90% in 30 min): t_R = 13.2 min. **HR-MS** (ESI): calcd. for $C_{24}H_{29}FN_3O_5^+$ 458.20858; found: 458.20883.

3-{4-[2-*N*-(*tert*-Butyloxycarbonyl)piperidin-4-ylethoxy]benzoylamino}-2-(*S*)-4-nitrophenylsulfonyl-aminopropionic acid (7)

Chemical Formula: $C_{28}H_{36}N_4O_{10}S$
Exact Mass: 620,21521
Molecular Weight: 620,67124
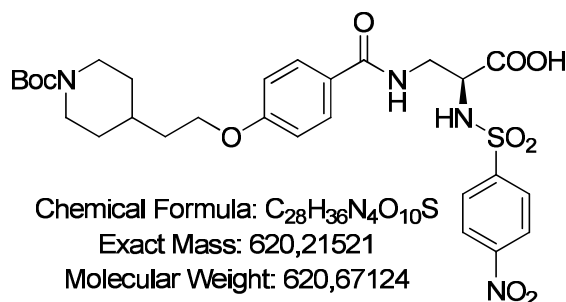
HATU (149 mg, 0.393 mmol), **1** (137 mg, 0.393 mmol) and DIEA (668 µL, 3.93 mmol) were dissolved in DMF (dry, 10 mL) and stirred at RT for 15 min. A solution of **8** (119 mg, 0.393 mmol) in DMF (dry, 3 mL) was added and stirred at RT for 16 h. The corresponding methyl ester was cleaved by saponification using LiOH. After evaporation of the DMF, the residue was dissolved in methanol-water 1:1. LiOH*H_2O (82.5 mg, 1.97 mmol) was added under stirring and the course of the reaction was monitored by analytical HPLC (usually 1 d). The solvents were removed and the resulting deprotected acid was purified by RP-HPLC to give **7** (212 mg, 0.342 mmol, 87%) as a white solid.

^{1}H NMR (500 MHz, DMSO-d$_6$, RT): δ (ppm) = 12.94 (br s, 1 H), 8.62 (d, ^3J = 8.8 Hz, 1 H), 8.20 (t, ^3J = 5.5 Hz, 1 H), 8.14 (d, ^2J = 9.0 Hz, 2 H), 7.92 (d, ^3J = 9.0 Hz, 2 H), 7.58 (d, ^3J = 8.2 Hz, 2 H), 6.88 (d, ^3J = 8.2 Hz, 2 H), 4.17-4.11 (m, 1 H), 4.04 (t, ^3J = 5.5 Hz, 2 H), 3.99-3.87 (m, 2 H), 3.60-3.47 (m, 2 H), 2.84-2.63 (m, 2 H), 1.75-1.60 (m, 5 H), 1.39 (s, 9 H), 1.12-1.01 (m, 2 H). **^{13}C NMR** (126 MHz, DMSO-d$_6$, RT): δ (ppm) = 171.1, 165.6, 161.0, 153.9, 148.9, 146.7, 128.9, 127.8, 125.5, 124.2, 113.7, 78.5, 65.3, 55.3, 35.1, 32.3, 28.1. **MS** (ESI): $^m/_z$ = 521.2 [M-Boc+2H]$^+$, 565.0 [M-^{t}Bu+2H]$^+$, 621.0 [M+H]$^+$, 643.2 [M+Na]$^+$, 1263.0 [2M+Na]$^+$. **RP-HPLC** (10-90% in 30 min): t_R = 25.6 min. **HR-MS** (ESI): calcd. for $C_{28}H_{37}N_4O_{10}S^+$ 621.22249; found: 621.22250

Methyl 3-amino-2-(*S*)-(4-nitrophenylsulfonamido)propanoate (8)
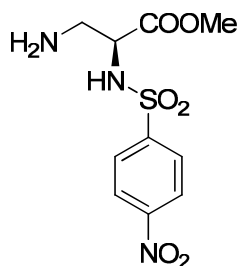
Chemical Formula: $C_{10}H_{13}N_3O_6S$
Exact Mass: 303,05251
Molecular Weight: 303,29172

4-Nitrobenzenesulfonyl chloride (87.0 mg, 0.393 mmol) was added to a solution of N^{β}-Boc-*L*-2,3-diaminopropionic acid methyl ester hydrochloride (100 mg, 0.393 mmol) and DIEA (668 µL, 3.93 mmol) in DCM (dry, 10 mL). The resulting yellow solution was stirred at RT for 5 h. After evaporation of the solvent, the residue was treated with a solution of TFA in DCM (10 mL, TFA/DCM = 3:1 v/v) for 1 h at RT. Removal of the TFA solution under reduced pressure gave **8** as crude product which was used without further purification.

^{1}H NMR (500 MHz, DMSO-d$_6$, RT): δ (ppm) = 9.03 (br s, 1 H), 8.44 (d, ^3J = 8.8 Hz, 2 H), 8.03 (d, ^3J = 8.8 Hz, 5 H), 4.28 (br s, 1 H), 3.36 (s, 3 H), 3.21-3.12 (m, 1 H), 2.99-2.88 (m, 1 H). **^{13}C NMR** (126 MHz, DMSO-d$_6$, RT): δ (ppm) = 168.4, 149.7, 145.9, 128.3, 124.5, 53.6, 52.6. **MS** (ESI): $^m/_z$ = 304.0 [M+H]$^+$. **RP-HPLC** (10-90% in 30 min): t_R = 11.9 min. **HR-MS** (ESI): calcd. for $C_{10}H_{14}N_3O_6S^+$ 304.05978; found: 304.05977.

2. Integrin Binding Assay (Fibrinogen – αIIbβ3 Assay)

The inhibiting activity of the integrin antagonists was determined in a solid-phase binding assay using coated extracellular matrix protein fibrinogen and soluble αIIbβ3 integrin.[2] Flat-bottom 96-well ELISA plates (*BRAND*, Wertheim, Germany) were coated overnight at 4 °C with 100 μL/well of 10 μg/mL fibrinogen (*Calbiochem*, Darmstadt, Germany) in carbonate-buffer [15 mM Na_2CO_3, 35 mM $NaHCO_3$ (pH 9.6)]. Wells were then washed three times with PBST buffer [137 mM NaCl, 2.7 mM KCl, 10 mM Na_2HPO_4, 2 mM KH_2PO_4, 0.01% Tween 20 (pH 7.4)] and blocked for 1 h at room temperature with 150 μL/well of TSB-buffer [20 mM Tris-HCl, 150 mM NaCl, 1 mM $CaCl_2$, 1 mM $MgCl_2$, 1 mM $MnCl_2$ (pH 7.5), and 1% BSA]. After being washed three times with PBST, equal amounts of controls (tirofiban, *Sigma-Aldrich*, Taufkirchen, Germany) or test compounds were mixed with 5.0 μg/mL human integrin αIIbβ3 (*Enzyme Research Lab.*, Swansea, UK) resulting in a final TSB buffer dilution of 0.00006 to 10 μM (10 μM, 1.43 μM, 204 nM, 29 nM, 4.2 nM and 0.6 nM) for the inhibitors and 2.5 μg/mL for integrin αIIbβ3. 100 μL/well of these solutions was incubated for 1 h at room temperature. The plate was washed three times with PBST buffer and 100 μL/well of 2.0 μg/mL primary antibody (mouse anti-human CD41b, *BD Biosciences*, Heidelberg, Germany) was added to the plate. After incubation for 1 h at room temperature, the plate was washed three times with PBST and 100 μL/well of 1.0 μg/mL of secondary peroxidase-labeled antibody (anti-mouse IgG-POD, *Sigma-Aldrich*, Taufkirchen, Germany) was added to the plate and incubated for 1 h at room temperature. After washing the plate three times with PBST the plate was developed by adding 50 μL/well of SeramunBlau® fast (*Seramun Diagnostic GmbH*, Heidesee, Germany) and incubated for 5 min at room temperature. The reaction was stopped with 50 μL/well of 3 M H_2SO_4 and the absorbance was measured at 450 nm with a plate reader (POLARstar Galaxy, *BMG Labtechnologies*). Each compound concentration was tested in duplicate and the resulting inhibition curves were analyzed using OriginPro 7.5G software. The inflection point describes the IC_{50} value. Each plate contained tirofiban as internal control.

3. Radiolabeling
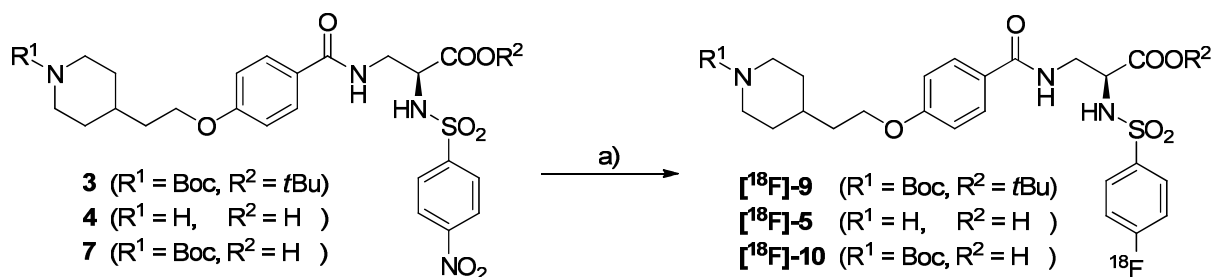
Supplementary Scheme 2. Radiosynthesis of ^{18}F-labeled compounds. a) K^{18}F, Kryptofix 2.2.2, K_2CO_3, $K_2C_2O_4$, DMSO, 150°C, 20min (optimized conditions).

General ^{18}F-Labeling Method:

$[^{18}F]$fluoride was produced through the $^{18}O(p,n)^{18}F$ nuclear reaction. The $[^{18}F]$fluoride was obtained in a 34 mM solution of K_2CO_3 (0.3 mL) and added to a 2 mL conical vial containing 0.5 mL dry MeCN (Merck, for DNA synthesis max 1 ppm H_2O) and 10 mg (39.9 µmol) Kryptofix 2.2.2. The solvent was evaporated by heating under stream of Argon gas. Azeotropic drying was repeated four times with 0.5 mL portions of MeCN. The precursor **3,4** or **7** (0.5-5 mg) was dissolved in 150 µL DMSO(Anhydrous ≥99.9%, Sigma Aldrich) and added to the dried kryptate [K$^+$⊂2.2.2]^{18}F$^-$, the vial was then sealed and heated to the desired temperature 100-150 °C for 10-60 min.

^{18}F-Labeling in presence of [K$^+$⊂2.2.2]CO$_3$ or [K$^+$⊂2.2.2]CO$_3$ and [K$^+$⊂2.2.2]C$_2$O$_4$:

The precursor (1-5 mg) was dissolved in 0.3 mL MeCN and added to already prepared [K$^+$⊂2.2.2]CO$_3$ or [K$^+$⊂2.2.2]CO$_3$ and [K$^+$⊂2.2.2]C$_2$O$_4$. The solvent was evaporated under stream of argon gas the mixture dissolved in 150 µL DMSO and added to the dried kryptate, [K$^+$⊂2.2.2]^{18}F$^-$, the vial was then sealed and heated to the desired temperature for 10-60 min.

Thereafter, the reaction mixture was diluted with 0.5 mL of water, loaded into a 2 mL injection loop and transferred onto a Cosmosil 5NPE C$_{18}$ column (12 nm average pore size, 5 µm particle size, 250 mm x 10 mm, *BGB*, Rheinfelden, Germany). The *Sykam* HPLC system uses H_2O (0.1% ammonium formate) and MeCN (0.1% ammonium formate) as eluents; 10-45% gradient, flow rate 10 mL/min. In-line HPLC detectors included a UV detector (*Sykam*) set at 254 nm and a radioactivity detector (Bioscan Flow-Count fitted with a PIN detector).

For animal experiments, the fractions containing the product were collected and diluted with water (1:1). The mixture was applied to a Sep-Pak C_{18} Classic (*Waters*) and the cartridge was subsequently washed with 10 mL water. The product was eluted with ethanol and diluted to the desired concentration with phosphate buffered saline. The pH of the final solution was between 7 and 8. [^{18}F]**5** was prepared in a specific activity of > 3000 mCi/µmol (111 GBq/µmol) at end-of-synthesis.

4. Biological Evaluation of Radiotracer [^{18}F]5

Platelet Aggregation Assay with ^{19}F Reference Compound 5

Whole blood was drained by intracardiac puncture from anesthetized 10-14 week old C57/Bl6 mice into hirudin coated tubes (*Multiplate*, Germany). Impedance-based whole blood aggregation measurements were performed according to the instruction manual (*Multiplate*, Germany). Briefly, 175 µL of whole blood were diluted 1:1 with 0.9% NaCl and incubated under stirring conditions in an aggregation chamber for 2 min at 37 °C. Subsequently the ^{19}F reference compound **5** (dissolved in 10%DMSO vehicle) was added with a final concentration of 10 µM, 1.43 µM, 204 nM, 29 nM, 4.2 nM, 0.6 nM or vehicle. After 5 min of incubation ADP (6.4 µM) and collagen (3.2 µM) were added respectively to trigger aggregation. Impedance curves were recorded for 6 min and the obtained AUC (area under the curve) values were used to determine EC_{50} values.[2]

Measurement of log*P*

Apparent drug lipophilicity was determined by a conventional partition method between 1-octanol and phosphate buffered saline (pH 7.4). The 1-octanol was saturated with PBS before use. Briefly, from a stock solution of 2 MBq no-carrier-added tracer, [^{18}F]**5,** in 2 mL PBS (pH 7.4), 0.2 mL was added to 0.2 mL of 1-octanol in a 1.5 mL polypropylene *Eppendorf* vial (n = 6). The vials were sealed and vortexed vigorously at room temperature for 5 min. The mixture was then centrifuged at 5000 rpm for 5 min. A 100 µL aliquot from each of the two phases was drawn and their radioactivity content was determined in a NaI (Tl) well-type detector.

The log $P_{oct/PBS}$ was calculated as follows:

log $P_{\text{oct/PBS}}$ = log (radioactivity concentration in the 1-octanol phase / radioactivity concentration in the PBS phase). The reported value represents the mean of six independent measurements.

Plasma Protein Binding

Human blood samples were collected in heparinized tubes and mixed with 2 MBq of n.c.a. [^{18}F]**5**, centrifuged (5 min, 5.000 rpm) for plasma isolatation, then supernatants were used for further evaluation. Samples (300 µL) of plasma were transferred to an ultrafiltration device (Vivacon 500, membrane: 30.000 MWCO HY, Sartoriusstedium biotech GmbH, Goetfingen, Germany) followed by centrifugation (10 min, 12.000 rpm) for the separation of proteins. The plasma protein values were determined by use of a γ-counter (a 1480 Wizard3 γ-counter from Wallac, PerkinElmer Life and Analytical Sciences) as described.[4]

Animal Experiments

The experiments were carried out with the approval of the institutional animal care committee (Regierung von Oberbayern, München, Germany), and in accordance with the German Animal Welfare Act (Deutsches Tierschutzgesetz). Animal husbandry followed the regulations of European Union (EU) guideline No. 86/609. Healthy C57Bl/6 male mice were obtained from Charles River laboratories Sulzfeld, Germany.

The animals were kept in a temperature-controlled environment (18-20 °C, 50-60 % relative humidity) on a 12:12 light/dark cycle with free access to a standard diet (Altromin 1326 mouse pellets, *Altromin*, Lage, Germany) and potable water. Mice were housed in type III cages (*Ehret*, Emmendingen, Germany), group size of ≤ 5 individuals with dust-reduced wood shavings as bedding. Upon arrival, all animals underwent an acclimatization period of ≥10 days prior to experiments.

Anesthesia

Inhalation anesthesia with isoflurane was used and the eyes of the animals were protected with dexpanthenol eye ointment. Anesthesia was initiated 15 min ahead of experimental procedures by placing the animal in a cage ventilated with oxygen (3.5 L/min) containing 3% isoflurane. During the experiments, anesthesia for the

duration of the procedure was maintained by adjusting the isoflurane content (0.6% to 2%) to ensure a respiratory rate in the range 80-100/min. Body temperature was held at 37 °C by employing a temperature-controlled heating pad.

Injection of Tracer

Access to a lateral tail vein was made by a 30 gauge needle which was connected via a polythene tubing (0.28 mm inner diameter) to a 1 mL syringe. Prior to injection of the tracer, the catheter filled with isotonic sodium chloride solution. The catheter was stabilized at the injection site with superglue.

General Biodistribution Studies in Wild-Type Mice

Biodistribution studies were performed in healthy C57Bl/6 male mice (body weight of 25-28 g). The mice were injected in a lateral tail vein with 4-14 MBq of n.c.a. [^{18}F]**5** contained in 0.1-0.15 ml of a solution of isotonic phosphate buffered saline. Groups of mice were sacrificed at 30 and 60 min p.i. The radioactivity of weighted tissue samples was measured in a γ-counter. Data are expressed as percent of the injected dose per gram tissue (% I.D or % I.D./g; mean ± sd, n ≥ 3).

General Procedures for Metabolite Analyses

Male healthy mice were prepared according to the procedure described for the biodistribution studies and were injected with 8-14 MBq of n.c.a. [^{18}F]**5** in a total volume of 0.1 mL PBS. The animals were sacrificed after 30 and 60 min p.i. and urine, spleen and liver samples were collected and analyzed. Blood was collected in heparinized tubes and centrifuged (5 min, 5000 rpm) for plasma isolation but unfortunately due to fast clearance of tracer from blood the rest of activity were not detectable. The spleen and liver were subsequently homogenized with a manual homogenizer for 5 min, the mixture vigorously vortexed, and 1 mL of MeCN:PBS (1:1) was added. After centrifugation for 5 min at 6000 rpm, the supernatant was collected followed by centrifugation (10 min, 12000 rpm) and the supernatants were used for further evaluation. Samples (300 µL) of plasma and homogenized organs were transferred to an ultrafiltration device (Vivacon 500, membrane: 30.000 MWCO HY, sartorius stedim biotech GmbH, Goetfingen, Germany) followed by centrifugation (10 min, 12000 rpm) for the separation of proteins. Approximately 0.1 mL of the supernatant solutions (15000 cpm) as well as a sample of [^{18}F]**5** (all sample were

approximately 15000 cpm, measured by γ-counter) were applied on a preparative TLC glass plate (PTLC silica gel with F_{254} indicator on glass plates with 4 × 20 cm preconcentration zone) for the quantification of the radiolabeled metabolic species and eluted with a mixture of 75% MeCN and 25% H_2O. The PTLC was detected by Phospho-Imager (CR 35 BIO, *Isotopenmeßgeräte GmbH*, Straubenhardt, Germany) and the resulting images analyzed using AIDA Image Analyzer software. The amount of intact tracer (Ti) was calculated as follows:

$$Ti = [FT / FT + FM] \times EE \times ER \times 1 \cdot 10^{-2}$$

where FT [%] represents the amount of intact tracer and FM [%] the amount of metabolites as determined by radio-HPLC, corrected for extraction efficiency EE [%] from the plasma samples and the recovery ER [%] of activity from the HPLC. The extraction efficiency was in the range 58-92 % among the compounds investigated.

PET Imaging

A subset of four animals was imaged using a small animal PET/CT scanner (Inveon, Siemens Medical Solutions, Knoxville, TN, USA.). The mice were anesthetized using 3% isoflurane. Breathing was monitored, and temperature maintained using a heating pad throughout the imaging procedures. A CT scan was performed for anatomical localization. The mice were then injected with 15 MBq of [^{18}F]**5** into the tail vein, and dynamic PET data were acquired from the start of the injection for 60 min in list mode.

PET data were reconstructed using a 3D-filtered back-projection algorithm. The resulting matrix was 128×128 pixels with 159 transverse slices (reconstructed voxel size of 0.80×0.80×0.80 mm^3). Data were normalized and corrected for randoms, dead time, and decay. No corrections were made for attenuation or scatter.

CT acquisition consisted of 121 projections acquired with exposure time of 200 ms, X-ray voltage of 80 kVp and anode current of 500 uA for 220° rotation. CT images were reconstructed using a modified Feldcamp algorithm. The resulting matrix was 256×256 pixels with 631 transverse slices (reconstructed voxel size 0.21×0.21×0.21 mm).

The PET and CT images were fused and the uptake was visualized using the Inveon Research Workplace (Siemens, Knoxville, TN, USA.). Regions of interest (ROI) were drawn manually. The mean radioactivity concentration within the ROIs was expressed as the percentage of injected dose per gram of tissue (% ID/g).

References

(1) Gottlieb, H. E.; Kotlyar, V.; Nudelman, A. NMR Chemical Shifts of Common Laboratory Solvents as Trace Impurities. *J. Org. Chem.* **1997,** *62*, 7512-7515.

(2) Bollinger, M.; Manzenrieder, F.; Kolb, R.; Bochen, A.; Neubauer, S.; Marinelli, L.; Limongelli, V.; Novellino, E.; Moessmer, G.; Pell, R.; Lindner, W.; Fanous, J.; Hoffman, A.; Kessler, H. Tailoring of Integrin Ligands: Probing the Charge Capability of the Metal Ion-Dependent Adhesion Site. *J. Med. Chem.* **2012,** *55*, 871-882.

(3) Duggan, M. E.; Duong, L. T.; Fisher, J. E.; Hamill, T. G.; Hoffman, W. F.; Huff, J. R.; Ihle, N. C.; Leu, C. T.; Nagy, R. M.; Perkins, J. J.; Rodan, S. B.; Wesolowski, G.; Whitman, D. B.; Zartman, A. E.; Rodan, G. A.; Hartman, G. D. Nonpeptide $\alpha_v\beta_3$ Antagonists. 1. Transformation of a Potent, Integrin-Selective $\alpha_{IIb}\beta_3$ Antagonist into a Potent $\alpha_v\beta_3$ Antagonist. *J. Med. Chem.* **2000,** *43*, 3736-3745.

(4) Wester, H.-J.; Willoch, F.; Tölle, T. R.; Munz, F.; Herz, M.; Øye, I.; Schadrack, J.; Schwaiger, M.; Bartenstein, P. 6-*O*-(2-[18F]Fluoroethyl)-6-*O*-Desmethyldiprenorphine ([18F]DPN): Synthesis, Biologic Evaluation, and Comparison with [11C]DPN in Humans. *J. Nucl. Med.* **2000,** *41*, 1279-1286.

APPENDIX III

Peptide Cyclization and Cyclodimerization by Cu^I-Mediated Azide−Alkyne Cycloaddition

Reshma Jagasia,[†] Justin M. Holub,[‡] Markus Bollinger,[†] Kent Kirshenbaum,[‡] and M. G. Finn*,[†]

Department of Chemistry and The Skaggs Institute for Chemical Biology, The Scripps Research Institute, 10550 North Torrey Pines Road, La Jolla, California 92037, and Department of Chemistry, New York University, New York, New York 10003

mgfinn@scripps.edu

Received September 21, 2008
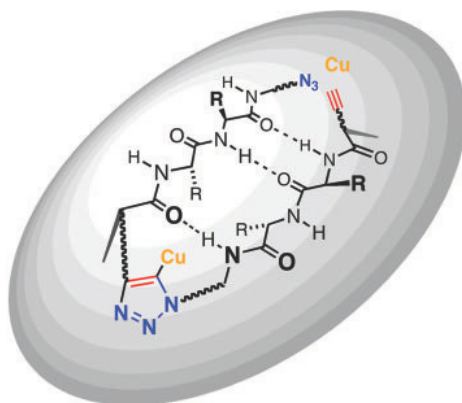
Head-to-tail cyclodimerization of resin-bound oligopeptides bearing azide and alkyne groups occurs readily by 1,3-dipolar cycloaddition upon treatment with Cu^I. The process was found to be independent of peptide sequence, sensitive to the proximity of the alkyne to the resin, sensitive to solvent composition, facile for α- and β-peptides but not for γ-peptides, and inhibited by the inclusion of tertiary amide linkages. Peptides shorter than hexamers were predominantly converted to cyclic monomers. Oligoglycine and oligo(β-alanine) chains underwent oligomerization by 1,3-dipolar cycloaddition in the absence of a copper catalyst. These results suggest that cyclodimerization depends on the ability of the azido−alkyne peptide to form in-frame hydrogen bonds between chains in order to place the reacting groups in close proximity and lower the entropic penalty for dimerization. The properties of the resin and solvent are crucial, giving rise to a productive balance between swelling and interstrand H-bonding. These findings allow for the design of optimal substrates for triazole-forming ring closure and for the course of the reaction to be controlled by the choice of conditions.

Introduction

Cyclic peptides and related structures are of longstanding interest as biologically active compounds because of their ability to display protein-like epitopes with restricted conformational flexibility.[1−3] Relative to their linear analogues, cyclic peptides are often more bioavailable, more stable toward metabolic degradation, and more selective in receptor binding.[4−11] It is therefore not surprising that peptide sequences are frequently evaluated for function in both linear and cyclic forms, creating a need for effective cyclization strategies.

† The Scripps Research Institute.
‡ New York University.
(1) Davies, J. S. In *Cyclic Polymers*, 2nd ed.; Semlyen, J. A., Ed.; Kluwer Academic Publishers: Dordrecht, Netherlands, 2000; pp 85−124.
(2) Davies, J. S. *Amino Acids, Peptides, and Proteins* 2002, 33, 238−294.
(3) Kessler, H.; Gratias, R.; Hessler, G.; Gurrath, M.; Mueller, G. *Pure Appl. Chem.* 1996, 68, 1201−1205.

(4) Colombo, G.; Curnis, F.; De Mori, G. M. S.; Gasparri, A.; Longoni, C.; Sacchi, A.; Longhi, R.; Corti, A. *J. Biol. Chem.* 2002, 277, 47891−47897.
(5) Craik, D. J.; Simonsen, S.; Daly, N. L. *Curr. Opin. Drug Discovery* 2002, 5, 251−260.
(6) Gobbo, M.; Biondi, L.; Filira, F.; Gennaro, R.; Benincasa, M.; Scolaro, B.; Rocchi, R. *J. Med. Chem.* 2002, 45, 4494−4504.
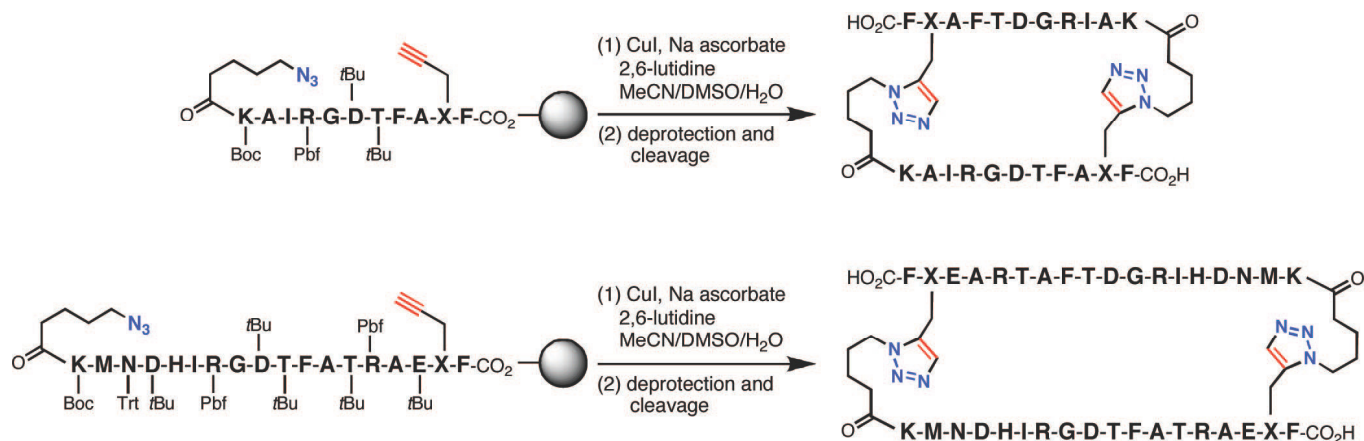(7) Barry, D. G.; Daly, N. L.; Clark, R. J.; Sando, L.; Craik, D. J. *Biochemistry* 2003, 42, 6688−6695.

FIGURE 1. On-resin peptide cyclodimerization of two sequences originally reported by Finn et al.[26] Amino acids are represented by their single-letter codes in bold print (X = propargylglycine).

Peptide cyclization is most often accomplished by the formation of amide, ester, thioester, disulfide, olefin, or C—C bonds.[12−14] Recently the copper(I)-mediated azide−alkyne cycloaddition (CuAAC) reaction has been employed as a means of orthogonal modification[15] and cyclization of peptides,[16−18] glycopeptides,[19] polymers,[20] and dendrimers.[21,22] In the context of peptides, this "click reaction"[23−25] methodology offers two important advantages. (1) Azide and alkyne units can be incorporated into peptide sequences during solid-phase peptide synthesis (SPPS) without protection, as both of these groups are stable to typical conditions of peptide synthesis and cleavage. (2) Azides and alkynes react selectively with each other, but do so very slowly unless catalyzed, allowing their ligation to be triggered at will.
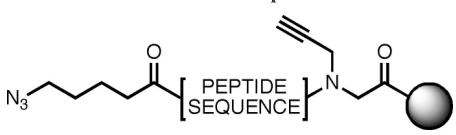
We previously described attempts to cyclize two peptides on resin via the CuAAC reaction (Figure 1).[26] The sequences used in this preliminary study were derived from an adenovirus serotype that binds several α_v integrins and contains the canonical Arg-Gly-Asp (RGD) triad. The alkyne, introduced as a propargylglycine unit, was located near the resin-bound C-terminus, while the azide group was incorporated as a 5-azidopentanoyl unit at the N-terminus. On-resin cyclization mediated by cuprous iodide gave high yields of head-to-tail cyclic dimer rather than the expected cyclic monomer, even for sequences of substantial length and no obvious conformational, steric, or torsional constraints.

Several examples of solution-phase Cu-mediated cyclodimerization of peptides and carbohydrates have been reported, all with azido−alkyne substrates for which monomeric ring closure is disfavored because of torsional or geometric factors (described in more detail in the Supporting Information).[27−30] Other investigators have described mixtures of peptide cyclic monomers and dimers as a function of ring strain and concentration,[31,32] as well as clean macrocyclization under the influence of conformational constraints.[17,18,33] These observations show that the CuAAC process is not inherently predisposed toward ring closure by head-to-tail dimerization. The unexpected and clean cyclodimerization of the two resin-bound peptides shown in Figure 1 therefore signaled to us the presence of an unexpected mechanistic feature. We suggested a sequence-dependent conformational bias and/or amide−Cu binding as two possible contributing factors in our original report.[26] We describe here experimental tests that disprove these hypotheses and suggest a crucial role for interchain hydrogen bonding. In addition, we wanted to explore the scope and limitations of the cyclodimerization method, since its products are both unique and potentially useful. When compared with monocyclic analogues, cyclic dimers test the contributions of both conformational rigidity and valency in the binding of peptide motifs to their targets.

(8) Yokoyama, F.; Suzuki, N.; Haruki, M.; Nishi, N.; Oishi, S.; Fujii, N.; Utaru, A.; Kleinman, H. K.; Nomizu, M. *Biochemistry* **2004**, *43*, 13590–13597.

(9) Dathe, M.; Nikolenko, H.; Klose, J.; Bienert, M. *Biochemistry* **2004**, *43*, 9140–9150.

(10) Kumar, A.; Ye, G.; Wang, Y.; Lin, x.; Sun, G.; Parang, K. *J. Med. Chem.* **2006**, *49*, 3395–3401.

(11) Monroc, S.; Badosa, E.; Feliu, L.; Planas, M.; Montesinos, E.; Bardají, E. *Peptides* **2006**, *27*, 2567–2574.

(12) Lambert, J. N.; Mitchell, J. P.; Roberts, K. D. *J. Chem. Soc., Perkin Trans. 1* **2001**, 471–484.

(13) Bordusa, F. *ChemBioChem* **2001**, *2*, 405–409.

(14) Li, P.; Roller, P. P.; Xu, J. *Curr. Org. Chem.* **2002**, *6*, 411–440.

(15) Franke, R.; Doll, C.; Eichler, J. *Tetrahedron Lett.* **2005**, *46*, 4479–4482.

(16) Roice, M.; Johannsen, I.; Meldal, M. *QSAR Comb. Sci.* **2004**, *23*, 662–673.

(17) Bock, V. D.; Perciaccante, R.; Jansen, T. P.; Hiemstra, H.; Van Maarseveen, J. H. *Org. Lett.* **2006**, *8*, 919–922.

(18) Ray, A.; Manoj, K.; Bhadbhade, M. M.; Mukhopadhyay, R.; Bhattacharjya, A. *Tetrahedron Lett.* **2006**, *47*, 2775–2778.

(19) Agren, J. K. M.; Billing, J. F.; Grundberg, H. E.; Nilsson, U. J. *Synthesis* **2006**, *18*, 3141–3145.

(20) Grayson, S. M.; Laurent, B. A.; Eugene, D. E. *Polym. Mater. Sci. Eng.* **2006**, *51*, 827–828.

(21) Rijkers, D. T. S.; Van Esse, G. W.; Merkx, R.; Brouwer, A. J.; Jacobs, H. J. F.; Pieters, R. J.; Liskamp, R. M. J. *Chem. Commun.* **2005**, 4581–4583.

(22) Wu, P.; Malkoch, M.; Hunt, J. N.; Vestberg, R.; Kaltgrad, E.; Finn, M. G.; Fokin, V. V.; Sharpless, K. B.; Hawker, C. J. *Chem. Commun.* **2005**, *46*, 5775–5777.

(23) Kolb, H. C.; Finn, M. G.; Sharpless, K. B. *Angew. Chem., Int. Ed.* **2001**, *40*, 2004–2021.

(24) Tornøe, C. W.; Christensen, C.; Meldal, M. *J. Org. Chem.* **2002**, *67*, 3057–3062.

(25) Rostovtsev, V. V.; Green, L. G.; Fokin, V. V.; Sharpless, K. B. *Angew. Chem., Int. Ed.* **2002**, *41*, 2596–2599.

(26) Punna, S.; Kuzelka, J.; Wang, Q.; Finn, M. G. *Angew. Chem., Int. Ed.* **2005**, *44*, 2215–2220.

(27) Van Maarseveen, J. H.; Horne, W. S.; Ghadiri, M. R. *Org. Lett.* **2005**, *7*, 4503–4506.

(28) Billing, J. F.; Nilsson, U. J. *J. Org. Chem.* **2005**, *70*, 4847–4850.

(29) Bodine, K. D.; Gin, D. Y.; Gin, M. S. *J. Am. Chem. Soc.* **2004**, *126*, 1638–1639.

(30) Bodine, K. D.; Gin, D. Y.; Gin, M. S. *Org. Lett.* **2005**, *7*, 4479–4482.

(31) Angell, Y.; Burgess, K. *J. Org. Chem.* **2005**, *70*, 9595–9598.

(32) Choi, W. J.; Shi, Z.-D.; Worthy, K. M.; Bindu, L.; Karki, R. G.; Nicklaus, M. C.; Fisher, R. J.; Burke, T. R., Jr. *Bioorg. Med. Chem. Lett.* **2006**, *16*, 5265–5269.

(33) Torres, O.; Yüksel, D.; Bernardina, M.; Kumar, K.; Bong, D. *ChemBioChem* **2008**, *9*, 1701–1705.

**TABLE 1. Peptide Sequences To Test the Dependence of Cyclodimerization on Amino Acid Composition[a]**

no.	sequence[b]	no.	sequence[b]	no.	sequence[b]
1	IDASTRLNA	12	SVAEYRLKA	23	HMFTMAKLF
2	KVASTRLNA	13	THMFAHLKA	24	ADFTMAKLF
3	YSMFTRLNA	14	SVMFAHLKA	25	MFAQTRIEF
4	VEMFTRLNA	15	IQASAHLKA	26	THAQTRIEF
5	RLASFKCLA	16	KVASAHLKA	27	KWANTRIEF
6	TWASFKCLA	17	RLRMFWKLF	28	SVANTRIEF
7	HTVMFKCLA	18	AKRMFWKLF	29	KNASHKIEF
8	KCVMFKCLA	19	SEMAFWKLF	30	IMASHKIEF
9	MHAQYRLKA	20	GYMAFWKLF	31	VTSFHKIEF
10	TLAQYRLKA	21	KRHDMAKLF	32	KASFHKIEF
11	KWAEYRLKA	22	FVHDMAKLF		

[a] All peptides bear protected side-chain functional groups as listed in the Experimental Section, and all were cyclodimerized successfully by treatment with Cu[I] in 4:1 MeCN:DMSO. [b] Single-letter amino acid codes represent the resin-bound N-to-C sequence present between azide and alkyne moieties with the general structure shown above the table.

Results and Discussion

Sequence Tolerance. The dependence of cyclodimerization on sequence identity was probed with a set of 32 peptides synthesized by batch splitting after coupling every second residue (Table 1). All proteinogenic amino acids were included except proline; the sequences tested the importance of several residues in the original sequence that were suspected of playing a role in the cyclodimerization outcome. Peptides were synthesized on Rink amide MBHA (4-methylbenzhydrylamine) resin with an initial loading of 0.70 mmol/g, similar to that in our previous report. As before, alkynes were installed near the C-terminus, although by N-propargylation rather than in propargylglycine for synthetic convenience, and azides were introduced by acylation of the N-terminus. Each linear sequence was individually cleaved and lyophilized after a standard workup procedure. All 32 peptides were obtained with good to excellent purity (>75%, estimated by MALDI mass spectrometry analysis of the lyophilized crude powders).

Each resin-bound protected peptide was subjected to cyclization in 20 mM solutions of cuprous iodide under the convenient reaction conditions employed in our previous report (20% DMSO in MeCN, room temperature, 40 h, in screw-cap reaction vials closed immediately after bubbling with a stream of dry N₂). Successful cyclodimerization was indicated by a clear transition from a dominant peak of monomer mass to a dominant peak of dimeric mass in the MALDI mass spectrum of the lyophilized powders. This result was observed for all of the 32 sequences shown in Table 1, although some were slower to react than others due to inconsistencies in the exclusion of oxygen, thereby giving rise to different amounts of active Cu[I] catalyst. To confirm the expected cyclic nature of the products, most of the samples were subjected to careful analysis by analytical reversed-phase (RP) HPLC after cleavage from the resin. In each case, a significantly shorter retention time was observed for the major product macrocycle in comparison with corresponding linear monomers. In contrast, linear dimers synthesized independently showed uniformly longer reversed-phase HPLC retention times than their monomeric counterparts. Moreover, the chromatogram and mass spectrum of each product was unchanged after treatment with excess triphenylphosphine,
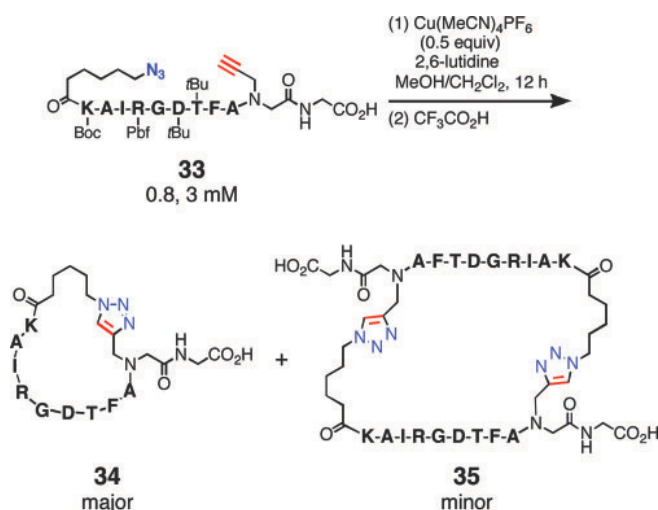
FIGURE 2. Solution-phase cyclization of an alkyne- and azide-derivatized peptide.

which would reduce the azide in a linear dimer. To the extent that our survey of sequence space is representative, it appears that *the CuAAC-mediated peptide cyclodimerization process is largely insensitive to the nature of the amino acids present in the sequence*, keeping in mind that side-chain functional groups are protected.

Solution-Phase Cyclization. To illuminate the role of the resin in the peptide cyclodimerization process, solution-phase reactions were performed with a protected peptide sequence similar to that in our original studies (Figure 2). Following solid-phase synthesis, cleavage (without deprotection), and purification, structure **33** was subjected to Cu[I]-mediated cycloaddition in a deoxygenated MeOH/CH₂Cl₂ mixture at concentrations of 0.8 and 3 mM, to promote an intra- and intermolecular reaction, respectively.[32] After side-chain deprotection, resin cleavage, and ether precipitation, the samples were analyzed by analytical HPLC and MALDI mass spectrometry. The major product peak in both reactions had monomer molecular weight, had significantly shorter retention time on RP-HPLC than the linear deprotected starting material, and was insensitive to reduction with phosphine, showing that monocyclization to structure **34** was the main pathway in the solution-phase reaction. A small amount of dimeric product **35** was also observed (approximately 10% and 20% when conducted at 0.8 and 3 mM, respectively, as determined by HPLC integration) which coeluted with an authentic sample of cyclic dimer. Therefore, *selective cyclodimerization of peptides of this length is facilitated by attachment to a resin*. However, a particular resin is not required. The use of three different polystyrene supports with different loading levels (chlorotrityl resin at 1.4 mmol/g starting functional group density, Rink amide MBHA resin at 0.70 mmol/g, and the PEGylated Rink-modified TentaGel (TGR) resin at 0.26 mmol/g) induced no substantial difference in the course of the reaction (Supporting Information).

Peptide Length. To evaluate the influence of peptide length on cyclodimerization, truncated versions of peptide **33** were prepared. When treated with Cu[I], resin-bound **36** was converted cleanly to the cyclic dimer, but the shorter sequence **37** gave an intractable mixture with no major peak on HPLC and a MALDI mass spectrum showing both monomer and dimer masses (Figure 3 and Supporting Information). The shortest sequence **38** produced a single major peak in the HPLC chromatogram with monomeric mass and a significantly shorter
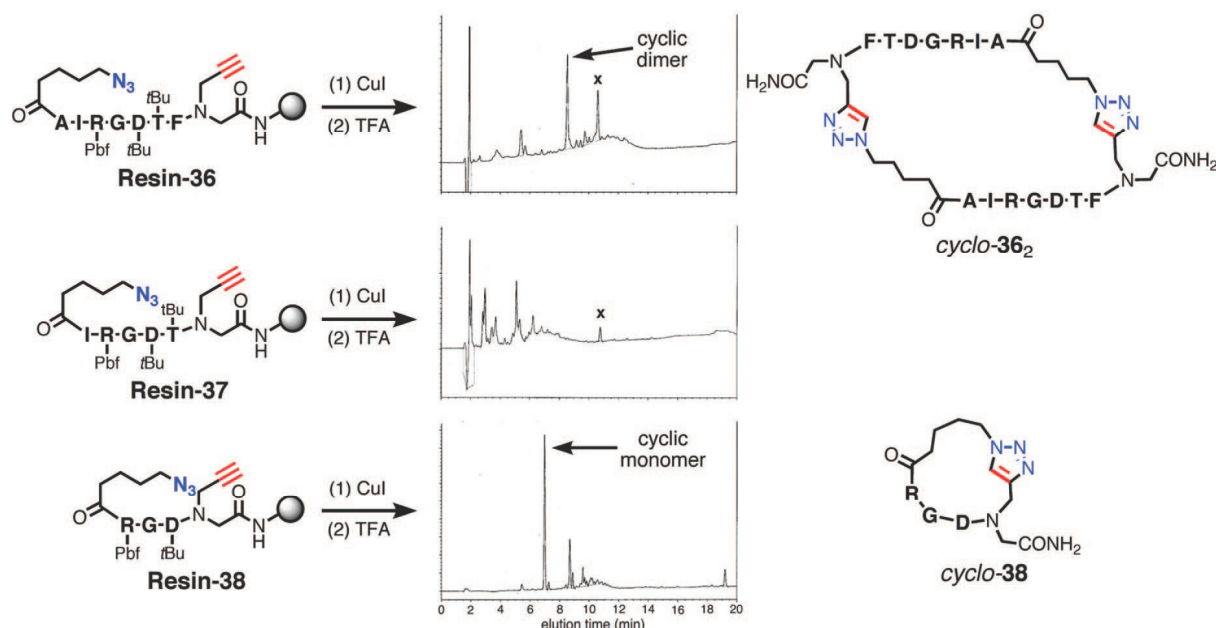
FIGURE 3. Test of the dependence of sequence length on cyclization. RP-HPLC chromatograms of the crude products. No linear monomers were observed, which was verified by coinjection of peptides before cyclization (not shown); "x" indicates peak due to a small amount of a chromophore with a high extinction coefficient.

retention time than the linear starting material; this material was unaffected by treatment with triphenylphosphine. Accordingly, this product was assigned as the cyclic monomer of sequence **38**. Monomeric cylization of peptides of this length was also shown to be independent of the sequence (Supporting Information). These results indicate that *a minimum peptide length of six residues is required in this case for selective cyclodimerization.*

Proximity of Alkyne to Resin. We previously demonstrated that cyclodimerization is favored by placement of the alkyne moiety at the C-terminal end of the peptide, which is attached to the resin polymer.[26] This phenomenon was further explored with sequences **39–43**, which provide an increasing number of glycine spacers between the resin and the alkyne (Figure 4). Under standard reaction conditions (5 or 20 mM Cu[I], 4:1 MeCN/DMSO with 2,6-lutidine), each of the sequences provided cyclic dimers as the sole detectable products by MALDI mass spectrometry. However, as the distance of the alkyne to the resin was increased, a progressive increase in the intensity of unresolved broad peaks was observed in the analytical RP-HPLC chromatograms. These side products are presumed to emerge from peptide degradation, which apparently becomes significant when cyclodimerization is not optimal (see Supporting Information for additional experiments). Thus, *cyclodimerization becomes less efficient as the alkyne is moved to peptide positions farther away from the resin.*

Availability of Alkyne. Figure 5 summarizes the outcome of experiments designed to test whether monocyclization could be made to occur if either azide or alkyne is made the limiting functional group. Resin-bound peptides were prepared in which only 25% of the chains displayed on the resin contained both groups necessary for triazole formation and 75% lacked either the azide (**44**) or the alkyne (**45**). Upon exposure to standard CuAAC conditions, no cyclic monomers were observed; in other words, chains containing both azide and alkyne were somehow prevented from closing upon themselves, even when the rate of cyclodimerization was necessarily reduced. Resin **44** provided only the linear heterodimer and remaining nonazide peptide,
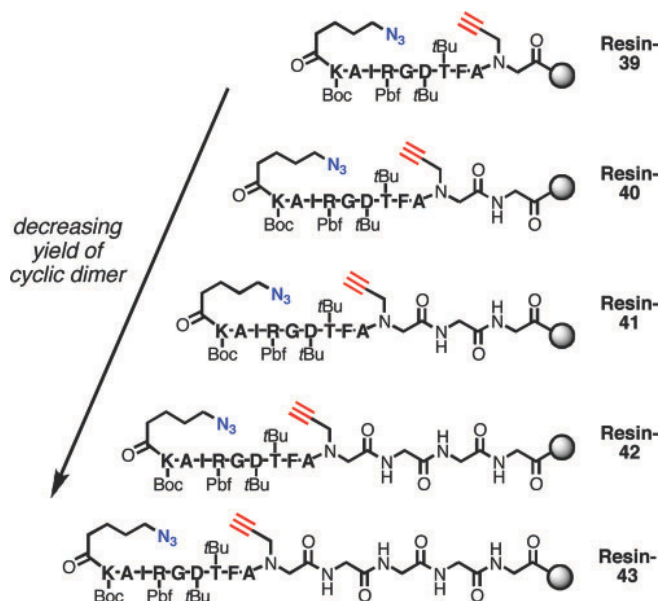

FIGURE 4. Sequences prepared to determine the efficacy of cyclodimerization when the distance between alkyne and solid support (Rink amide MBHA resin) is increased.

whereas resin **45** returned the linear mixed dimer, cyclic dimer, and both starting peptide sequences. A significant difference was also noted in the extent of completion for the two reactions. Resin **44**, which bears alkynes on every peptide chain, gave complete consumption of the limiting (azide) group, whereas even extended treatment of **45** with Cu[I] failed to consume all of the limiting reagent (alkyne). This is consistent with the expectation that alkynes are converted rapidly to Cu-acetylides, and that two Cu atoms are required for triazole formation.[34–36]

(34) Rodionov, V. O.; Fokin, V. V.; Finn, M. G. *Angew. Chem., Int. Ed.* **2005**, *44*, 2210–2215.

(35) Ahlquist, M.; Fokin, V. V. *Organometallics* **2007**, *26*, 4389–4391.

(36) Rodionov, V. O.; Presolski, S.; Díaz, D. D.; Fokin, V. V.; Finn, M. G. *J. Am. Chem. Soc.* **2007**, *129*, 12705–12712.
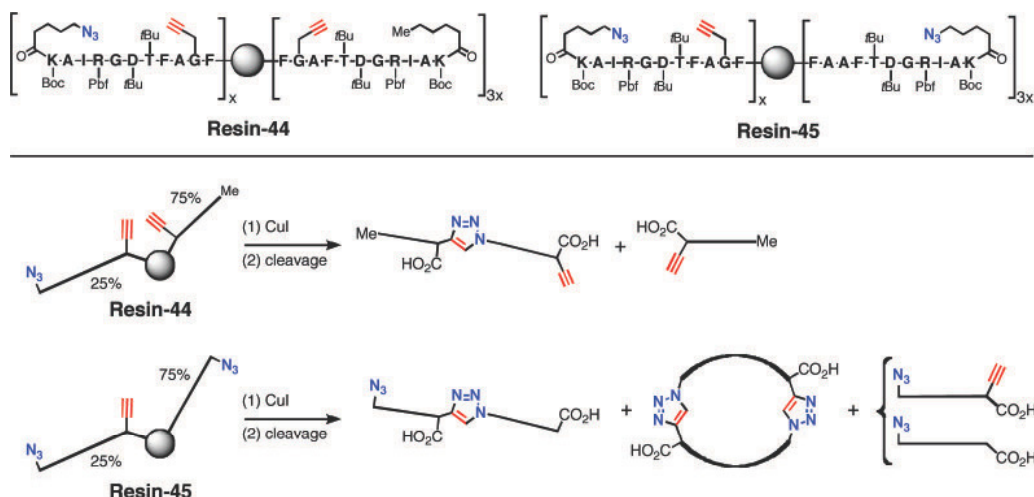
FIGURE 5. (Top) Mixed peptide sequences with substoichiometric quantities of azide or alkyne groups. (Bottom) Summary of the results from exposure to cyclization reaction conditions.
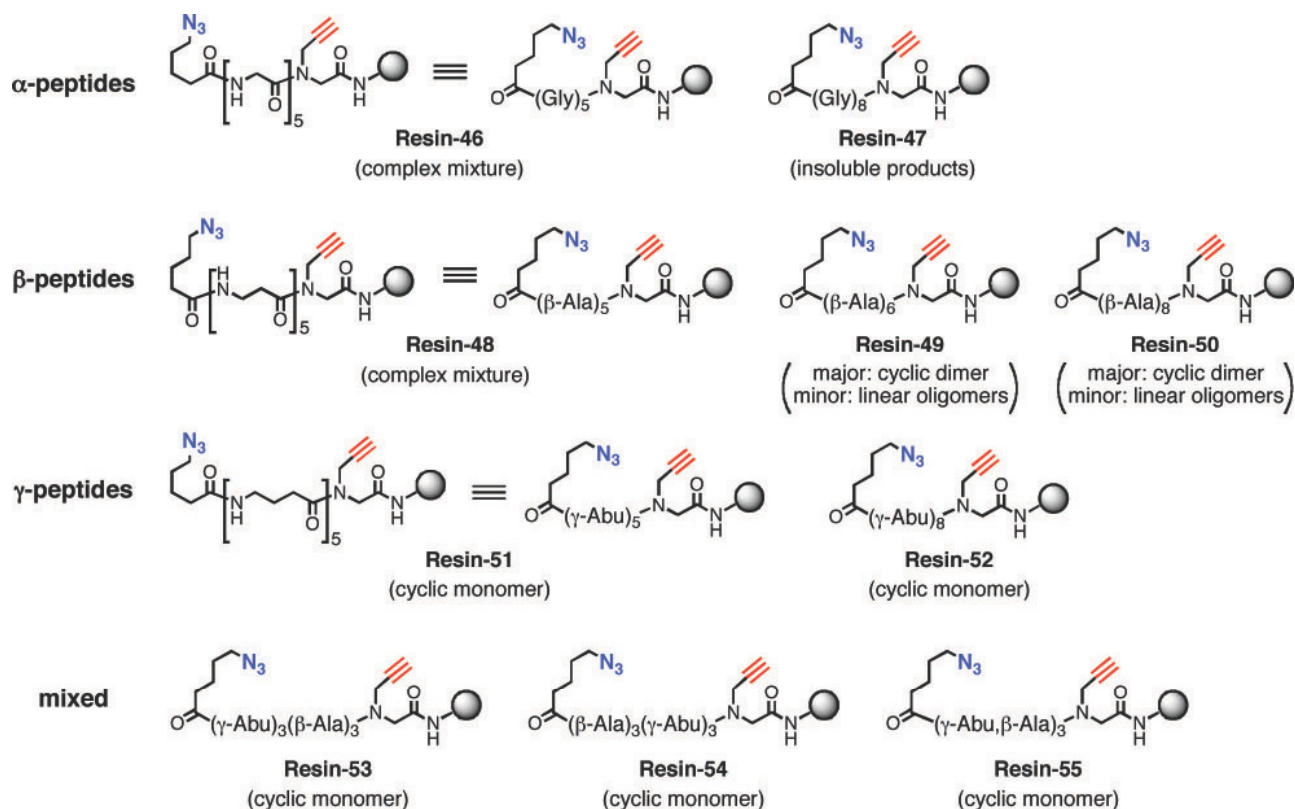

FIGURE 6. Oligomers of β-Ala, γ-Abu, and Gly tested for on-resin CuAAC cyclization. The observed products of standard Cu^I treatment are indicated in parentheses.

Non-Peptide Oligoamides. In an attempt to establish the structural requirements for cyclodimerization, we prepared resin-bound oligoamides lacking side chains and with differing numbers of main-chain methylene spacers and different lengths: glycine oligomers **46** and **47**, β-alanine oligomers **48**–**50**, and γ-aminobutyrate oligomers **51** and **52** (Figure 6). Mixed β-Ala/γ-Abu sequences **53**–**54** were also synthesized. Upon exposure to Cu^I under standard conditions, the penta(α-peptide) **46** and penta(β-peptide) **48** afforded complex product mixtures (linear and cyclic monomers, dimers, and oligomers), similar to pentapeptide **37** (Figure 3) used to establish the length dependence of cyclodimerization. Unfortunately, the octapeptide **47** yielded only highly insoluble material (likely due to β-sheet aggregation characteristic of long oligoglycines), the composi-

tion of which could not be analyzed. More revealingly, lengthening the β-peptide chain by one (**49**) or three (**50**) units gave rise to a change in the product distribution, providing substantial amounts of cyclic dimers. It is therefore evident that cyclodimerization does not require the presence of oligopeptide side chains.

Sequences **49** and **50** also returned significant amounts (approximately 15% total) of linear oligomers with mass values ranging from dimer to pentamer (M$_2$–M$_5$). This phenomenon was investigated with **49** and was found to arise from triazole formation in the absence of copper with both the resin-bound protected peptide and the linear deprotected peptide after cleavage from the resin, when each was stored in the absence of solvent at room temperature. We have previously observed
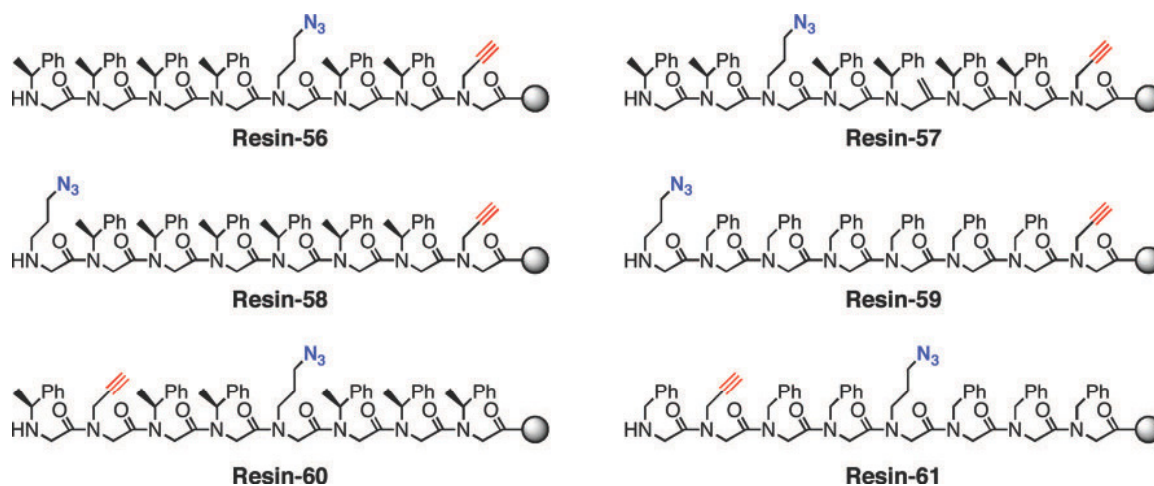
FIGURE 7. Resin-bound peptoid sequences subjected to standard CuAAC conditions and subsequent cleavage with TFA. All returned cyclic monomers were in clean fashion, with the exception of **61**, which gave a cyclic monomer and oligomers.

such solid-state (or neat oil) oligomerization of other small-molecule α,ω-azido−alkynes during the course of polymerization studies.[37] This phenomenon has interesting implications for metal-independent triazole formation[38−41] on surfaces or in the context of materials synthesis.[37]

In contrast to the β-Ala oligomers, oligo(γ-Abu) sequences **51** and **52** were completely converted to cyclic monomers, the latter being particularly notable because it contains eight backbone amide bonds in the chain, the same number that gave reliable cyclodimerization with oligopeptides. Sequences **49** and **51** are nearly the same length but have different numbers and relative spacings of their amide bonds. To determine which of these two factors is responsible for selective cyclodimerization, mixed β-Ala and γ-Abu sequences **53−55** were prepared, where the number of amide bonds was conserved (equivalent to **49**, which readily cyclodimerizes) but their spacing along the oligoamide strand was varied. Upon exposure to Cu^I, sequences **53−55** all afforded cyclic monomers, suggesting that *the spacing of amide bonds influences the cyclization process, with closer amide linkages (α- or β-peptides) favoring cyclodimer formation.*

Tertiary Amides. Peptoids, oligomeric peptides in which the side chains are placed on the amide nitrogen atom, have attracted a great deal of interest for their resistance to proteolytic cleavage,[42] fascinating structural and conformational properties,[43−45] and their ability to display a wide array of chemical function-

alities that enhance structural diversity and biomedical relevance.[46,47] We reasoned that the treatment of azido-alkynyl derivatives of such molecules with Cu^I would provide novel cyclic structures and would begin to test our prior hypothesis (now discredited, see below and Supporting Information) that interactions of copper with the backbone amide groups are of importance to cyclodimerization.[26] Experiments were performed using the series of N-benzylated octamers shown in Figure 7, designed to exhibit various properties of conformational structure and rigidity.

Homochiral α-substitution on nitrogen confers well-characterized helicity to the peptoid architecture with a helical pitch of three residues.[43−45] Sequence **56** thereby places its azide and alkyne groups in close proximity to each other on the same side of the helix, while **57** places them a greater distance apart and on different faces of the helix.[33,47] Structures **58** and **59** mimic the alkyne and azide positions of the peptides tested above. The lack of α-substituents in the latter sequence removes the steric and torsional interactions between side chains and hence any predisposition toward helicity, creating an unstructured, more flexible peptoid strand.[48] In all of these cases (**56−59**), cyclic monomers were produced exclusively from an on-resin CuAAC reaction. The cyclic monomers were identified by mass spectrometry and their substantially different retention times on analytical RP-HPLC compared with the linear starting material.

Limited N-alkylation of a peptide was also able to abolish cyclodimerization, as shown in Figure 8. Thus, while the resin-bound decamer **62** underwent facile cyclodimerization under standard conditions, N-methylation of a central glycine (**63**) induced the formation of significant amounts of both cyclic monomer and cyclic dimer, along with some trimeric material. N-Methylation of two flanking positions (Leu and Phe, structure **64**) diverted the CuAAC reaction products to mostly cyclic monomer, along with small amounts of cyclic dimer and oligomeric materials with masses ranging from M$_3$ to M$_5$. The complete absence of cyclic dimers from the reactions of peptoids and the decrease in cyclodimerization upon N-methylation of

(37) Díaz, D. D.; Punna, S.; Holzer, P.; McPherson, A. K.; Sharpless, K. B.; Fokin, V. V.; Finn, M. G. *J. Polym. Sci., Part A: Polym. Chem.* **2004**, *42*, 4392−4403.

(38) Mock, W. L.; Irra, T. A.; Wepsiec, J. P.; Manimaran, T. L. *J. Org. Chem.* **1983**, *48*, 3619−3620.

(39) Mock, W. L.; Irra, T. A.; Wepsiec, J. P.; Adhya, M. *J. Org. Chem.* **1989**, *54*, 5302−5308.

(40) Rozkiewicz, D. I.; Janczewski, D.; Verboom, W.; Ravoo, B. J.; Reinhoudt, D. N. *Angew. Chem., Int. Ed.* **2006**, *45*, 5292−5296.

(41) Zhang, H.; Piacham, T.; Drew, M.; Patek, M.; Mosbach, K.; Ye, L. *J. Am. Chem. Soc.* **2006**, *128*, 4178−4179.

(42) Miller, S. M.; Simon, R. J.; Ng, S.; Zuckermann, R. N.; Kerr, J. M.; Moos, W. H. *Drug Devel. Res.* **1995**, *35*, 20−32.

(43) Yoo, B.; Kirshenbaum, K. *Curr. Opin. Chem. Biol.* **2008**, *12*, 714−721.

(44) Kirshenbaum, K.; Barron, A. E.; Goldsmith, R. A.; Armand, P.; Bradley, E. K.; Truong, K. T. V.; Dill, K. A.; Cohen, F. E.; Zuckermann, R. N. *Proc. Natl. Acad. Sci. U.S.A.* **1998**, *95*, 4309−4314.

(45) Wu, C. W.; Kirshenbaum, K.; Sanborn, T. J.; Patch, J. A.; Huang, K.; Dill, K. A.; Zuckermann, R. N.; Barron, A. E. *J. Am. Chem. Soc.* **2003**, *125*, 13525−13530.

(46) Holub, J. M.; Jang, H. J.; Kirshenbaum, K. *Org. Lett.* **2007**, *9*, 3275−3278.

(47) Jang, H.; Fafarman, A.; Holub, J. M.; Kirshenbaum, K. *Org. Lett.* **2005**, *7*, 1951−1954.

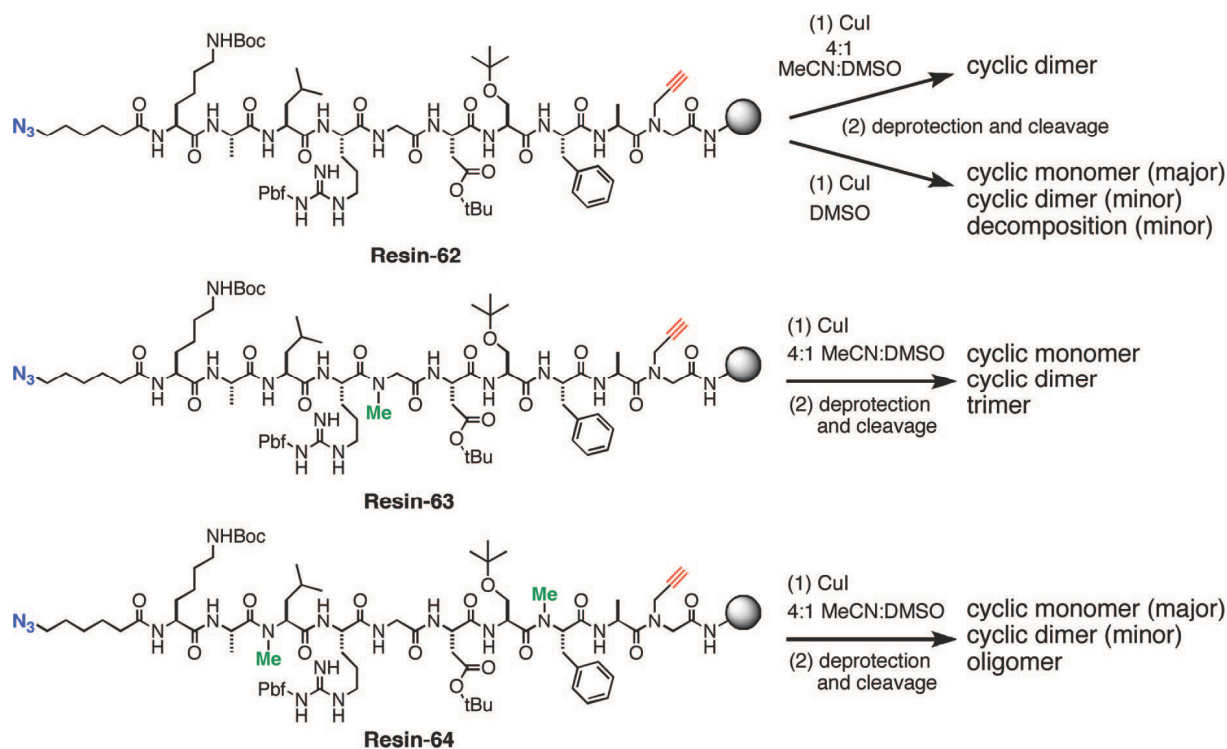(48) Fafarman, A. T.; Borbat, P. P.; Freed, J. H.; Kirshenbaum, K. *Chem. Commun.* **2007**, 377−379.

FIGURE 8. Peptides used to test the dependence of backbone amide methylation on cyclodimerization, and their results after applying standard reaction conditions.
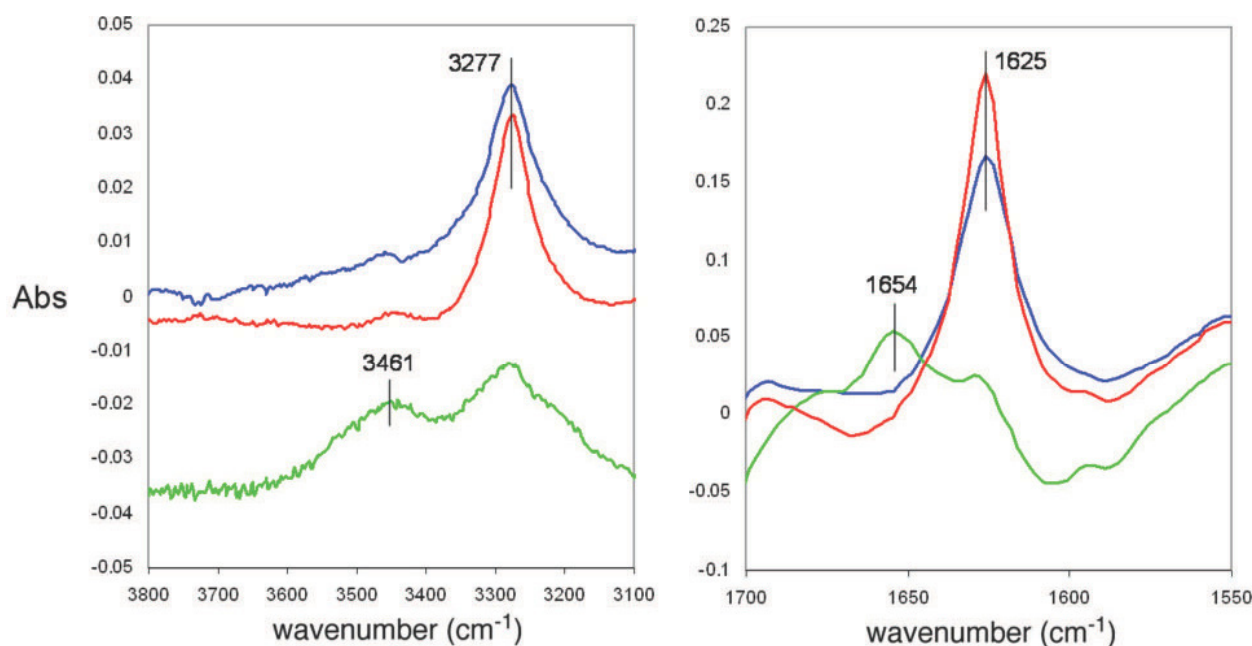

FIGURE 9. IR spectra of protected resin-bound nonapeptide **39** swollen overnight in CH_2Cl_2 (blue), DMSO (green), or the standard reaction solvent system of 4:1 MeCN/DMSO (red).

peptides, demonstrate that *secondary, not tertiary, amide bonds are required for cyclodimerization*.

Proposed Mechanism of Cyclodimerization. An examination of the resin-bound protected peptides by IR spectroscopy revealed an important solvent-dependent change in the state of hydrogen bonding by the backbone amide groups. Both CH_2Cl_2 and DMSO swell polystyrene resins, but the latter solvent is far better at disrupting inter- and intrachain peptide H-bonding. Figure 9 shows the representative case of resin-bound protected peptide **39**, which in CH_2Cl_2 exhibited an amide carbonyl

stretching band at 1625 cm^{-1} and an amide N−H absorbance at 3277 cm^{-1}, both characteristic of strong hydrogen bonding. In DMSO, new bands appeared at 1654 and 3461 cm^{-1}, consistent with the expected loss of H-bonding due to interactions of the peptide chains with the solvent.[49−52] In the standard reaction solvent system of 4:1 MeCN/DMSO, the IR spectrum

(49) Narita, M.; Honda, S.; Umeyama, H.; Ogura, T. *Bull. Chem. Soc. Jpn.* **1999**, *61*, 1201−1206.

(50) Narita, M.; Lee, J.-S.; Hayashi, S.; Hitomi, M. *Bull. Chem. Soc. Jpn.* **1993**, *66*, 489−493.

TABLE 2. Conditions Found To Promote Dimeric vs Monomeric CuAAC Cyclization of Peptides

dimeric cyclization	competing monomeric cyclization	reliable monomeric cyclization
side-chain groups protected polystyrene-based resin swelled in 4:1 MeCN:DMSO	side-chain groups protected	side-chain groups protected polystyrene-based resin swelled in DMSO or protic solvent, or reaction done in solution
six or more amino acids in length	four or fewer amino acids in length	tertiary backbone amide bonds
α- or β-peptides	γ-peptides	
alkyne group installed close to polystyrene backbone		

matched that in CH_2Cl_2, showing that this mixture contains an insufficient amount of DMSO to disrupt peptide H-bonding. We therefore propose that head-to-tail interchain H-bonding is the organizing phenomenon responsible for cyclodimerization by CuAAC.

Two important corollaries to this hypothesis concern the role of resin and solvent: (a) the resin provides a relatively hydrophobic environment that promotes hydrogen bonding,[53,54] and (b) the 4:1 MeCN:DMSO solvent mixture solvates (swells) the resin, allowing Cu^I access to all of the reactants, without disrupting H-bonding between pairs of chains. This solvent system was originally chosen for a very different reason: to provide the Cu^I center with what was thought to be advantageous coordination by the acetonitrile ligand, a notion that later kinetic studies on solution-phase CuAAC reactions proved to be erroneous. The crucially balanced role of the solvent was verified by the CuAAC reaction of resin **62** in pure DMSO (Figure 8), which is commonly used for solid-phase peptide synthesis due to its H-bond disrupting ability. Correlating with the observed change in H-bonding (Figure 9), this change in solvent changed the outcome of the reaction from cyclodimerization to monomeric cyclization, with small amounts of cyclic dimer observed along with some degraded material. We also note that monocyclization of two azido—alkyne oligopeptides has recently been reported using the highly polar and protic combination of 20% H_2O in *N*-methylpyrrolidinone (NMP) as the solvent.[55]

A summary of the experimental factors favoring cyclodimerization vs monomeric cylization is given in Table 2. The hypothesis of head-to-tail preorganization by interstrand H-bonding, along with the above two corollaries, are consistent with these findings, as follows:

(1) Backbone secondary amide groups in sufficient numbers are required. When H-bonding cannot occur, as with tertiary amides (Figures 7 and 8) or is too weak, as with shorter peptides (Figure 3), monomeric cyclization is favored as each alkyne finds itself in closest proximity to the azide of its own chain.

(2) Cyclodimerization is a function of main-chain amide linkages and is independent of the identity of protected peptide side chains, at least in the series of nonamers tested in Table 1.

(3) Solution-phase cyclization of a protected peptide affords a predominantly cyclic monomer, whereas on-resin reaction of the same species gives a cyclic dimer (Figure 2). When performed in solution (in this case, in MeOH—CH_2Cl_2), hydrogen bonding between chains is likely to be disrupted. On the contrary, variation in resin loadings of 0.26—1.4 mmol/g

do not affect the cyclodimerization efficiency, suggesting that H-bonding in the resin environment is a powerful force.

(4) Cu-mediated cyclodimerization occurs for resin-bound α- and β-oligopeptides but not γ-peptides (Figure 6). A potential antiparallel arrangement for each of these amide oligomers is shown in Figure 10; head-to-head alignments are somewhat less favorable and would not be productive in terms of azide—alkyne ligation. Sufficiently stable interchain interactions could arise from a combination of H-bonding density and dipolar stabilization. Oligo(α-peptides) have the greatest number of H-bonds per unit length, enough to overcome a less favorable dipolar arrangement derived from the alternating pattern of H-bond donors and acceptors.[56] Oligo(β-peptides)[57] compensate for the lesser H-bond density with a favorable H-bond dipolar arrangement.[56] Oligo(γ-peptides) have their H-bonds too far apart to stabilize interchain interactions and do not undergo cyclodimerization.

(5) Cyclic dimers are less efficiently produced when peptides are inserted between the alkyne and the polystyrene backbone (Figure 4). We suggest that when H-bonding is maximized in these extended sequences, alkyne and azide are not placed optimally for cyclodimerization, as shown at the left of Figure 11. The productive alignment (Figure 11, right) is less favorable with respect to H-bonding, and so, a poor yield of cyclic dimer is obtained.

(6) Uncatalyzed azide—alkyne cycloaddition reactions are extremely slow when the alkyne is not electron-deficient and so require the reactants to be held in close proximity in order to occur, even to a small degree, at room temperature.[38,39,58] The observation of Cu-free solid-phase oligomerization for oligo(β-Ala) species **49** and **50** (and probably oligo(Gly) **47**), but not for sequences containing γ-peptides, therefore supports the proposed existence of a preorganizing interaction between peptide chains. We suggest that the slow reaction in the absence of copper begins to link the head-to-tail oriented chains and that cyclic dimers are formed when triazole formation is accelerated under conditions where H-bonding is maintained.

Peptide Cyclization and Cyclodimerization on Preparative Scale. To demonstrate the capability of the CuAAC process to produce substantial quantities of a large cyclic peptide, 240 mg of resin **65** was prepared (Figure 12) and cleaved to obtain 57 mg of crude linear peptide (approximately 60% of the maximum yield based on the initial functional group loading of the resin) and 30 mg of purified peptide after reversed-phase HPLC. Cyclization of a parallel batch under standard dimerization conditions (20 mL of 4:1 MeCN:DMSO,

(51) Narita, M.; Lee, J.-S.; Hayashi, S.; Yamazaki, Y.; Sugiyama, T. *Bull. Chem. Soc. Jpn.* **1993**, *66*, 500–505.

(52) Narita, M.; Tomotake, Y.; Isokawa, S.; Matsuzawa, T.; Miyauchi, T. *Macromolecules* **1984**, *17*, 1903–1906.

(53) Merrifield, B. *Br. Polym. J.* **1984**, *16*, 173–178.

(54) Sherrington, D. C. *J. Chem. Soc., Chem. Commun.* **1999**, 2275–2286.

(55) Goncalves, V.; Gautier, B.; Regazzetti, A.; Coric, P.; Bouaziz, S.; Garbay, C.; Vidal, M.; Inguimbert, N. *Bioorg. Med. Chem. Lett.* **2007**, *17*, 5590–5594.

(56) Murray, T. J.; Zimmerman, S. C. *J. Am. Chem. Soc.* **1992**, *114*, 4010–4011.

(57) Cheng, R. P.; Gellman, S. H.; DeGrado, W. F. *Chem. Rev.* **2001**, *101*, 3219–3232.

(58) Lewis, W. G.; Green, L. G.; Grynszpan, F.; Radic, Z.; Carlier, P. R.; Taylor, P.; Finn, M. G.; Sharpless, K. B. *Angew. Chem., Int. Ed.* **2002**, *41*, 1053–1057.
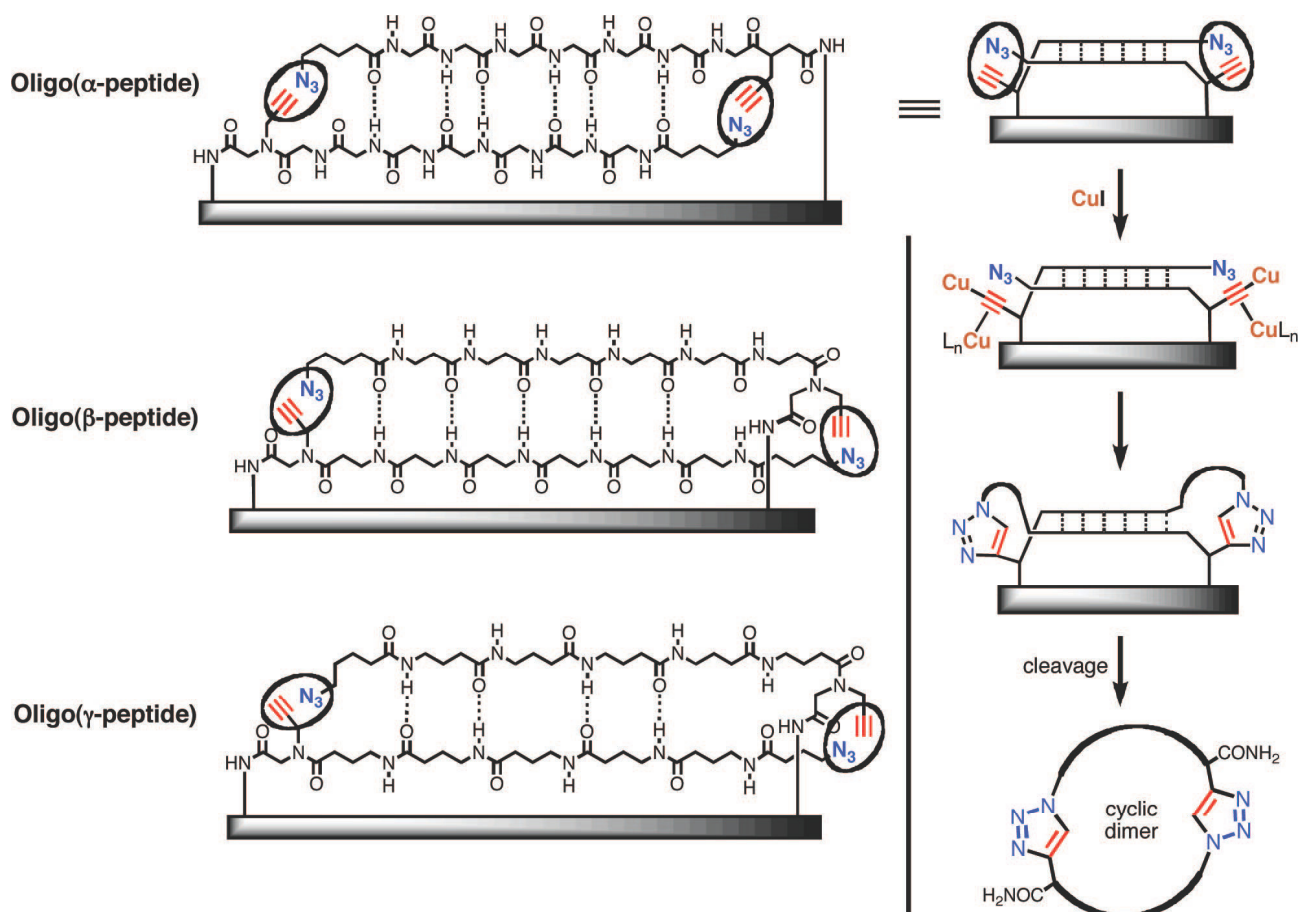
FIGURE 10. (Left) Potential hydrogen patterns formed by head-to-tail alignments of oligo(Gly), oligo(β-Ala), and oligo(γ-Abu), placing interstrand alkyne and azide moieties in close proximity to each other. The shaded bar represents the polystyrene chains to which the peptides are attached. (Right) Proposed CuAAC cyclodimerization pathway directed by head-to-tail H-bonding.
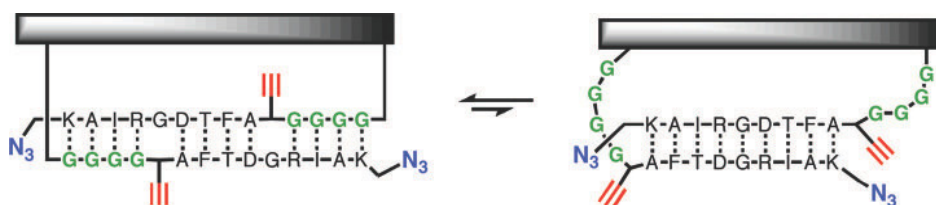

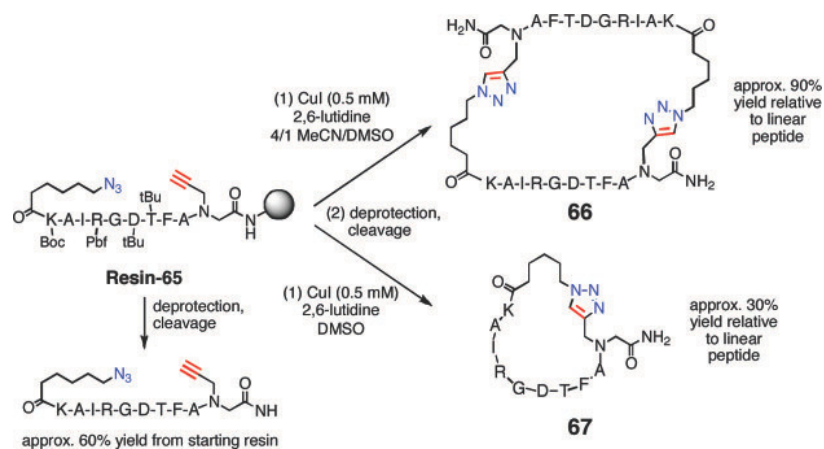**FIGURE 11.** Proposed hydrogen-bonded alignments formed by resin **43** (Figure 4).

FIGURE 12. Preparative-scale syntheses of a representative cyclic dimer and monomer.

495 mg of resin **62**, 5 mM Cu^I, 30 μL of 2,6-lutidine, sparged with N$_2$), followed by cleavage and deprotection, returned 52 mg of crude cyclized material (compound **66**, 91% of the amount of the linear peptide obtained without CuAAC treatment) and 32 mg after purification. Thus, the cyclodimerization process was conducted with little or no loss of material. A third
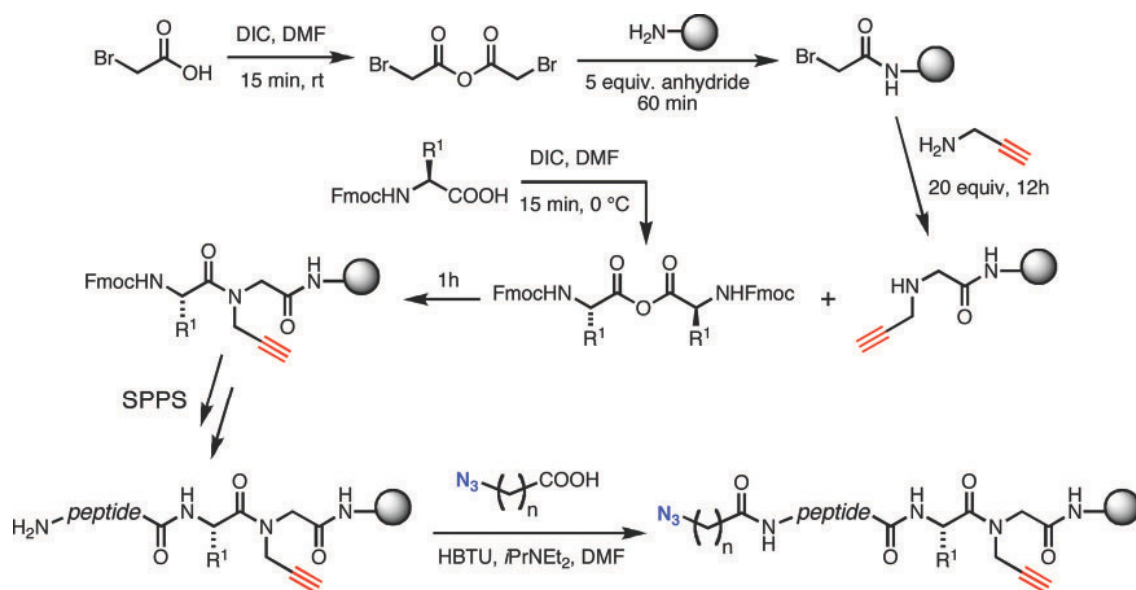
FIGURE 13. Incorporation of alkyne and azide groups during solid-phase peptide synthesis.

parallel batch of resin **65** was cyclized under conditions to promote monomeric ring closure (20 mL of DMSO + 1 drop of H_2O, 5 mM Cu^I, 30 μL of 2,6-lutidine, sparged with N_2) and cleaved from the resin to give only 25 mg of crude product, reflecting a difficulty in precipitating the more soluble cyclic monomer, and 8.5 mg of monocyclic triazole **67** after HPLC purification. In each case, HPLC and MALDI analysis showed the expected species (linear azido−alkyne peptide, cyclic monomer, or cyclic dimer) as the dominant species in the unpurified product mixture, and the purified products were characterized by HPLC, NMR, and high-resolution mass spectrometry (Supporting Information).

Conclusions

The CuAAC cyclodimerization process is quite robust for peptides of six residues or longer, allowing the convenient synthesis of large bivalent[59] cyclic peptides. Furthermore, the analogous cyclic monomers can be obtained from the same resin-bound precursor with a simple change in solvent.

The success of peptide cyclodimerization derives from a fortuitous combination of resin and solvent properties. The discovery of the beneficial effects of the 4:1 MeCN:DMSO solvent mixture provides a useful lesson in the properties of resin-bound peptides or rather reinforces an old one. Merrifield's focus on the role of resin in maintaining oligopeptide solubility as the key enabling feature of solid-phase peptide synthesis[53] is perhaps underappreciated today even by some who use Merrifield's methods. Our reaction conditions maintain a state intermediate between the full resin swelling desired for SPPS and the collapsed aggregates that bedevil peptide-bearing resins when insufficiently solvated. Furthermore, we failed to initially recognize interchain hydrogen bonding as the key organizing event for cyclodimerization, because we assumed that 20% DMSO was enough to disrupt all H-bonding interactions.

The CuAAC reaction is well suited to joining together of such noncovalently organized fragments into larger structures.

Azides and alkynes are incorporated with ease into peptide building blocks and remain undisturbed under conditions of standard protection, deprotection, and coupling steps. The rate of the reaction is fast, which is crucial to the overall outcome. However, these features are not unique to CuAAC, and it should be possible to find other ligation reactions, such as olefin metathesis,[60−62] nitrile imine-olefin cycloaddition,[63,64] or thiol-ene condensation,[65] to accomplish the same task. In addition to such studies, we will continue the development of cyclic triazole-linked peptides for biological and materials science.

Experimental Section

Peptide Synthesis. All peptides were prepared by Fmoc SPPS methods using Rink amide MBHA resin with an initial loading of 0.70 mmol/g, unless otherwise noted. Resins were swollen in DMF for 45 min prior to synthesis. For sequence extension, the Fmoc-protected amino acid (4 equiv) was activated by treatment with HBTU or HCTU (3.9 equiv) and *N,N*-diisopropylethylamine (500 μL per mmol of amino acid) in DMF (4 mL per mmol of amino acid) for 2 min. This solution was added to the free amine on resin, and the coupling reaction was allowed to proceed for 15 min (longer for difficult couplings) with intermittent stirring. After washing with DMF, Fmoc deprotection was achieved with 20% 4-methylpiperi-dine in DMF (2 × 7 min). The resin was washed once again, and the process was repeated for the next amino acid.

The alkyne group was usually incorporated as an *N*-propargylg-lycine unit by the method shown in Figure 13. The symmetric anhydride of 2-bromoacetic acid (5 equiv of anhydride relative to free amine) was prepared by mixing the acid (10 equiv) with *N,N'*-diisopropylcarbodiimide (DIC, 5 equiv) in DMF at room temper-ature for 15 min. This mixture was then added to the resin and allowed to react for 1 h with intermittent stirring. The resin was washed and then treated with propargylamine (20 equiv) in DMF

(59) We have verified our earlier report (ref 26) that the synthesis of two different sequences, A and B, on a resin bead results in the production of AA, AB, and BB cyclic dimers under standard CuAAC cyclodimerization conditions. Thus, mixtures of nonsymmetrical cyclic peptides can be prepared by this method.

(60) Clark, T. D.; Ghadiri, M. R. *J. Am. Chem. Soc.* **1995**, *117*, 12364–12365.

(61) Miller, S. J.; Blackwell, H. E.; Grubbs, R. H. *J. Am. Chem. Soc.* **1996**, *118*, 9606–9614.

(62) Kazmaier, U.; Hebach, C.; Watzke, A.; Maier, S.; Mues, H.; Huch, V. *Org. Biomol. Chem.* **2005**, *3*, 136–145.

(63) Song, W.; Wang, Y.; Lin, Q. *J. Am. Chem. Soc.* **2008**, *130*, 9654–9655.

(64) Song, W.; Wang, Y.; Qu, J.; Madden, M. M.; Lin, Q. *Angew. Chem., Int. Ed.* **2008**, *47*, 2832–2835.

(65) Dondoni, A. *Angew. Chem., Int. Ed.* **2008**, *47*, 8995–8997.

for 12−16 h. After washing, coupling of the next residue to the resultant secondary amine was achieved by preparing the symmetrical anhydride of that protected residue (5 equiv of anhydride) with DIC in DMF at 0 °C for 15 min and coupling this mixture to the amine for 1 h with occasional stirring. This same coupling method was used for all instances when acylation of a secondary amine was required. Where the alkyne was incorporated by coupling Fmoc-L-propargylglycine, preactivation was carried out by mixing the protected unnatural amino acid with HOBt and DIC (4 equiv each) in DMF at 0 °C for 20 min. Azide was incorporated by the attachment of either 5-azidopentanoic acid or 6-azidohexanoic acid by the standard peptide coupling procedure.

The following Fmoc-protected amino acids with side-chain protecting groups were obtained from a commercial supplier and used as received: Fmoc-γAbu-OH, Fmoc-Ala-OH, Fmoc-βAla-OH, Fmoc-Arg(Pbf)-OH, Fmoc-Asn(Trt)-OH, Fmoc-Asp(OtBu)-OH, Fmoc-Cys(Trt)-OH, Fmoc-Gln(Trt)-OH, Fmoc-Glu(OtBu)-OH, Fmoc-Gly-OH, Fmoc-His(Mtt)-OH, Fmoc-Ile-OH, Fmoc-Leu-OH, Fmoc-Lys(Boc)-OH, Fmoc-Met-OH, Fmoc-Phe-OH, Fmoc-Ser(tBu)-OH, Fmoc-Thr(tBu)-OH, Fmoc-Trp(Boc)-OH, Fmoc-Tyr(tBu)-OH, and Fmoc-Val-OH.

Peptide Cyclization. On-resin cyclization was carried out at the bench with solvents freshly deoxygenated by bubbling with nitrogen for at least 5 min. A Cu^I solution (usually 5 mM, but 20 mM was used in early experiments) was prepared using a solvent mixture of 20% DMSO in MeCN. Acetonitrile was required for solublizing the copper salt, while DMSO was crucial for resin swelling and peptide accessibility. A 4 mL vial was charged with 50 mg of peptide-loaded resin, to which was added 2 mL of a Cu^I solution and 5 μL of 2,6-lutidine. Cyclizations on a larger scale were carried out in 20 or 40 mL scintillation vials as required. Nitrogen was gently bubbled through the mixture for 3 min, and the vial was capped, sealed with parafilm or electrical tape, and gently agitated on a rotisserie at room temperature for 16 or 40 h. After the reaction, the resin was washed successively with DMF, MeCN, and water. The resin was then gently stirred in a saturated aqueous solution of disodium EDTA (2 × 10 min) to remove residual bound copper, followed by sequential washing with water, MeCN, CH$_2$Cl$_2$, and diethyl ether, and drying in a vacuum desiccator.

Peptide Cleavage. Linear and cyclized peptides were cleaved from the resin with 2% triisopropylsilane (TIS) in trifluoroacetic acid (TFA, approximately 1 mL of TFA/TIS per g of resin) for 2.5 h. The cleavage mixture (including resin) was mixed with cold ether to precipitate the peptide and then filtered. The filtrate was washed with cold ether, and the peptide was extracted from the residue with H$_2$O/MeCN mixtures (typically 5−20% MeCN in water, 50% for peptoids) containing 0.1% TFA. The resulting solution was frozen and lyophilized to afford a white, solid product. A similar procedure was used for release of fully protected peptides from the resin, using 4% TFA in CH$_2$Cl$_2$ for 4 h. The peptide was precipitated from cold ether, filtered, extracted with 20% MeOH in CH$_2$Cl$_2$, evaporated to dryness, and purified by preparatory HPLC to give a white powder.

Analytical Methods. Peptides were analyzed by reversed-phase analytical HPLC (RP-HPLC) at a 1.0 mL/min flow rate and a 4.7

× 150 mm column (5 μm particle size), with detection at 220 nm. Gradients of 0−35% or 15−50% MeCN in H$_2$O over 20 min (with constant 0.1% TFA) were used. Preparatory HPLC was performed at 10 mL/min on a Dynamax SD-1 instrument using a C18 column (22 × 250 mm, 10 μm particle size) and MeCN/H$_2$O with 0.1% TFA gradients as needed. MALDI mass spectra were obtained.

Peptoid Synthesis. N-Substituted glycine oligomers (peptoids) were synthesized on solid-phase support using modified submonomer synthesis protocols reported previously by Zuckermann et al.[66] Peptoid oligomers were synthesized by manual techniques as well as automated procedures on a robotic peptide synthesizer with software program files written in-house. All reactions were completed at room temperature.

Rink amide resin (100 mg, 0.69 mmol/g) was swollen in 3 mL of CH$_2$Cl$_2$ for 45 min before Fmoc deprotection. Typically, the resin was washed with DMF (4 × 2 mL) and CH$_2$Cl$_2$ (3 × 2 mL) between each synthetic step described below. Stoichiometries are based on the loading of the starting resin functional groups, that is, assuming quantitative yield at each coupling step. Fmoc deprotection was performed by treatment of the resin with 20% piperidine in DMF (20 min, 15 mL per g of resin). The resin was washed, and 20 equiv of bromoacetic acid (1.2 M in DMF, 8.5 mL per g of resin) and 24 equiv DIC (2 mL per g of resin) were added. The reaction mixture was agitated at room temperature for 20 min. After another resin wash, 20 equiv of the monomer amine (1.0 M in DMF, 10 mL per g of resin) was added, and the reaction mixture was shaken for 20 min at room temperature. Subsequent bromoacylation and amine displacement steps were performed to prepare peptoids of desired length.

Linear and cyclized peptoid products were cleaved from the solid support by treatment with 50% TFA in CH$_2$Cl$_2$ (40 mL per g of resin) for 10 min at room temperature. The cleavage cocktail was evaporated under nitrogen gas flow, and the products were resuspended at an approximate concentration of 2 mM in HPLC solvent (50% acetonitrile in water, with 0.1% TFA) for analysis by RP-HPLC and electrospray ionization mass spectrometry.

Supporting Information Available: Experimental details and representative HPLC and MALDI mass spectrometry data. This material is available free of charge via the Internet at http://pubs.acs.org.

JO802097M

(66) Zuckermann, R. N.; Kerr, J. M.; Kent, S. B. H.; Moos, W. H. *J. Am. Chem. Soc.* **1992**, *114*, 10646−10647.

Peptide Cyclization and Cyclodimerization by Cu$^\text{I}$-Mediated Azide-Alkyne Cycloaddition

Reshma Jagasia, Justin M. Holub, Markus Bollinger, Kent Kirshenbaum, and M.G. Finn*

Supporting Information

Table of Contents

1. Other CuAAC peptide ring closures in the literature

Ghadiri and coworkers described the solution phase head-to-tail assembly of dipeptides in up to 80% yield (Figure S1a),[1] Nilsson and colleagues reported a similar transformation of functionalized glycodipeptide monomers, with a maximum yield of 64% after 72 h (Figure S1b),[2] and Gin and coworkers accomplished an efficient synthesis of cyclodextrins from a trisaccharide in 80% yield (Figure S1c).[3,4] In each case, cyclic trimer and linear oligomers comprised most of the byproducts.

Figure S1. Reported examples of solution-phase cyclodimerization via the CuAAC reaction. (A) Ghadiri *et al.*[1] (B) Nilsson *et al.*[2] (C) Gin *et al.*[3] (D) Burgess *et al.*[5] (E) Burke *et al.*[6].
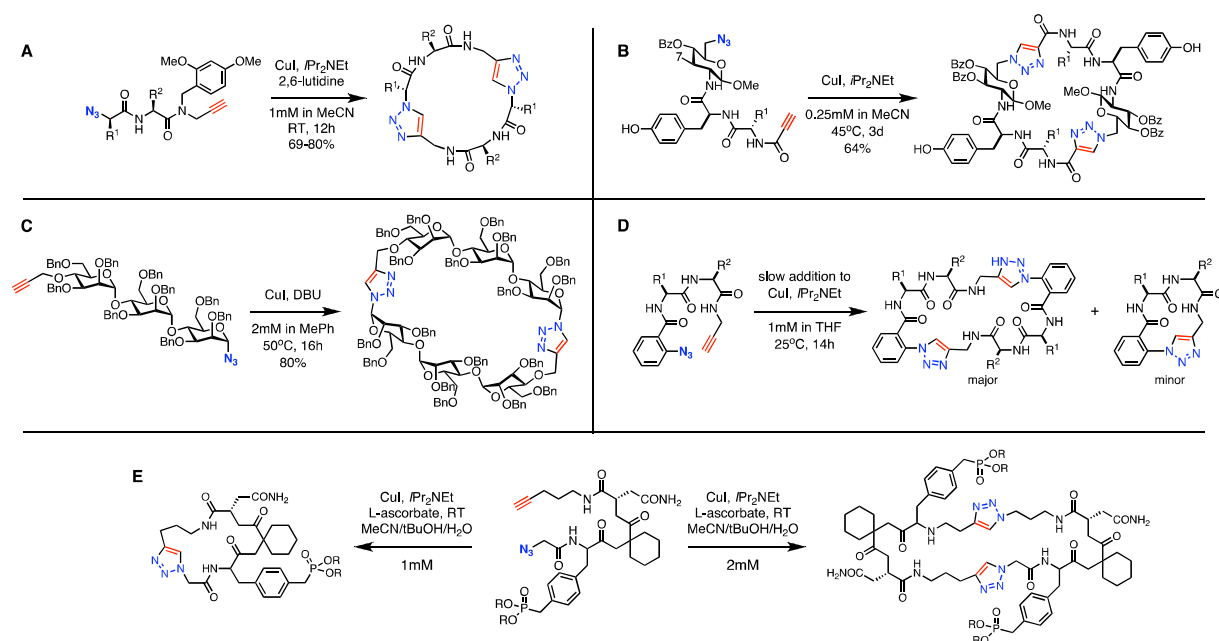
Burgess and coworkers have made several attempts to monocyclize azido-alkynyl dipeptides to produce 14-membered rings as β-turn mimics (Figure S1d).[5] In order to favor an intramolecular reaction, the dipeptide was slowly added to a solution of copper catalyst, and the final dipeptide concentration was kept no higher than 1 mM. While cyclic monomers were produced, the major product in most cases was cyclic dimer. The authors offered a sensible rationale based on torsional strain that would come into play upon monocyclization incorporating the 1,4-triazole moiety. In contrast, a conformationally biased diketodipeptide azido-alkyne was found by Burke and coworkers to provide cyclic monomer under dilute conditions(Figure S1e).[6]

2. Solution phase cyclization.

Figure S2. (a) HPLC analysis of peptide **33** cleaved from resin; (b) MALDI-MS of the material eluted at the major peak in (a); (c) HPLC of protected peptide obtained after Cu-mediated cyclization of **33** in 0.8 mM solution as described in the text; (d) HPLC of protected peptide obtained after Cu-mediated cyclization of **33** in 3.0 mM solution as described in the text; (e) HPLC of (c) to which a small amount of linear **33** was added. A comparison of this trace to (c) shows that no linear peptide remained after the CuAAC reaction. (f) MALDI-MS of the material eluted at the peak marked [M]$_1$ in (e); (g) MALDI-MS of the material eluted at the peak marked [M]$_2$ in (e). All analytical HPLC runs were performed with an elution gradient of 15 to 50% MeCN over 20 min, in 0.1% aqueous trifluoroacetic acid, except for (a), in which a gradient of 50-95% MeCN was used. All panels show the analysis of crude protected peptide, isolated without purification after cleavage from the resin.
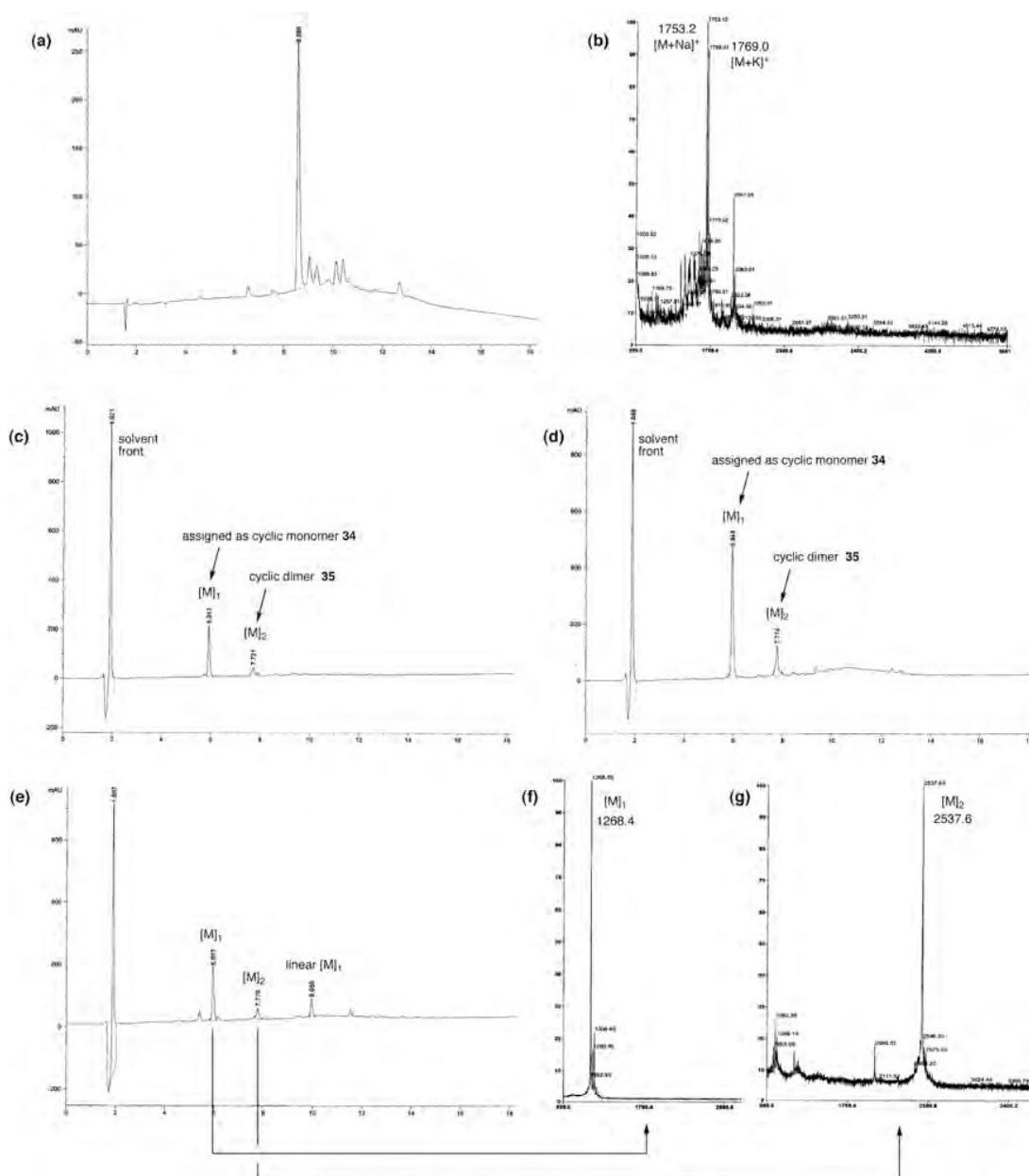
3. Dependence on resin linkage, loading, and Cu(I) concentration.

To explore the dependence of resin-based cyclodimerization on the nature of the resin and the density of peptide chains on the support, the same 9-mer sequence in **33** was prepared on three polystyrene-based resins with different loading levels, as shown in Figure S3: (1) chlorotrityl resin with a starting functional group density of 1.4 mmol/g (approximately 1 functional group for every 5 styrene monomers, **Resin-S1**); (2) rink amide MBHA resin with starting functional group density of 0.70 mmol/g (approximately 1 functional group for every 10 styrenes, our standard resin for peptide cyclodimerization, **Resin-S2**); and (3) TGR resin (Rink-modified TentaGel, a PEGylated polystyrene) with starting functional group density of 0.26 mmol/g (**Resin-S3**).[7] Oligopeptide syntheses proceeded satisfactorily on all supports, and on-resin cyclizations were conducted in the presence of varying amounts of CuI for standard (16 h) and extended (40 h) reaction times in order to test the susceptibility of the peptides to Cu-mediated degradation.

Figure S3. Peptide sequences and resins used to determine the dependence of resin type and loading density on cyclodimerization.
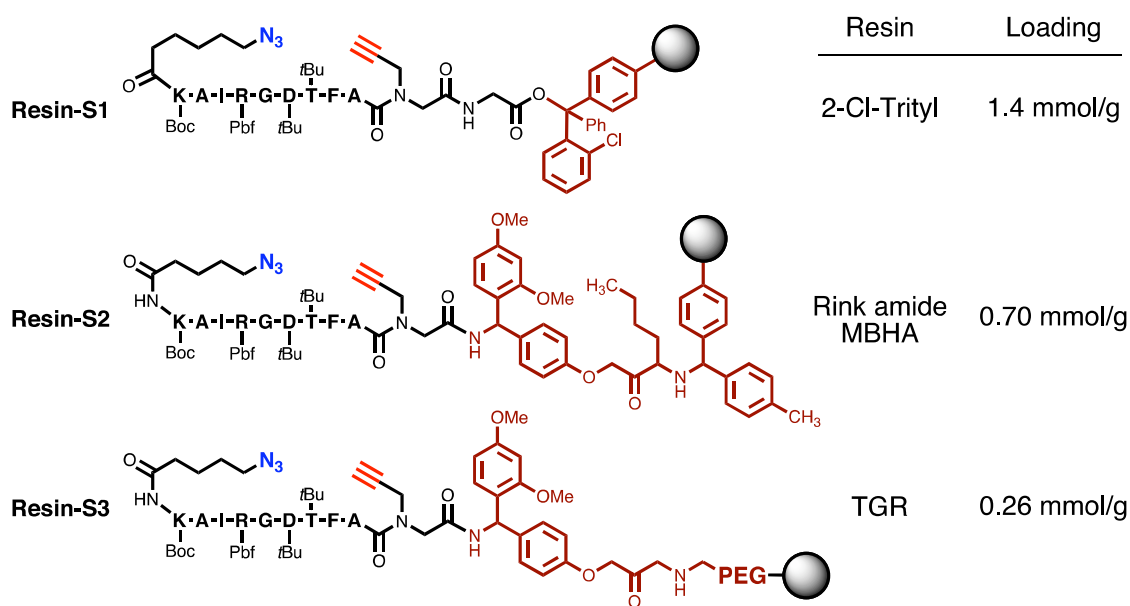
In all cases, cyclodimerization was the predominant reaction observed, showing that the process tolerates various resin-anchoring functionalities and loading densities. The highly loaded 2-chlorotrityl chloride resin **S1** did not afford larger cyclic or linear products, and the lower density of peptides on the TGR resin **S3** did not promote cyclic monomer production. Copper concentrations up to several equivalents with respect to resin-bound alkyne did not hinder the reaction. No evidence was found for increased peptide yield or product deterioration (amide bond cleavage) with additional reaction time. The chlorotrityl resin was found to be significantly less attractive with regard to the purity of the linear and cyclic peptides obtained, and the PEG-based TGR resin was found to be marginally better than the Rink amide resin. We

suggest that non-amide linkage units, even long ones such as the PEG spacer in resin-**S3**, do not disrupt cyclodimerization because they do not engage in competitive H-bonding, avoiding the type of misalignment suggested for **43**.

Reactions were conducted at various Cu(I) concentrations ranging from 5 to 20 mM, representing 0.5 to 4 equiv relative to peptide. Each reaction was carried out for 16 h and 40 h. For each resin, results were similar for all reaction modifications tested. Representative data are shown in Figure S4.

Figure S4. HPLCs of crude material released from the following resins (insets show MALDI mass spectra of the indicated peak collected from the HPLC run): (a) **Resin-S1**; (b) **Resin-S1** treated with CuI under standard conditions; (c) **Resin-S2**; (d) **Resin-S2** treated with CuI under standard conditions; (e) **Resin-S3**; (f) **Resin-S3** treated with CuI under standard conditions. All analytical HPLC runs were performed with an elution gradient of 15 to 50% MeCN over 20 min, in

0.1% aqueous trifluoroacetic acid. In each case, the linear peptide was completely consumed by the CuAAC reaction, as shown by co-injection (data not shown). In (b) and (d), x = organic impurity (collected and shown to represent a negligible amount of material of low molecular weight).

4. Dependence on peptide length.

Figure S5 shows data supporting Figure 4.

Figure S5. HPLCs and MALDI mass spectra of crude material released from the following resins: (a,b) **Resin-36**; (c,d) **Resin-36** treated with CuI under standard conditions; (e,f) **Resin-36**; (g,h) **Resin-36** treated with CuI under standard conditions; (i,j) **Resin-36**; (k,l) **Resin-36** treated with CuI under standard conditions. All analytical HPLC runs were performed with an elution gradient of 15 to 50% MeCN over 20

min, in 0.1% aqueous trifluoroacetic acid. In each case, the linear peptide was completely consumed by the CuAAC reaction, as shown by co-injection (data not shown, position indicated by an arrow. In (c) and (g), x = organic impurity (collected and shown to represent a negligible amount of material of low molecular weight).
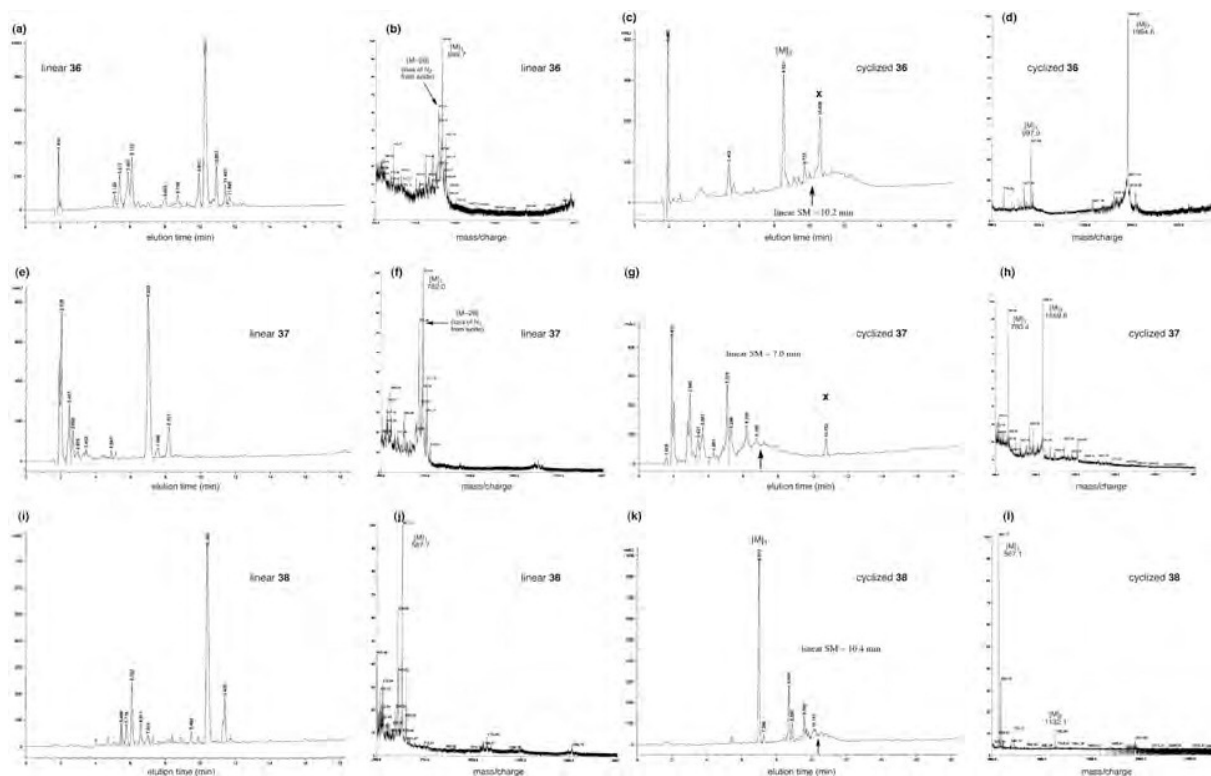
These results mark the first instance of intra-strand ring closure by the on-resin CuAAC reaction with these respective placements of azide and alkyne in the sequence. To confirm that monomeric cyclization is the result of the shortened peptide length and not an artifact of the sequence, **Resin-S4** was exposed to Cu^I (Figures S6 and S7), returning cyclic monomer cleanly. The integrity of the resin and side-chain protecting groups after exposure to the Cu^I cyclization conditions was verified by further elaboration of the peptide derived from **Resin-S5**, which is identical to **Resin-38** except for the presence of a secondary amine in the *N*-terminal azide cap. After cyclization, the resin was washed, acylated with 6-azidohexanoic acid, and treated with trifluoroacetic acid (TFA) to provide a clean cyclic-RGD product (**S6**) functionalized for ligation to an alkyne.
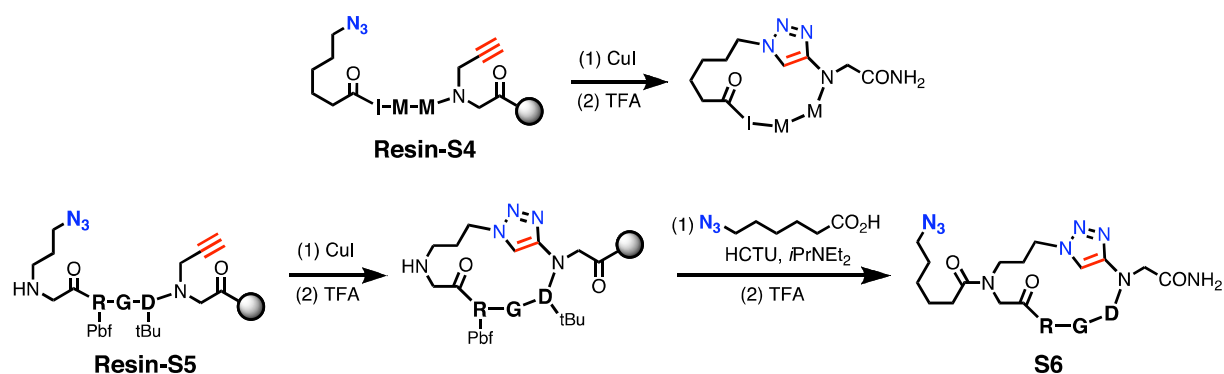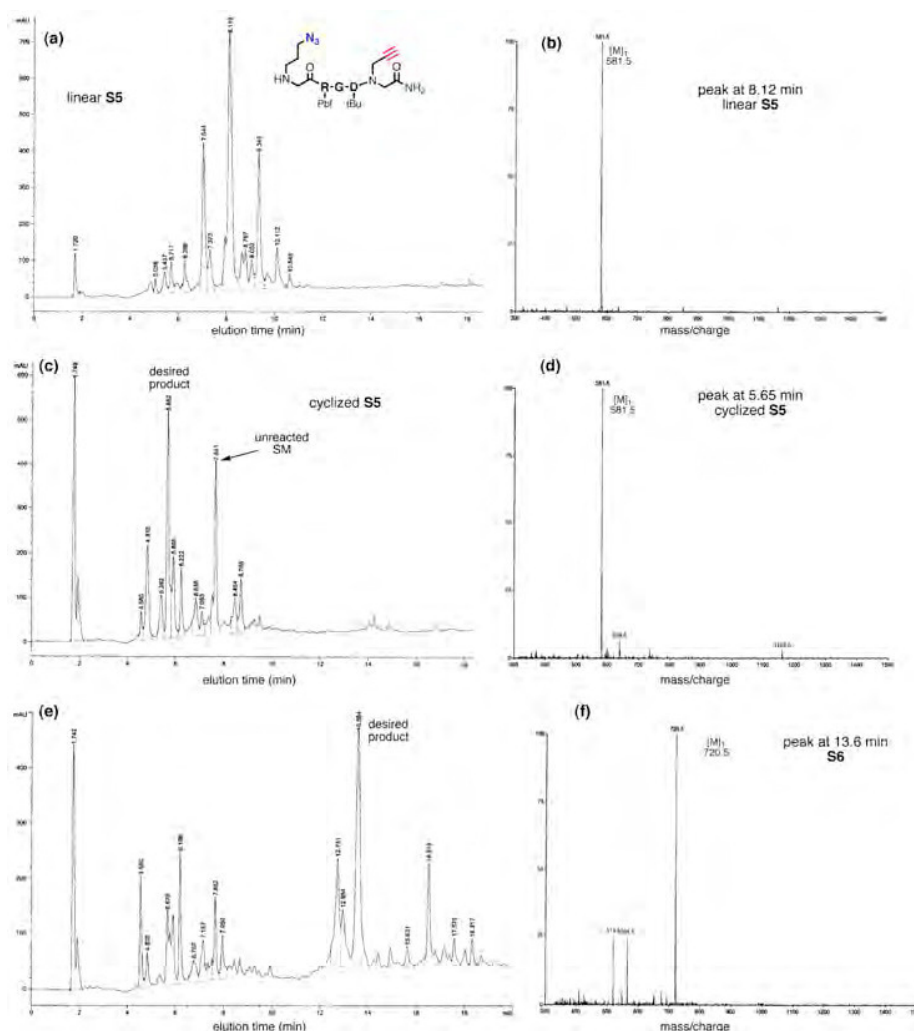
Figure S6. Monocyclization and elaboration of tripeptide derivatives.

Figure S7. HPLCs of crude material released from the following resins (insets show MALDI mass spectra of the indicated peak collected from the HPLC run):
(a) **Resin-S1**;
(b) **Resin-S1** treated with CuI under standard conditions;
(c) **Resin-S2**;
(d) **Resin-S2** treated with CuI under standard conditions;
(e) **Resin-S3**;
(f) **Resin-S3** treated with CuI under standard conditions.
All analytical HPLC runs were performed with an elution gradient of 0 to 35% MeCN over 20 min, in 0.1% aqueous trifluoroacetic acid. In each case, the linear peptide was completely consumed by the CuAAC reaction, as shown by co-injection (data not shown).

In (b) and (d), x = organic impurity (collected and shown to represent a negligible amount of material of low molecular weight

5. Dependence on proximity of alkyne to resin.

Figure S8 shows data supporting Figure 5.

Figure S8. HPLCs of the crude material released from the following resins, along with MALDI mass spectra of the indicated eluted samples: (a,b) **Resin-40**; (c,d) **Resin-40** treated with CuI under standard conditions; (e,f) **Resin-41**; (g,h) **Resin-41** treated with CuI under standard conditions; (i,j) **Resin-42**; (k,l) **Resin-42** treated with CuI under standard conditions; (m,n) **Resin-43**; (o,p) **Resin-43** treated with CuI under standard conditions. All analytical HPLC runs were performed with an elution gradient of 15 to 50% MeCN over 20 min, in 0.1% aqueous trifluoroacetic acid. In (c), (g), (k), and (o), x = organic impurity (collected and shown to represent a negligible amount of material of low molecular weight).
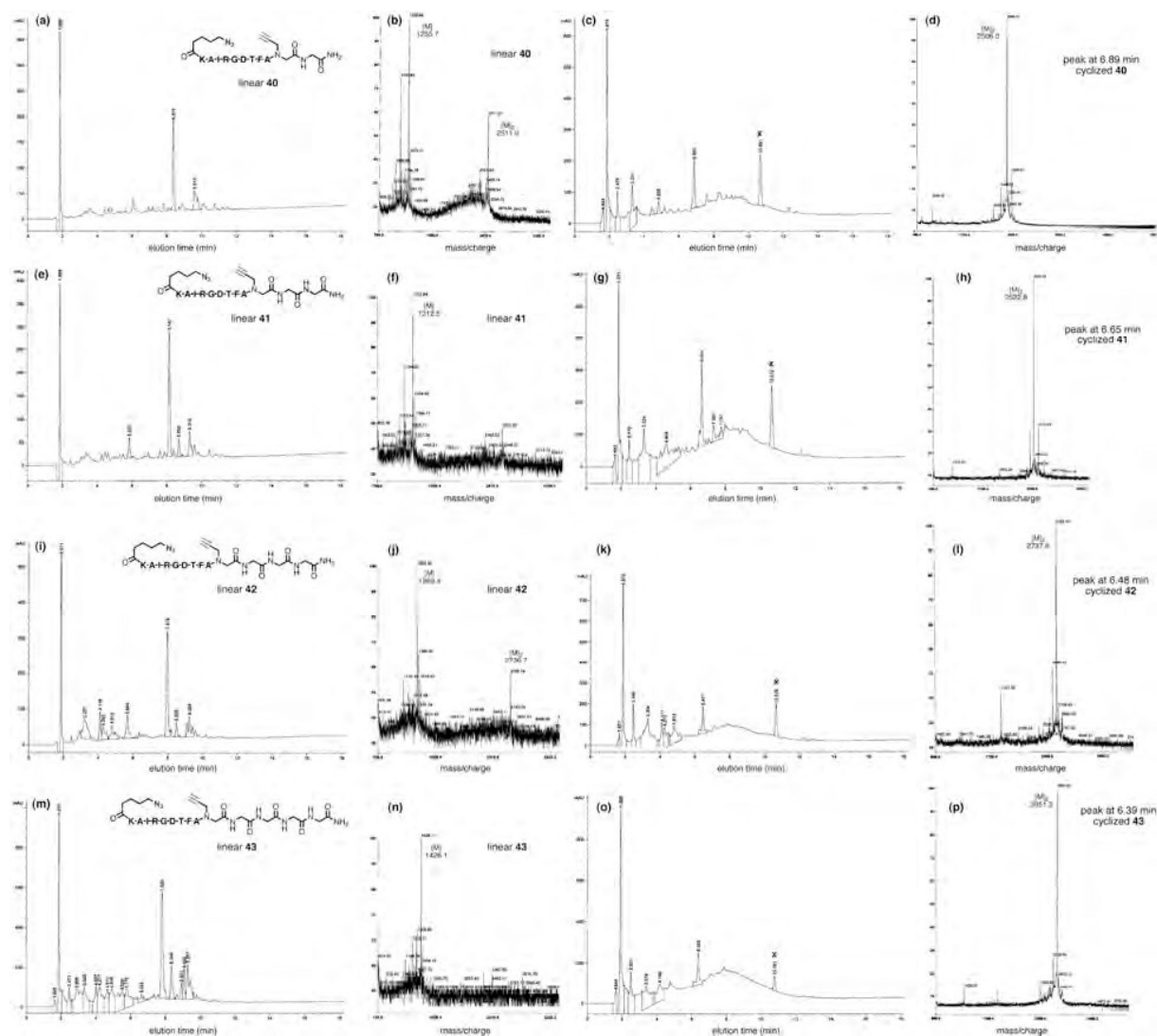
6. Peptide degradation in cases of non–optimal cyclization.

The occurrence of peptide degradation for non-optimal cyclodimerization substrates was examined using sequences **S7–S9**, analogous to **37** but lacking either or both of the alkyne and azide functionalities (Figure S9, related to Figure 5).   After exposure to standard cyclodimerization conditions, workup, and resin cleavage, no peptide degradation was observed: in each case, analytical HPLC chromatograms were identical to those of the linear material before being exposed to CuI (Figure S10).   While CuI ions (or CuII accessible by disproportionation or air oxidation in the absence of reducing agent) may have the capacity to enhance the cleavage of peptide bonds,[8,9] they apparently do not do so here. The only difference between **37** (which does undergo decomposition) and **S7-S9** (which do not) is the presence in the former of both components that are required to form triazoles. Therefore, if degradation is occurring in the absence of facile cyclization, it is likely caused by Cu complexes of the triazole product or by the organometallic Cu-triazolyl intermediate that precedes release of triazole in the CuAAC catalytic cycle.[10,11]

Figure S9. Sequences prepared to test peptide decomposition.

Resin-37   **Resin-S7**   **Resin-S8**   **Resin-S9**
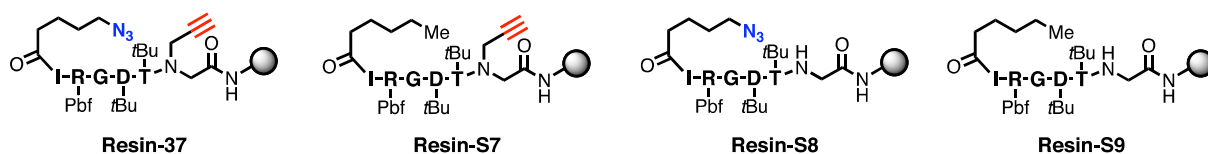
Figure S10. HPLCs and MALDI mass spectra of the crude material released from the indicated resins: (a) **Resin-S7**; (b,c) **Resin-S7** treated with CuI under standard conditions; (d) **Resin-S8**; (e,f) **Resin-S8** treated with CuI under standard conditions; (g) **Resin-S9**; (h,i) **Resin-S9** treated with CuI under standard conditions. All analytical HPLC runs were performed with an elution gradient of 15 to 50% MeCN over 20 min, in 0.1% aqueous trifluoroacetic acid.
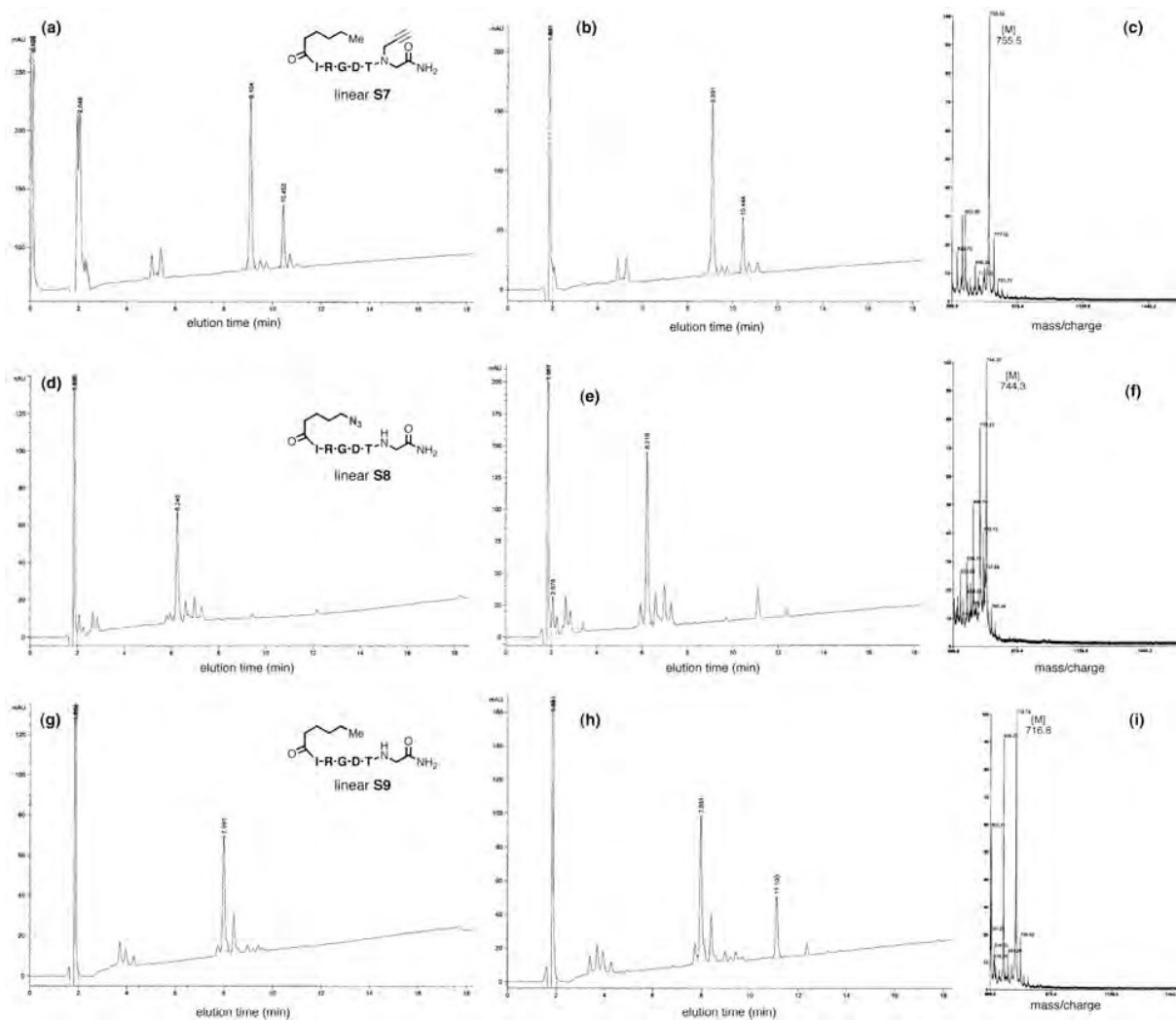
7. Peptide cyclodimerization on preparative scale.

Structures and HPLC traces for the crude and purified peptides described in this section of the text are shown in Figure S11; ^{1}H and ^{1}H-^{1}H COSY NMR spectra of the purified peptides are shown in Figure S12. High resolution MALDI-TOF MS: for the peptide cleaved from resin-**62** [M+H]$^+$ = [C$_{54}$H$_{87}$N$_{18}$O$_{14}$]$^+$, calcd *m/z* 1211.6651, observed *m/z* 1211.7875; for cyclic dimer **35** [M+2H]$^{2+}$ = [C$_{108}$H$_{174}$N$_{36}$O$_{28}$]$^{2+}$, calcd *m/z* 1211.6651, observed *m/z* 1211.6644; for cyclic monomer **34** [M+H]$^+$ = [C$_{54}$H$_{87}$N$_{18}$O$_{14}$]$^+$, calcd *m/z* 1211.6651, observed *m/z* 1211.6654. In the case of the linear and cyclic monomers, introducing a small amount of D$_2$O into the H$_2$O solution produced unit mass increases in the mass spectrum, whereas the cyclic dimer showed half-unit increases, as expected for the doubly charged dimeric ions.

Figure S11. HPLCs of crude material released from Rink amide MBHA resin as described in the text, and purified samples after reversed-phased preparative HPLC. All runs were performed with an elution gradient of 15 to 50% MeCN over 20 min, in 0.1% aqueous trifluoroacetic acid.
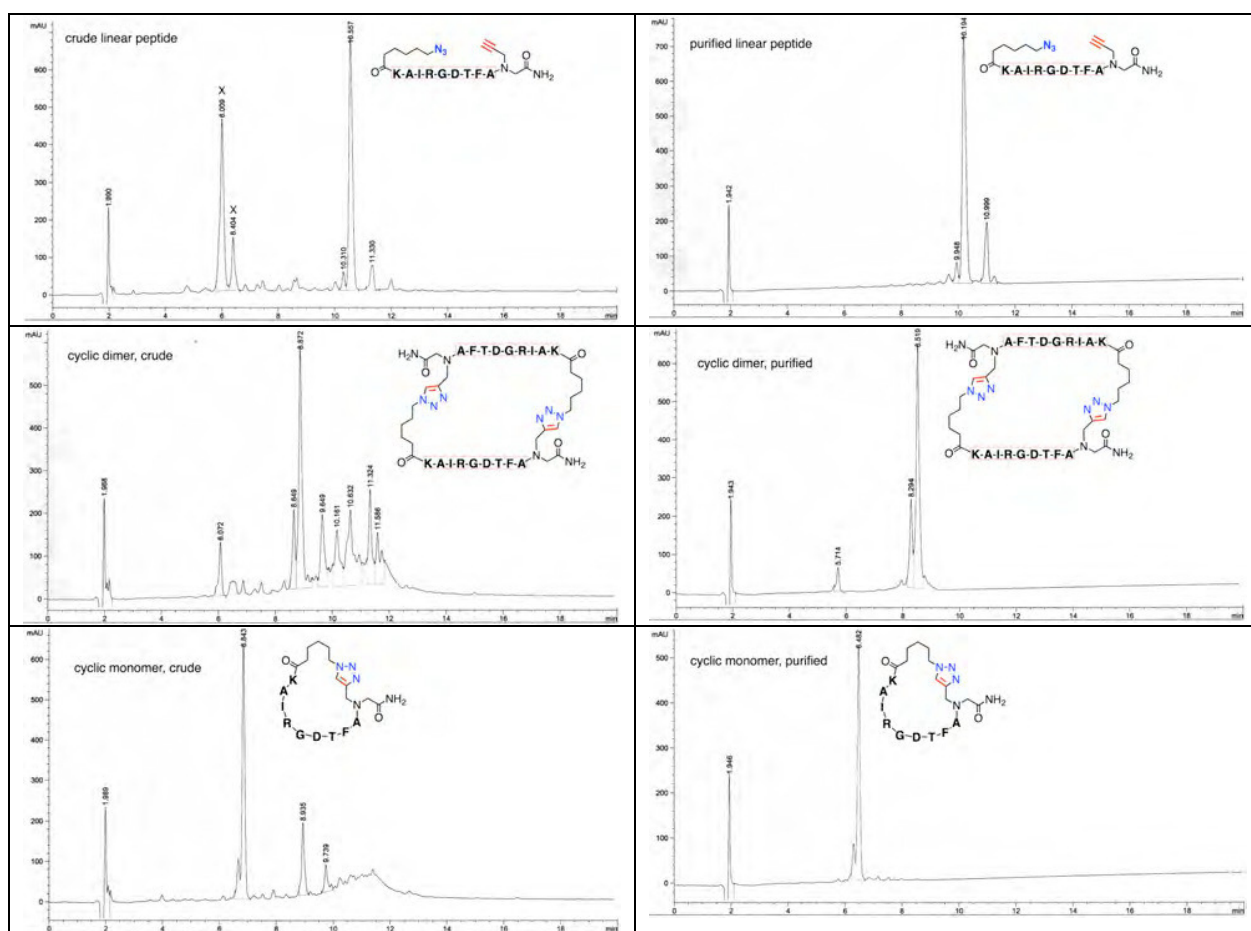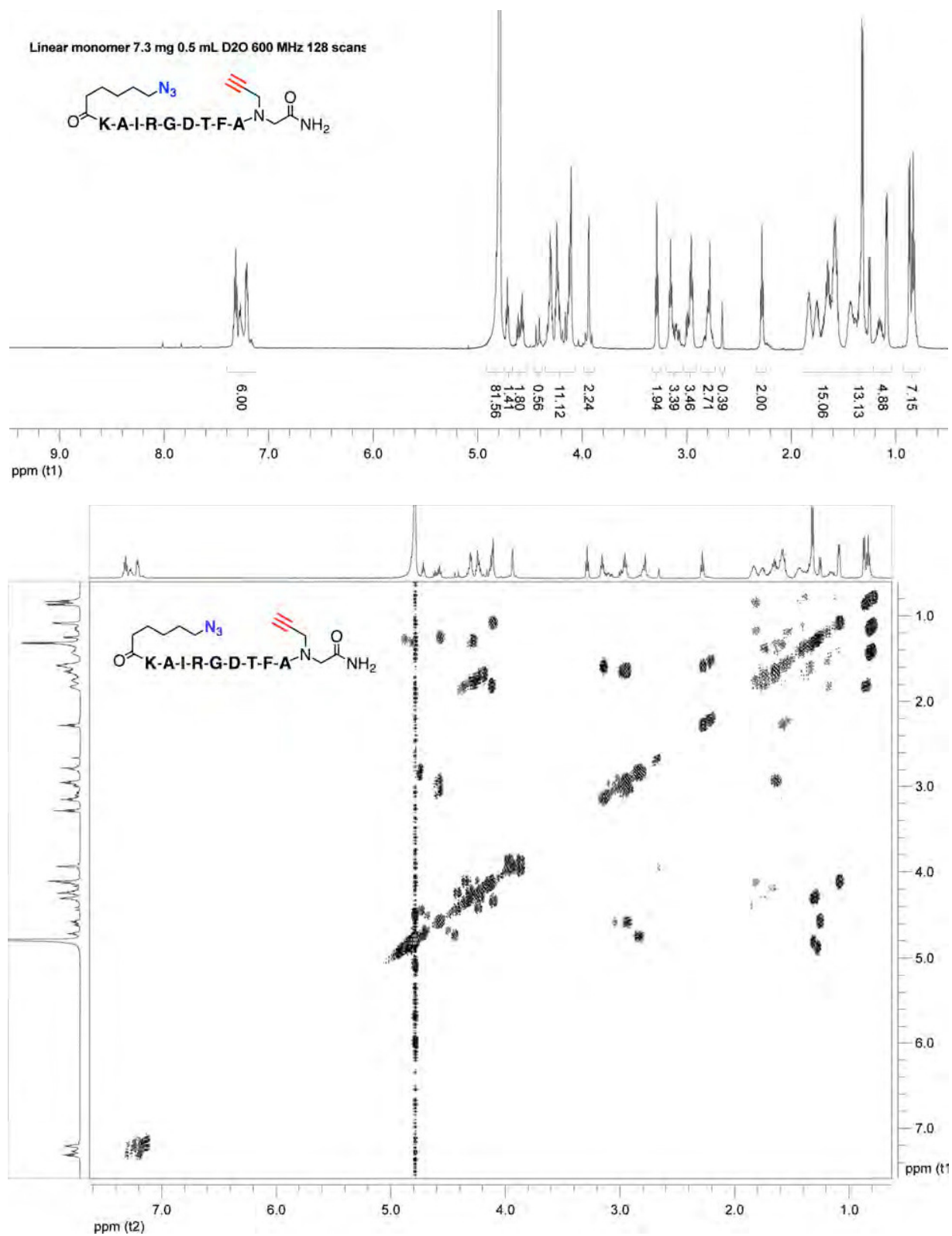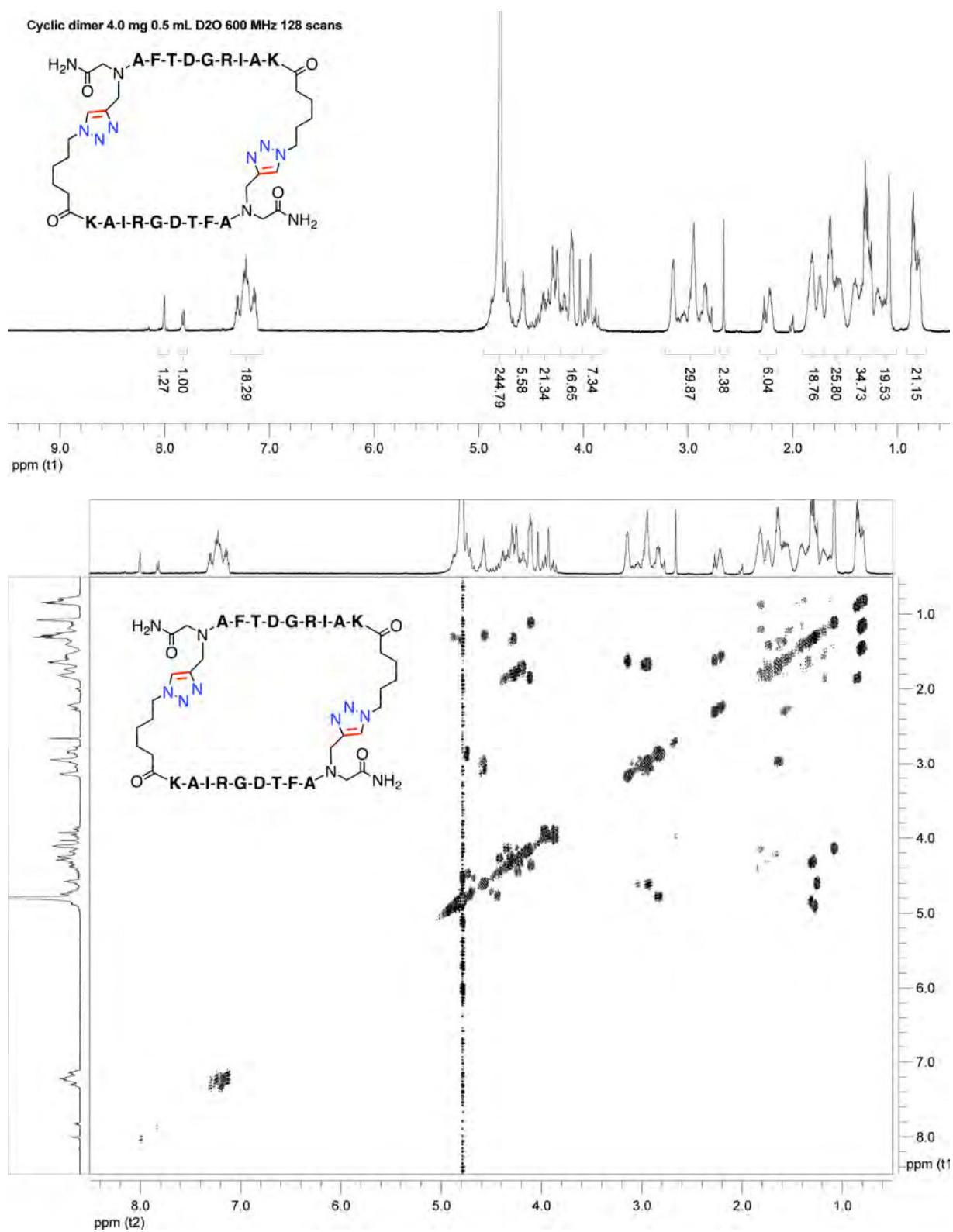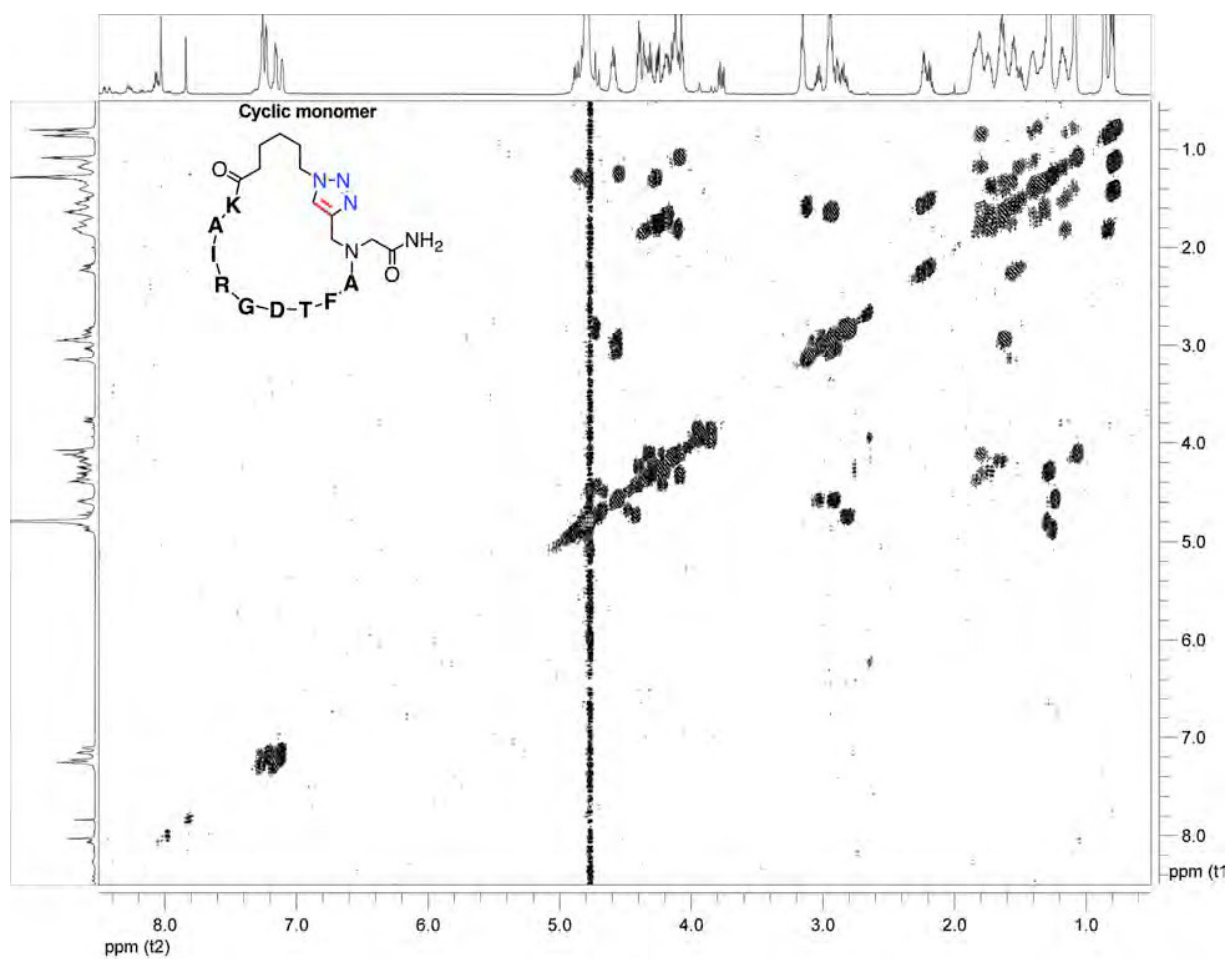
Figure S12. ^{1}H NMR and ^{1}H-^{1}H-correlation (COSY) NMR spectra of the indicated peptides.

Cyclic dimer 4.0 mg 0.5 mL D2O 600 MHz 128 scans

Cyclic monomer 3.9 mg 0.3 mL D2O 600 MHz 60 scans
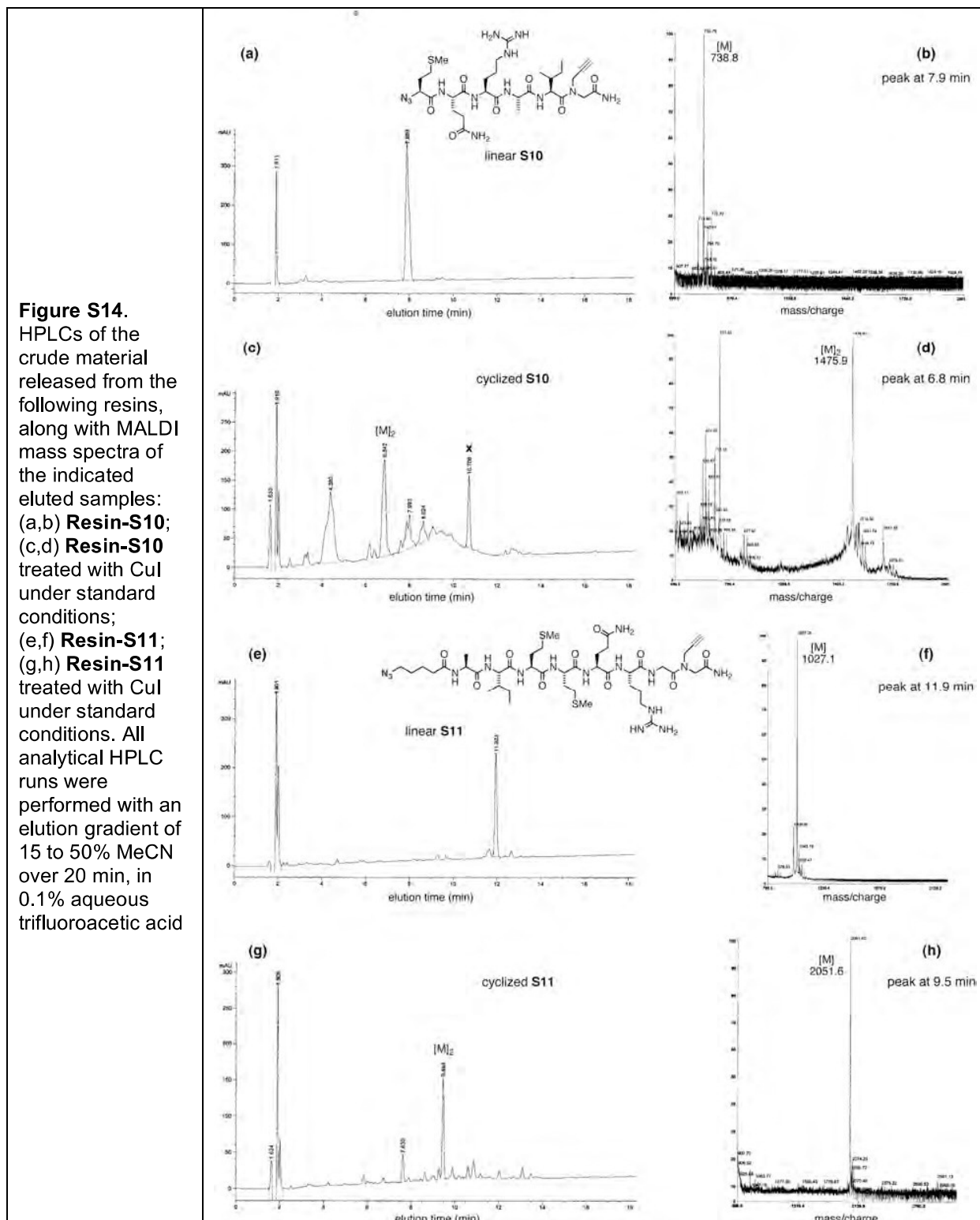

Cyclic monomer
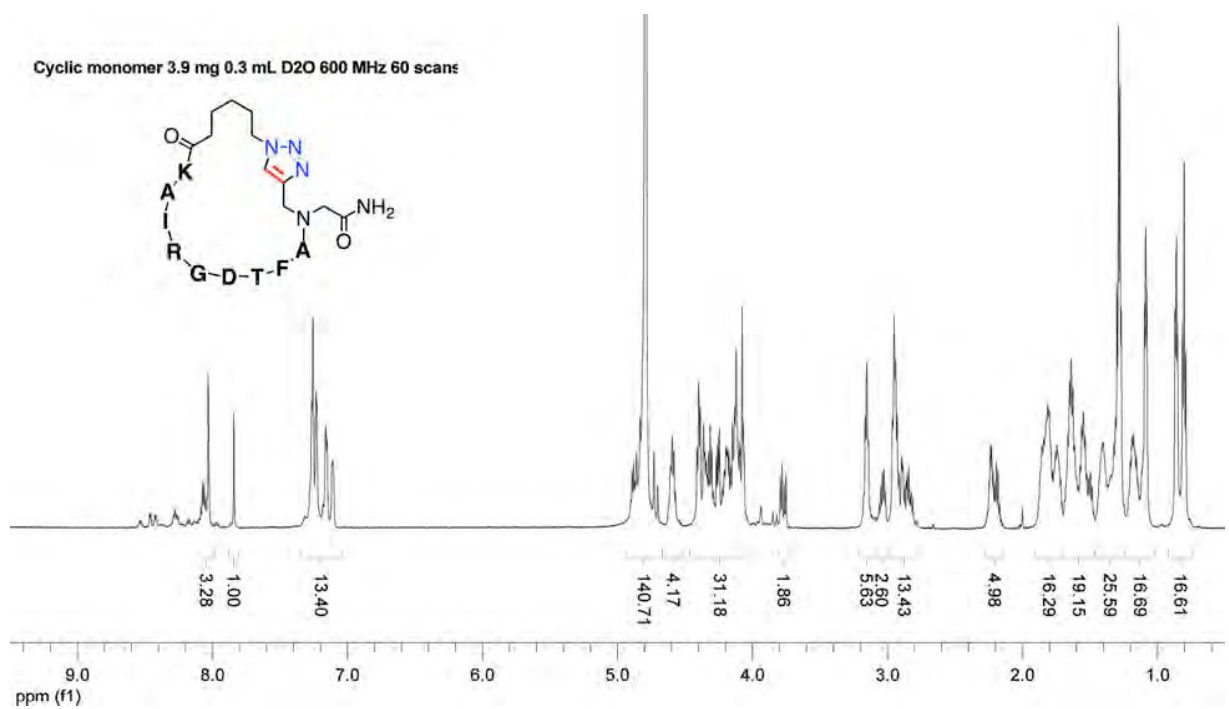
We also performed similar experiments on larger scale with two other sequences, **S10** (encompassing the pentapeptide sequence MQRAI) and **S11** (AIMMQRG), prepared on several hundred milligrams of the standard Rink amide MBHA resin (Figure S13). After dimeric cyclization as above (suspension in 20 mL of 1:4 DMSO:MeCN, 5 mM CuI, 2,6-lutidine), standard cleavage from the resin, and purification by preparatory RP-HPLC, and lyophilization, the desired cyclic dimers were obtained as white powders in 5.7 and 9.0 mg yields, respectively (Figure S14). The successful cyclodimerization of **S10**, incorporating the azide moiety as an azidomethionine derivative,[12] shows that the longer tether to the azide used in all other cases described here is not required. It also demonstrates that a pentamer can be cyclodimerized, although the efficiency of this process is somewhat less than that for hexamers or longer oligopeptides.

Figure S13. Linear peptides used to prepare cyclic dimers on preparative scale.

Resin-S10   **Resin-S11**

Figure S14.
HPLCs of the crude material released from the following resins, along with MALDI mass spectra of the indicated eluted samples: (a,b) **Resin-S10**; (c,d) **Resin-S10** treated with CuI under standard conditions; (e,f) **Resin-S11**; (g,h) **Resin-S11** treated with CuI under standard conditions. All analytical HPLC runs were performed with an elution gradient of 15 to 50% MeCN over 20 min, in 0.1% aqueous trifluoroacetic acid

8. Oligomerization in the absence of copper with non-peptide polyamides

Figure S15 shows a graphical representation of the phenomenon described in the text associated with Figure 7. Figure S16 shows some of the data supporting that discussion.

Figure S15. Spontaneous cycloaddition reactions of resin-bound oligo(β-Ala) peptides, represented in cartoon fashion. For clarity, tetramer and pentamer products are not shown.
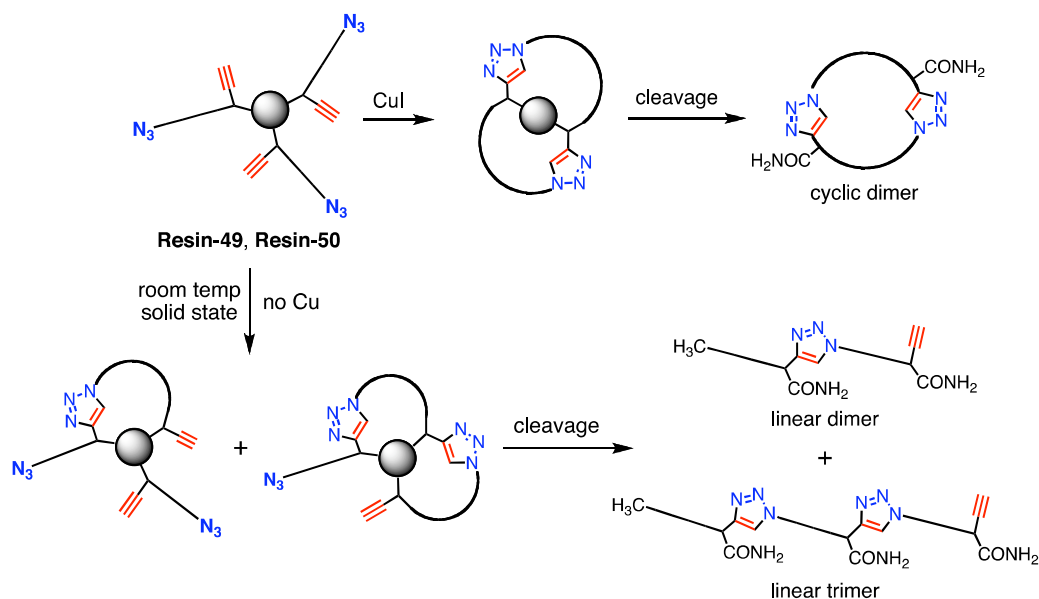
A similar observation was also made with the longer oligo(β-Ala) sequence **50**. In this case, after Cu[I] treatment the resin was washed extensively with aqueous EDTA to remove copper ions and the peptide cleaved away from the resin. The resulting crude, lyophilized powder was stored at room temperature for one month. HPLC analysis of the sample revealed a decrease in the amount of linear starting material and a corresponding increase in the amount of linear oligomers over time, with the amounts of cyclic monomer and cyclic dimer remaining unchanged (Figure S17).

Figure S16. HPLCs and MALDI mass spectra of the crude material released from the indicated resins. HPLC peak labels describe the result of MALDI-MS on the material obtained by collection of that peak (data not shown). (a) **Resin-46**; (b,c) **Resin-46** treated with CuI under standard conditions; (d) **Resin-48**; (e,f) **Resin-48** treated with CuI under standard conditions; (g) **Resin-49**; (h,i) **Resin-49** treated with CuI under standard conditions; (j) **Resin-49** allowed to stand for 3 weeks in the solid state. A comparison with (g) shows the growth in linear oligomers. All analytical HPLC runs were performed with an elution gradient of 0 to 35% MeCN over 20 min, in 0.1% aqueous trifluoroacetic acid.
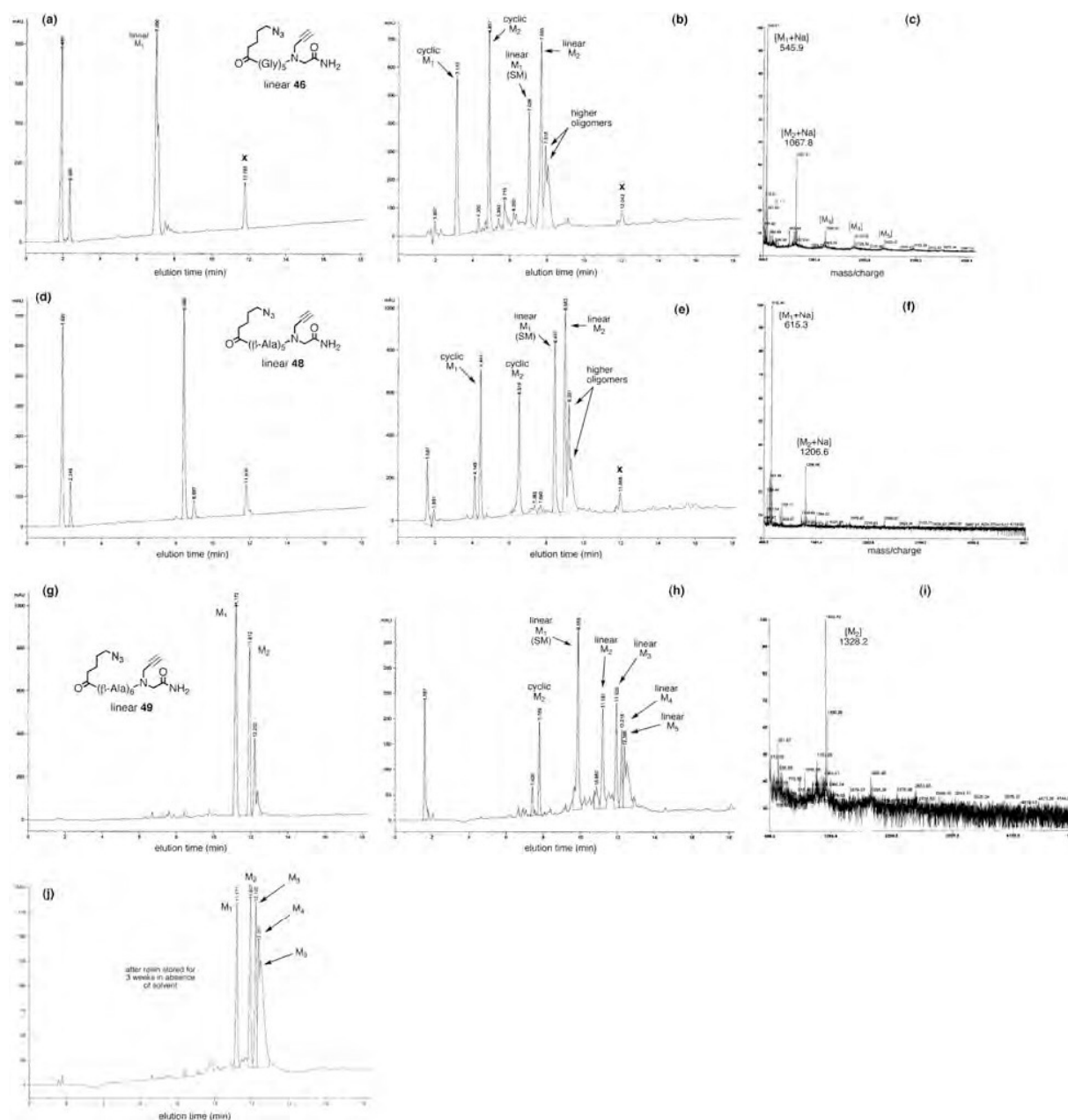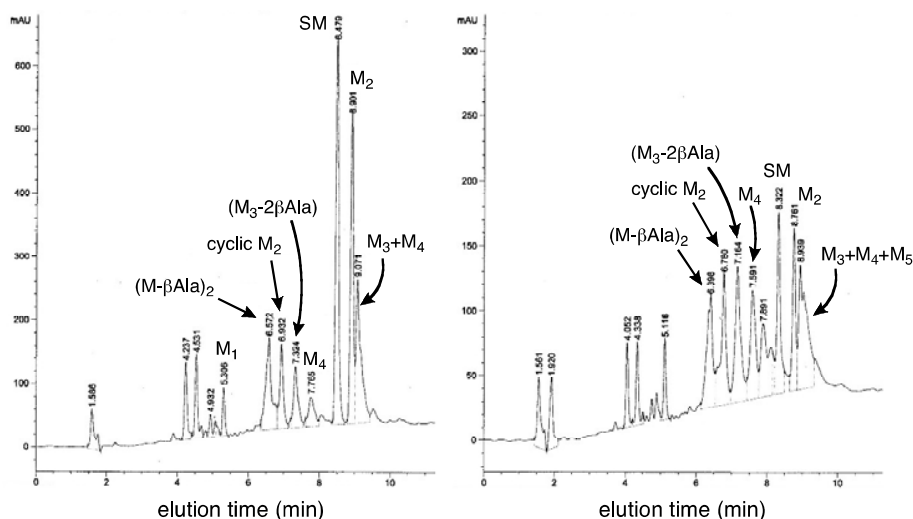
Figure S17. HPLCs (0 to 35% MeCN over 20 min, in 0.1% aqueous trifluoroacetic acid) of material released from (left) **Resin-50** after CuAAC reaction, and (right) the crude product from that reaction after storage as a lyophilized solid for three weeks. HPLC peak labels describe the result of MALDI-MS on the material obtained by collection of that peak (data not shown).

9. Tertiary Amides

Homochiral α-substitution on nitrogen confers well-characterized helicity to the peptoid architecture with a helical pitch of three residues.[13-15] Sequence **56** thereby places its azide and alkyne groups in close proximity to each other on the same side of the helix, while **57** places them a greater distance apart and on different faces of the helix (Figure 8). Structures **58** and **59** mimic the alkyne and azide positions of the peptides tested above. The lack of α-substituents in the latter sequence removes the steric and torsional interactions between side chains and hence any predisposition toward helicity, creating an unstructured, more flexible peptoid strand. In all of these cases (**56-59**), cyclic monomers were produced exclusively from on-resin CuAAC reaction. The cyclic monomers were identified by mass spectrometry and their substantially different retention times on analytical RP-HPLC compared to the linear starting material.

The helical peptoid sequence **60** and its unstructured analogue **61** were prepared to further explore the role of alkyne position relative to the resin backbone (see Figure 5 and associated discussion). When alkyne and azide were placed three residues apart, and thus in close proximity on the more rigid helix of **60**, cyclic monomer was formed exclusively upon treatment with Cu^I. The more flexible sequence **61**, however, afforded products of oligomeric mass (M_2-M_5) as well as cyclic monomer, and also stands in contrast to the exclusive monocyclization behavior of **59**. These results correspond with observations made in our previous report[16] in which oligomeric products were observed for peptide sequences with reversed alkyne and azide positions, highlighting the extra control provided by the installation of alkyne near the polymeric resin backbone.

Figures S18 and S19 show data supporting this discussion (Figures 8 and 9).

Figure S18. HPLCs and MALDI mass spectra of the crude material released from the indicated resins. HPLC peak labels describe the result of MALDI-MS on the material obtained by collection of that peak (data not shown). (a, d, g, j, m, p) **Resins-56–61**. Each of these materials gave a clean MALDI-MS showing the expected monomer parent ion (data not shown). The other panels on each line show HPLC and MALDI-MS data for each material after treatment with CuI under standard conditions and cleavage from the resin. HPLC runs were performed with an elution gradient of 0 to 95% MeCN over 20 min, in 0.1% aqueous trifluoroacetic acid. Peaks labeled as cyclic M_1 elute at a different retention time than the linear peptoid, as shown by co-injection (data not shown). **x** = organic impurity (collected and shown to represent a negligible amount of material of low molecular weight); **z** = material giving a parent ion in the mass spectrum corresponding to the peptoid monomer minus all six of the methyl groups.
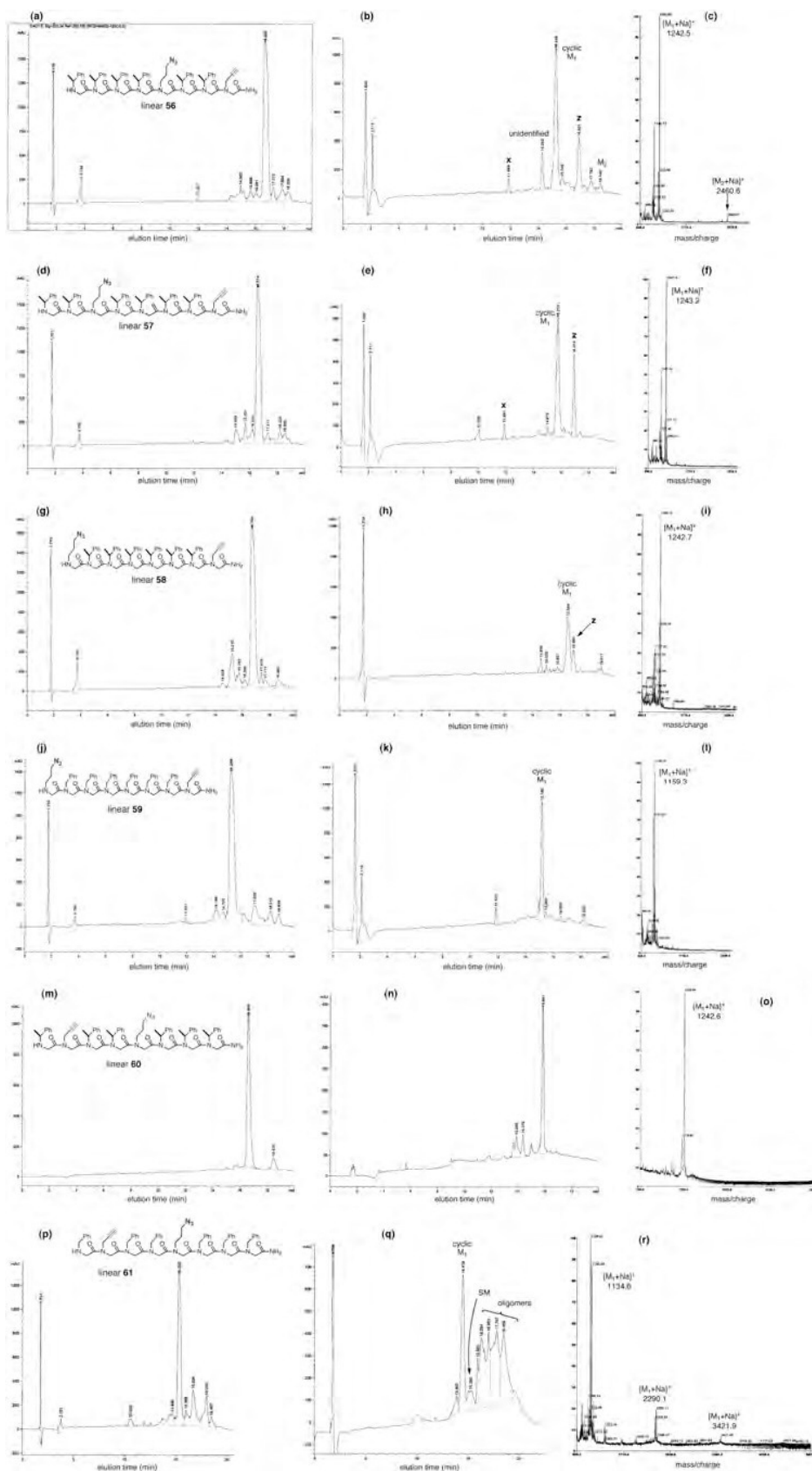
Figure S19. HPLCs and MALDI mass spectra of the crude material released from the indicated resins. HPLC peak labels describe the result of MALDI-MS on the material obtained by collection of that peak (data not shown).
(a) **Resin-62**; (b,c) **Resin-62** treated with CuI under standard conditions. (d,e) **Resin-62** treated with CuI in DMSO. (f) **Resin-63**; (g,h) **Resin-63** treated with CuI under standard conditions. (i) **Resin-64**; (j,k) **Resin-64** treated with CuI under standard conditions. All analytical HPLC runs were performed with an elution gradient of 15 to 50% MeCN over 20 min, in 0.1% aqueous trifluoroacetic acid. In (d) the two peaks designated "M_1" are likely diastereomers of the monocyclized peptide.
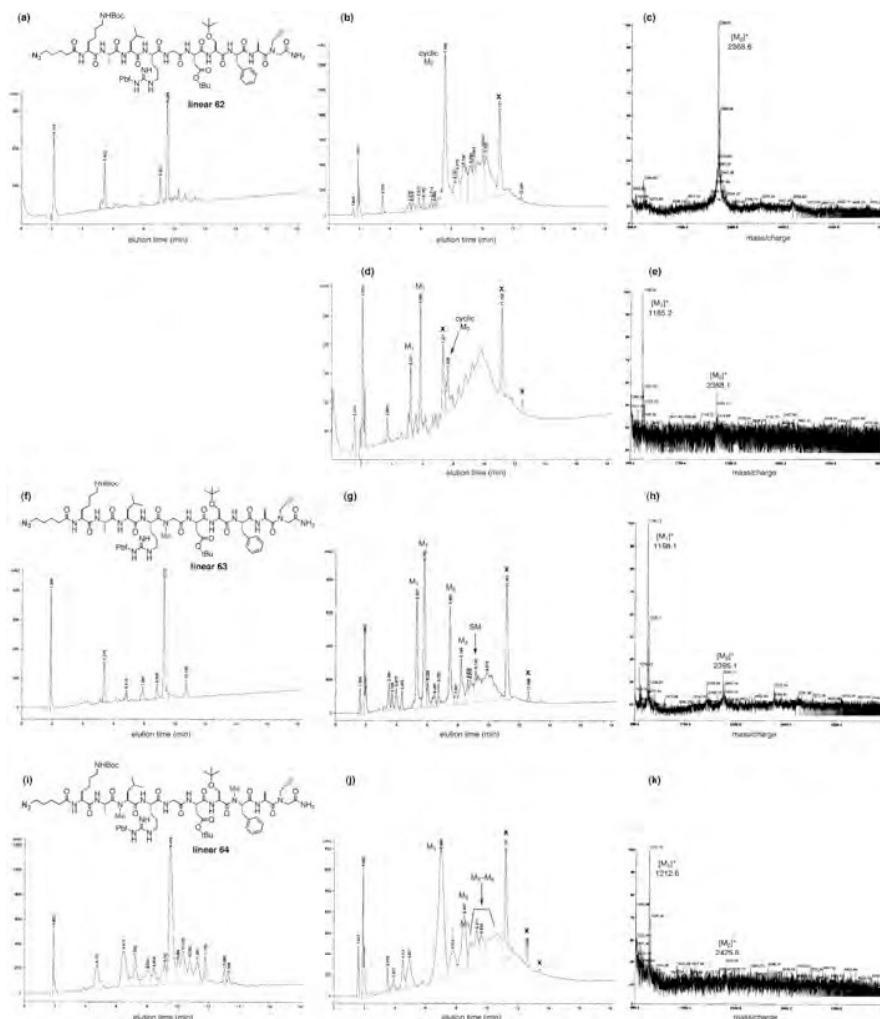
10. Potential participation of Cu(II) in cyclodimerization

In our original report, we suggested that the binding of copper with the peptide backbone might help orient the chains to favor the formation of head-to-tail dimers.[16] Such an interaction would be expected to be much stronger for Cu^{II} than for Cu^{I}, since the former is a better match for the relatively hard donor properties of the amide group, and there are many more examples known of Cu^{II}-peptide interactions, albeit aided in most cases by binding to side chain donor groups.[17,18] Since our standard reaction conditions do not exclude oxygen with the most rigorous care (resin suspensions are degassed, sealed in vials with polycarbonate or Teflon caps, and agitated gently at the bench for 16 or 40 hours), one might expect the mixtures to become exposed to oxygen and thus to generate some Cu^{II}. To test this possibility, the standard resin **33** was treated with $Cu(MeCN)_4OTf$ in rigorously degassed solvent (4:1 MeCN:DMSO) and allowed to react in a drybox under nitrogen atmosphere kept at <1 ppm O_2. Cyclic dimer was returned in normal fashion, ruling out the participation of Cu^{II} since significant quantities would not be expected from disproportionation of Cu^{I} in organic solvent.

References

(1)   Van Maarseveen, J. H.; Horne, W. S.; Ghadiri, M. R. *Org. Lett.* **2005**, *7*, 4503-4506.
(2)   Billing, J. F.; Nilsson, U. J. *J. Org. Chem.* **2005**, *70*, 4847-4850.
(3)   Bodine, K. D.; Gin, D. Y.; Gin, M. S. *J. Am. Chem. Soc.* **2004**, *126*, 1638-1639.
(4)   Bodine, K. D.; Gin, D. Y.; Gin, M. S. *Org. Lett.* **2005**, *7*, 4479 -4482.
(5)   Angell, Y.; Burgess, K. *J. Org. Chem.* **2005**, *70*, 9595-9598.
(6)   Choi, W. J.; Shi, Z.-D.; Worthy, K. M.; Bindu, L.; Karki, R. G.; Nicklaus, M. C.; Fisher, R. J.; Burke, T. R., Jr. *Bioorg. Med. Chem. Lett.* **2006**, *16*, 5265-5269.
(7)   Bayer, E. *Angew. Chem. Int. Ed. Engl.* **1991**, *30*, 113-216.
(8)   de Oliveira, M. C. B.; Scarpellini, M.; Neves, A.; Terenzi, H.; Bortoluzzi, A. J.; Szpoganics, B.; Greatti, A.; Mangrich, A. S.; de Souza, e. M.; Fernandez, P. M.; Soares, M. R. *Inorg. Chem.* **2005**, *44*, 921-929.
(9)   Hegg, E. L.; Burstyn, J. N. *J. Am. Chem. Soc.* **1995**, *117*, 7015-7016.
(10) Nolte, C.; Mayer, P.; Straub, B. F. *Angew. Chem. Int. Ed.* **2006**, *46*, 2101-2103.
(11) Rodionov, V. O.; Fokin, V. V.; Finn, M. G. *Angew. Chem. Int. Ed.* **2005**, *44*, 2210-2215.
(12) Lundquist, J. T., IV; Pelletier, J. C. *Org. Lett.* **2001**, *3*, 781-783.
(13) Armand, P.; Kirshenbaum, K.; Goldsmith, R. A.; S., F.-J.; Barron, A. E.; Truong, K. T. V.; Dill, K. A.; Mierke, D. F.; Cohen, F. E.; Zuckermann, R. N.; Bradley, E. K. *Proc. Natl. Acad. Sci. USA* **1998**, *95*, 4303-4308.
(14) Kirshenbaum, K.; Barron, A. E.; Goldsmith, R. A.; Armand, P.; Bradley, E. K.; Truong, K. T. V.; Dill, K. A.; Cohen, F. E.; Zuckermann, R. N. *Proc. Natl. Acad. Sci. USA* **1998**, *95*, 4309-4314.
(15) Wu, C. W.; Kirshenbaum, K.; Sanborn, T. J.; Patch, J. A.; Huang, K.; Dill, K. A.; Zuckermann, R. N.; Barron, A. E. *J. Am. Chem. Soc.* **2003**, *125*, 13525-13530.
(16) Punna, S.; Kuzelka, J.; Wang, Q.; Finn, M. G. *Angew. Chem. Int. Ed.* **2005**, *44*, 2215-2220.
(17) Groves, J. T.; Chambers, J., R.R. *J. Am. Chem. Soc.* **1984**, *106*, 630-638.
(18) Yokoi, H.; Hanaki, A. *Chem. Lett.* **1983**, *8*, 1319-1322.